GEOLOGICAL SURVEY OF CANADA
CURRENT RESEARCH 1998-F

RADIOGENIC AGE AND ISOTOPIC STUDIES: REPORT 11

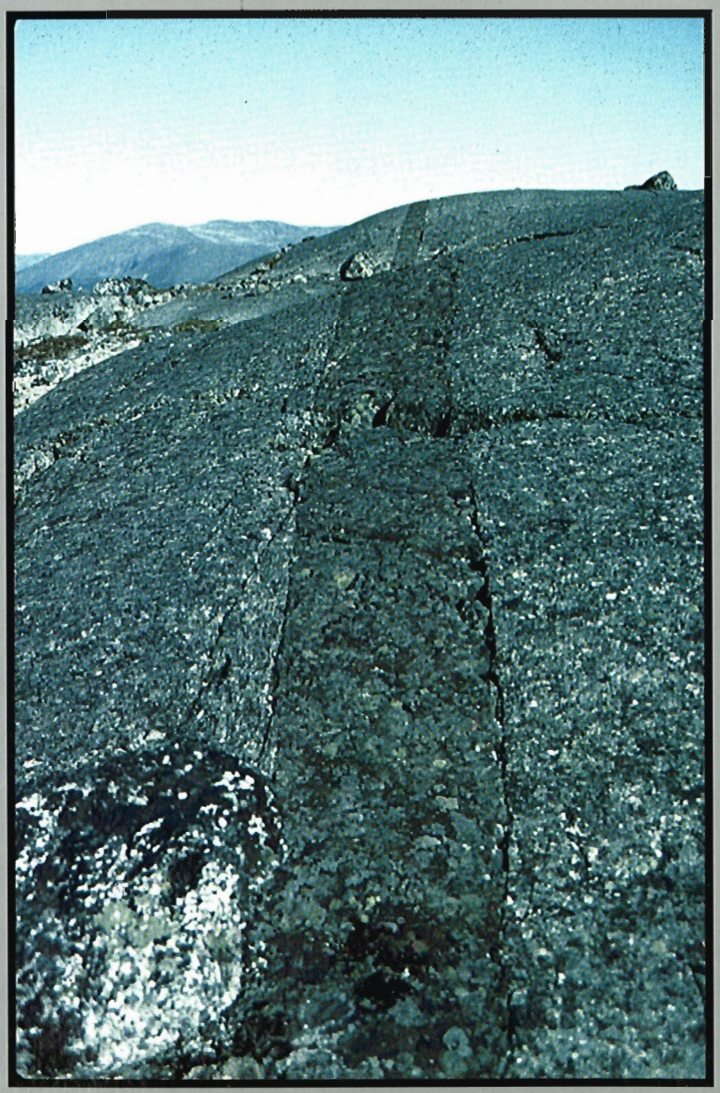

1998

Natural Resources Canada Ressources naturelles Canada

Canada

STAFF, GEOCHRONOLOGY SUBDIVISION GEOLOGICAL SURVEY OF CANADA

Research Scientists:	Otto van Breemen Bill Davis Mike Hamilton Hamish Sandeman Richard Stern Natasha Wodicka
Physical Scientists:	Vicki McNicoll Réginald Thériault Mike Villeneuve
Technical Staff:	Diane Bellerive Ron Christie Gerald Gagnon Jack MacRae Natalie Morisset Fred Quigg Klaus Santowski

GEOLOGICAL SURVEY OF CANADA
CURRENT RESEARCH 1998-F

RADIOGENIC AGE AND ISOTOPIC STUDIES: REPORT 11

1998

Catalogue No. M44-1998/6E
ISBN 0-660-17673-4

Available in Canada from
Geological Survey of Canada offices:

601 Booth Street
Ottawa, Ontario K1A 0E8

3303-33rd Street N.W.
Calgary, Alberta T2L 2A7

101-605 Robson Street
Vancouver, B.C. V6B 5J3

or from

Canada Communication Group – Publishing
Ottawa, Ontario K1A 0S9

A deposit copy of this publication is also available for reference
in selected public libraries across Canada

Price subject to change without notice

Cover illustration

Along the northeast flanks of the Mesoproterozoic Nain Plutonic Suite in Labrador, a newly recognized complex of Paleoproterozoic leucogabbros and anorthosites are intruded by a swarm of dominantly southeast-trending (140°) metagabbroic and metadiabase dykes.

The photo shows a thin dyke splay (<1 m), parallel to a larger 11 m wide metadiabase (not shown), which was dated at about 2045 Ma. The host leucogabbros are correlated with similar rocks to the northwest which crystallized at 2112 +5/-4 Ma. Weak metamorphism and foliation affecting the rocks are ascribed to the effects of Torngat Orogen, between about 1860 and 1740 Ma.

Photo from hilltop east of Iglusuataliksuak Lake, by M.A. Hamilton. GSC 1998-031

CONTENTS

RADIOGENIC AGE AND ISOTOPIC STUDIES: REPORT 11

INTRODUCTION

Radiogenic Age and Isotopic Studies is an annual report on recently obtained radiometric age and tracer isotope data generated by the Geochronology Subdivision at the Geological Survey of Canada. Report 11 consists of fourteen papers on various geoscience research topics within the fields of U-Pb, Sm-Nd, and Rb-Sr isotopic studies. Readers are reminded that the contributions often contain provisional results and interpretations of ongoing research, or consist of completed studies of limited scope. Typically, articles of greater depth and magnitude are published in external journals, and a list of such recent works is provided at the end of this volume. Nonetheless, all reports herein present brief regional and local field settings, and relate data in an appropriate geological context.

This year saw the commencement of U-Pb zircon dating projects using the SHRIMP (Sensitive HighResolution Ion Microprobe), housed in the J.C. Roddick Ion Microprobe Laboratory, and the development of analytical methods for U-Pb-Th analysis of monazite. The monazite analytical techniques are detailed in the first paper of this volume, complementing the zircon analytical methods reported in last year's publication (Report 10). Monazite geochronology by SHRIMP is a novel technique that provides a powerful new tool in the dating of metamorphic rocks, among many other potential applications. Furthermore, methods for Pb-Th dating using conventional TIMS (thermal ionization mass spectrometry) are described, and augment the analytical capabilities of the subdivision.

Other papers presented in this volume exemplify the span of the Geochronology Subdivision's involvement, both in time through the geological eons, and in space across the Canadian landmass. Included are reports on the age and evolution of the Archean Slave and Churchill crust. Contributions on the Proterozoic include papers on the Trans-Hudson Orogen in southern Baffin Island, the Saguenay–Lac Saint-Jean area of the Grenville Province, and Paleoproterozoic magmatism in the vicinity of the Nain Plutonic Suite of Labrador. Also included are reports on aspects of the evolution of the northern Cordillera.

The continued vitality of the Geochronology Subdivision's program would not be possible without the diligent work of its support staff. Gerry Gagnon and Ron Christie produce pure mineral separates from rock specimens. Fred Quigg assures continued production of $^{40}Ar/^{39}Ar$ data. Diane Bellerive and Jack MacRae

INTRODUCTION

La publication *Radiogenic Age and Isotopic Studies* est un rapport annuel renfermant les données récentes relatives à la datation radiométrique et aux isotopes traceurs obtenues par la Sous-division de la géochronologie de la Commission géologique du Canada. Le rapport n° 11 comprend quatorze articles portant sur divers sujets de recherche géoscientifique sur les isotopes U-Pb, Sm-Nd et Rb-Sr. Rappelons aux lecteurs que ces articles renferment souvent les résultats et les interprétations provisoires de recherches en cours ou qu'ils consistent souvent en un compte rendu final d'études de portée limitée. En général, les articles plus approfondis et plus fouillés sont publiés dans des revues externes. Une liste des articles publiés récemment est fournie à la fin du présent volume. Néanmoins, tous les articles publiés dans ce rapport présentent les contextes régionaux et locaux et contiennent une interprétation qui place les données dans le contexte géologique approprié.

Cette année, des projets de datation U-Pb sur zircon utilisant la microsonde ionique à haute résolution et à haut niveau de sensibilité (SHRIMP), installée dans le Laboratoire d'analyse à la microsonde J.C. Roddick, ont vu le jour et des méthodes analytiques pour l'analyse U-Pb-Th de la monazite ont été mises au point. Les méthodes d'analyse de la monazite sont décrites en détail dans le premier article de ce volume et viennent en complément des méthodes d'analyse du zircon présentées dans le rapport de l'année dernière (rapport n°10). La géochronologie de la monazite effectuée à l'aide de la microsonde SHRIMP est une technique novatrice qui offre un nouvel outil puissant de datation des roches métamorphiques, entre autres applications possibles. De plus, les méthodes de datation Pb-Th par spectrométrie de masse à thermoionisation (TIMS) décrites dans ce rapport viennent accroître les capacités analytiques de la sous-division.

D'autres articles publiés dans ce volume viennent illustrer la portée de l'intérêt de la Sous-division de la géochronologie à la fois dans le temps, par l'étude des éons géologiques, et dans l'espace, par l'étude de la masse continentale du Canada. Certains articles traitent de l'âge et de l'évolution de la croûte terrestre archéenne des provinces des Esclaves et de Churchill. D'autres portent sur le Protérozoïque, notamment sur l'orogène trans-hudsonien dans le sud de l'île de Baffin, de la Province de Grenville dans la région du Saguenay–Lac Saint-Jean, et sur le magmatisme du Paléoproterozoïque à proximité de la Suite plutonique de Nain au Labrador. Enfin, des articles traitent des aspects de l'évolution de la partie nord de la Cordillère.

Le dynamisme soutenu du programme de la Sous-division de la géochronologie est rendu possible grâce au travail assidu du personnel de soutien. La préparation des fractions minéralogiques pures à partir de carottes d'échantillons est assurée par Gerry Gagnon et Ron Christie et la collecte des données $^{40}Ar/^{39}Ar$, par Fred Quigg. Diane Bellerive et Jack MacRae sont responsables de la délicate

perform the delicate procedures to extract nanogram levels of Pb and U from carefully selected mineral separates. Klaus Santowski meticulously measures isotopic ratios on a solid-source mass spectrometer. All are warmly thanked for their reliability and commitment.

opération d'extraction de nanogrammes de plomb et d'uranium à partir de fractions minéralogiques qu'ils sélectionnent avec soin. Klaus Santowski mesure méticuleusement les rapports isotopiques sur un spectromètre de masse à source solide. Qu'ils soient tous chaleureusement remerciés de leur dévouement et de leur grande disponibilité.

Réginald J. Thériault

Monazite U-Pb and Th-Pb geochronology by high-resolution secondary ion mass spectrometry

R.A. Stern[1] and N. Sanborn[2]

Stern, R.A. and Sanborn, N., 1998: Monazite U-Pb and Th-Pb geochronology by high-resolution secondary ion mass spectrometry; in *Radiogenic Age and Isotopic Studies: Report 11; Geological Survey of Canada, Current Research 1998-F, p. 1-18.*

Abstract: Analytical techniques have been developed for the determination of monazite U-Pb and Th-Pb isotopic ages using the SHRIMP II ion microprobe. Nine isotopes of Pb, U, Th, and Ce are sequentially analyzed at a mass resolution of 5700. An unidentified isobar at ~203.960 amu complicates the determination of ^{204}Pb in monazites with moderate to high Th contents. The $^{207}Pb^*/^{206}Pb^*$ ratios of individual spots can be determined to ±0.3-0.5% (1se), whereas the uncertainty in the mean of 10 or more spots is typically ±0.1-0.4% (2se). Instrumental bias in the measured Pb/U and Pb/Th values is corrected for using linear relationships between $^{206}Pb^+/UO^+$ vs. UO_2^+/UO^+ and $^{208}Pb^+/ThO^+$ vs. UO_2^+/UO^+, empirically derived from natural monazite standards; bias varies with monazite Th content, necessitating the use of low-, medium- and high-thorium standards. Individual spot determinations of the $^{206}Pb/^{238}U$ and $^{208}Pb/^{232}Th$ ratios in unknown monazites of low to moderate Th can generally be determined to ±2% (1se).

Résumé : Des méthodes analytiques de datation de la monazite par U-Pb et Th-Pb ont été mises au point à l'aide de la microsonde ionique SHRIMP II. Neuf isotopes de Pb, U, Th et Ce ont été analysés séquentiellement à une résolution de masse de 5 700. Une isobare non identifiée d'environ 203,960 uma rend difficile la détermination du ^{204}Pb dans les monazites à teneur modérée à élevée de thorium. Les rapports de $^{207}Pb^*/^{206}Pb^*$ déterminés ponctuellement sont estimés à ±0,3 à 0,5 p. 100 (1se), alors que le degré d'incertitude en ce qui concerne la moyenne de 10 points ou plus est généralement de ±0,1 à 0,4 p. 100 (2se). La distorsion, liée aux instruments, des valeurs Pb/U et Pb/Th mesurées a été corrigée afin qu'il soit possible d'utiliser les relations linéaires entre $^{206}Pb^+/UO^+$ contre UO_2^+/UO^+ et entre $^{208}Pb^+/ThO^+$ contre UO_2^+/UO^+, dérivées empiriquement d'étalons de monazite naturelle. L'erreur varie en fonction de la teneur en thorium de la monazite et requiert l'utilisation d'étalons à teneur faible, modérée et élevée de thorium. On peut déterminer ponctuellement des rapports individuels $^{206}Pb/^{238}U$ et $^{238}Pb/^{232}Th$ dans des échantillons de monazite inconnus à teneur faible à modérée de thorium et les évaluer à ±2 p. 100 près (1se).

[1] Geological Survey of Canada, 601 Booth Street, Ottawa, Ontario K1A 0E8
[2] Department of Earth Sciences, Carleton University, Ottawa, Ontario K1S 5B6

INTRODUCTION

Monazite is a light-rare-earth-element phosphate, LREE(PO_4), occurring as a common igneous accessory mineral in granitic rocks, as a metamorphic mineral in amphibolite- to granulite-grade paragneisses and pelitic schists, and as a detrital mineral in sedimentary and metasedimentary rocks (Parrish, 1990). The determination of high-precision U-Pb ages of single monazite grains is a standard analytical procedure now carried out widely in laboratories conducting isotope-dilution thermal ionization mass spectrometry (ID-TIMS), usually as a complement to zircon dating. Monazite is an ideal mineral from which to acquire U-Pb and Th-Pb isotopic ages, generally having thousands of parts-per-million U and Th, and very low initial Pb contents. Nevertheless, compared to zircon, the applications of U-Th-Pb geochronology of monazite are fewer, and the isotope systematics have received less attention. For example, estimates of the U-Pb closure temperatures of monazite in the literature show a considerable range, from 700–750°C to greater than 800°C (Parrish, 1990; Suzuki et al., 1994; Spear and Parrish, 1996; Smith and Giletti, 1997). Furthermore, the stability and dating of monazite in relation to specific metamorphic reactions has been studied in few cases (e.g. Smith and Barreiro, 1990; Kingsbury et al., 1993; Bingen et al., 1996), and, until very recently, the intra-grain complexities that may exist in monazites have been downplayed, despite evidence that age heterogeneities exist in some cases (e.g. Copeland et al., 1988; Parrish, 1990; Harrison et al., 1995).

The development of monazite geochronology by secondary ion mass spectrometry (SIMS) using the Geological Survey of Canada's Sensitive High-Resolution Ion Microprobe (SHRIMP II; Stern, 1996, 1997) was undertaken principally to open up the field of intra-grain and in situ (in thin section or rock chip) contextual studies of monazite, principally in metamorphic rocks. The field of metamorphic petrology would be significantly aided by the capability to estimate the time of growth of monazite in relation to the specific metamorphic minerals used in calculating pressure-temperature conditions. The issue of monazite closure temperatures and Pb diffusion would also be greatly aided by the ability to analyze specific parts of monazite grains from experimental or geological case studies. There also exists a demand for the acquistion of large numbers of detrital monazite grains to complement the zircon data for provenance characterization, an application well suited to the SHRIMP (Stern, 1996).

Only recently has the analysis of monazite been accomplished by high-resolution SIMS. The technique has been applied mainly to studies of metamorphic rocks (e.g. DeWolf et al., 1993; Williams et al., 1996; Vry et al., 1996), including studies in thin section (Zhu et al., 1997a, b). Harrison et al. (1995) applied the method to Th-Pb dating of leucogranites, whereas Sircombe and Compston (1994) have applied it to the U-Pb dating of detrital monazites. Despite the emergence of SIMS monazite chronology, few descriptions of the analytical methods are provided, the most detailed being that of Harrison et al. (1995). Reported here are the results from our laboratory, perhaps the most exhaustive examination of the method to date. We believe the findings will be of interest, practical utility, and concern to all those conducting SIMS analysis of monazite.

ANALYTICAL METHODS

The study employed the Geological Survey of Canada's SHRIMP II ion microprobe, which is described in detail by Stern (1997). A full description of monazite analysis by SHRIMP follows (*see* 'Monazite analysis'). SHRIMP and ID-TIMS analyses were carried out on different grains from the same population of monazites. Ideally, it would have been better to study identical grains by conducting SHRIMP analyses first, extracting the grains from the mount, and analyzing them by ID-TIMS. However, much of the ID-TIMS data existed prior to the study, and we were reluctant to destroy grains analyzed by SHRIMP, finding it necessary to return to the mounts several times over the course of the study in order to clarify problems. Additional studies could now involve extraction of grains from the SHRIMP mounts for ID-TIMS analysis.

The ID-TIMS data for single grains of monazite (≈10–20 μg) were obtained from existing published and unpublished data from our laboratory (*see* Table 1), supplemented by additional U-Pb and Th-Pb analyses conducted for this study. In all cases, analytical methods for monazite U-Pb age determinations followed the methods described in Parrish et al. (1987). The techniques of monazite Th-Pb age determinations and the Th-Pb data used in this study are provided by Davis et al. (1998).

Cathodoluminescence (CL) and back-scattered electron (BSE) imaging of monazite was carried out using a Cambridge Instruments S360 scanning electron microcope operating at 20kV accelerating potential and using an electron beam current of 2–5 nA. The CL detector is off-axis and has an optical bandwidth of 350-850 nm.

MONAZITE CHEMICAL VARIATIONS

Monazite is chemically more variable than zircon, a concern in SIMS analysis as target composition plays an important role in the complexity of the secondary ion spectrum and in calibrating inter-element ratios. In particular, monazite shows large abundance variations in what are referred to here as 'intermediate' elements. Hanson (1980) described three types of elements present in minerals: 1) essential structural constituents (ESCs), whose abundance is fixed by the stoichiometry of the mineral and are normally tens of weight percent; 2) trace elements, whose abundances (usually <1000 ppm) can vary widely without affecting the mineral stability and which are not determined by stoichiometry, nor can they be predicted without a knowledge of the growth environment; and 3) intermediate elements, whose abundances can vary, but only within a restricted range, usually ranging from a few thousand parts-per-million to a few tens of weight per cent, determined by both the growth environment and mineral stoichiometry.

Phosphorus may be considered as an ESC in monazite, and Ce occurs as an ESC only in the uncommon, pure, end member. In many monazites, intermediate elements occupy the LREE site in monazite in nine-fold co-ordination with oxygen (e.g. Yunxiang et al., 1995), including Ce^{3+} (ionic radius = 1.20 Å, Shannon, 1976), La^{3+} (1.22 Å), Pr^{3+} (1.18 Å), Nd^{3+} (1.16 Å), Th^{4+} (1.09 Å), U^{4+} (1.05 Å), Pb^{2+} (1.35 Å), Ca^{2+} (1.18 Å), and Y^{3+} (1.08 Å). Examples of REE distributions in various monazites are reported by Stern (1992). Most monazites contain Si^{4+} (0.26 Å) as an intermediate element replacing P^{5+} (0.17 Å) in tetrahedral co-ordination with oxygen. As many of the cations in monazite are intermediate elements, their abundance is determined by the environment of formation and by stoichiometric reactions, the most important of which is summarized as:

$$4REE^{3+} + P^{5+} = 3Th^{4+} + Si^{4+} + Ca^{2+} + [F^{-}, (OH)^{-}]$$

Apparently, the REE can be substituted by Th accompanied by one or more of Si^{4+}, Ca^{2+}, F^{-}, or $(OH)^{-}$. According to Kucha (1980), $Th/[Si+F_4+(OH_4)]$ is $\cong 1$ (atomic proportions). For the SHRIMP, the presence of F^{-} or OH^{-} in the structure of some monazites is cause for concern, as the formation of metal fluorides or metal hydrides could result in irresolvable mass interferences (*see* below). As we will illustrate below, the Th content of monazite is an important issue during SHRIMP analysis. The natural variation in Th contents in monazites is large (e.g. Overstreet, 1967; Rapp and Watson, 1986), and to simplify this discussion we refer in this paper to the following ranges: very low (<1 wt %), low (1–3%), medium (3–8%), and high (>8%).

Internal compositional zonation of monazite appears to be common, but not particularly well studied (e.g. Mohr, 1984; DeWolf et al., 1993; Zhu et al., 1997a). Back-scattered electron (BSE) images of selected grains of monazite used in this study are shown in Figure 1 and are quite typical of the sample suite. A monazite from leucosome within paragneiss (Fig 1a) has a complex, patchy, central region that gives the appearance of being a recrystallization or replacement texture of what may have been a grain with regular igneous zoning as indicated in the lower left part of the grain. The rounded

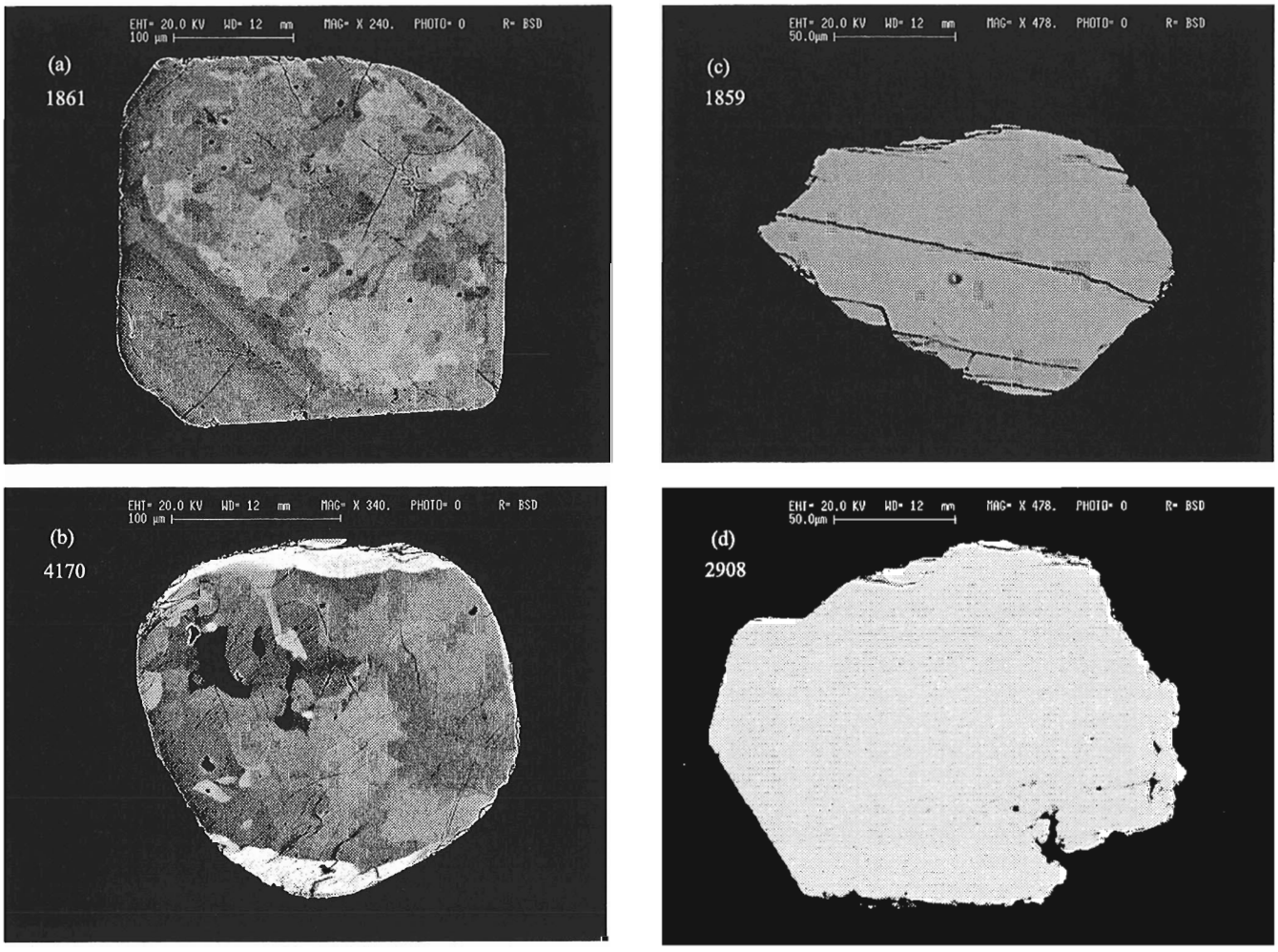

Figure 1. *Backscattered electron (BSE) images of selected monazite grains.* ***a****) Archean igneous monazite sample 1861 with patchy interior replacement texture;* ***b****) Paleoproterozoic metamorphic monazite sample 4170, with characteristic bright (high-thorium) rims;* ***c****) and* ***d****) show Archean and Paleoproterozoic monazites 1859 and 2908, respectively, having homogeneous BSE images and internally uniform U and Th contents.*

monazite from monzogranite in Figure 1b shows patchy, irregular features in the centre, cut off by a discontinuous, bright rim. The SHRIMP analysis indicates that the rim contains several times more Th than the darker patches, but only a fraction of the U. In this instance, brighter BSE zones correlate with higher Th concentrations. These complex features contrast with the uniform BSE images observed in a diatexite (Fig. 1c) and deformed muscovite granite (Fig. 1d). The BSE images of Figure 1c and 1d were taken under identical analytical conditions, and it is evident that the image for Figure 1d is significantly brighter. The SHRIMP analysis indicates that this monazite contains ~2% Th and 3000 ppm U, whereas, the monazite in Figure 1c contains much higher Th (~7%) but lower U (800 ppm). It appears in this case that factors in addition to Th content, perhaps U and REE levels, are required to explain the relative BSE brightness, a reflection of average atomic weight. More work is needed to document the elemental variations responsible for the BSE contrasts. In general, however, these monazites and the others studied showed little evidence in the BSE images of the regular zoning commonly observed in zircons.

MONAZITE SECONDARY ION MASS SPECTRUM

The critical issue in monazite analysis is identifying if there are any isotopes present in the secondary ion mass spectrum that could interfere with the isotopes of interest. The chemical complexity of monazite would lead one to suspect a high potential for isobars (different ionic species having the same nominal mass); however, an isobar will be a problem only if it cannot be resolved from the peak of interest. The best way to check for isobars is to examine the mass spectra of natural monazites and compare them with theoretical mass spectra derived by combinations of the constituent elements. Monazite mass spectra were obtained upon several of the natural monazites in our suite at a mass resolution (R) of 5700 (1% peak height definition), centred on the masses of interest (203, 204, 206, 207, 208, 248, 254, and 270 amu) and ±0.25 amu on either side. Representative mass scans are illustrated in Figure 2.

Similar to the mass spectrum of zircon (Stern, 1997), the Pb, Th, and U isotopes of interest occur at higher mass than all the other isobars present. The determination of the identity of the isobars was aided by the use of specialized software used to calculate the mass of all secondary ions (monoatomic and polyatomic species) that could exist in a given mass range under specified conditions. The following elements were considered in these calculations: O, P, Si, Al, La, Ce, Pr, Nd, Sm, Eu, Gd, Dy, Er, Yb, Y, Th, Pb, U, Ca, Ba, Fe, Mg, F, and H. We allowed a maximum of four different elements in molecular ions ('clusters'), a maximum of two of any single element, but only one hydrogen ion.

The mass scans shown in Figure 2 indicate that most of the isotopes of interest are well resolved from the numerous other isobars present. Although we attempted to identify the isobars present based on mass and intensity, confirmation of their identity would require study with synthetic or very pure monazites of appropriate composition. The chemical complexity of natural monazites is such that there are theoretically several possible isotopes that could be generating the observed isobars. At mass resolution (R) = 5700, the isobars that are clearly resolvable appear to be mainly molecular ions involving combinations of Nd, Pr, Gd, Er, Yb, Ca, Si, P, Pb, and O. For example, ^{206}Pb and ^{207}Pb (Fig. 2d,e) are easily resolved from large $NdPO_2^+$ peaks and smaller YbP^+.

While the mass scans provide evidence of the types of isobars present, they seldom are helpful in identifying isobars that may be present but masked by the much larger isotopes of interest. $^{203}CePO_2^+$ is an exception, as it can be seen by the mass scan (Fig. 2a) to be only partially resolved from $GdPO^+$ at 202.891 amu (Fig. 2a). This situation is not a serious problem, as $^{203}CePO_2^+$ is not used for age calculations (*see* below). The only other isobars that we believe, based on *theoretical* calculations, could potentially interfere with monazite analysis at R = 5700 are metal hydroxides or metal fluorides. If they were present, the most serious problem would occur in resolving $^{206}PbH^+$ from $^{207}Pb^+$, and $^{207}PbH^+$ from $^{208}Pb^+$, as there are no other fluorides or hydrides that are sufficiently abundant to cause problems. Subsequent analytical work demonstrates that metal hydrides are not significant, if present at all.

For ^{204}Pb, however, despite the above calculations, we have evidence from actual mass scans and subsequent analytical work (detailed below) of an isobar at ~203.960 ± 0.005 amu. In our initial scans of the 204 mass region, we observed a small peak very close to where we expected $^{203.973}Pb$ (e.g. Fig. 2b). Further scans of this mass region in high-thorium monazite and comparison with the exact position of ^{204}Pb determined from Pb-feldspar revealed a mass difference of ~.010–.015 amu (*see* Fig. 2b). Unfortunately, the identity of the isobar remains unknown, as our calculations of potential isobars have revealed no isotope of any fractional abundance with this particular mass. To resolve this 204 isobar from $^{203.973}Pb$ would require R~15 000, which is achievable but certainly not desirable for routine operation as there would be no flat top to the peaks. The intensity of the 204 isobar is directly correlated with Th content (*see* below), much lower or absent in low-thorium monazite, as illustrated in the mass scan of Figure 2c. The presence of this isobar is a serious problem for common Pb correction of monazites.

MONAZITE ANALYSIS

The following is a description of the analytical techniques and rationale employed in SHRIMP monazite geochronology at the GSC laboratory. The methods discussed refer to analysis of polished grain mounts rather than thin sections, as the former are essential for technique development. The methodology was developed over the course of several months, during which grains of monazite from nine different rocks were examined with the SHRIMP on three separate grain mounts (IP36, IP50, and IP52).

Table 1 is a summary of the ID-TIMS isotopic data of the nine test samples, ranging in age from 1.02 Ga to 2.67 Ga, and including metamorphic and igneous monazites. These monazites were initially selected based on their high degree of concordance, absolute age, and Th content. Included in Table 1 is our best estimate of the 'correct' age of the sample. Three samples in particular show in their ID-TIMS data evidence for isotopic heterogeneity. The ID-TIMS $^{207}Pb/^{206}Pb$ ages for sample 2234 range from 1012–1025 Ma, sample 1861 exhibits one population of ages at ~2666 Ma and one fraction at 2675 Ma, and sample 4170 has one fraction that is 7 Ma older than the mean age of 1836 Ma (Table 1). For samples 2234 and 1861 the 'correct' age is unclear and therefore these two samples are excluded from subsequent discussions on SHRIMP accuracy.

We had three objectives at the outset of this study. Firstly, we wanted to test various methods in calibrating the Pb/U and Pb/Th ratios, and also the U and Th abundances. Although previous workers have had success using various methods, our investigations eventually led us to adopt analytical protocols that are distinct from other laboratories. Secondly, and obviously related to the first objective, we needed to identify

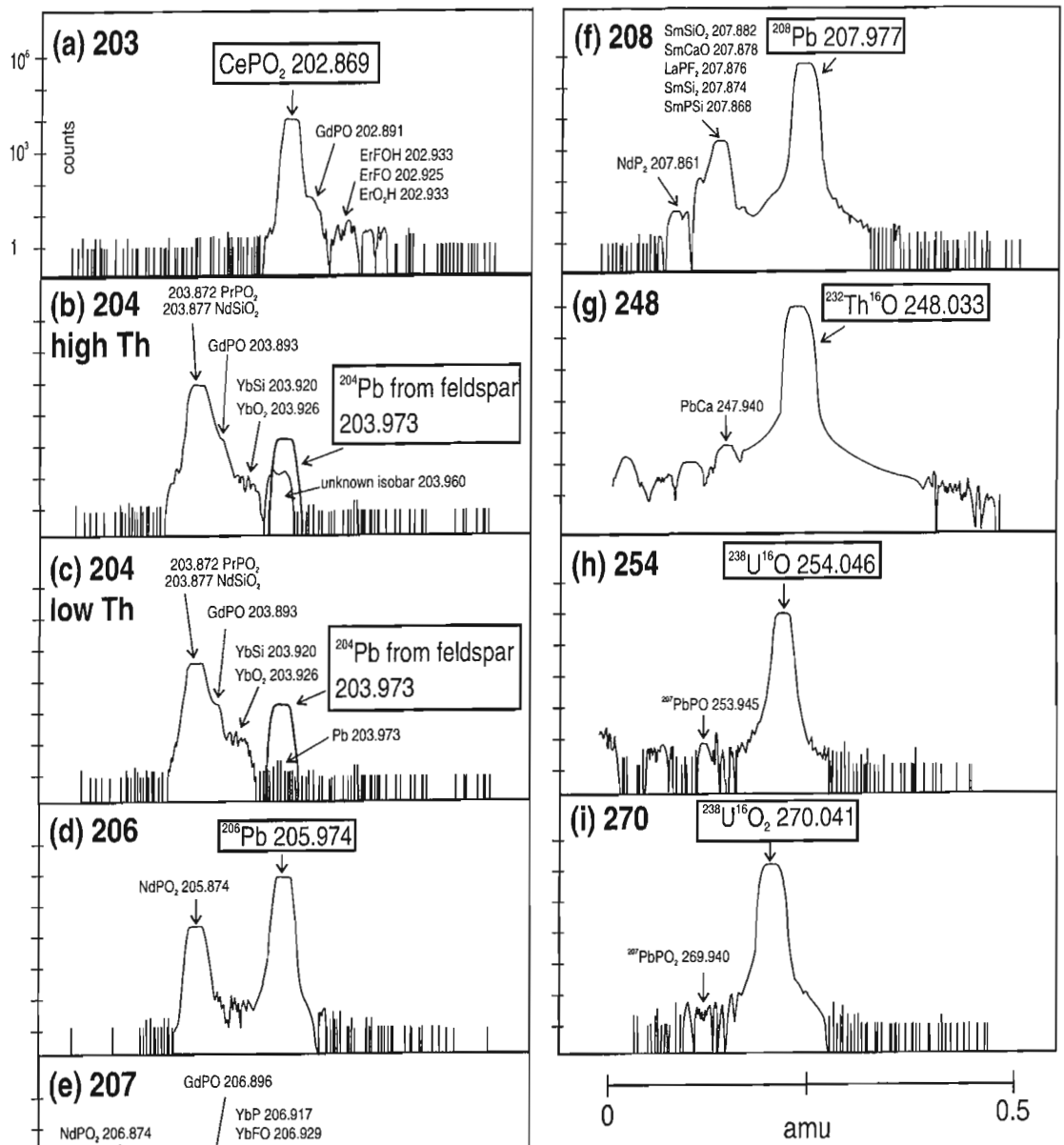

Figure 2. *Mass scans of Paleoproterozoic high-thorium monazite 4170 (**a, b, d-i**) and low-thorium monazite 2908 (**c**), centred on the masses of interest and ±0.25 amu, with increasing mass to the right. Operating conditions were R=5700 and retardation lens deactivated, except for 204 mass region (**b, c**).*

a monazite standard(s). And thirdly, we needed to establish that the analytical techniques gave us the expected results, both in terms of the Pb-Pb, Pb-U, and Pb-Th ages.

Conventions used in this paper are as follows. A '+' sign indicates a raw count rate or isotopic ratio (e.g. $^{204}Pb^{+}$), the use of '*' indicates that the Pb isotope has been corrected for common Pb (e.g. $^{206}Pb^{*}$), and where no signs are present (e.g. $^{206}Pb/^{238}U$), it is assumed that all corrections have been applied. For brevity, $^{270}UO_2^{+}$, $^{254}UO^{+}$, $^{248}ThO^{+}$, $^{238}U^{+}$, and $^{232}Th^{+}$ are frequently abbreviated without the mass numbers. The designation for 1 standard deviation is '1s', and 2 standard errors or 95% confidence interval are indicated by '2se'. Decay constants used in age calculations are from Steiger and Jäger (1977).

Table 1. U-Pb and Th-Pb isotopic data on monazite determined by ID-TIMS. Th-Pb data from Davis et al. (1998), and other data as referenced.

Lab number (original sample number) & rock description	$^{207}Pb/^{206}Pb$ age (Ma, ±2se)	$^{232}Th/^{208}Pb$ age (Ma, ±2se)	Pb-U % discord.	U (ppm)	Th (wt. %)	best age estimate (Ma, ±2se)	best $^{207}Pb/^{206}Pb$ estimate
4170 (HVA-95-D094B) **High-Th Standard**	1837 ±1.0		0	1202	10.06		
	1838 ±1.0		0	1273	10.09		
	1837 ±1.0		0.1	1050	9.30		
	1834 ±1.1	1828 ±9	0.3	1169	9.64		
	1833 ±1.1	1834 ±9	0.0	918	8.15		
monzogranite, S. Baffin Is. Island;	1836 ±1.0	1833 ±9	-0.1	796	7.44		
Wodicka and Scott (1997)	(1843 ±1.0)	(1848 ±9)	(-0.4)	(7025)	(18.12)	**1836 ±1**	**0.11224**
3345 (BIB-92-S074) **Medium-Th Standard**	1821 ±1.0		-0.01	3428	6.81		
	1820 ±1.0		0.01	2583	7.37		
	1823 ±1.0		-0.04	2976	7.47		
sillimanite, migmatite paragneiss, Baffin	1821 ±1.0		0.02	4009	8.06		
Island;	1820 ±1.0	1822 ±9	0.1	3141	6.68		
Bethune and Scammell (1997)						**1821 ±1**	**0.11132**
2908 (PCA-C509-9) **Low-Th Standard**	1794 ±1.1		0	2041	1.52		
	1795 ±1.0		-0.09	2349	2.05		
	1796 ±1.0		-0.3	3708	2.80		
deformed muscovite granite, E. Athabasca	1794 ±1.6		0.1	1731	1.92		
mylonite zone; Parrish and Hanmer	1796 ±1.0	1787 ±9	1.4	1765	1.58		
(unpublished data)						**1795 ±1**	**0.10973**
1861 (PBA-85-75)	2666 ±0.9		0.06	1999	4.78		
leucosome in paragneiss, Ashuanipi	2665 ±0.9		0.07	2061	4.91		
Complex, Superior Province; Percival et al,	2666 ±0.9		0.1	1872	4.38		
(1992)	2675 ±0.9	2667 ±13	0.3	2698	4.18	2666?	
1859 (PBA-85-68)	2664 ±0.9		-0.77	783	7.70		
diatexite, Ashuanipi Complex, Superior	2665 ±1.1		-0.51	697	6.35		
Province; Percival et al. (1992)	2659 ±0.9	2676 ±13	-1.0	775	6.86	2664 ±2	0.18110
4323 (87BK-369Y)	1935 ±1.0		0.16	2844	4.35		
deformed megacrystic syenogranite,	1937 ±1.1		0.04	2340	3.39		
Taltson magmatic zone	1934 ±1.0		0.03	2538	2.94		
	1935 ±1.0		-0.11	5091	5.12		
Bostock and van Breemen	1936 ±1.0		0.17	7164	8.59		
(unpublished data, 1996)	1933 ±1.0		0.14	5202	5.57		
	1936 ±1.0	1938 ±9	0	6998	7.53	1935±1	0.11858
1409 (WBT-329)	1767 ±1.2		-1.71	1605	11.09		
pegmatite, Thompson belt; Roddick and	1771 ±1.1		-0.06	2087	11.40		
Bleeker (unpublished data, 1990)	1766 ±1.0		-0.22	2583	13.97		
	1768 ±1.0		0	2088	11.28		
	1770 ±1.0	1777 ±9	-0.3	2259	12.33	1768 ±2	0.10812
2775 (CQA-2688)	1166 ±2.4		0.23	411	6.08		
granulite facies orthogneiss, Grenville Prov.	1167 ±2.8		0.25	141	5.25		
Corriveau et al (1996)	1164 ±1.5	1169 ±6	-0.1	365	4.51	1166 ±2	0.07876
2234 (31-87)	1025 ±4.5		-0.1	258	0.65		
fenite, Grenville Province	1020 ±3.9		-0.53	252	0.83		
	1025 ±5.6		-0.16	236	0.61		
Hogarth and van Breemen (1996)	1014 ±4.2	1017 ±5	-0.4	299	0.81		
	1012 ±1.9		0	188	0.55	1025 ?	

Grain mount preparation

The selected monazites were arranged as tightly clustered groups upon double-sided tape within a 25 mm diameter x 7 mm deep Teflon mould. Araldite resin (Struers Epofix) was then poured into the mould and allowed to harden overnight. The mounts were polished with diamond polishing compound (9, 6, and 1 micron) to reveal the grain centers. The mounts were then washed with a soap solution, rinsed in deionized water, and photographed in reflected and transmitted plane light. The mounts were then washed again with soap and deionized water, and dried under a heat lamp at 40°C.

The cleaned mounts were coated evaporatively with 5.8-6.0 nm of Au (99.9999%). Although not used in this study, our experience with thin sections and rock chips indicates that they generally require 8–12 nm of Au due to their higher surface relief. Following coating, BSE images were obtained using a scanning electron microscope (SEM). Following SEM imaging, the mounts were readied for the SHRIMP. The samples were placed within a steel holder and surface conductivity measured, generally 10–20 ohms. The mounts were then placed within the SHRIMP sample lock, and held at high vacuum for a minimum of 12 hours.

SHRIMP setup

The SHRIMP analytical setup for monazite was identical to that of zircon (Stern, 1997). The primary ion species used for age determinations was O_2^- focused to a spot measuring 17 x 21 μm using a 120 μm Kohler aperture. Primary ion currents were typically 1–2 nA. Total secondary ion accelerating voltage is nominally 10 kV, with the first extraction electrode at 750 V with respect to the sample surface. The source slit width is set at 100 μm, and collector at 90 μm, giving an operating mass resolution (1% peak height) of 5500–5700, with flat top peaks ~0.012–0.013 amu wide. Acceptance to the electrostatic analyzer (ESA) is set at 7.9 mm, and the width of the post-ESA energy window is 2.5 mm, equivalent to an energy bandwidth of 20 eV. Ion arrival is detected using a single electron multiplier coupled with an ion counting system. Deadtime for the system has been measured using Pb standards at 25 ns. Overall instrumental Pb sensitivity for monazite is estimated to be 30–35 cps/ppm/nA using primary O_2^-, based on analysis of monazite 1859. These intrumental conditions are maintained at all times during analysis, i.e. no energy offsets were employed (c.f. Harrison et al., 1995).

For unknown reasons, monazite produces higher background count rates than zircon, approximately three times greater (*see* below). An energy-filtering device called the retardation lens is provided within the collector housing of the SHRIMP for rejection of ions that have lost energy due to scattering, and this device was highly effective at reducing background. The disadvantage of the retardation lens is that its use resulted in the loss of approximately 15% of the ion beam reaching the electron multiplier. It was felt that the use of the retardation lens was not warranted at this time.

Pre-analysis rastering

For reasons explained below, it is vital in the analysis of monazite to reduce the sources of common Pb to those contained only within the monazite. As shown by Stern (1997), the sample preparation procedure and conductive Au coating contribute measurable common Pb to the surface of the mount. The surface Pb contamination can be reduced or eliminated if the primary beam is used to clean Au and any polishing residues from the area immediately surrounding the analysis spot. Testing zircon with undetectable common Pb has shown that total elimination of surface common Pb is achieved in 2–3 minutes of rastering with the O^- primary ion prior to analysis. The O^- primary species is significantly stronger and therefore more effective at surface cleaning than O_2^-, the primary ion used during analysis. Accordingly, we believe that there is no detectable common Pb being contributed by contaminants on the surface of the mount.

Analyzed isotopes

Following a period of investigation, we settled on the sequential analysis of the following nine mass stations: $^{203}CePO_2^+$, $^{204}Pb^+$, 204.1 (background), $^{206}Pb^+$, $^{207}Pb^+$, $^{208}Pb^+$, $^{248}ThO^+$, $^{254}UO^+$, and $^{270}UO_2^+$. Table 2 summarizes the masses and typical count times for each, separated by delays for magnet settling. Typically, 5–8 sequential measurements of each isotope are carried out, with each sequence constituting a 'scan', and the group of scans termed a 'run'. A typical run lasts 10–15 minutes. The objective of the analysis is to estimate the composition of the monazite at the midpoint in time of the run period. The reader is referred to Stern (1997) for a description of the method of deriving count rates and errors for each isotope at the midpoint time.

$^{203}CePO_2^+$, UO^+, ThO^+: determining U and Th abundances and Th/U

For the determination of minor- or trace-element abundances in monazite, there is a need to monitor an isotope of a major element (an ESC preferably) that can be used to cancel out variations in total secondary ion emission, principally due to

Table 2. Mass stations and count times for monazite analysis.

Mass station	Isotope	Mass (amu)	Typical count time (s)	Delay for magnetic settling (s)
1	$^{203}CePO_2$	202.869	2	2
2	^{204}Pb	203.973	20	1
3	background	204.100	20	1
4	^{206}Pb	205.974	10	1
5	^{207}Pb	206.976	25	1
6	^{208}Pb	207.977	3	1
7	^{248}ThO	248.033	3	1
8	^{254}UO	254.046	5	1
9	$^{270}UO_2$	270.041	5	1

varying primary beam currents. Although Ce is commonly an intermediate element in monazite, its abundance range is relatively limited in most natural monazites, typically 25% (±5%) by weight of the element. Phosphorus, as an ESC in monazite, shows much less variation, about ±5%. Accordingly, the intensity of the $^{203}CePO_2^+$ isotope should not vary widely for the majority of monazites, and thus is appropriate as a 'matrix' isotope close to mass 204. Harrison et al. (1995) alternatively selected the $^{204}PrPO_2^+$ isotope for this purpose.

The determination of the U content in monazite is derived from the emiprical relationship shown in Figure 3, and does not require the use of a separate monazite U standard. This plot shows $^{203}CePO_2^+/UO^+$ measured in several of the samples from three separate mounts versus the U content (ppm) measured by ID-TIMS. Both the SHRIMP and TIMS data show a certain degree of variability (shown by 1s bars), which in the case of TIMS represents natural variations in U content. Despite the scatter in both data sets, a systematic linear relationship between U content and $^{203}CePO_2^+/UO^+$ can be derived from Figure 3:

1) $U_{unk} = 460/(^{203}CePO_2^+/UO^+)$

where U_{unk} is the U content of the unknown in ppm (weight), and $^{203}CePO_2^+/UO^+$ is the value measured for the unknown. The uncertainty in the calculated U content is estimated at ±20%, dominated by the uncertainty in the empirical calibration. We caution that the calibration is probably valid only for 'average' monazites, and probably within the range of U contents and $^{203}CePO_2^+/UO^+$ ratios in Figure 3. This relationship could be improved by extraction of the exact grains used in the SHRIMP analysis and subsequent measurement of U concentrations using ID-TIMS.

Once the U content has been determined, the Th content can be also be determined from the measured ThO^+/UO^+ ratios and a knowledge of the instrumental fractionation of ThO^+ and UO^+. The method used in determining the ThO^+/UO^+ fractionation was identical to that of zircon (Stern, 1997), and is summarized here.

For the test monazites, assumed to have remained closed to exchange of Pb, U, and Th since crystallization, there is an expected relationship between the measured $^{208}Pb/^{206}Pb$ ratio and ThO^+/UO^+, i.e.:

2) $^{208}Pb^*/^{206}Pb^* = f_{ThO\text{-}UO}$
$(ThO^+/UO^+)(e^{t\lambda 232}-1)/(e^{t\lambda 238}-1)$

where t is the current age of the monazite in millions of years, $f_{ThO\text{-}UO}$ is the relative sensitivity factor of ThO^+ relative to UO^+, and λ_{232} and λ_{238} are the relevant decay constants. For a monazite of known age and analyzed by SHRIMP, equation 2) produces a straight line on a graph of ThO^+/UO^+ vs. $^{208}Pb^*/^{206}Pb^*$ with

3) (measured slope) $= f_{ThO\text{-}UO}\ (e^{t\lambda 232}-1)/(e^{t\lambda 238}-1)$

4) (measured slope) $= f_{ThO\text{-}UO}$ (expected slope)

5) $f_{ThO\text{-}UO}$ = (measured slope)/(expected slope)

The expected slope can be calculated from the age of the sample. An example of these relationships is shown in Figure 4 for monazite 3345. Here, the expected slope is 0.2888, based on an age of 1821 Ma. The measured slope is 0.2470, and from equation 5), $f_{ThO\text{-}UO} = 0.855$. This experiment was repeated for the nine monazite samples on three separate mounts, and the results are summarized in Table 3. The $f_{ThO\text{-}UO}$ values are seemingly constant, having a mean of 0.857 and standard deviation of 0.004. This result shows that for monazite, ThO^+ ionization is enhanced over UO^+, which is opposite to the relationship for zircon. Williams et al. (1996) measured a $f_{ThO\text{-}UO}$ value of 0.835 for the ANU SHRIMP II, and Harrison et al. (1995) determined a value of 0.888 for the Cameca IMS 1270, indicating that the relative sensitivity factor is a fundamental property of SIMS analysis of monazite and not influenced greatly by the specific instrumentation.

Consequently,

6) $^{232}Th/^{238}U = 0.857 \times (ThO^+/UO^+)$

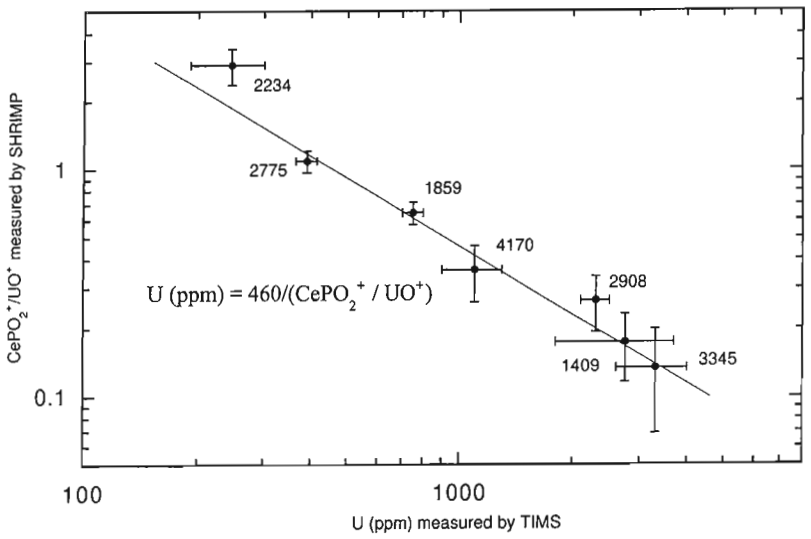

Figure 3.

Uranium abundances measured by ID-TIMS vs. $^{203}CePO_2^+/UO^+$ ratios measured by SHRIMP for the study samples. One standard deviation is indicated to give some idea of the natural variability within each sample. The equation indicated is derived from the data and used to determine the U contents in a SHRIMP analysis.

and, converting to weight fractions,

7) $Th/U = 0.968 \times {}^{232}Th/{}^{238}U$

The Th content can then be calculated from the known U content. The uncertainty associated with calculation of Th/U ratios in monazite is <0.5%, and is added in quadrature to the counting errors. Typically, Th/U can be determined to <±1%. A blanket uncertainty of ±20% is applied to the Th abundances, a value derived from the uncertainty in determining the U content (*see* above).

The Th and U contents can also be calculated relatively accurately from the isotope count rates normalized to the total primary beam current, i.e.:

8) $U(ppm) = [UO^+]/6.67$

9) $Th\ (wt\ \%) = [ThO^+]/86460$

where [ ] is the isotope count rate normalized to the total primary beam current (cps/nA). These abundance determinations are useful for the analyst during data collection, but the former methods are preferred.

Equations 8) and 9) and, indeed 1), depend on the secondary ion yields specific to the individual monazite sample, sample mount, and the analytical conditions used in this study. These variables appear to be essentially constant for the purposes of U and Th abundance determinations at the ±20% uncertainty level. Higher precision in the abundance determinations could be achieved if monazite standards more homogeneous in U and Th content were available for calibration.

Background measurements

Background count rate is monitored at 204.1 amu, closest to the isotope (^{204}Pb) for which a background correction will be most important. As explained previously, for reasons to do with instrument performance, the collector retardation lens was not employed. Background count rates for monazite average 0.3 ± 0.1 cps per nA primary O_2^- beam, compared to zircon which averages 0.1 ± 0.05 cps/nA.

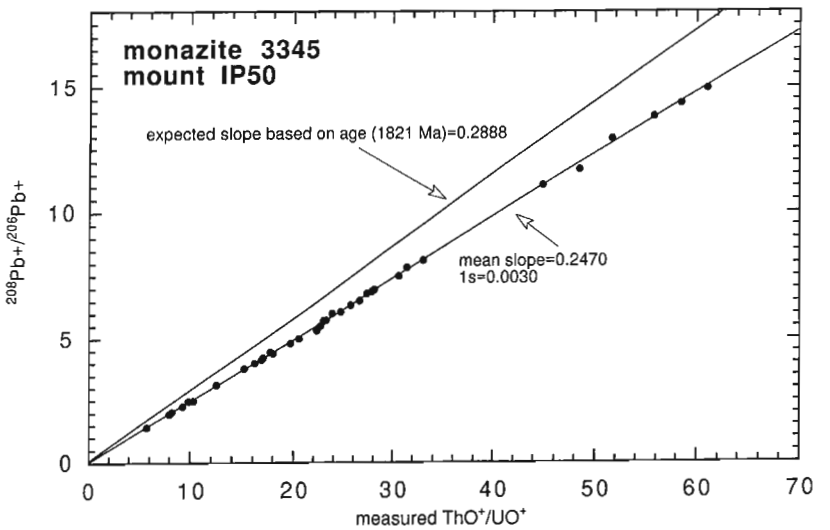

Figure 4.

Plot of ThO^+/UO^+ vs. $^{208}Pb^+/^{206}Pb^+$ for 35 separate spots on several grains from monazite 3345. The slope of the correlation line is compared with the expected slope based on the age to derive a relative sensitivity factor, $f_{ThO\text{-}UO}$, required to correct the Th/U ratios for inter-element bias.

Table 3. Summary of data used to assess the relative instrumental fractionation of ThO^+ and UO^+, with mean $f_{(ThO+/UO+)}$ indicated.

Sample	mount #	mean UO_2^+/UO^+	age (Ma)	expected slope	measured slope (mean)	1s	$f_{(ThO/UO)}$
1409	52	1.51	1768	0.2897	0.2489	0.0027	0.8591
1409	36	1.51	1768	0.2897	0.2491	0.0026	0.8597
2908	50	1.52	1795	0.2892	0.2448	0.0028	0.8464
3345	50	1.58	1821	0.2888	0.2470	0.0030	0.8551
4170	36	1.58	1836	0.2886	0.2478	0.0026	0.8586
4170	50	1.55	1836	0.2886	0.2477	0.0169	0.8582
4323	50	1.37	1935	0.2870	0.2474	0.0024	0.8620
1859	50	1.61	2663	0.2753	0.2355	0.0013	0.8554
1559	50	1.63	2668	0.2752	0.2359	0.0038	0.8570
						mean=	**0.857**
						1s=	0.004

Pb ISOTOPES

The mass scans and peak interference calculations indicate that the *radiogenic* Pb isotopes appear to be free of significant isobaric interferences, except for the potential of Pb hydrides. In order to verify that the Pb isotopes can be analyzed accurately we have examined in detail the Pb-isotopic ratios from our test samples. Between 7 and 35 spot analyses were obtained on several grains from each monazite sample. Table 4 presents a summary of the data, reported as the mean values. Typical uncertainty (1se) per spot for the raw $^{207}Pb^{+}/^{206}Pb^{+}$ values is ±0.3–0.5%.

In Figure 5a, the weighted mean raw $^{207}Pb^{+}/^{206}Pb^{+}$ data are plotted as the percentage difference relative to the 'correct' value (i.e. ID-TIMS, Table 1) vs. mean $^{204}Pb^{+}/^{206}Pb^{+}$ ratio. The mean $^{207}Pb^{+}/^{206}Pb^{+}$ data generally have 2se uncertainties of ±0.2%. Note that in comparing the SHRIMP Pb-isotope data with the ID-TIMS data we have omitted the heterogeneous samples 2234 and 1861, as discussed previously. The raw $^{207}Pb^{+}/^{206}Pb^{+}$ values deviate from the accepted values by +0.03% to +1.10%, increasing with $^{204}Pb^{+}/^{206}Pb^{+}$. That the raw $^{207}Pb^{+}/^{206}Pb^{+}$ values are greater than the accepted values is consistent with a small contribution from intrinsic common Pb in the monazite. As explained previously, we feel certain that any common Pb in the analysis must be due entirely to that within the monazite. For samples with mean $^{204}Pb^{+}/^{206}Pb^{+}$ values <0.00015, the percentage difference of raw $^{207}Pb^{+}/^{206}Pb^{+}$ values relative to true values is very small, ranging from +0.03% to +0.29%, almost within the 2se uncertainty of the means (Table 4). Those samples with $^{204}Pb^{+}/^{206}Pb^{+}$ <0.00005 deviate by <+0.11% from the accepted values, well within the 2se uncertainties. Samples with mean $^{204}Pb^{+}/^{206}Pb^{+}$ values >0.00015 deviate more significantly, +0.82% to +1.10%, reflecting a higher proportion of common Pb.

Figure 5b shows the same data set corrected for presence of common Pb (compositions from Cumming and Richards, 1975) using the measured mass-204 count rate (204 method, *see* Stern, 1997). All the samples now have $^{207}Pb^{*}/^{206}Pb^{*}$ values that are systematically lower than the accepted values (*see* Table 4). Generally, the amount of overcorrection correlates with the $^{204}Pb^{+}/^{206}Pb^{+}$, i.e., being least (-0.2%) for samples with $^{204}Pb^{+}/^{206}Pb^{+}$ values of $2–3x10^{-5}$, and quite large (-8.7%) for the sample with highest mean $^{204}Pb^{+}/^{206}Pb^{+}$. In all cases, correction for common Pb using the 204 method would bias the $^{207}Pb/^{206}Pb$ ages low, and the results actually

Table 4. SHRIMP weighted-mean Pb isotope ratios and other related parameters for test samples.

sample	1409	3345	4323	1859	4170	2908	2775
mount #	52	50	50	50	50	50	50
# spots	9	35	8	35	15	12	7
$^{207}Pb^{*}/^{206}Pb^{*}$ accepted (Table 1)	0.10812	0.11132	0.11858	0.18110	0.11224	0.10973	0.07876
$^{207}Pb^{+}/^{206}Pb^{+}$ (raw data); ±2se	0.10843 ±0.00022	0.11147 ±0.00010	0.11861 ±0.00018	0.18160 ±0.00022	0.11316 ±0.00030	0.10985 ±0.00021	0.07963 ±0.00055
% difference from accepted	+0.29	+0.13	+0.03	+0.28	+0.82	+0.11	+1.10
$^{207}Pb^{*}/^{206}Pb^{*}$ (204-corrected); ±2se	0.10674 ±0.00025	0.11090 ±0.00011	0.11836 ±0.00019	0.18036 ±0.00024	0.11085 ±0.00035	0.10950 ±0.00022	0.07194 ±0.00160
% difference from accepted	-1.28	-0.38	-0.19	-0.41	-1.24	-0.21	-8.66
$^{207}Pb^{*i}/^{206}Pb^{*i}$ (isobar- & 204-corrected); ±2se	0.10801 ±0.00036	0.11125 ±0.00012	0.11854 ±0.00021	0.18146 ±0.00024	0.11272 ±0.00039	0.10966 ±0.00026	0.07884 ±0.00101
% difference from accepted	+0.33	+0.11	+0.18	+0.13	+0.35	+0.24	+0.10
$^{204}Pb^{+}/^{206}Pb^{+}$	1.30×10^{-4}	4.70×10^{-5}	2.20×10^{-5}	9.90×10^{-5}	1.80×10^{-4}	2.60×10^{-5}	5.60×10^{-4}
$^{203}CePO_2^{+}/^{254}UO^{+}$	0.265	0.134	0.031	0.645	0.361	0.174	1.09
ThO^{+}/UO^{+}	63.6	22.5	11.4	109.2	99.6	9.9	172.8
Th/U (wt.)	52.8	18.7	9.4	90.6	82.6	8.2	143.4
U (ppm)	1736	3433	14839	713	1274	2644	422
Th (wt.%)	12.0	7.3	5.4	7.0	9.1	2.0	5.3
[204] cps/nA	1.5	1.1	1.9	0.7	1.6	0.4	1.0
[204 isobar]	1.3	0.8	1.6	0.4	1.0	0.1	0.9
$[^{204}Pb]$ cps/nA	0.2	0.3	0.3	0.3	0.6	0.3	0.1

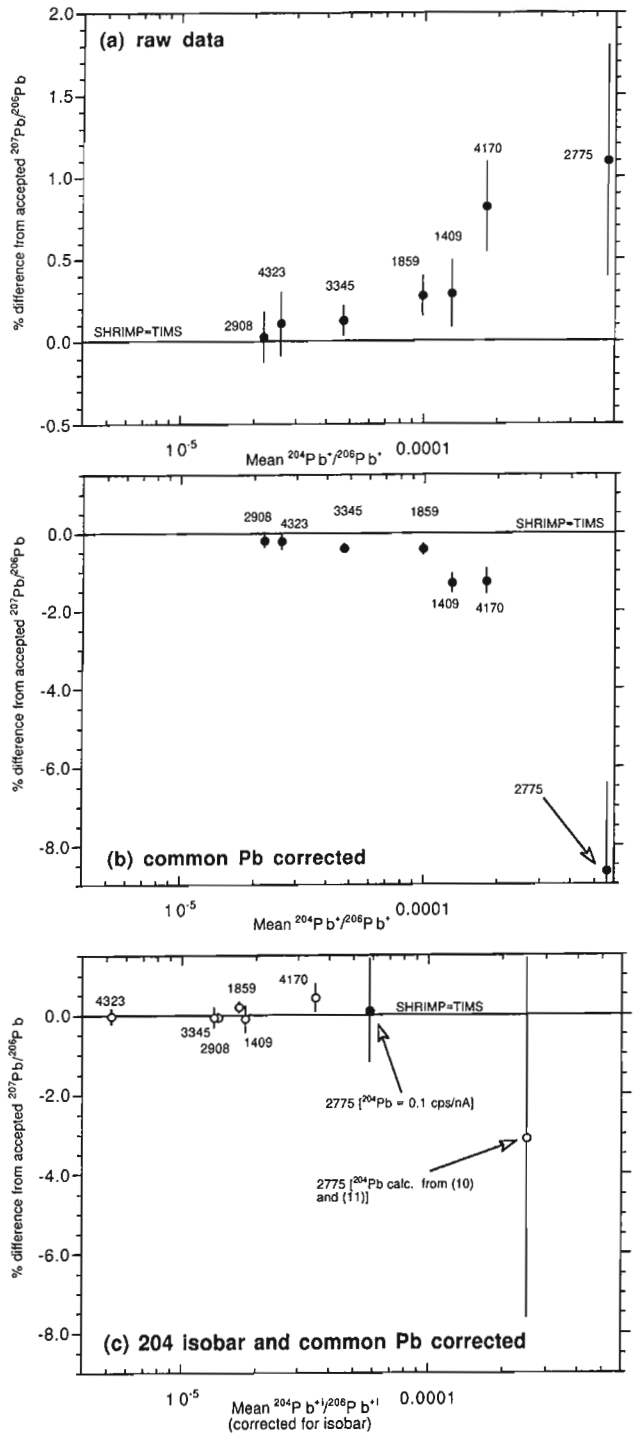

*Figure 5. Per cent difference between SHRIMP weighted mean $^{207}Pb/^{206}Pb$ ratios and the accepted values (ID-TIMS, Table 1) vs. $^{204}Pb/^{206}Pb$: **a**) raw data; **b**) corrected for common Pb using measured $^{204+}Pb/^{206+}Pb$ ratios (204 method, see Stern, 1997) and a Cumming and Richards (1975) model for the common Pb composition; **c**) corrected for the presence of a 204 isobar (see text) and then common Pb corrected. The ±2se uncertainties are shown where larger than symbol.*

deviate further from the accepted value than the uncorrected values. If ^{204}Pb is being measured accurately there is no reason to expect the inverse correlation displayed in Figure 5b.

The inverse correlation between $^{204}Pb^{+}/^{206}Pb^{+}$ and $^{207}Pb^{*}/^{206}Pb^{*}$ observed in Figure 5b is also evident when considering individual data sets, an example of which is shown in Figure 6. Relative to the accepted value, the raw data are uniformly high due to the presence of common Pb in the monazite (Fig. 6a). The 204-corrected data (Fig. 6b) show an inverse correlation. The higher the measured $^{204}Pb^{+}/^{206}Pb^{+}$, the more the overcorrection for common Pb. The data set shown in Figure 6 is typical of what would normally be encountered by SHRIMP users; it is shown here to emphasize that such a pattern indicates a problem with the accuracy of the ^{204}Pb measurements.

204 isobar and related corrections

It was the systematics of the overcorrection for common Pb that led us suspect the presence of a mass-204 isobar. Further evidence for the isobar came from a systematic relationship

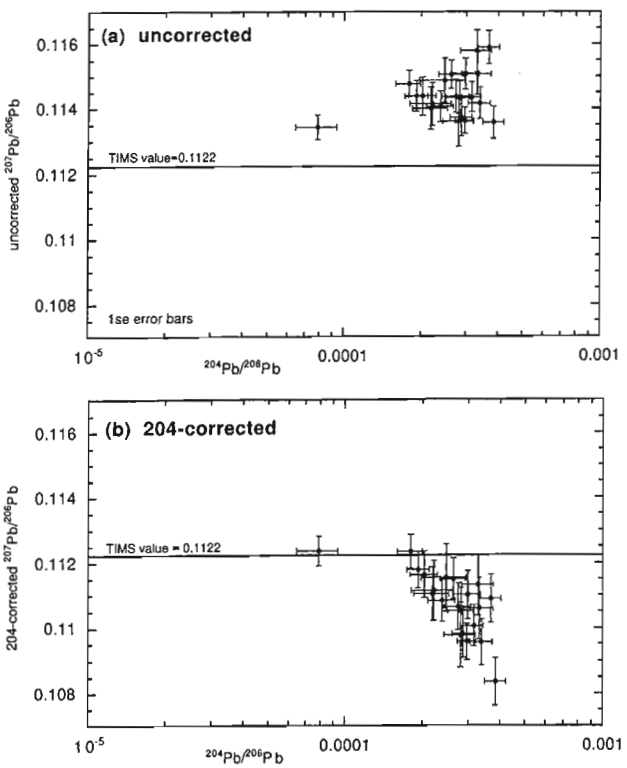

*Figure 6. An example of a SHRIMP $^{204}Pb^{+}/^{206}Pb^{+}$ vs. $^{207}Pb^{+}/^{206}Pb^{+}$ data set for monazite 4170 in which the 204 isobar is quite easily recognized. **a**) Uncorrected for common Pb, showing a relatively tight cluster of data, nevertheless ~2% high due to intrinsic common Pb in the monazite. **b**) Corrected for common Pb by the 204 method, the data show the characteristic inverse correlation indicative of an isobaric interference on mass 204.*

between 204 count rate and monazite composition. Figure 7 shows a graph of mean measured 204 cps/nA, the count rate of $^{204}Pb^{+}$ normalized to the total primary O_2^- beam current, vs. mean Th content as measured by the SHRIMP. The graph shows that 204 count rate is positively correlated with Th content. The ID-TIMS data, however, provide no support for the results in Figure 7. Our data indicate that there is no systematic relationship between the ^{204}Pb concentration measured by ID-TIMS and Th content, i.e. high-thorium monazites have about the same level of common Pb as low-thorium monazites. These observations led us to conduct further mass scans of monazites, ultimately revealing the presence of an unidentified isobar at mass ~203.960 amu in high-thorium monazites (compare Fig. 2b and 2c). Based on these observations, we concluded that

10) $[204] = [^{204}Pb] + [204\ isobar]$

where [ ] denotes count rate in cps/nA.

The $[^{204}Pb]$ can be estimated by calculating what would be required to correct the observed $^{207}Pb^{+}/^{206}Pb^{+}$ values to the accepted values. The mean $[^{204}Pb]$ for the samples based on these calculations range from 0.1 to 0.6 cps/nA (Table 4). It is straightforward then to calculate [204 isobar] for our test samples (Table 4), i.e. [204 isobar] = [204] -$[^{204}Pb]$, and these results are plotted against Th content in Figure 8. This diagram indicates that [204 isobar] is directly correlated with Th content. Based on this data set, it is possible to predict the intensity of the isobaric interference using the following equation:

11) [204 isobar] = 0.12•(Th) - 0.08

where [ ] denotes count rate in cps/nA and Th is in wt % of the element. There appears to be an uncertainty of about ±30–50% in [204 isobar].

Equation 11) serves as a basis for making corrections for the presence of the 204 isobar to the $^{207}Pb^{+}/^{206}Pb^{+}$ values of individual data points in unknown monazites, a result that we term $^{207}Pb^{*i}/^{206}Pb^{*i}$. The following sequence of calculations is performed:

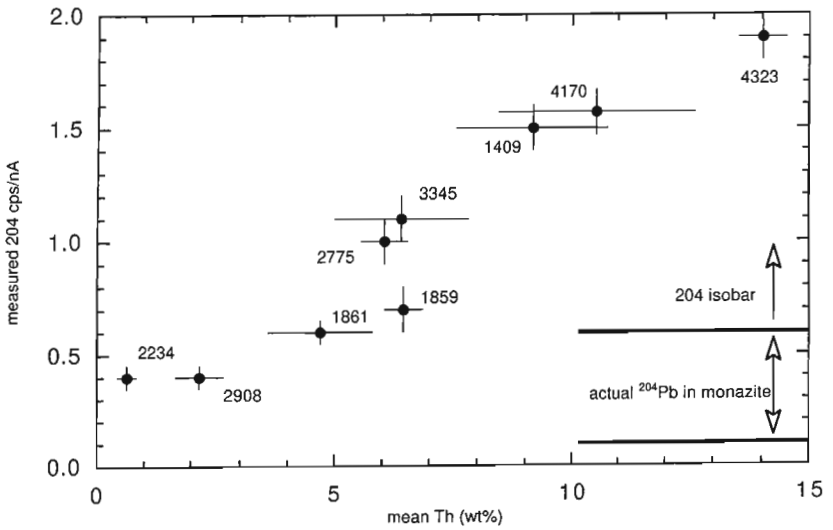

Figure 7.

SHRIMP mean Th abundance vs. mean 204 cps/nA primary beam; 1s is indicated. The indicated region shows the typical range that is actual ^{204}Pb, determined as explained in the text.

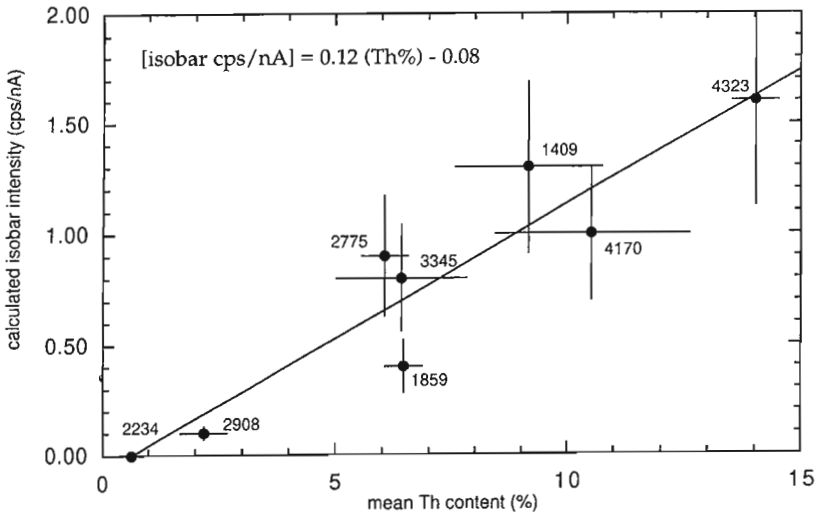

Figure 8.

SHRIMP mean Th abundance vs. intensity of the interfering 204 isobar (in cps/nA), calculated using the observed and accepted $^{207}Pb/^{206}Pb$ values (see text). The indicated equation is used to estimate the 204 isobar intensity in an unknown.

1. Calculate Th content from the U content and ThO^+/UO^+, as explained above.
2. Calculate [204 isobar] from equation 11).
3. Calculate the $[^{204}Pb]$ by difference from total [204], generally 0.1-0.6 cps/nA.
4. Correct $^{204}Pb^+/^{206}Pb^+$ by multiplying by $[^{204}Pb]/[204]$.
5. Assign 1s errors to $^{204}Pb^i/^{206}Pb^+$, estimated as ±100% of absolute value.
6. Carry out common Pb correction using the 204 method (Stern, 1997).

The above calculations were carried out for the test monazites (Fig. 5c). Compared to the raw data (Fig. 5a), the $^{207}Pb^{*i}/^{206}Pb^{*i}$ values are both slightly higher and lower than the accepted value, indicating that bias has been minimized (Table 4). Note that $^{204}Pb^i/^{206}Pb^+$ values are now lower than $^{204}Pb^+/^{206}Pb^+$. In all but one case the deviation from the accepted value is the same as or lower than for the raw data (Table 4), and the 2se errors for the means (±0.1–0.4%) are not significantly worsened.

The exception to these results is the youngest sample, 2775 (1166 Ma), in which a large common Pb correction results in $^{207}Pb^{*i}/^{206}Pb^{*i}$ values that are further from the accepted value compared to the raw ratio, although within the increased and rather large ±4.5% error. The accuracy of determining [204 isobar] from equation 11) becomes a limiting factor in the accuracy of corrections for common Pb in 'young' samples. It is recommended that monazites whose $^{204}Pb^i/^{206}Pb^+$ values are >0.00005 be corrected by assuming a low and constant value for $[^{204}Pb]$ = 0.1 cps/nA. This ensures that the data are closer to the true value than the uncorrected value, but very unlikely to cause overcorrection. The data for sample 2775 have been corrected assuming this fixed value, and are suitably closer to the accepted value (*see* Fig. 5c).

Calibration of Pb/U and Pb/Th ratios

At the beginning of our investigation we examined various methods of correcting for variable bias in the secondary ion yields of Pb^+ relative to U^+ and Th^+ (metals or metal oxides). This problem is similar to that experienced with zircon (Stern, 1997), whereby the measured $^{206}Pb^+/U^+$ and $^{208}Pb^+/Th^+$ values exceed the actual values in the target by about a factor of 3 ± 0.5. For the monazite geochronological technique to be useful, the inter-element bias for an unknown must be predictable to within a few per cent. Harrison et al. (1995) and Zhu et al. (1997a) adopted an empirical linear relationship between ThO_2^+/Th^+ and $^{208}Pb^+/Th^+$, and achieved uncertainties of few per cent in the determination of $^{208}Pb/^{232}Th$. Williams et al. (1996) and Sircombe and Compston (1994) adopted a second-order power law relationship between $^{206}Pb^+/U^+$ and $^{208}Pb^+/ThO^+$ vs. UO^+/U^+, and appear to have achieved similar results. We tested these methods as well as other combinations of isotopes, and found that the best relationships were achieved in linear correlations between $^{206}Pb^+/UO^+$ vs. UO_2^+/UO^+ and $^{208}Pb^+/ThO^+$ vs. UO_2^+/UO^+. Examples of the Pb-U and Pb-Th correlations are shown in Figure 9 for a low-, medium-, and high-thorium monazite from mount IP50. The one standard deviation of $^{206}Pb^+/UO^+$ and $^{208}Pb^+/ThO^+$ about the regression lines ranges from ±1-2%. Note that the MSWD values are high (3.4–109) compared to what is typically observed in calibrating zircons, a result of the more favourable counting statistics and thus higher analytical precision of the measured Pb/U and Pb/Th ratios in monazite, and possibly real age variations within the grains. It needs to be emphasized that the Pb-U and Pb-Th calibration schemes are empirical; there is no expectation of a perfect correlation even within a 100% concordant monazite.

Based on these and other data sets, we have selected three Paleoproterozoic monazites as our laboratory standards: 2908, 3345, and 4170. The accepted ages and ratios for these three are summarized in Table 1. The precision on the $^{206}Pb^+/UO^+$ and $^{208}Pb^+/ThO^+$ ratios of individual spots is very high, typically 0.1-0.4% (1se). Nevertheless, the one standard deviation uncertainty obtained for the standard monazite (i.e. ±1–2%) must be added quadratically to the counting statistical error of an individual analyses to obtain the 1se uncertainty in $^{206}Pb/^{238}U$ and $^{208}Pb/^{232}Th$ for an unknown single spot. Unfortunately, as in zircon, our analytical ability to directly measure inter-element ratios is far better than our ability to correct them for inter-element bias. The latter factor dominates the analytical uncertainty.

Calculation of the $^{206}Pb/^{238}U$ and $^{208}Pb/^{232}Th$ for the unknown spot follows from the following equations:

$$12)\ (^{206}Pb^+/UO^+)_{unk} / (^{206}Pb^+/UO^+)_{std} = (^{206}Pb/^{238}U)_{unk} / (^{206}Pb/^{238}U)_{std}$$

$$\therefore\ 13)\ (^{206}Pb/^{238}U)_{unk} = (^{206}Pb^+/UO^+)_{unk} \bullet (^{206}Pb/^{238}U)_{std} / (^{206}Pb^+/UO^+)_{std}$$

and similarly,

$$14)\ (^{208}Pb^+/ThO^+)_{unk} / (^{208}Pb^+/ThO^+)_{std} = (^{208}Pb/^{238}Th)_{unk} / (^{208}Pb/^{232}Th)_{std}$$

$$\therefore\ 15)\ (^{208}Pb/^{232}Th)_{unk} = (^{208}Pb^+/ThO^+)_{unk} \bullet (^{208}Pb/^{232}Th)_{std} / (^{208}Pb^+/ThO^+)_{std}$$

where $(^{206}Pb^+/UO^+)_{std}$ and $(^{208}Pb^+/ThO^+)_{std}$ are the values for the standard calculated from the linear regression calibration at the UO_2^+/UO^+ of the unknown (Fig. 9), and $(^{206}Pb/^{238}U)_{std}$ and $(^{208}Pb/^{232}Th)_{std}$ are the values assumed for the concordant age of the standard.

The $(^{207}Pb/^{235}U)_{unk}$ is not directly measured, but calculated as follows:

$$16)\ (^{207}Pb/^{235}U)_{unk} = (^{206}Pb/^{238}U)_{unk} \bullet {}^{207}Pb^*/^{206}Pb^* \bullet {}^{238}U/^{235}U$$

where $^{238}U/^{235}U$ = 137.88 (Steiger and Jäger, 1977).

Isotopic results for four Early Proterozoic and Archean monazite samples from mount IP50 are presented on standard Wetherill (1956) concordia plots (Fig. 10). The data are also plotted as $^{206}Pb/^{238}U$ vs. $^{208}Pb/^{232}Th$ (Fig. 11). In the latter diagram, the concordia curve is almost linear (actually slightly convex to the lower right) and vectors for relative mobility of Pb, Th, or U are, for all practical purposes, along concordia. The calibration standard used was monazite 3345, and a 1s error of ±2% for the standard was applied to the unknowns. The SHRIMP results for samples 2908 and 1859 (Fig. 10a, b and 11 a, b) are both highly concordant and cluster near the ID-TIMS results (large black dots). For samples 4170 and 4323, however, the SHRIMP $^{206}Pb/^{238}U$, $^{207}Pb/^{235}U$, and $^{208}Pb/^{232}Th$ ages are too high by a few per cent, and the $^{208}Pb/^{232}Th$ ages are also biased about 2% higher than the $^{206}Pb/^{238}U$ ages (Fig. 10 c, d and 11 c, d).

For the reduced data, there is a relationship between the accuracy of the SHRIMP $^{206}Pb/^{238}U$ and $^{208}Pb/^{232}Th$ ages and the mean Th abundance of the sample relative to the

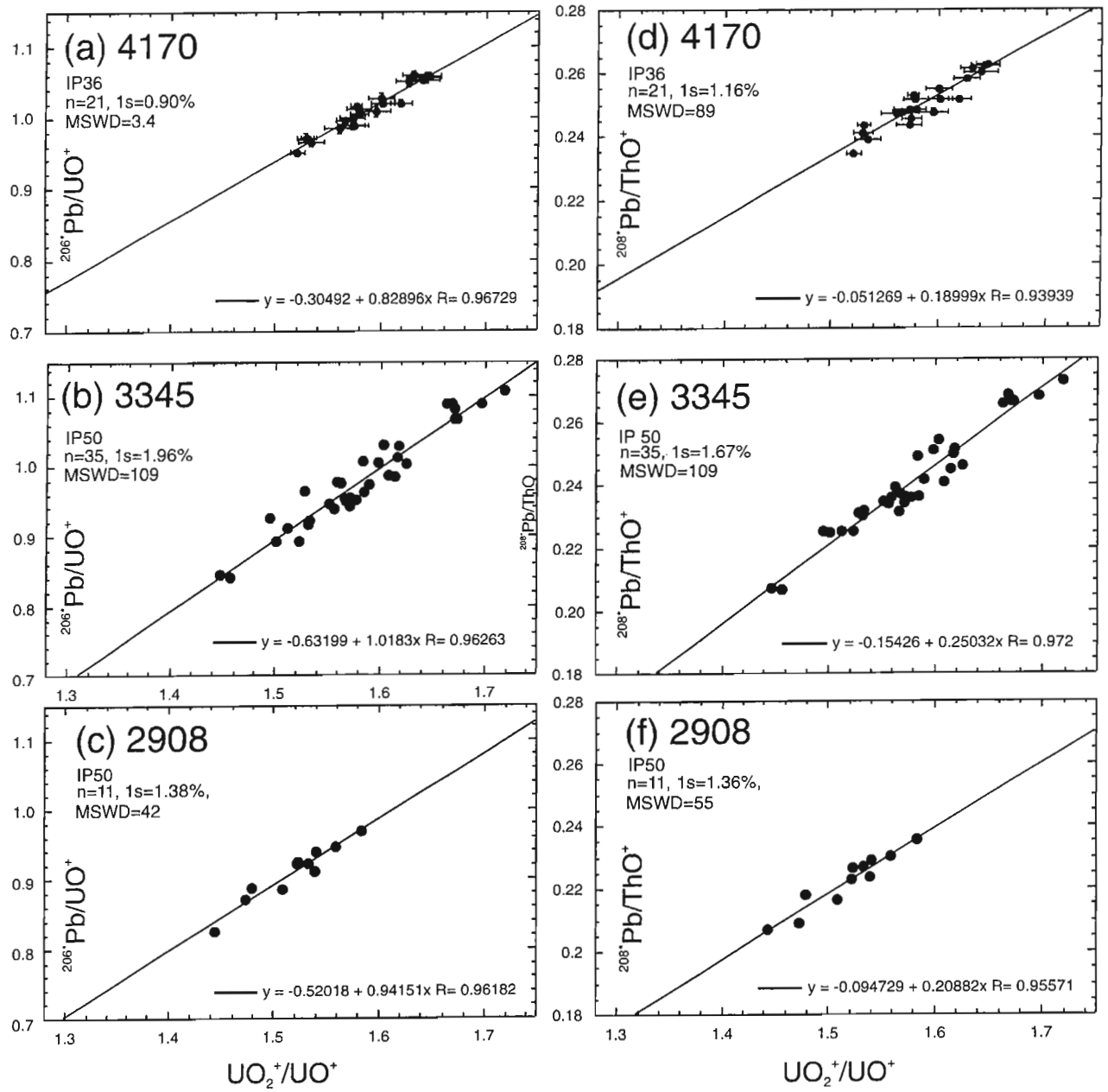

Figure 9. *Examples of linear correlations of $^{206}Pb^*/UO^+$ vs. UO_2^+/UO^+ and $^{208}Pb^*/ThO^+$ vs. UO_2^+/UO^+ for monazites 4170 (**a, d**), 3345 (**b, e**), and 2908 (**c, f**), now adopted as monazite standards. One or more of these calibration lines need to be established for each grain mount or thin section in order to correct for variable bias in measuring $^{206}Pb^+/UO^+$ and $^{208}Pb^+/ThO^+$ in unknown monazites.*

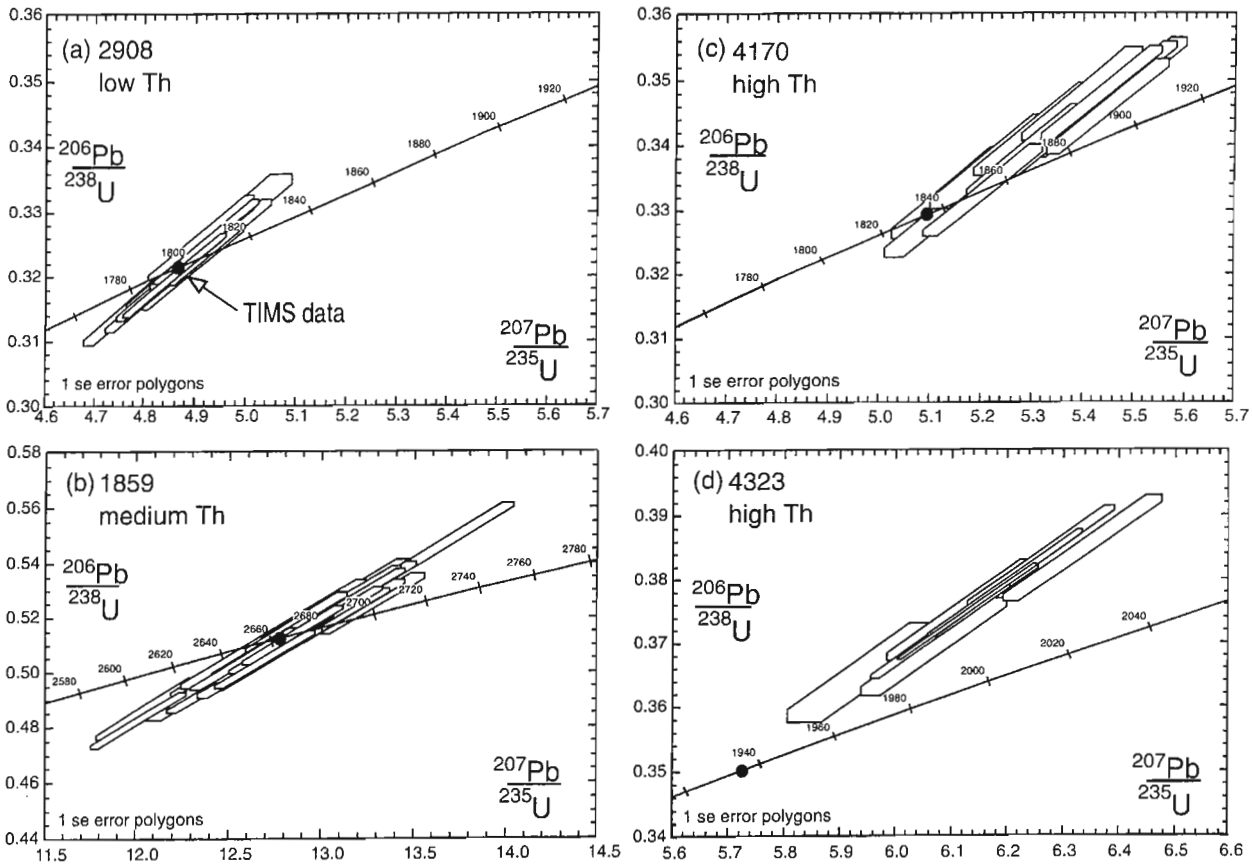

Figure 10. *U-Pb concordia plots of SHRIMP monazite data. The U/Pb ratios have been calibrated relative to monazite standard 3345 (see Fig. 9). Dots show ID-TIMS ages. Note that the U/Pb calibration is effective for* ***a)*** *and* ***b)****, but in* ***c)*** *and* ***d)*** *the SHRIMP data appear to be reversely discordant, an artifact of the U/Pb calibration. It is important in such high-thorium monazites to use a separate high-thorium standard for U/Pb calibrations.*

standard with 6.4% Th (Table 4). For samples 2908 and 1859, with mean Th contents similar to or less than the standard, the mean SHRIMP $^{206}Pb/^{238}U$ and $^{208}Pb/^{232}Th$ ages are within 0.5% of the accepted values, and well within the analytical errors (*see* Fig. 12). However, the SHRIMP $^{206}Pb/^{238}U$ and $^{208}Pb/^{232}Th$ ages for sample 4170, with 10.5% Th, are, respectively, 3% and 5% older than the ID-TIMS age (Fig. 12). For sample 4323, with 14% Th, the mean $^{206}Pb/^{238}U$ and $^{208}Pb/^{232}Th$ ages are, respectively, 6% and 8% older than the ID-TIMS ages (Fig. 12). As there is no evidence from the TIMS data that there is excess ^{206}Pb or ^{208}Pb in these samples, there must be a problem with the calibration of the inter-element ratios.

We interpret these results as indicating a compositional dependence on the calibration of the inter-element ratios. Compared to low- and medium-thorium monazites, secondary ion yields of Pb^+ from high-thorium monazites appear to be enhanced relative to U^+ and Th^+. This situation is analagous to that encountered in SHRIMP analyses of certain high-U zircons which, when referenced to zircon standards with lower U, plot above concordia (e.g. McLaren et al., 1994). Consequently, the effect observed in high-thorium monazite likely relates to a crystal structural difference compared with other monazites, perhaps damage caused by decay of Th, or some other differences relating to the substitution in the structure of Th, Si, Ca, F, or OH^-.

The calibration of the Pb/U and Pb/Th ratios in monazites requires standard with similar Th contents. Monazites with 1-8% Th form one group in which the relative secondary ion yields of Pb^+, U^+, and Th^+ appear to be similar. The Pb/U and Pb/Th ratios in these low- to medium-thorium monazites can be calibrated using a standard monazite with Th contents in this range. In our laboratory, either or both of standards 2908 and 3345 are suitable, and both are recommended for added confidence in the calibration. We have some evidence, not yet fully documented, that inter-element calibration for very low-thorium monazites (<1 wt %) may require a similarly very low-thorium monazite. Monazite 2234, although not ideal, could serve this purpose (Table 4).

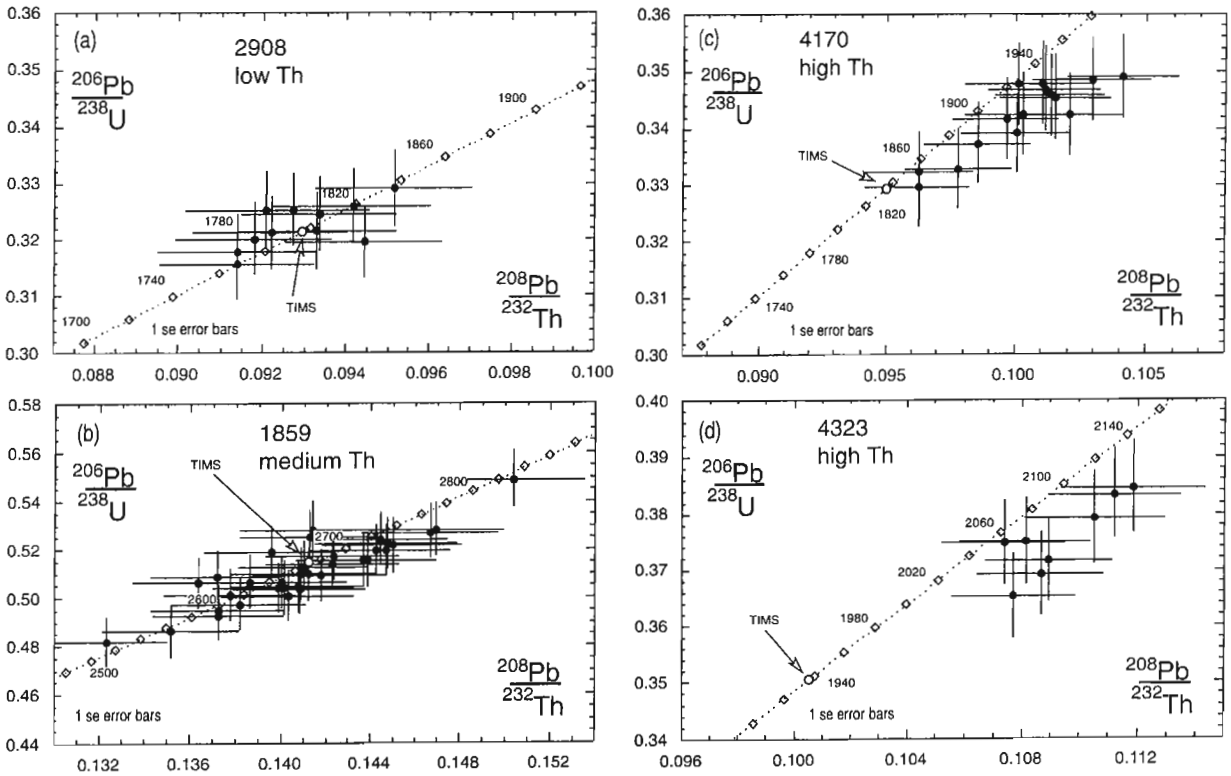

Figure 11. *U-Pb-Th concordia plots of SHRIMP data, with U/Pb and Th/Pb ratios referenced to monazite 3345. As for Figure 10, the data for high-thorium monazites* ***c)*** *and* ***d)*** *have U-Pb and Th-Pb ages that are inaccurately high.*

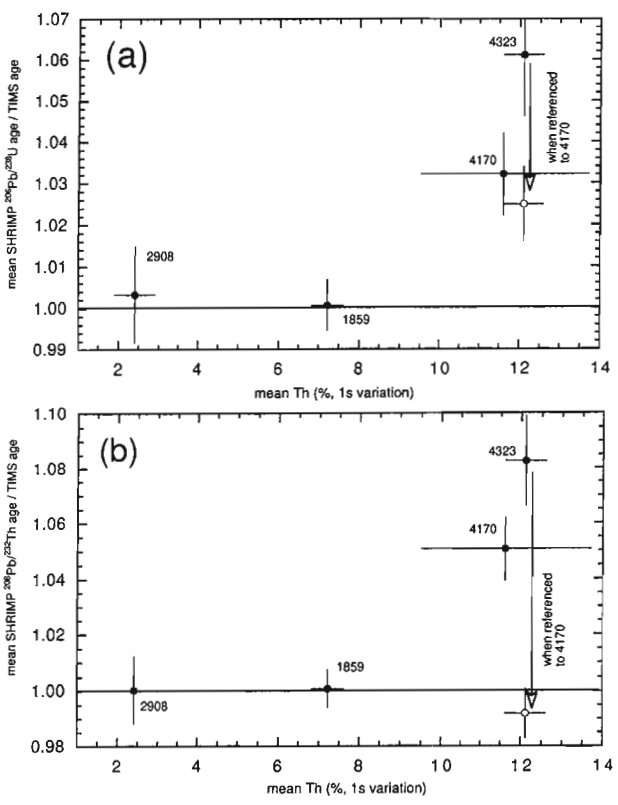

High-thorium monazites (>8 % Th) are more problematic, as it appears that accurate calibration requires even more careful matching of Th content. For example, if the data for sample 4323 are instead referenced to monazite 4170, the mean $^{208}Pb/^{232}Th$ age is now within error of the accepted value (Fig. 12b, open symbols), but the $^{206}Pb/^{238}U$ age remains biased high by ~2.5% (Fig. 12a, open symbols). It is unclear why a residual bias remains with the $^{206}Pb/^{238}U$ ratio. Perhaps one would need to match the standard and unknown more precisely in both Th and U content and age. More work is needed to understand the inter-element calibration in high-thorium monazite, but monazite 4170 has been adopted as the high-thorium standard for the time being. Typically, all three monazite standards would be mounted along with the unknowns in anticipation of a range of monazite compositions.

Despite the compositional dependence observed in calibrating the Pb/Th and Pb/U ratios, there is no evidence in monazite of the extreme bias observed in high-uranium

Figure 12. *Mean SHRIMP Th abundance in four samples vs.* ***a)*** *mean SHRIMP $^{206}Pb/^{238}U$ age, normalized to the accepted age, and* ***b)*** *mean SHRIMP $^{208}Pb/^{232}Th$ age, normalized to the accepted age. The age error bars are ±2se. The arrows and open symbols show how the data for high-thorium monazite 4323 would plot when normalized to high-thorium monazite 4170.*

zircons (e.g. McLaren et al., 1994), so it is unlikely to be a serious impediment in most studies. Individual spot determinations of the $^{206}Pb/^{238}U$ and $^{208}Pb/^{232}Th$ ratios in unknown monazites with <8 wt % Th can generally be determined with an accuracy to better than ±2% (1se) using either of the two laboratory standards, 2908 and 3345 (Table 1).

SUMMARY

In this study, analytical techniques have been developed for the determination of monazite U-Pb and Th-Pb ages using the SHRIMP II ion microprobe. The basis for the study was a reference suite comprising natural monazite samples having more or less isotopically concordant ID-TIMS ages ranging from 1.02 Ga to 2.67 Ga. The following points summarize the key findings of this study:

1. Analysis by SHRIMP requires monitoring of nine mass stations, $^{203}CePO_2^+$, $^{204}Pb^+$, 204.1 (background), $^{206}Pb^+$, $^{207}Pb^+$, $^{208}Pb^+$, $^{248}ThO^+$, $^{254}UO^+$, and $^{270}UO_2^+$, which are sequentially analyzed at a mass resolution (1%) of 5700. Instrumental setup is identical to that for zircon, permitting either mineral to be analyzed during an analytical session.

2. Uranium abundances in most monazites can be determined to ±20% of the actual value by an empirically derived inverse relationship between measured $^{203}CePO_2^+/UO^+$ and U content. A separate monazite U standard is not required. The relative instrumental discrimination ('sensitivity factor') between Th and U is virtually constant, enabling Th/U ratios to be very accurately determined (≤1%).

3. An unidentified isobar at ~203.960 ± 0.005 amu interferes with the accurate determination of ^{204}Pb in monazites with moderate to high Th contents. The $^{207}Pb^*/^{206}Pb^*$ ratios are consistently biased low by up to a few per cent if all the data are corrected using the measured ^{204}Pb. A positive correlation between the 204 isobar intensity and Th content permits ^{204}Pb count rates to be corrected. The $^{207}Pb^*/^{206}Pb^*$ ratios, corrected for common Pb following removal of the 204 isobar according to the guidelines provided, are generally indistiguishable from the accepted values. The $^{207}Pb^*/^{206}Pb^*$ ratios of individual spots can typically be determined to a precision (1se) of ±0.3–0.5%, whereas, a precision of ±0.1–0.4% at the 95% confidence level is possible for the mean of approximately 10 or more spots from the same monazite generation.

4. Instrumental bias in the measured $^{206}Pb^+/UO^+$ and $^{208}Pb^+/ThO^+$ ratios in unknown monazites is corrected for using linear relationships between $^{206}Pb^+/UO^+$ vs. UO_2^+/UO^+ and $^{208}Pb^+/ThO^+$ vs. UO_2^+/UO^+, empirically derived from natural monazite standards. The relative instrumental fractionation of Pb^+ with respect to UO^+ and ThO^+ varies with monazite composition, and it is important to match the Th content of unknowns and standards. Individual spot determinations of the $^{206}Pb/^{238}U$ and $^{208}Pb/^{232}Th$ ratios in unknown monazites with 1–8 wt % Th can generally be determined with an accuracy to better than ±2% (1se) using either of the recommended standards (2908, 3345, Table 1). Accuracy may be a factor of two worse for monazites with >8% Th calibrated using the suggested standard (4170, Table 1).

CONCLUSIONS

This study illustrates well the importance of testing new SIMS geochronological methods against samples that have been precisely and accurately analyzed by ID-TIMS. We used our extensive collection of monazites analyzed by ID-TIMS to locate suitable monazite standards, and to refine and ultimately verify the technique. This iterative process led to the documentation for the first time of an irresolvable isobar at mass 204 amu. The isobar was suspected by Williams et al. (1996), and considered as a possibility by Harrison et al. (1995) who found no evidence of it in a synthetic Nd-monazite. The presence and mitigation of the isobar is an important issue for the accuracy of SHRIMP ^{207}Pb-^{206}Pb age data, particularly for Mesoproterozoic or younger monazites. If unrecognized, the presence of the isobar would cause such ages to be biased low when corrected for common Pb.

The iterative testing technique also led to the recognition of a compositional dependence in the relative secondary ion yields of Pb^+ relative to UO^+ and ThO^+. We suspect that this relationship is fundamental to the sputtering characteristics of monazite. The latter point is a crucial one for studies of young monazites in which $^{206}Pb/^{238}U$ or $^{208}Pb/^{232}Th$ ratios are relied upon for absolute age determinations (e.g. Harrison et al., 1995). Depending on the circumstances, such ages could be biased high or low by several percent if the standard and unknowns are not matched in Th content.

SHRIMP U-Pb and Th-Pb geochronology of monazite is rapid, accurate, and permits similar or better precision than is possible with zircon (Stern, 1997). Although not reported on here, the technique has already allowed us to identify intragrain age heterogeneities within at least two of the test monazite suites (4170, 1861). Coupled with the complexity of the monazite BSE images (Fig. 1), it is clear that the field of monazite chronology, formerly considered quite simple in comparison to zircon, may shortly be overturned now that the age complexity of the grains can be documented with the ion microprobe. Application of the technique to in situ studies of metamorphic rocks has commenced and proving highly successful in resolving the ages of metamorphism recorded in monazite occurring in various mineralogical contexts.

ACKNOWLEDGMENTS

Development of SIMS monazite chronology was aided by discussions with K. Sircombe, I. Williams, and W. Compston. Thanks go to numerous GSC staff in providing access to monazite samples and unpublished data. A work-term report of J. Robillard was valuable in assessing peak interferences. R. Berman is thanked for pushing R.S. to study monazite sooner than later. The manuscript benefitted immensely from

discussions and critical review by W. J. Davis, who graciously provided Th-Pb ID-TIMS data for this study. Thanks go to Reg Thériault for thorough editing.

REFERENCES

Bethune, K. and Scammell, R.J.
1997: Precambrian geology, Koch Island area (part of NTS 37C), District of Franklin, Northwest Territories; Geological Survey of Canada, Open File 3391, scale 1:50 000.

Bingen, B., Demaiffe, D., and Hertogen, J.
1996: Redistribution of rare earth elements, thorium, and uranium over accessory minerals in the course of amphibolite to granulite facies metamorphism: the role of apatite and monazite in orthogneisses from southwestern Norway; Geochimica et Cosmochimica Acta, v. 60, p. 1341-1354.

Copeland, P., Parrish, R.R., and Harrison, T.M.
1988: Identification of inherited radiogenic Pb in monazite and its implications for U-Pb systematics; Nature, v. 333, p. 760-763.

Corriveau, L., van Breemen, O., Morin, D., Amelin, Y., Rivard, B., and Sharma, K.N.M.
1996: New light on the Central Metasedimentary Belt of Quebec and its lithosphere; Rapport du transect de LITHOPROBE Abitibi-Grenville, v. 49, p. 23-27.

Cumming, G.L. and Richards, J.R.
1975: Ore lead in a continuously changing Earth; Earth and Planetary Science Letters, v. 28, p. 155-171.

Davis, W.J., Parrish, R.R., McNicoll, V.J., and Bellerive, D.
1998: Analytical techniques for the determination of $^{208}Pb/^{232}Th$ ages of monazite and zircon at the geochronology laboratory, Geological Survey of Canada; *in* Radiogenic Age and Isotopic Studies: Report 11; Geological Survey of Canada, Current Research 1998-F.

DeWolf, C.P., Belshaw, and O'Nions, R.K.
1993: A metamorphic history from micron-scale $^{207}Pb/^{206}Pb$ chronometry of Archean monazite; Earth and Planetary Science Letters, v. 120, p. 207-220.

Hanson, G.N.
1980: Rare earth elements in petrogenetic studies of igneous systems; Annual Reviews of Earth and Planetary Science, v. 8, p. 371-406.

Harrison, T.M., McKeegan, K.D., and LeFort, P.
1995: Detection of inherited monazite in the Manaslu leucogranite by $^{208}Pb/^{232}Th$ ion microprobe dating: crystallization age and tectonic implications; Earth and Planetary Science Letters, v. 133, p. 271-282.

Hogarth, D.D. and van Breemen, O.
1996: Geology and age of the Lac à la Perdrix fenite, southern Gatineau district, Quebec; *in* Radiogenic Age and Isotopic Studies: Report 9; Geological Survey of Canada, Current Research 1995-F, p. 33-41.

Kingsbury, J.A., Miller, C.D., Wooden, J.L., and Harrison, T.M.
1993: Monazite paragenesis and U/Pb systematics in rocks of the eastern Mojave Desert, California: implications for thermochronometry; Chemical Geology, v. 110, p. 147-167.

Kucha, H.
1980: Continuity in the monazite-huttonite series; Mineralogical Magazine, v. 43, p. 1031-1034.

McLaren, A.C., Fitz Gerald, J.D., and Williams, I.S.
1994: The microstructure of zircon and its influence on the age determination from Pb/U isotopic ratios measured by ion microprobe; Geochimica et Cosmochimica Acta, v. 58, p. 993-1005.

Mohr, D.V.
1984: Zoned porphyroblasts of metamorphic monazite in the Anakeesta Formation, Great Amoky Mountain, North Carolina; American Mineralogist, v. 69, p. 98-103.

Overstreet, W.C.
1967: The geologic occurrence of monazite; United States Geological Survey Professional Paper, v. 530, p. 1-327.

Parrish, R.R.
1990: U-Pb dating of monazite and its application to geological problems; Canadian Journal of Earth Sciences, v. 27, p. 1431-1450.

Parrish, R.R, Roddick, J.C., Loveridge, W.D., and Sullivan, R.W.
1987: Uranium-lead analytical techniques at the geochronology laboratory, Geological Survey of Canada; *in* Radiogenic Age and Isotopic Studies: Report 1; Geological Survey of Canada, Paper 87-2, p. 3-7.

Percival, J.A., Mortensen, J.K., Stern, R.A., Card, K.D., and Begin, N.J.
1992: Giant granulite terranes of northeastern Superior Province: the Ashuanipi Complex and Minto Block; Canadian Journal of Earth Sciences, v. 29, p. 2287-2308.

Rapp, R.P. and Watson, E.B.
1986: Monazite solubility and dissolution kinetics: implications for the thorium and light rare earth chemistry of felsic magmas; Contributions to Mineralogy and Petrology; v. 94, p. 304-316.

Shannon, R.D.
1976: Revised effective ionic radii and systematic studies of interatomic distances in halides and chalcogenides; Acta Crystallographica, v. A32, p. 751-767.

Sircombe, K. and Compston, W.
1994: SHRIMP analysis of monazite and application for provenance studies; Geological Society of Australia, Abstracts, No. 37, p. 409.

Smith, H.A. and Barreiro, B.
1990: Monazite U-Pb dating of staurolite grade metamorphism in pelitic schists; Contributions to Mineralogy and Petrology, v. 105, p. 602-615.

Smith, H.A. and Giletti, B.
1997: Lead diffusion in monazite; Geochimica et Cosmochimica Acta, v. 61, p. 1047-1055.

Spear, F.S. and Parrish, R.R.
1996: Petrology and cooling rate of the Valhalla Complex, British Columbia, Canada; Journal of Petrology, v. 37, p. 733-765.

Steiger, R.H. and Jäger, E.
1977: Subcommission on geochronology: convention on the use of decay constants in geo- and cosmochronology; Earth and Planetary Science Letters, v. 36, p. 359-362.

Stern, R.A.
1992: Nd- and Pb-isotope studies of monazite, zircon and other minerals in granitoids: examples from northeastern Superior Province, Quebec and Mount Everest, Tibet; *in* Radiogenic Age and Isotopic Studies: Report 5; Geological Survey of Canada, Paper 91-2, p. 43-50.
1996: A SHRIMP II ion microprobe at the Geological Survey of Canada; Geoscience Canada, v. 23, p. 73-76.
1997: The GSC Sensitive High Resolution Ion Microprobe (SHRIMP): analytical techniques of zircon U-Th-Pb age determinations and performance evaluation; *in* Radiogenic Age and Isotopic Studies: Report 10; Geological Survey of Canada, Current Research 1997-F, p. 1-31.

Suzuki, K., Adachi, M., and Kajizuka, I.
1994: Electron microprobe observations of Pb diffusion in metamorphosed detrital monazites; Earth and Planetary Science Letters, v. 128, p. 391-405.

Vry, J., Compston, W., and Cartwright, I.
1996: SHRIMP II dating of zircons and monazites: reassessing the timing of high-grade metamorphism and fluid flow in the Reynolds Range, northern Arunta Block, Australia; Journal of Metamorphic Petrology, v. 14, p. 335-350.

Wetherill, G.W.
1956: Discordant uranium-lead ages; Transactions of the American Geophysical Union, v. 37, p. 320-326.

Wodicka, N. and Scott, D.J.
1997: A preliminary report on the U-Pb geochronology of the Meta Incognita Peninsula, southern Baffin Island, Northwest Territories; *in* Current Research 1997-C; Geological Survey of Canada, p. 167-178.

Williams, I.S., Buick, I.S., and Cartwright, I.
1996: An extended episode of early Mesoproterozoic metamorphic fluid flow in the Reynolds Range, central Australia; Journal of Metamorphic Petrology, v. 14, p. 29-47.

Yunxiang, N., Hughes, J.M., and Mariano, A.N.
1995: Crystal chemistry of the monazite and xenotime structures; American Mineralogist, v. 80, p. 21-26.

Zhu, X.K., O'Nions, R.K., Belshaw, N.S., and Gibb, A.J.
1997a: Significance of in situ SIMS chronometry of zoned monazite from the Lewisian granulites, northwest Scotland; Chemical Geology, v. 135, p. 35-53.
1997b: Lewisian crustal history from in situ SIMS mineral chronometry and related metamorphic textures; Chemical Geology, v. 136, p. 205-218.

Analytical techniques for the determination of $^{208}Pb/^{232}Th$ ages of monazite and zircon at the Geochronology Laboratory, Geological Survey of Canada

W.J. Davis[1], R.R. Parrish[2], V. McNicoll[1], and D. Bellerive[1]

Davis, W.J., Parrish, R.R., McNicoll, V. and Bellerive, D., 1998. Analytical techniques for the determination of $^{208}Pb/^{232}Th$ ages of monazite and zircon at the Geochronology Laboratory, Geological Survey of Canada; in *Radiogenic Age and Isotopic Studies: Report 11; Geological Survey of Canada, Current Research 1998-F, p. 19-22.*

Abstract: A mixed ^{230}Th-^{233}U-^{235}U-^{205}Pb isotopic spike has been prepared for the analyses of thorium, uranium, and lead isotopes by isotope-dilution methods, and the determination of $^{208}Pb/^{232}Th$, $^{207}Pb/^{235}U$, and $^{206}Pb/^{238}U$ mineral ages. The chemical separation procedure uses Dowex (1X8)^{TM} anion exchange resin to separate Th from Pb and U, and a separate column containing TEVA-SPEC^{TM} anion exchange resin to further purify Th. Thorium isotopes are analyzed either in static multicollector mode, or by single, secondary electron multiplier on a Finnigan-Mat 261 mass spectrometer. Analyses of high-optical-quality, concordant or near concordant (<±0.5%) monazites from 12 Paleoproterozoic and Neoarchean rocks show good agreement between $^{208}Pb/^{232}Th$ and $^{206}Pb/^{238}U$ ages (average <0.1% relative difference).

Résumé : On a préparé un échantillon isotopique dopé renfermant ^{230}Th-^{233}U-^{235}U-^{205}Pb pour le dosage des isotopes de thorium, d'uranium et de plomb par les méthodes de dilution isotopique, et pour la datation des minéraux d'après les rapports $^{208}Pb/^{232}Th$, $^{207}Pb/^{235}U$ et $^{206}Pb/^{238}U$. Le thorium a été séparé chimiquement du plomb et de l'uranium à l'aide de résine échangeuse d'anions Dowex (1X8)^{MC}; une colonne distincte contenant une résine échangeuse d'anions TEVA-SPEC^{MC} a été utilisée afin de purifier davantage le thorium. Les isotopes du thorium ont été analysés soit en mode multicollecteur statique, soit par multiplicateur unique d'électrons secondaires relié au spectromètre de masse Finnigan-Mat 261. Les analyses de monazites concordantes ou subconcordantes de grande qualité optique (< ± 0,5 %) de douze roches du Paléoprotérozoïque et du Néoarchéen montrent une bonne concordance entres les âges obtenus avec $^{208}Pb/^{232}Th$ et $^{206}Pb/^{238}U$ (moyenne de l'écart relatif de < 0,1 %).

[1] Geological Survey of Canada, 601 Booth Street, Ottawa, Ontario K1A 0E8
[2] NERC Isotope Geosciences Laboratory, Keyworth, Notts NG12 5GG, U.K.

INTRODUCTION

A new mixed spike (^{230}Th-^{233}U-^{235}U-^{205}Pb) has been prepared at the Geochronology Laboratory, Geological Survey of Canada, to permit the determination of precise ^{208}Pb/^{232}Th, ^{207}Pb/^{235}U, and ^{206}Pb/^{238}U ages from the same mineral fractions. The ^{232}Th/^{208}Pb ages are particularly useful in addressing uncertainties in the interpretation of reversely discordant U-Pb ages caused by incorporation of disequilibrium ^{230}Th, and subsequent production of excess ^{206}Pb, in high-thorium minerals such as monazite and allanite (e.g. Scharer, 1984; Parrish, 1990). These ^{232}Th/^{208}Pb ages may also prove useful in recognizing and evaluating the significance of other potential disturbances in the U-Pb systematics of minerals, such as relative uranium gain or loss (e.g. Gibson et al. 1997).

This paper describes preparation of a mixed ^{230}Th-^{233}U-^{235}U-^{205}Pb isotopic tracer solution, and the chemical and mass spectrometric techniques employed at the Geological Survey of Canada laboratory for the separation, purification, and analysis of Th in monazite and zircon by thermal ionization mass spectrometry. We also report Th-U-Pb analyses of Paleoproterozoic and Neoarchean monazites as a measure of the accuracy and reproducibility of the method. Many of these monazites were analyzed for their ^{208}Pb/^{232}Th ratios to evaluate their suitability as SHRIMP ion microprobe standards (Stern and Sanborn, 1998).

ANALYTICAL METHODS

Preparation and calibration of spike solution

A tracer solution comprising enriched ^{230}Th (99.87%) was sequentially precleaned in Dowex (1X8) and TEVA-SPEC™ resin to remove any Pb and U, respectively. A predetermined quantity of this tracer solution was added to an existing ^{205}Pb-^{233}U-^{235}U tracer whose Pb/U, Pb isotopic, and U isotopic compositions were previously known. After appropriate dilution of the combined ^{230}Th-^{233}U-^{235}U-^{205}Pb tracer solution, a weighed quantity of it was added to a weighed quantity of U-Th-Pb reference solution prepared from pure natural Th metal (Ames), natural U (SRM960), and SRM 982 Pb whose concentrations and isotopic compositions were known. This reference solution was prepared in 1996 and its composition uncertainty relates almost exclusively to the purity of the trace elements at the ppm level in the metals. The isotopic composition of the tracer-reference mixture was measured by thermal ionization mass spectrometry (TIMS) in static multicollection mode for U, Th, and Pb. The U, Th, and Pb concentrations of the tracer were calculated by unmixing using isotope-dilution equations.

The uncertainty of Th concentration of the spike remains higher than U or Pb because of greater uncertainties in the corrections for isotopic fractionation determined with the TIMS technique. The U and Pb concentrations and Pb/U concentration ratio of the tracer solution are known to a very high precision, mostly because of the ability to precisely correct for isotopic fractionation in the measurements (Roddick et al., 1987). The isotopic composition of the U in the tracer was determined precisely by the critical-mixture technique, and U fractionation is corrected using a double-spike technique. Lead fractionation on the Finnigan-Mat 261 mass spectrometer is well characterized from repeated analysis of SRM Pb 981 solution (0.09 ± 0.03%). Thorium fractionation for TIMS analysis was determined by comparative analysis of a mixed isotopic solution (^{230}Th, ^{232}Th) on the Finnigan-Mat 261 mass spectrometer at the GSC and on the VG Elemental P54 multicollector mass spectrometer in Cheshire (UK). The ICP-MS P54 measurements used the mixed Th isotopic solution spiked with an equal-atom U solution (U500). Th fractionation on the ICP-MS P54 could then be precisely measured, and a fractionation-corrected, 'absolute' value of the mixed isotopic solution determined. The P54 determined ratio of the solution was then used to calculate the relative mass fractionation for TIMS analysis on the Finnigan-Mat 261. A value of 0.07%/amu (atomic mass units) was determined, and used to determine the isotopic composition of the ^{230}Th spike, and Th concentration of the spike.

Column chemistry

Details of U-Pb analytical methods for analysis of monazite and zircon, including mineral preparation and selection, chemical dissolution, ion exchange chemistry, and mass spectrometry are described in Parrish et al. (1987). Modifications to recover and purify Th for thermal ionization mass spectrometry analysis are described below. Monazites are washed, weighed, and spiked with a mixed ^{230}Th-^{233}U-^{235}U-^{205}Pb isotopic tracer solution, and dissolved in 12 N HCl in Teflon™ pressure bombs at 210°C. The solutions are taken to dryness, checked for dissolution, and redissolved in 3.1 N HCl. Th is separated from Pb and U using anionic (Dowex 1X8) exchange chemistry with 3.1 N HCl. This step is part of the standard ion-exchange chemistry for monazite and zircon (Parrish et al., 1987). Pb and U are then collected in 6 N HCl and H_2O respectively (Parrish et al., 1987). The 3.1 N HCl solution is taken to dryness and redissolved in 0.1 mL of 2 N HNO_3. Purification of Th is carried out using TEVA-SPEC™ chromatographic resin (Horowitz et al., 1995) in Teflon columns with a resin volume of 55 µL and bed length of 12.5 mm. The procedure is outlined in Table 1. After cleaning and conditioning of the resin in the column, the sample is added to the column in 0.1 mL 2 N HNO_3. Most analytes other than Th and the tetravalent actinides are removed by repeated washings in 2 N HNO_3 (≈8 free column volumes (fcv)). Thorium is then stripped in 0.1 mL of H_2O and 0.2 mL of 6 N HCl. One drop of H_3PO_4 is added and the solution is evaporated to dryness and ready for mass spectrometry. Measured Th procedural blanks are <5 pg.

Mass spectrometry

Uranium and lead are loaded separately onto single Re filaments with Si gel and H_3PO_4, and analyzed as UO_2^+ and Pb^+, respectively (Parrish et al., 1987; Roddick et al., 1987). Th is loaded onto the side filament of a double Re filament assembly and analyzed as a positive metal ion on a Finnigan-Mat

261 mass spectrometer in static Faraday multicollection or single, secondary electron multiplier (SEM) collector mode. A stable ion beam is achieved at 4.9 A on the ionization filament, and 2.7–3.0 A on the evaporation filament. This yields a stable signal of 30–100 mV of ^{232}Th for sample loads of 0.1–1 μg. Thorium isotopic ratios are corrected for an estimated mass fractionation value of 0.07%/amu (*see* above). Reproducibility of the $^{232}Th/^{230}Th$ ratio determined for 50–150 ng loads of a spiked reference solution is 0.11% (1σ; n=9), corresponding to an error in the mass fractionation value of 0.07 ± 0.056%/amu (1σ). The SEM was utilized for signal intensities of less than 10 mV. The SEM was calibrated for non-linearity following methods modified from Loveridge (1986). The SEM to Faraday mass bias was determined by repeated analysis of a spiked standard solution on Faraday and SEM collectors. The mass bias of the SEM was calculated to be 0.19 ± .07%/amu (average of seven determinations over several month period; error at 1σ level).

Table 1. Procedure for separation of thorium using TEVA-SPEC resin.

Clean TEVA -SPEC™ resin by rinsing and decanting with:	
Milli-Q water (2x)	
2 N HNO_3 (2x)	
6 N HCl (2x)	
Load 0.50 μL of TEVA resin into pre-cleaned, 55 μL column	
Add and discard:	
0.35 mL	H_2O
0.35 mL	2 N HNO_3
0.35 mL	6 N HCl
0.15 mL	H_2O
0.15 mL	2 N HNO_3
Load sample into column as 0.1 mL 2M HNO_3 solution	
Add and discard:	
0.10 mL	2 N HNO_3
0.35 mL	2 N HNO_3
Add and collect (Th) in clean beaker:	
0.10 mL	H_2O
0.10 mL	6 N HCl
0.10 mL	6 N HCl
Add one drop of H_3PO_4 and evaporate to dryness.	

Data reduction for U and Pb follow methods outlined in Parrish et al., (1987) and errors in Pb/U ratios are calculated following methods of Roddick (1987), and incorporate reproducibility of standard solutions. Thorium concentrations are calculated by standard isotope-dilution methods and are corrected for blanks of <5 pg. Two-sigma errors in the $^{208}Pb/^{232}Th$ ratio are estimated to be 0.5%, and take into account uncertainty in measurement errors, Pb and Th mass fractionation, and common and blank ^{208}Pb corrections. Errors in the Pb/Th ratio of the spike are not included.

Th-U-Pb ANALYTICAL RESULTS AND DISCUSSION

Table 2 presents Th-U-Pb analytical data for monazites from 12 samples. Monazites from all these samples had previously been analyzed for U and Pb composition at the GSC laboratory, and most of these samples were selected for evaluation as potential SHRIMP standards (all samples excluding Z4598, Z4599 in Table 2; *see* Stern and Sanborn, 1998). Monazites from those samples considered as potential SHRIMP standards show a high degree of concordance and little variation in $^{207}Pb/^{206}Pb$ ratios. However, Stern and Sanborn (1998) report evidence for age heterogeneity within monazite populations from some of these samples (e.g. Z4170; Z2234). Samples Z4598 through Z4600 are Archean granitoids from the Yellowknife area of the Slave Province, northwest Canada. Monazites in these rocks are of poorer optical quality and some exhibit discordance in the U-Pb system.

In most cases the $^{232}Th/^{208}Pb$ ages determined for the monazites agree with their $^{206}Pb/^{238}U$ ages, within analytical uncertainty (Fig. 1). The largest deviations are for analyses of poor-optical-quality monazites that exhibit discordance in the U-Pb system. Analyses of high-optical-quality

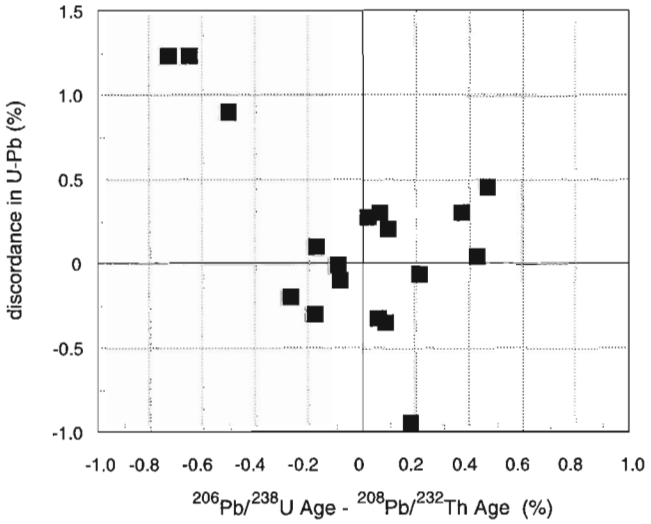

Figure 1. *Plot of discordance in U-Pb data vs. relative difference in $^{206}Pb/^{238}U$-$^{208}Pb/^{232}Th$ age. Discordance in the U-Pb system is defined in terms of the relative difference in $^{207}Pb/^{206}Pb$-$^{206}Pb/^{238}U$ ages. Concordant Pb/U and Pb/Th ages plot at origin in this diagram.*

Table 2. U-Th-Pb analytical data.

Sample[1]	Concentrations[2]					Atomic Ratios[3]						Ages (Ma)[4]				
	Wt. µg	Th ppm	U ppm	Pb* ppm	Pbc pg	$^{206}Pb/^{204}Pb$	$^{208}Pb/^{206}Pb$	$^{208}Pb/^{232}Th$	$^{207}Pb/^{235}U$	$^{206}Pb/^{238}U$	$^{207}Pb/^{206}Pb$	$^{208}Pb/^{232}Th$	$^{207}Pb/^{235}U$	$^{206}Pb/^{238}U$	$^{207}Pb/^{206}Pb$	% disc
Z2234 - D	13	7941	299	414	24	1763	8.266	0.05159	1.721	0.1710	0.07300	1016.8 ± 5.0	1016.4 ± 2.1	1017.4 ± 3.0	1014.1 ± 4.2	-0.33
Z4170 - MF	29	72735	796	6439	18	24504	27.173	0.09492	5.101	0.3297	0.11222	1832.9 ± 8.8	1836.3 ± 2.8	1836.8 ± 5.1	1835.6 ± 2.0	-0.07
Z4170 - MG	24	176826	7025	17409	69	46707	7.493	0.09575	5.164	0.3324	0.11269	1848.2 ± 8.8	1846.7 ± 2.8	1849.8 ± 5.1	1843.3 ± 2.0	-0.35
Z4170 - MD	13	79321	918	7043	11	20793	25.801	0.09500	5.079	0.3288	0.11202	1834.4 ± 8.8	1832.6 ± 2.8	1832.7 ± 5.1	1832.5 ± 2.0	-0.01
Z4170 - ME	27	93917	1169	8336	48	12575	23.970	0.09468	5.070	0.3280	0.11211	1828.4 ± 8.7	1831.1 ± 2.8	1828.8 ± 5.1	1833.8 ± 2.0	0.27
Z2908 - M4	7	15314	1765	1802	5	43796	2.616	0.09243	4.795	0.3167	0.10979	1786.8 ± 8.7	1784.0 ± 2.8	1773.8 ± 5.0	1795.9 ± 2.0	1.23
Z3345 - ME	18	65024	3141	6474	30	36031	6.191	0.09431	5.000	0.3259	0.11127	1821.6 ± 8.5	1819.3 ± 2.8	1818.4 ± 5.1	1820.2 ± 2.0	0.10
Z4598 - M1	15	35767	508	4629	141	1476	20.286	0.13655	11.797	0.4899	0.17463	2587.2 ± 12.1	2588.4 ± 3.1	2570.4 ± 6.8	2602.5 ± 2.0	1.23
Z4598 - M2	8	42178	785	5563	19	9505	15.450	0.13684	11.848	0.4920	0.17465	2592.3 ± 12.2	2592.5 ± 3.1	2579.3 ± 6.8	2602.7 ± 1.8	0.90
Z4598 - M3	21	33654	1505	4865	23	38351	6.355	0.13631	11.963	0.4956	0.17506	2582.9 ± 12.1	2601.5 ± 3.1	2595.0 ± 6.8	2606.7 ± 1.8	0.45
Z4599 - M2	4	39227	7484	8499	6	132330	1.491	0.13582	11.762	0.4933	0.17292	2574.1 ± 12.1	2585.6 ± 3.1	2585.1 ± 6.8	2586.1 ± 1.8	0.04
Z4599 - M3	4	22158	4917	5141	2	258729	1.287	0.13599	11.723	0.4921	0.17279	2577.2 ± 12.1	2582.5 ± 3.1	2579.6 ± 6.8	2584.9 ± 1.8	0.21
Z1859 - L	42	67035	775	8911	27	38760	24.537	0.14155	12.848	0.5156	0.18071	2675.8 ± 12.5	2668.5 ± 3.1	2680.6 ± 7.0	2659.4 ± 1.8	-1.0
Z1861 - L	19	40755	2698	6560	22	75300	4.293	0.14106	12.902	0.5129	0.18244	2667.2 ± 12.5	2672.5 ± 3.1	2668.9 ± 7.0	2675.2 ± 1.8	0.3
Z1409 - M1	58.4	119979	2259	10570	75	34560	15.920	0.09192	4.728	0.3168	0.10822	1777.4 ± 8.5	1772.2 ± 3.1	1774.2 ± 5.5	1769.7 ± 2.0	-0.3
Z4323 - M8	3.6	73358	6998	8976	4	123900	3.111	0.10065	5.734	0.3505	0.11866	1938.4 ± 9.2	1936.5 ± 2.9	1936.8 ± 5.4	1936.2 ± 2.0	-0.1
Z2775 - C	8.9	43727	364	2400	5	7811	37.263	0.05952	2.149	0.1982	0.07866	1168.7 ± 5.7	1164.9 ± 2.3	1165.5 ± 3.4	1163.6 ± 2.2	-0.2
Z662 - Da	11	49373	3854	5715	17	56680	3.785	0.09990	5.718	0.3494	0.11869	1924.6 ± 9.2	1934.1 ± 2.9	1931.7 ± 5.4	1936.6 ± 2.0	0.3

1. Z1234 - Geological Survey of Canada, Geochronology Laboratory sample numbers; letter code identifies individual fraction.
2. Sample weight error of ±1 µg. Concentration uncertainty varies with sample weight: >10% for sample weights <10 µg, <10% for sample weights above 10 µg. Pb* = radiogenic Pb corrected for fractionation, spike, blank and common Pb. Pbc = total common Pb corrected for spike and fractionation.
3. Ratios corrected for spike, fractionation, blank and initial common Pb, except $^{206}Pb/^{204}Pb$ ratio corrected for spike and fractionation only. One sigma errors on ratios are $^{206}Pb/^{238}U$ = 0.160%; $^{207}Pb/^{235}U$ = 0.17%; $^{208}Pb/^{232}Th$ = 0.25%.
4. $^{206}Pb/^{238}U$; $^{207}Pb/^{235}U$; $^{208}Pb/^{232}Th$; and $^{207}Pb/^{206}Pb$ ages with 2 sigma absolute error in Ma.

monazites, which are less than 0.5% discordant (normal or reverse), show good agreement between their $^{206}Pb/^{238}U$ and $^{232}Th/^{208}Pb$ ages (Fig. 1). Excluding the three analyses which are more than 0.5% discordant, the differences in $^{232}Th/^{208}Pb$ ages relative to $^{206}Pb/^{238}U$ ages are less than ±0.5%, with most analyses (~75%) differing less than 0.2%, and an average difference of less than 0.1%. The average % difference is less than the estimated two-sigma uncertainties in the individual $^{206}Pb/^{238}U$ (0.25–0.30%) and $^{232}Th/^{208}Pb$ (0.45–0.50%) ages.

Four single-grain analyses of monazites from sample Z4170 were analyzed as a measure of reproducibility of the $^{208}Pb/^{232}Th$ ages. As previously noted, SHRIMP analyses identified more than a single age population within this sample (Stern and Sanborn, 1998), and this is also observed in the U-Th-Pb TIMS data, with fraction MG having a significantly older Pb/U, Pb/Th and Pb/Pb age. The other three analyses are concordant and exhibit reproducible $^{208}Pb/^{232}Th$ ages, with a weighted mean age of 1832 ± 5 Ma (95% confidence; MSWD = 0.5). This age is within error of the weighted mean $^{207}Pb/^{206}Pb$, $^{206}Pb/^{238}U$ and $^{207}Pb/^{235}U$ ages of 1834 ± 4 Ma, 1833 ± 3 Ma, and 1833 ± 7 Ma, respectively. These data demonstrate the accuracy and reproducibility of the measured $^{208}Pb/^{232}Th$ ages.

ACKNOWLEDGMENTS

We would like to thank the staff at the geochronology laboratory who provided monazite fractions for analysis in this study. Richard Stern is thanked for his help and comments on the manuscript. Nicole Sanborn picked many of the analyzed monazite fractions. We thank Jack McRae and Klaus Santowski for technical support and Reg Thériault for his patient editing.

REFERENCES

Gibson, D.H., Parrish, R.R., and Brown, R.L.
1997: Th-Pb dating and U-Th-Pb systematics of metamorphic monazite: new insight into the interpretation of monazite crystallization ages using an example from southeastern British Columbia; Geological Association of Canada, Abstract Volume 22, p.A54.

Horowitz, E. P., Dietz, M.L., Chiarizia, R., Diamond, H., Maxwell, S.L. III, and Nelson, M.R.
1995: Separation and preconcentration of actinides by extraction chromatography using a supported liquid anion exchanger: application to the characterization of high-level nuclear waste solutions; Analytica Chimica Acta, v. 310, p. 63-78.

Loveridge, W.D.
1986: Measurement of biases in the electron multiplier ion detection system of a Finnigan-Mat model 261 mass spectrometer; International Journal of Mass Spectrometry and Ion Processes, v. 74, p. 197-206.

Parrish, R.R.
1990: U-Pb dating of monazite and its application to geological problems; Canadian Journal of Earth Sciences, v. 27, p. 1431-1450.

Parrish, R.R., Roddick, J.C., Loveridge, W.D., and Sullivan, R.W.
1987: Uranium-lead analytical techniques at the geochronology laboratory, Geological Survey of Canada; *in* Radiogenic Age and Isotopic Studies: Report 1; Geological Survey of Canada, Paper 87-2, p. 3-7.

Roddick, J.C.
1987: Generalized numerical error analysis with applications to geochronology and thermodynamics; Geochimica et Cosmochimica Acta, v. 51, p. 2129-2135.

Roddick, J.C., Loveridge, W.D., and Parrish, R.R.
1987: Precise U/Pb dating of zircon at the sub-nanogram Pb level; Chemical Geology, v. 66, p. 111-121.

Scharer, U.
1984: The effect of initial ^{230}Th equilibrium on young U-Pb ages: the Makalu case, Himalaya; Earth and Planetary Science Letters, v. 26, p. 207-221.

Stern, R.A. and Sanborn, N.
1998: Monazite U-Pb and Th-Pb geochronology by high-resolution mass spectrometry (SHRIMP): *in* Radiogenic Age and Isotopic Studies: Report 11, Geological Survey of Canada, Current Research 1998-F.

Identification of Paleoproterozoic anorthositic and monzonitic rocks in the vicinity of the Mesoproterozoic Nain Plutonic Suite, Labrador: U-Pb evidence

M.A. Hamilton[1], A.B. Ryan[2], R.F. Emslie[1], and I.F. Ermanovics[1]

Hamilton, M.A., Ryan, A.B., Emslie, R.F., and Ermanovics, I.F., 1998: Identification of Paleoproterozoic anorthositic and monzonitic rocks in the vicinity of the Mesoproterozoic Nain Plutonic Suite, Labrador: U-Pb evidence; in *Radiogenic Age and Isotopic Studies: Report 11; Geological Survey of Canada, Current Research 1998-F, p. 23-40.*

Abstract: Recent mapping along the northeast margin of the Mesoproterozoic Nain Plutonic Suite has revealed an important suite of locally deformed and variably altered anorthositic rocks. Uranium-lead zircon dating of one of these anorthositic rocks reveals a Paleoproterozoic emplacement age (2112 +5/-4 Ma), broadly equivalent to established ages of nearby 2135–2110 Ma granitic plutons in Nain craton. New Paleoproterozoic emplacement ages (2128 to 2109 Ma) are also reported here for variably foliated dioritic-monzonitic-granitic rocks in the immediate region, and together with the basic rocks belie the general lithological similarities shared with the younger anorogenic Nain Plutonic Suite plutonic assemblage.

Emplacement of diabase dyke swarms at 2121 ± 1.5 Ma and (crosscutting leucogabbro) at ca. 2045 Ma further substantiate the regional importance of Paleoproterozoic basic magmatism. Leuconoritic and monzodioritic members of the northern Nain Plutonic Suite yield crystallization ages of 1322 ± 1 Ma and 1330 ± 1 Ma, respectively. Recognition of significant Paleoproterozoic anorthositic rocks within this dominantly Mesoproterozoic magmatic province imposes important new constraints on massif anorthosite petrogenesis.

Résumé : La cartographie récente de la marge nord-est de la suite plutonique de nain du Mésoprotérozoïque a révélé la présence d'un cortège important de roches anorthositiques qui montrent une déformation locale et une altération d'importance variée. La datation d'une de ces roches par la méthode U-Pb sur zircons indique que la mise en place remonte au Paléoprotérozoïque (2 112 +5/-4 Ma), ce qui correspond largement aux âges établis (2 135–2 110 Ma) des plutons granitiques voisins du craton de Nain. Des âges paléoprotérozoïques de mise en place (2 128–2 109 Ma) des roches dioritiques, monzonitiques et granitiques inégalement feuilletées dans la région sont présentés et, avec les roches basiques, ils infirment les similarités lithologiques générales avec le cortège plutonique anorogénique plus jeune de la suite plutonique de Nain.

La mise en place d'essaims de dykes de diabase à 2 121 ± 1.5 Ma et (leucogabbro) vers 2 045 Ma confirme l'importance régionale du magmatisme basique du Paléoprotérozoïque. Des membres de la partie nord de la suite plutonique de Nain donnent des âges de cristallisation de 1 322 ± 1 Ma (leuconorite) et de 1 330 ± 1 Ma (monzodiorite). L'individualisation de roches anorthositiques paléoprotérozoïques importantes dans cette province magmatique principalement mésoprotérozoïque impose de nouvelles contraintes sur la pétrogenèse des anorthosites massives.

[1] Geological Survey of Canada, 601 Booth Street, Ottawa, Ontario K1A 0E8

[2] Geological Survey of Newfoundland and Labrador, Department of Mines and Energy, P.O. Box 8700, St. John's, Newfoundland A1B 3X5

INTRODUCTION

The discovery in recent years of a world-class Ni-Cu-Co sulphide deposit within troctolitic rocks of the Nain Plutonic Suite at Voisey's Bay has provided considerable impetus towards a more detailed investigation of its relationship to magmatic rocks of the Nain Plutonic Suite as well as to its earlier Proterozoic and Archean gneissic country rocks. Since 1995, focused exploration activity by junior mineral companies has outlined several sulphide prospects in the Alliger Lake–Puttuaalu Lake–Okak Bay area (Fig. 1; NTS 14 E/1 and 14 E/8), a northeastern region marginal to the Nain Plutonic Suite which has received comparably less mapping and fewer petrological studies to date than southern and coastal areas that are typically more accessible and better exposed.

A 1996 field program in the northern environs of the Nain Plutonic Suite, conceived by the Geological Survey of Newfoundland and Labrador and building on ongoing studies of their own and of the GSC, developed into a joint federal-provincial effort whose aim was to address, in part, the following:

1. Provision of new geological maps at 1:50 000 scale, for eventual compilation at 1:100 000 scale for this part of Labrador. Principal among these in 1996 was detailed mapping in the Alliger Lake map area (NTS 14 E/1), although additional reconnaissance mapping was accomplished elsewhere between 57°00′N and 57°30′N.
2. Investigation of detailed plutonic relations within the Alliger Lake map area, where considerable exploration for magmatic Ni sulphide was ongoing by junior companies, despite a lack of updated and comprehensive geological control.
3. Determination of precise radiometric ages for key geological units identified through the mapping program, as an exploration aid, and elucidation of the nature of the northern Nain Plutonic Suite and surrounding rocks in the context of an evolving framework of Archean and Proterozoic geochronology (e.g. Emslie and Loveridge, 1992; Hamilton et al., 1994; Connelly and Ryan, 1994; Ryan and Connelly, 1996).

This report addresses the last aim and provides new U-Pb geochronological constraints on field observations made from earlier reconnaissance studies as well as the more recent detailed mapping program. The significance of these ages is discussed with respect to Paleoproterozoic tectonic models for the western Nain craton, and to the implications for massif anorthosite genesis during the Paleo- and Mesoproterozoic.

GEOLOGICAL SETTING

Parts of the Nain Plutonic Suite were mapped as early as 1926 by E. P. Wheeler, and he continued to do so over most areas of the erstwhile Nain Anorthosite Complex up until 1974 (e.g. Wheeler, 1960; 1969). Intensive study of individual components of the troctolite-anorthosite-diorite-granite complex began with Morse (1969), which led to a decade of work with researchers and numerous students associated with the Nain Anorthosite Project from 1971 to 1981 (e.g. Berg, 1974; Ranson, 1976; Wiebe, 1988; *see* Morse, 1983 for full bibliography). Reconnaissance coverage of the Nain Plutonic Suite and its basement rocks was also provided by Taylor (1979). Field work continued in the mid-1980s with an attempt at systematic mapping of the plutonic suite and surrounding gneisses, culminating in a revised geological compilation of the Nain–Okak Bay area at 1:500 000 scale (Ryan, 1990b). Detailed petrological, geochemical, and mineralogical studies begun by Emslie and coworkers (Emslie and Russell, 1988; Emslie and Stirling, 1993) were combined with similar Nd, Sr, and Pb isotopic studies by Hamilton (1993) to establish the Nain Plutonic Suite as a working paradigm for anorthosite-mangerite-charnockite-granite complexes elsewhere (Emslie et al., 1994). More recently, detailed high-precision U-Pb analyses have been obtained on zircon- and baddeleyite-bearing members of the Nain Plutonic Suite, which define a well-constrained emplacement history for these Mesoproterozoic plutons, mostly between about 1335 and 1290 Ma (Hamilton et al., 1994), though smaller volumes of slightly older monzonitic rocks are known (to ca. 1350 Ma; Connelly, 1993; Connelly and Ryan, 1994).

In this study area (Fig. 1), the earliest descriptions of geological field relations stem from Wheeler's unpublished manuscript maps and notes, from reconnaissance mapping by Taylor (1979), and by a detailed mapping transect by Ranson (1976; 1977) in the Puttuaalu Brook–Aupalukitak Mountain–Alliger Lake area (Fig. 2). Emslie and Russell (1988) described the geology of monzonitic and granitic rocks related to the Nain Plutonic Suite around Umiakovik Lake, and intrusive relationships of syenitic and monzonitic rocks in anorthosites and leuconorites around Umiakoviarusek Lake. The polydeformational history of 3.7–2.6 Ga Nain Province Archean rocks immediately north of the field area has been summarized most recently by Ermanovics and Van Kranendonk (1998); description of these gneisses further south is provided by Ryan et al. (1997) and by Emslie et al. (1997).

The U-Pb geochronological studies of stocks of granite dated at 2137 ± 2 Ma and 2134 +3/-1 Ma (Wheeler Mountain granites; Emslie and Loveridge, 1992), and at 2110 +5/-2 Ma (Sheet Hill pluton), 2047 +14/-11 Ma (Loon Island granite), and 2032 +17/-14 Ma (Satok Island monzonite; all in Connelly and Ryan, 1994), document episodic crustal melting events of uncertain tectonic significance within Nain Province gneisses.

With the exception of areas underlain by true Nain Plutonic Suite rocks, many parts of the eastern half of the study area are transected by metagabbroic and metadiabase dykes. Principal (but not exclusive) among these are a swarm of southeast-trending (roughly 140°) dykes that locally show well preserved igneous textures, but have a widely developed metamorphic alteration to amphibole-rich assemblages (Ryan et al., 1997). These dykes are possibly correlative with the tholeiitic Napaktok dykes further north (*see* Ermanovics and Van Kranendonk, 1998). Although they have poorly constrained ages, a component of the Napaktok dykes crosscuts, and must be younger than, the ca. 2135 Ma Wheeler

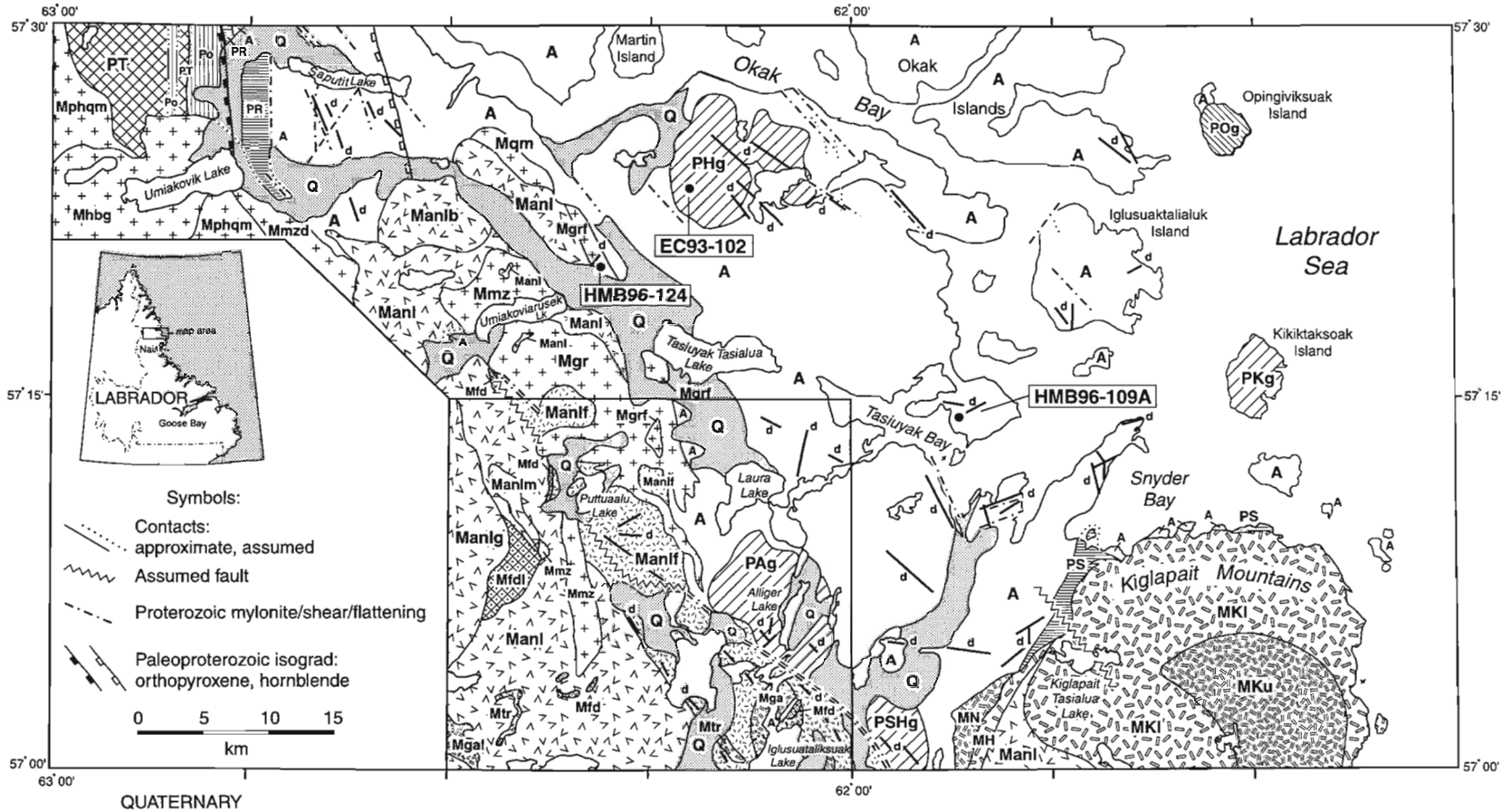

QUATERNARY

Q, Drift-covered, generally forested, areas

MESOPROTEROZOIC (M) (Nain Plutonic Suite)

Granitoid (mainly Umiakovik Lake batholith, ca.1320 Ma):
Mphqm, pyroxene-hornblende quartz monzonite; **Mhbg**, hornblende-biotite granite; **Mmzd**, monzodiorite; **Mmz**, monzonite; **Mqm**, quartz monzonite; **Mgr**, granitic rocks **Mgrf**, granitic rocks variably foliated, recrystallized (hydrated) and intruded by metadiabase (may be Paleoproterozoic)

Dioritic: **Mfd**, ferrodiorite; **Mfdl**, layered, leucoferrodiorite

Anorthositic - gabbroic: **Manl**, anorthosite - leuconorite - leucotroctolite
Manlb, black; **Manlg**, dark grey; **Manlm**, mauve

Mtr, Troctolite

Mga, Gabbroic rocks; **Mgal**, layered gabbroic rocks

Individual intrusions:
MKu and **MKl**, Kiglapait intrusion upper olivine gabbro - ferrosyenite and lower troctolite
MH, Hettasch intrusion leucotroctolite - anorthosite;
MN, North Ridge gabbro

PALEOPROTEROZOIC (P)

Torngat Orogen (Churchill Province): **PT**, Tasiuyak gneiss (1940-1895 Ma); **Po**, mainly orthogneiss

Metasedimentary rocks:
PR, Ramah Group; **PS**, Snyder Group

d, Metadiabase and metabasic dykes

Manlf, Anorthositic - leucogabbronoritic rocks variably foliated, recrystallized (hydrated) and intruded by metadiabase

Granite stocks: **PHg**, Halbach;
PAg, Alliger Lake; **PSHg**, Sheet Hill; **PKg**, Kikiktaksoak Island
POg, (ca. 1770 Ma) Opingiviksuak and Orphan islands

ARCHEAN (A)

A, Undivided quartzofeldspathic metaplutonic rocks (includes minor metasedimentary rocks, mafic granulite, ultramafic and meta-anorthositic gneiss)

***Figure 1**. Generalized geological map of the northern part of the Nain Plutonic Suite and surrounding rocks (Kiglapait Mountains to Okak Bay). The Alliger Lake map area (NTS 14 E/1) of Fig. 2 is outlined. Sample localities for geochronological studies lying outside of NTS 14 E/1 are also shown.*

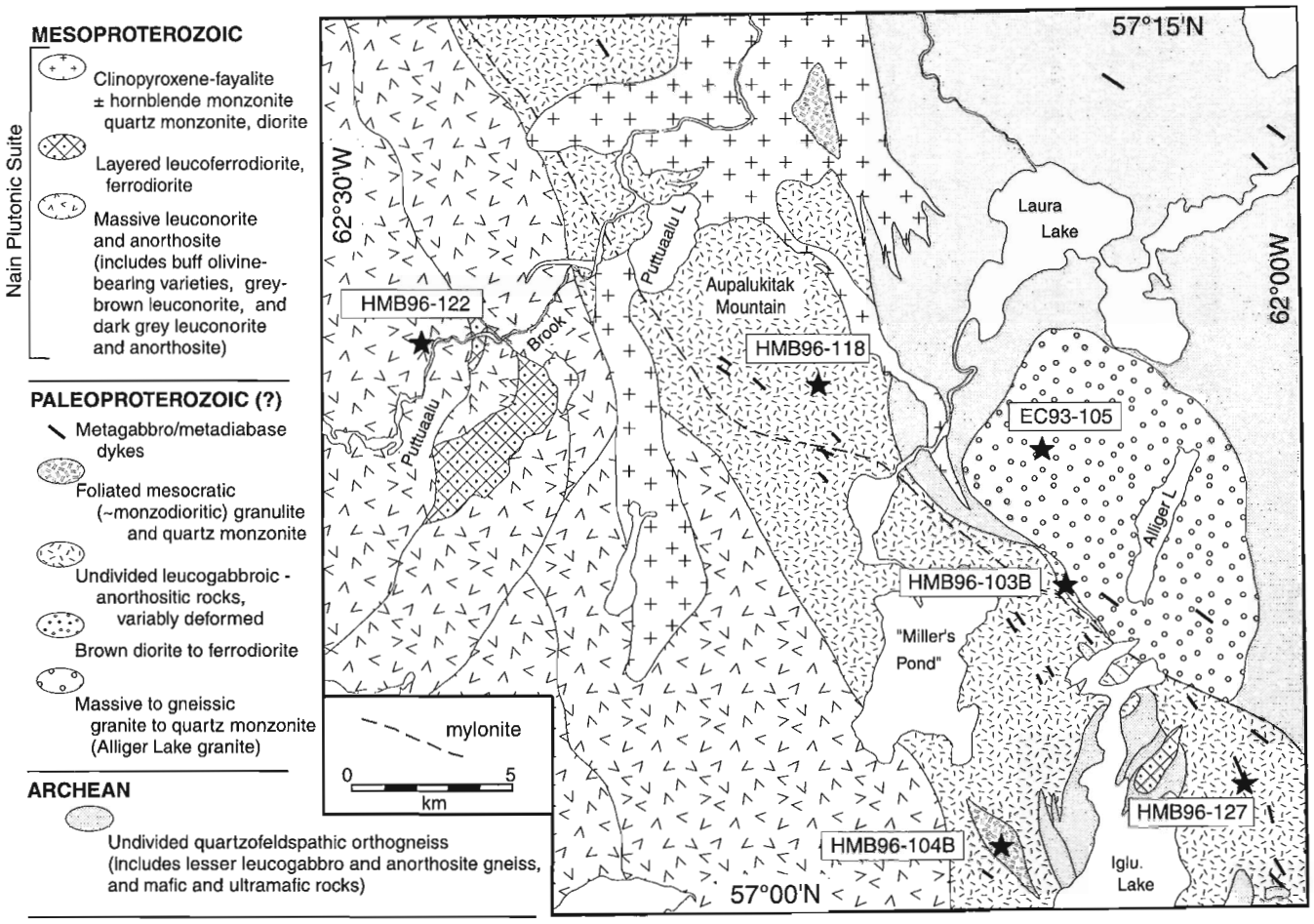

Figure 2. *Geological sketch and sample locality map of the Alliger Lake map sheet (NTS 14 E/1). Quaternary drift cover omitted for clarity.*

Mountain granites. A younger age limit for Napaktok dykes is established by the fact that in the foreland of the Torngat Orogen, they are affected by ca. 1860 Ma deformation resulting from collision of the Rae Province with the western Nain craton (Bertrand et al., 1993).

Emslie and Loveridge (1992) have also documented the intrusion of a suite of massive, locally fluorite-bearing, stocks of granite northeast of the Nain Plutonic Suite. These plutons are of limited spatial extent, occurring largely offshore, and have crystallization ages around 1778 Ma (U-Pb, zircon).

During the course of the 1996 field-mapping season, it became evident that a widespread suite of variably deformed and altered leucogabbroic to anorthositic rocks occupied the central portion of the Alliger Lake map area between Iglusuataliksuak Lake and Puttuaalu Lake (Ryan et al., 1997). Subjacent to and northeast of these rocks are several massive to foliated monzonitic intrusions lithologically similar to certain components of dated Paleoproterozoic granitoids mentioned above. Secondary mineral assemblages and deformational fabrics, likely a consequence of Torngat tectonism at ca. 1860 Ma, serve to distinguish these units from superficially similar plutonic rocks allied with the Nain Plutonic Suite that dominate the western half of the field area.

U-Pb GEOCHRONOLOGY

Geochronological sampling of representatives of some of the variably foliated and altered leuconoritic/gabbroic and monzonitic units was carried out in order to resolve first-order uncertainties regarding whether the rocks could be Paleoproterozoic magmatic rocks, or simply deformed early members of the Mesoproterozoic Nain Plutonic Suite. A southeast-trending metadiabase dyke, typical of many intruding the aforementioned leucogabbros, was sampled with the aim of providing a minimum age for the latter, as well as establishing a link between these and less-deformed diabase dykes exposed further north and east. Two samples of suspected Mesoproterozoic intrusive rocks were collected in order to provide critically underrepresented geochronological information for northern Nain Plutonic Suite magmatism.

Analytical methods

Heavy minerals were concentrated from representative samples via conventional crushing, grinding, shaking (Wilfley) table, and heavy liquid techniques. Purification of the heavy mineral concentrates was carried out using a Frantz

LB-1 isodynamic separator. Zircon grains were selected for analysis based on morphology, optical clarity, rarity of cracks, and absence of inclusions or apparent cores. In all cases, zircon grains were strongly abraded. The U-Pb analytical techniques used in this study are those outlined in Parrish et al. (1987). Treatment of analytical errors follows that outlined by Roddick (1987), with regression procedures modified after York (1969). For samples whose analyses are concordant or nearly concordant within error, the cited age is the weighted average of the $^{207}Pb/^{206}Pb$ ages, calculated according to the inverse variance of the individual analyses, following the treatment of Ludwig (1991). Analytical results, keyed to lettered fractions in the concordia diagrams, are presented in Table 1; errors on the ages are presented in the text and in concordia plots at 95% confidence limits (2σ). Where weighted mean $^{207}Pb/^{206}Pb$ ages are provided in the figures, a graphical representation of averages is presented along with the mean square of the weighted deviates (MSWD).

Paleoproterozoic magmatism

Halbach granite (EC93-102)

Immediately south of central Okak Bay, an irregular, but generally oval, stock of pink to grey, biotite-hornblende granite is exposed over some 60 km^2 (Fig. 1). Originally described and informally named by Wheeler (unpublished manuscript and maps), the Halbach granite was ascribed to the adamellite group of the Mesoproterozoic Nain Plutonic Suite. More recent investigation has shown that the intrusion is instead chemically and petrographically similar to the fluorite-bearing Wheeler Mountain, Alliger Lake, and Sheet Hill granites (Emslie et al., 1997). Like other granites in the region known or suspected to be Paleoproterozoic in age, Halbach granite locally shows recrystallization textures and is massive to moderately foliated. A suite of southeast-trending, altered diabase dykes intrudes the Halbach granite. These dykes show strong similarity to other southeast-trending dykes (ca. 2.13–1.86 Ga Napaktok dykes) which intrude both Nain Province Archean gneisses and the ca. 2135 Ma Wheeler Mountain granites.

Sample EC93-102 is a slightly pinkish-grey, fluorite-bearing, biotite-hornblende granite sampled from a prominent hilltop on the western flank of the Halbach intrusion, with a 3–5 mm grain size and rare, larger perthite grains. It has elevated whole-rock Zr concentrations (940 ppm Zr; Emslie et al., 1997) and yielded abundant colourless, water-clear, elongate, euhedral zircon prisms, some of which show rod (apatite?) and bubble inclusions. The grains lack core or overgrowth features, or well defined magmatic growth zoning (Fig. 3).

Analysis of four zircon fractions, each comprising two to eight grains, shows that U contents are consistently low (≤35 ppm). The data display only minor discordance (0.6% at worst), with the least discordant fraction (A3), being the most strongly abraded (Fig. 3). A weighted mean $^{207}Pb/^{206}Pb$ age of the fractions A2, A3, and A4 yields 2128 ± 1 Ma (MSWD = 0.11). Fraction A1, whose error ellipse and lower $^{207}Pb/^{206}Pb$ age slightly overlaps those of the other three, possibly shows minor Pb loss due to reheating during Mesoproterozoic emplacement of Nain Plutonic Suite plutons; inclusion of this fraction with the other three results in an identical weighted mean age but with a poorer fit (MSWD = 2.0). An age of 2128 ± 1 Ma is therefore regarded as the timing of crystallization of the Halbach granite.

The crystallization ages of 2137 ± 2 Ma and 2134 +3/-1 Ma determined for the Wheeler Mountain granites by Emslie and Loveridge (1992) represent the earliest recognized Paleoproterozoic magmatic activity in central Nain craton. These granites, though lying outside the area shown in Figure 1, outcrop immediately north of Martin Island and Okak Bay, and have been shown to have considerable chemical similarities to Halbach granite as well as other recognized or suspected early Paleoproterozoic granitoids in the area (Emslie et al., 1997). The age for the Halbach granite, at 2128 ± 1 Ma, is broadly similar to, but distinct from, the Wheeler Mountain suite despite their close proximity; their chemical and petrologic similarities nonetheless imply that comparable magma sources or melting processes were operating over this 6–9 million-year interval or perhaps longer (*see* below).

Illuilik monzonite, Illuilik ridge (HMB96-124)

An elongate body of variably foliated, recrystallized clinopyroxene+hornblende-bearing granite to quartz monzonite intrudes Archean quartzofeldspathic metaplutonic rocks on Illuilik ridge, south of Okak Bay and north of Tasiuyak Tasialua Lake (Fig. 1, 4). Sample HMB96-124, a moderately foliated quartz monzonite, yielded abundant elongate zircon prisms with square cross-sections (fractions A1 and A2) and well-faceted equant grains (fraction B1), all of which have very low uranium contents (38–58 ppm). Small population (n=3-7) fractions of zircon having no visible overgrowths gave nearly concordant results (0.25–0.8% discordant), which together provide a weighted mean age of 2124 ± 1 Ma (Fig. 5). This age is interpreted as the magmatic crystallization age for the quartz monzonite, and is similar to currently recognized ages of Paleoproterozoic granitoid rocks in the immediate vicinity (Wheeler Mountain granite, 2137 ± 2 Ma, 2134 +3/-1 Ma, Emslie and Loveridge, 1992; Halbach granite, 2128 ± 1 Ma (this report); Sheet Hill granite, 2110 +5/-2 Ma, Connelly and Ryan, 1994).

Tikkigatsiagak diabase, Tikkigatsiagak peninsula (HMB96-109A)

Grey- to buff-weathering quartzofeldspathic and dioritic Archean gneisses of the Nain Province, commonly displaying amphibolite- to granulite-facies metamorphic assemblages, are, in many places within the field area, intruded by variably metamorphosed basic dykes. These dykes, or subsets of them, have been considered by Ryan et al. (1997) to possibly represent equivalents of the Paleoproterozoic Domes dykes described from the Saglek Fiord area (Ryan, 1990a) and/or the Napaktok dykes of the Okak to Hebron Fiord region (Ermanovics and Van Kranendonk, 1990).

Table 1. U-Pb isotopic data.

Fraction[a]	Wt.[b] (µg)	U (ppm)	Pb[c] (ppm)	$^{206}Pb/^{204}Pb$[d]	Pb[e] (pg)	$^{208}Pb/^{206}Pb$[f]	Radiogenic ratios (± 1σ, %)[f] $^{207}Pb/^{235}U$	$^{206}Pb/^{238}U$	$^{207}Pb/^{206}Pb$	$^{207}Pb/^{206}Pb$[g] Age (Ma)	Disc.[h] %
1. EC93-102 Halbach granite (UTM Zone 20 548110 E, 6361510 N; NTS 14 E/8)											
A1 (Z)	53	34	15	4154	11	0.176	7.076 ± 0.10	0.3885 ± 0.09	0.13210 ± 0.03	2126 ± 1	0.56
A2 (Z)	51	25	11	1657	19	0.179	7.088 ± 0.12	0.3887 ± 0.09	0.13224 ± 0.06	2128 ± 2	0.61
A3 (Z)	30	17	7	1080	12	0.150	7.121 ± 0.14	0.3904 ± 0.12	0.13230 ± 0.08	2129 ± 3	0.23
A4 (Z)	23	35	15	2278	9	0.176	7.104 ± 0.12	0.3896 ± 0.10	0.13224 ± 0.05	2128 ± 2	0.38
2. HMB96-124 Illuilik quartz monzonite (UTM Zone 20 540600 E, 6356550 N; NTS 14 E/8)											
A1 (Z)	36	39	17	3233	11	0.210	7.053 ± 0.12	0.3876 ± 0.11	0.13197 ± 0.05	2124 ± 2	0.69
A2 (Z)	44	38	17	4649	9	0.199	7.072 ± 0.10	0.3890 ± 0.09	0.13184 ± 0.04	2123 ± 1	0.25
B1 (Z)	40	58	25	13612	0	0.152	7.045 ± 0.10	0.3872 ± 0.09	0.13197 ± 0.03	2124 ± 1	0.80
3. HMB96-109A Tikkigatsiagak diabase (UTM Zone 20 568945 E, 6344650 N; NTS 14 F/4)											
A (Z)	-	-	-	2868	10	0.676	6.895 ± 0.11	0.3809 ± 0.10	0.13129 ± 0.05	2115 ± 2	1.92
B (Z)	-	-	-	2015	11	0.610	6.587 ± 0.11	0.3660 ± 0.10	0.13053 ± 0.05	2105 ± 2	5.22
A1 (B)	-	-	-	795	21	0.019	7.012 ± 0.16	0.3866 ± 0.10	0.13157 ± 0.10	2119 ± 4	0.67
A2 (B)	-	-	-	903	26	0.022	7.027 ± 0.15	0.3876 ± 0.10	0.13147 ± 0.09	2118 ± 3	0.32
B1 (B)	-	-	-	2190	15	0.025	6.989 ± 0.11	0.3854 ± 0.09	0.13154 ± 0.05	2119 ± 2	0.95
B2 (B)	-	-	-	1034	25	0.021	6.981 ± 0.15	0.3851 ± 0.10	0.13148 ± 0.09	2118 ± 3	0.99
B3 (B)	-	-	-	349	8	0.023	6.960 ± 0.45	0.3841 ± 0.41	0.13143 ± 0.23	2117 ± 8	1.21
4. HMB96-118 Aupalukitak leuconorite (UTM Zone 20 545700 E, 6334000 N; NTS 14 E/1)											
A1 (Z)	366	88	38	12950	57	0.225	6.445 ± 0.10	0.3671 ± 0.08	0.12735 ± 0.03	2062 ± 1	2.60
A2 (Z)	238	70	30	35218	11	0.212	6.718 ± 0.09	0.3771 ± 0.08	0.12921 ± 0.03	2087 ± 1	1.38
A3 (Z)	-	-	-	19792	6	0.212	6.852 ± 0.10	0.3820 ± 0.08	0.13009 ± 0.03	2099 ± 1	0.74
A4 (Z)	-	-	-	11969	18	0.202	6.541 ± 0.10	0.3703 ± 0.08	0.12809 ± 0.03	2072 ± 1	2.31
5. EC93-105 Alliger Lake granite (UTM Zone 20 551400 E, 6331750 N; NTS 14 E/1)											
B (Z)	30	41	20	1442	20	0.323	6.979 ± 0.12	0.3871 ± 0.10	0.13075 ± 0.06	2108 ± 2	-0.08
C (Z)	50	20	10	1116	22	0.314	6.982 ± 0.13	0.3870 ± 0.10	0.13083 ± 0.08	2109 ± 3	0.00
D1 (Z)	15	14	7	816	6	0.359	6.984 ± 0.17	0.3860 ± 0.15	0.13121 ± 0.11	2114 ± 4	0.54
D2 (Z)	11	30	14	1576	5	0.305	6.976 ± 0.15	0.3863 ± 0.15	0.13098 ± 0.08	2111 ± 3	0.30
6. HMB96-103B Alliger diorite (UTM Zone 20 553100 E, 6327720 N; NTS 14 E/1)											
A1 (B)	4	96	36	1919	2	0.001	6.967 ± 0.14	0.3860 ± 0.13	0.13090 ± 0.06	2110 ± 2	0.31
B1 (B)	7	119	45	2868	7	0.002	6.933 ± 0.11	0.3846 ± 0.10	0.13073 ± 0.04	2108 ± 2	0.56
7. HMB96-127 Iglusuataliksuak diabase (UTM Zone 20 558550 E, 6321840 N; NTS 14 E/1											
A (B)	-	-	-	1268	9	0.015	6.393 ± 0.17	0.3676 ± 0.17	0.12612 ± 0.10	2045 ± 3	1.50
A2 (Z)	3	77	43	806	10	0.096	13.384 ± 0.22	0.5070 ± 0.19	0.19147 ± 0.09	2755 ± 3	4.92
A3 (Z)	2	72	40	1021	5	0.031	13.890 ± 0.25	0.5295 ± 0.24	0.19026 ± 0.07	2744 ± 2	0.23
8. HMB96-104B quartz monzodiorite, (UTM Zone 20 551500 E, 6319450 N; NTS 14 E/1)											
A1 (Z)	43	367	87	15014	15	0.122	2.696 ± 0.10	0.2284 ± 0.08	0.08560 ± 0.03	1329 ± 1	0.23
A2 (Z)	11	318	72	8580	6	0.063	2.699 ± 0.10	0.2286 ± 0.09	0.08563 ± 0.03	1330 ± 1	0.22
A3 (Z)	-	-	-	14812	5	0.157	2.712 ± 0.10	0.2296 ± 0.09	0.08566 ± 0.03	1330 ± 1	-0.17
9. HMB96-122 Puttuaalu Brook leuconorite (UTM Zone 20 533580 E, 6335000 N; NTS 14 E/1)											
A1 (Z)	551	36	10	11466	24	0.285	2.669 ± 0.10	0.2270 ± 0.09	0.08526 ± 0.03	1322 ± 1	0.22
A2 (Z)	770	29	8	73848	4	0.269	2.670 ± 0.10	0.2270 ± 0.08	0.08531 ± 0.03	1323 ± 1	0.30
A4 (Z)	-	-	-	3287	10	0.255	2.668 ± 0.11	0.2269 ± 0.09	0.08527 ± 0.05	1322 ± 2	0.30

[a] All zircon fractions were strongly air-abraded; (Z) = Zircon, (B) = Baddeleyite.
[b] Error on weight = ± 0.001mg. "-" = weight and concentrations not determined.
[c] Radiogenic Pb.
[d] Measured ratio corrected for spike and Pb fractionation of 0.09+0.03%/AMU.
[e] Total common Pb in analysis, corrected for fractionation and spike.
[f] Corrected for spike and blank Pb and U, and common Pb (Stacey-Kramers model Pb composition equivalent to the $^{207}Pb/^{206}Pb$ age).
[g] Age error is ± 2 s.e. in Ma.
[h] Discordance (along discordia to origin).

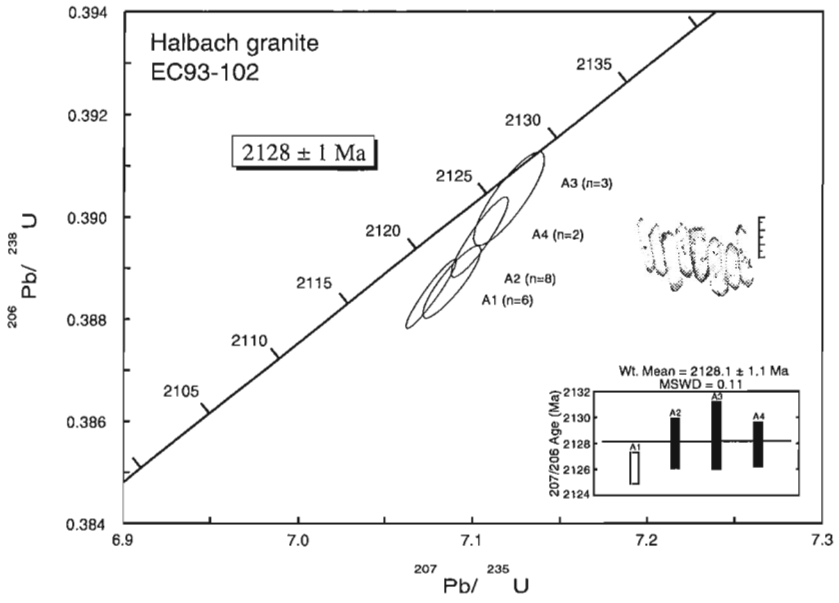

Figure 3.

Concordia diagram showing U-Pb isotopic data for zircon from the Halbach granite. Error ellipses are 2σ. Length of scale bar in photograph is 300 μm.

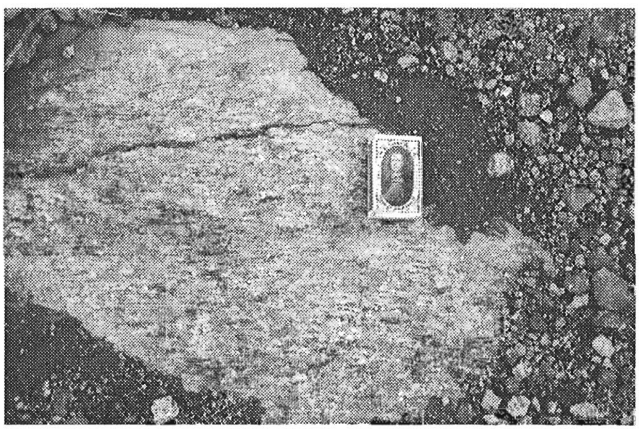

Figure 4.

Foliated quartz monzonite, Illuilik ridge (sample locality HMB96-124).

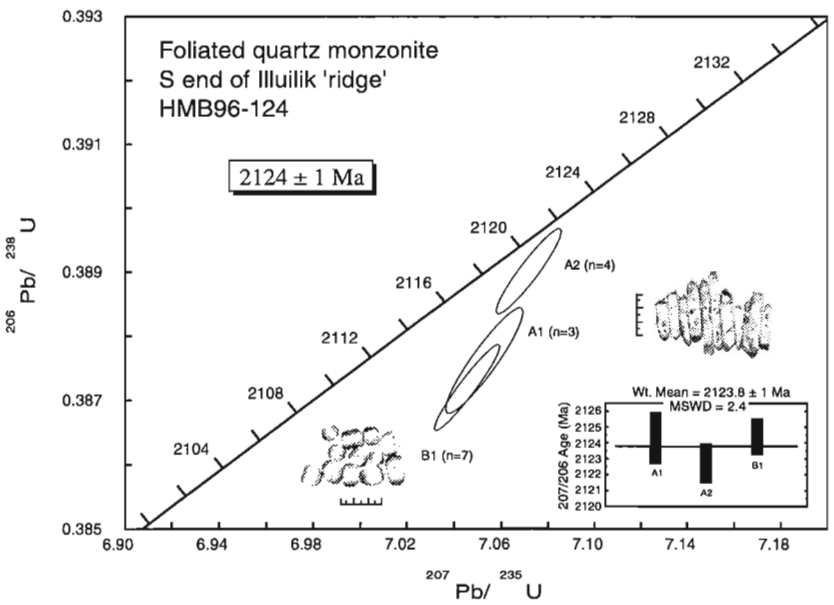

Figure 5.

Concordia diagram showing U-Pb isotopic data for zircon from the foliated quartz monzonite from the south end of Illuilik Ridge. Error ellipses are 2σ. Length of smallest scale bar division in photographs is 50 μm.

Most of these dykes are subvertical planar intrusions, less than about 15 m wide, that are traceable along strike for hundreds of metres. On Tikkigatsiagak Island, on the east side of Tasiuyak Bay and immediately east of the Alliger Lake map area, at least two sets of very thick (up to 100 m) gabbroic dykes of this type occur, striking at roughly 060° and 100° (Fig. 1). Both dyke sets are characterized by very coarse-grained diabase or gabbro with well preserved subophitic textures between pyroxene and plagioclase (Fig. 6). Foliation is locally present along dyke margins, where primary minerals are also largely replaced by secondary minerals including hornblende. Samples were collected for geochronological study from a massive, very coarse-grained (2-3 cm) northeast-striking (058°) subophitic gabbro dyke.

Abundant zircon and baddeleyite were recovered from one of the samples (HMB96-109A). Several fractions of zircon and baddeleyite were separated, hand picked and analyzed from the sample. Zircons (~50x50x100 μm) from the dyke are clear, colourless, and have a 'skeletal' appearance not uncommon in zircon precipitated from mafic magmas. Many of the grains show hollow cores (elongate to the c-axis of the crystals), while no grains show evidence of inherited cores or metamorphic overgrowths. Abundant, deep honey-coloured, striated thin blades and blade fragments of baddeleyite (~30x100 μm) are present and show very rare twins and good clarity. Extreme conditions of static electricity during sample processing precluded accurate weighing of zircon and baddeleyite grains and determination of U and Pb concentrations.

Figure 6. *Coarse-grained interior of Tikkigatsiagak diabase dyke, east side of Tasiuyak Bay (see HMB96-109A).*

Data for all analyzed grains (zircon and baddeleyite) are collinear and regression yields an upper intercept of 2121 ± 1.5 Ma, with a lower intercept of approximately 468 Ma (MSWD = 0.36; Fig. 7). The upper intercept is interpreted as the crystallization age of this dyke, and is similar to the known crystallization ages of some of the granitoid rocks in the Nain–Okak region mentioned earlier. However, no other mafic rocks in the region are known from this span of time, and the Tikkigatsiagak diabase dyke represents the first documented case of basic magmatism that appears to have attended the more widely known granitic plutonic activity such as the Wheeler Mountain granite (ca. 2135 Ma), Halbach granite (2128 Ma; *see* above), Sheet Hill granite (2110 Ma) and the Alliger Lake granite (*see* below). The Paleoproterozoic dyke is distinct in age, however, from the known 2235 Ma tholeiitic and high-magnesium noritic Kikkertavak dykes from the Hopedale block in southern coastal Labrador (Cadman et al., 1993, 1997), as well as from the ca. 1953 Ma Mugford Group, northeast of the field area, which is dominated by mafic tholeiitic lavas (Hamilton, 1994).

Aupalukitak leucogabbro to anorthosite (HMB96-118)

Rocks comprising predominantly leucogabbroic to anorthositic compositions, and likely representing several different plutons, form a northwest to southeast-trending belt across the central part of the Alliger Lake map area (Fig. 2). Between Puttuaalu and Iglusuataliksuak lakes, metaplutonic

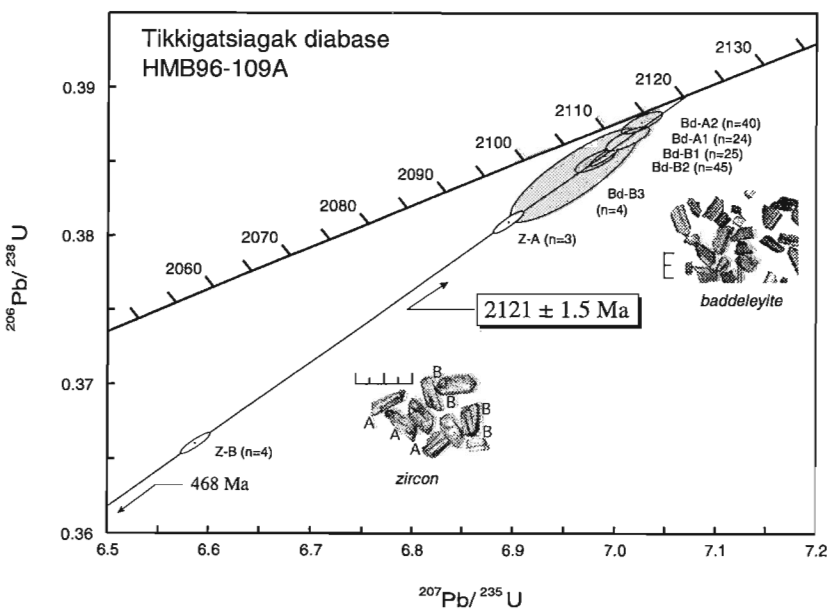

Figure 7.

Concordia diagram showing U-Pb isotopic data for zircon (Z-A, Z-B; open ellipses) and baddeleyite (Bd; shaded ellipses) from the Tikkigatsiagak diabase dyke, Tasiuyak Bay. Error ellipses are 2σ. Length of smallest scale bar division in photographs is 50 μm.

rocks of leucogabbroic composition predominate, and consist mostly of grey- to white-weathering (recrystallized) leucogabbro to anorthosite. An important observation is that the unit is intruded by abundant metamorphosed basic dykes, comprising hornblendite and metagabbro/metadiabase (see HMB96-127, below), among other compositions (Ryan et al., 1997; Emslie et al., 1997). In the Aupalukitak Mountain area (Fig. 2, centre), medium- and coarse-grained, brown orthopyroxene-bearing leuconorite and anorthosite is common, locally with secondary hornblende present as a black rim on orthopyroxene (Fig. 8). Elsewhere, pyroxene may be replaced almost entirely by pale green amphibole.

A single large prism of cloudy, pale brown zircon, over 2 cm in length, was extracted from a 0.5 m pegmatitic pod interpreted to represent trapped, fractionated magma in cumulate leuconorite on the south flank of Aupalukitak Mountain (HMB96-118). Fragments of this zircon showed no evident signs of overgrowths or cores, but were highly fractured and therefore given moderate air abrasion to minimize effects of Pb loss along these surfaces. Fractions from this sample show low concentrations of uranium (~70–90 ppm), yield relatively discordant results (0.7–2.6%), but define a moderately well constrained discordia having an upper intercept of 2112 +5/-4 Ma, and a lower intercept of 1321 ± 61 Ma (MSWD = 1.66; Fig. 9).

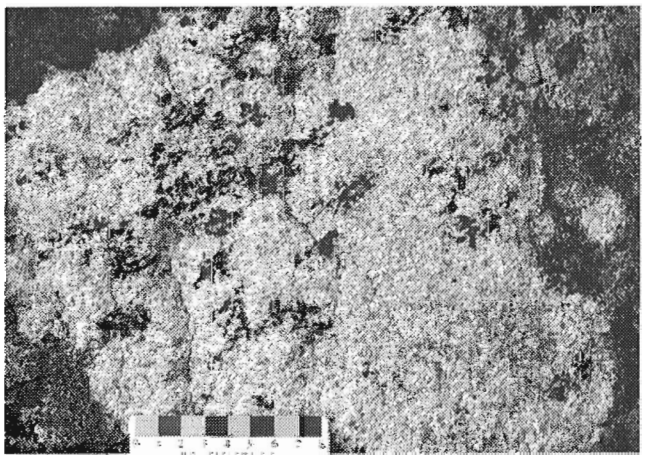

Figure 8. *Pale leuconorite in which most pyroxene is altered to amphibole, Aupalukitak Mountain area (BR96-236).*

The lower intercept age of ca. 1321 Ma is interpreted as the time of Pb loss due to a reheating event coincident with the intrusion of the voluminous Nain Plutonic Suite rocks, while the upper intercept age is interpreted as the crystallization age of the coarse-grained leuconorite unit. The elongate prismatic zircon morphology, and lack of obvious discrete metamorphic zircon grains within this unit, preclude the likelihood that the older age instead represents some Paleoproterozoic metamorphic episode. Indeed, no evidence for the ca. 1.85 Ga widespread Torngat metamorphic event is manifest, except for an associated and locally developed foliation within the Aupalukitak leucogabbro-anorthosite. The 2112 Ma crystallization age for the Aupalukitak intrusion represents a newly recognized, but previously postulated (Ryan and Connelly, 1996), period of Paleoproterozoic anorthosite formation, now known to coincide with the span of age-related 2135–2109 Ma granitoid rocks in the vicinity, and broadly with the coastal swarm of 2121 Ma basic dykes described above (Tikkigatsiagak diabase).

Alliger Lake granite (EC93-105)

Granitic rocks are generally subordinate to Proterozoic gabbroic and anorthositic units and to Archean quartzofeldspathic gneisses in the Alliger Lake map area. The Alliger Lake granite, however, is one of a number of felsic intrusions, including the Wheeler Mountain and Sheet Hill granites, that form a north-northwest–south-southeast-trending belt between Okak Bay and Webb Bay (*see* Ryan, 1990b). The Alliger Lake granite is medium grained, biotite- and hornblende-bearing, grey to pale pink, and contains distinctive opalescent blue quartz. Earlier studies by Ranson (1976),

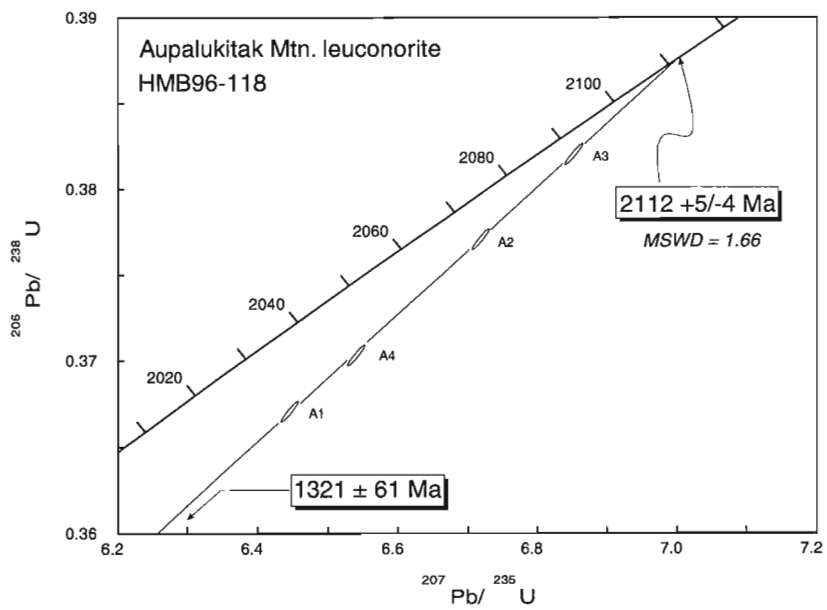

Figure 9.

Concordia diagram showing U-Pb isotopic data for zircon from the leuconorite at Aupalukitak Mountain. Error ellipses are 2σ.

together with recent remapping, has shown that this generally internally massive granite is locally strongly foliated and has complex contact relationships with surrounding country rocks. A quartz monzonitic phase of Alliger Lake 'granite' (Fig. 2) was sampled as part of a reconnaissance mapping and petrological program in 1993, with the aim of also establishing a precise crystallization age for the unit.

Four multigrain (n=7-14) fractions of clear, colourless to very pale yellow, stubby to subequant multifaceted zircon prisms were selected for analysis (sample EC93-105). Minor overgrowths were visible on some grains, but were removed through moderate air abrasion. Most of the zircons have very low U contents (<40 ppm). Two fractions are concordant, whereas fractions D1 and D2 show signs of possible minor inheritance or Pb loss (Fig. 10). The best estimate for the crystallization age of this granite is taken as the weighted mean of the two most concordant fractions (B, C), as well as fraction D2 (having overlapping errors with B, C), which yields 2109 ± 2 Ma. This age is indistinguishable from the age of the Sheet Hill pluton, lying some 10 km southeast of Alliger Lake. Further work is aimed at resolving the age of the thin zircon overgrowths.

Alliger diorite (HMB96-103B)

Immediately adjacent to the western margin of the Alliger Lake granite occurs a narrow unit of fine- to medium-grained dioritic rocks (Fig. 2). These rocks, like the Alliger Lake granite, contain opalescent blue quartz and were considered by Ranson (1976) to be gradational towards not only Alliger Lake granite to the east, but also to gabbroic rocks to the west. This relationship led Ranson to conclude that all three units

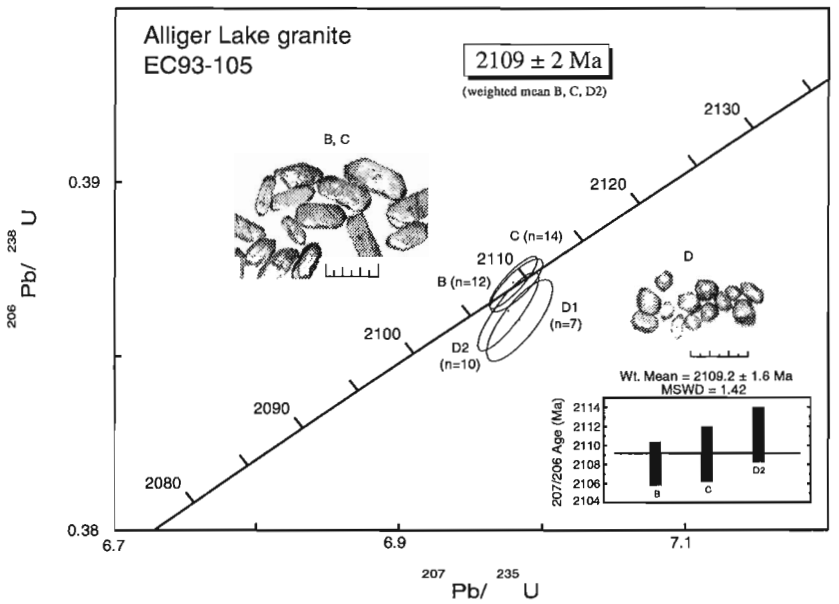

Figure 10.

Concordia diagram showing U-Pb isotopic data for zircon from the Alliger Lake granite. The age shown is the weighted mean of the three most concordant analyses (B, C, D2). Error ellipses are 2σ. Length of scale bar in photographs is 300 μm.

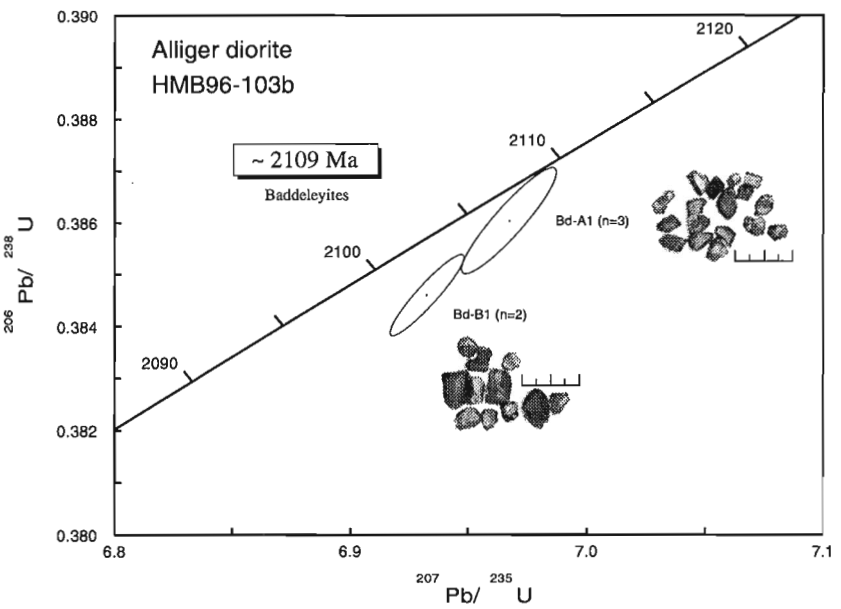

Figure 11.

Concordia diagram showing U-Pb isotopic data for baddeleyite from the Alliger diorite. Error ellipses are 2σ. Length of scale bar in photographs is 200 μm.

were likely the same age as the gabbroic rocks, then assumed to be the same age as the Nain Plutonic Suite, or Mesoproterozoic. Ryan et al., (1997, p. 33) argued, however, that field relations between these units pointed strongly to a Paleoproterozoic age. In light of the possibility of Paleoproterozoic magmatism in the area, the dioritic phase west of the Alliger Lake granite was sampled (HMB96-103B) to improve age resolution.

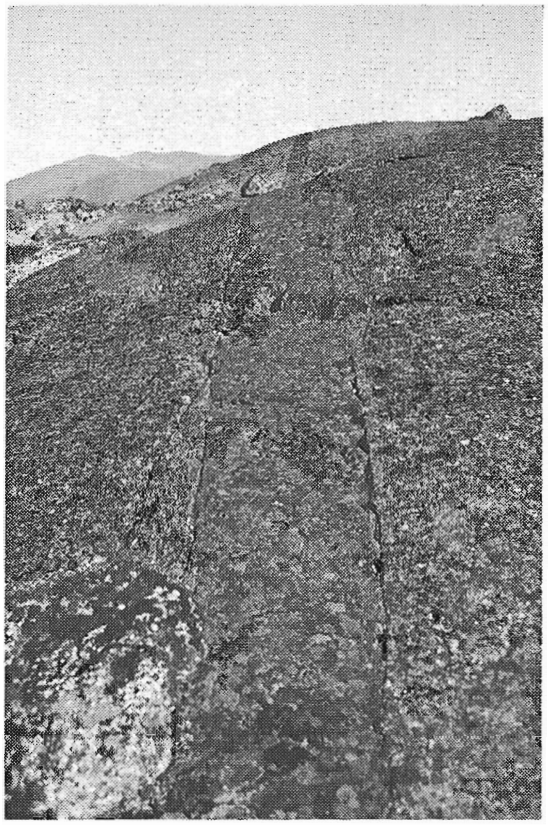

Figure 12. *Thin (<1 m) splay, adjacent main 11 m metadiabase dyke, trending 140°, intruding leucogabbro of Aupalukitak type, east of Iglusuataliksuak Lake (HMB96-127).*

Dark red-brown, blocky, subhedral to anhedral, clear baddeleyite grains were readily separated from the Alliger diorite. U-Pb data have been obtained for two baddeleyite fractions comprising 2–3 grains of ~50x100 μm dimension. These grains were morphologically robust, and fraction A1 was given one hour of standard air abrasion. Though fraction B1 (unabraded) is slightly more discordant (0.6%) than fraction A1 (0.3%), both baddeleyite fractions yield similar U contents (~100 ppm) and nearly identical $^{207}Pb/^{206}Pb$ ages (2110 ± 2 Ma, 2108 ± 2 Ma), indicating an average age of ~2109 Ma (Fig. 11), indistinguishable from that of the Alliger Lake granite. The results support the inferences from the field relations that the units described above are broadly contemporaneous.

Iglusuataliksuak metadiabase dyke (HMB96-127)

Many representatives of the anorthositic and granitoid suites described and dated above are intruded by foliated metabasic dykes which suggests that their host rocks might predate Nain Plutonic Suite plutonism (cf. Ryan et al., 1997). As an independent test of the age of the leucogabbroic rocks in the Alliger Lake map area predating the Nain Plutonic Suite, an 11 m wide metagabbroic/metadiabase dyke trending 140° was sampled east of Iglusuataliksuak Lake (HMB96-127; Fig. 2, 12). A primary crystallization age was sought to establish the accuracy of correlating metamorphosed dykes in this area with regional Paleoproterozoic dykes to the north and northeast, as well as to provide a minimum age for the gabbroic intrusions in which it occurs.

Sample HMB96-127 yielded approximately a dozen grains of non-magnetic zircon of varying quality, colour, and shape. A single, abraded grain (elongate prism) fraction (A3)

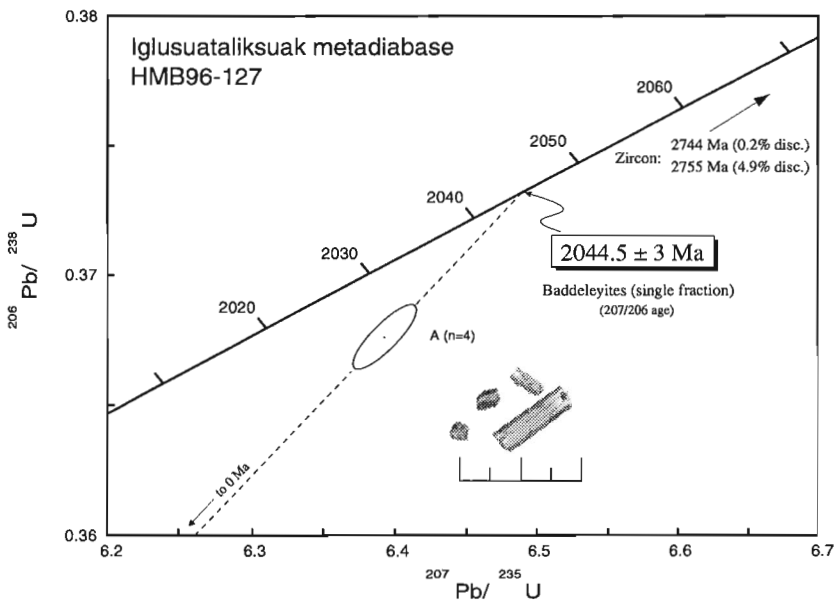

Figure 13.

Concordia diagram showing U-Pb isotopic data and preliminary age for a single fraction of baddeleyite (4 grains) from the metadiabase dyke cutting leucogabbro east of Iglusuataliksuak Lake. Reference chord through origin shown with dashed line. Error ellipses are 2σ. Length of scale bar in photograph is 200 μm.

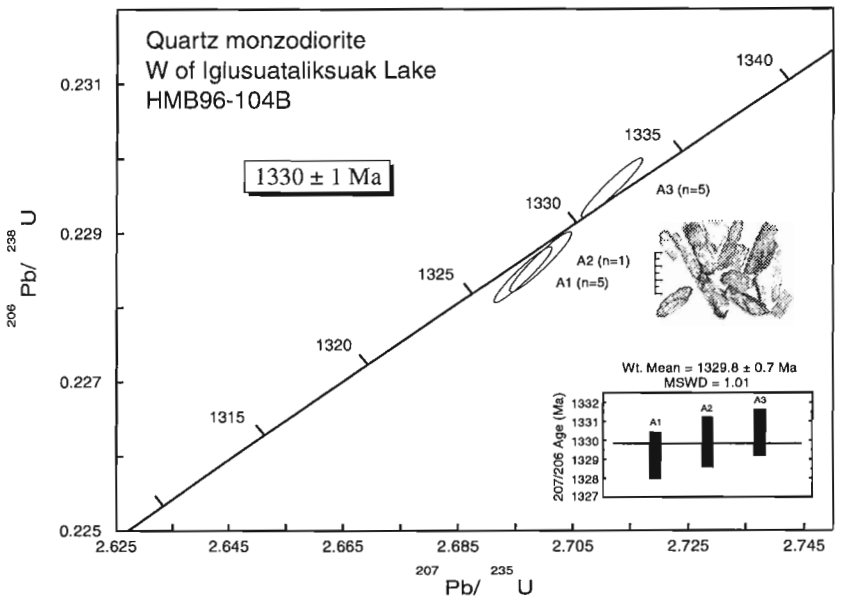

Figure 14.

Concordia diagram showing U-Pb isotopic data for zircon from the quartz monzodiorite dyke west of Iglusuataliksuak Lake. Error ellipses are 2σ. Length of scale bar in photograph is 300 μm.

yields a concordant age at 2744 ± 2 Ma, while a small multigrain fraction (A2; n=3) is somewhat discordant (5%), but has a similar $^{207}Pb/^{206}Pb$ apparent age of 2755 ± 3 Ma. Both of these ages are clearly too old for the diabase (the dyke intrudes leucogabbros equated with the Paleoproterozoic anorthositic rocks of Aupalukitak Mountain); taken together with their slightly rounded morphology, the zircons of this age are interpreted as xenocrystic. Nonetheless, they provide indirect information about the underlying Nain Province crust, whose history is poorly known, but thought to encompass components within the age range 2700–2800 Ma.

The Iglusuataliksuak dyke sample also yielded sparse (n=4) grains of baddeleyite, up to 125 μm in length (but typically <50 μm), honey-brown in colour and present as blades and blade fragments. No overgrowths of zircon were present. U-Pb data for one fraction (all grains) are slightly discordant (1.5%), but yield a $^{207}Pb/^{206}Pb$ age of 2044.5 ± 3 Ma (Fig. 13; reference line shown passes through origin). Until more data are obtained from this dyke, this age of 2045 Ma is provisionally interpreted as a minimum magmatic crystallization age for the metagabbro. The age is in good agreement with the observed field relationships because the dyke intrudes leucogabbros assumed to be temporally equivalent to analogous 2112 Ma anorthositic rocks from Aupalukitak Mountain. Moreover, the weak foliation developed in this metabasic dyke can logically be ascribed to a younger tectonometamorphism during Torngat orogenesis (ca. 1860–1775 Ma).

The provisional 2045 Ma age for the Iglusuataliksuak metadiabase dyke falls within the age range of *felsic* magmatic activity in the coastal region further southeast (Satok Island monzonite, 2032 +17/-14 Ma; Loon Island granite, 2047 +14/-11 Ma; Connelly and Ryan, 1994). Nonetheless, Ryan (1992) has described at least one set of synplutonic basic dykes within the Loon Island granite, and has noted a suite of layered basic plutonic rocks associated with monzonite on Satok Island (some 40 km southeast of Nain). It seems reasonable, therefore, to expect that a more regionally distributed mafic magmatic component of this age may be present.

Mesoproterozoic magmatism

Quartz monzodiorite dyke (HMB96-104B)

Immediately west of Iglusuataliksuak Lake, a lens-shaped unit of foliated biotite+two pyroxene monzodiorite, intruding, and locally containing blocks and fragments of, white Paleoproterozoic (?) leucogabbronorite and anorthosite, is intruded by a foliation-parallel, fresh, greenish dyke of quartz monzodiorite. This relatively fine-grained dyke is approximately 20m in maximum width and contains subcalcic augite and inverted pigeonite as its principal mafic silicates. Based on its mineralogical similarities to monzonitic varieties within the Nain Plutonic Suite, and because it transgresses older fragmental 'granulites', a sample of the dyke was collected to test age correlations and provide a minimum age for the older intrusion that hosts blocks of even older leucogabbro (Fig. 2).

Sample HMB96-104B from the quartz monzodiorite sheet yielded abundant 'woody'-textured, generally elongate, but highly fractured zircons and zircon fragments having moderate U contents (318–367 ppm). Two fractions comprising five grains (A1, A3), and one single grain fraction (A2) are less than 0.25% discordant and yield a well constrained weighted mean $^{207}Pb/^{206}Pb$ age of 1330 ± 1 Ma (MSWD = 1.0), interpreted as the time of crystallization for the monzodiorite sheet (Fig. 14).

This quartz monzodioritic dyke unambiguously represents a member of the Nain Plutonic Suite, as is suggested by compositional similarities described above, as well as its lack of deformation. The crystallization age is equivalent to certain older members of the Mesoproterozoic Nain granitoid suite, demonstrated to range, with minor exceptions, from 1335–1290 Ma (Hamilton et al., 1994; Emslie and Loveridge, 1992; Ryan et al., 1991).

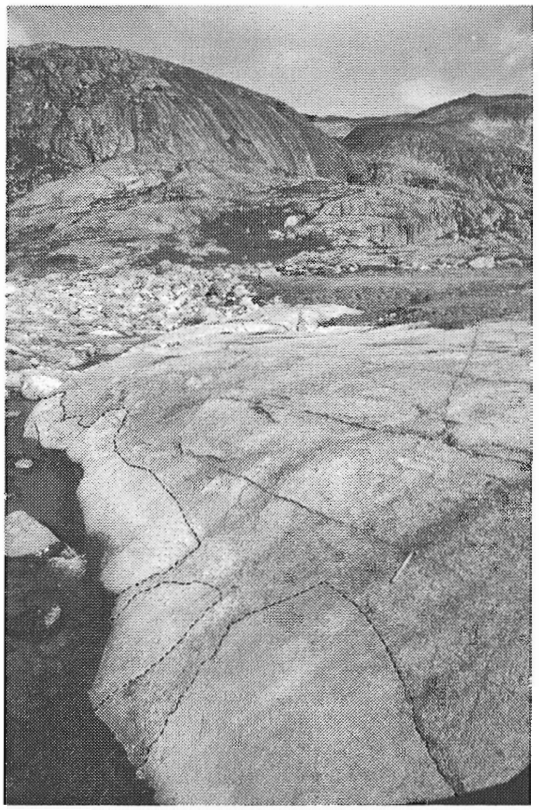

Figure 15. *Pale grey to white anorthosite blocks (outlined by dashed lines; at stream level) enclosed by dark grey leuconorite. Puttuaalu Brook area. Hammer, for scale, lies 0.5 m above block-host contact.*

Puttuaalu Brook leuconorite (HMB96-122)

Much of the western one-third of the Alliger Lake map area (14 E/1; Fig. 2) is underlain by a variety of gently dipping to locally steep, nested plutons and sheets of anorthositic, leuconoritic, and monzonitic rocks, all of which can locally be olivine-bearing, and which are typical of Mesoproterozoic intrusive rocks of the Nain Plutonic Suite. Lesser volumes of iron-rich basic rocks also occur. The westernmost marginal phase in the Alliger Lake area is a coarse-grained to pegmatoidal, dark grey Nain Plutonic Suite leuconorite-anorthosite characterized by plagioclase locally showing dark to pale blue labradorite iridescence. Inclusions of older pale grey anorthosite are present locally, and, along the central part of its eastern contact, an extensive intrusion-breccia occurs (Fig. 15).

Within a megabreccia zone along Puttuaalu Brook, dark grey pegmatoidal leuconorite matrix locally contains intergranular patches in which trapped magma has fractionated to evolved granitoid compositions. These pockets comprise quartz-K-feldspar-biotite assemblages in which stubby, pink to dark brown zircons are well developed; this type of zircon has been observed and exploited for age determination in anorthositic and troctolitic intrusions elsewhere in the Nain Plutonic Suite (e.g. Hamilton et al., 1994).

Zircons recovered from one of these patches (HMB96-122; Fig. 2) are large, clear, deep honey-coloured grains and are relatively fracture-free. Three fractions, taken from fragments of two large (1–2 mm sized) grains, have low U concentrations and yield overlapping results plotting very close to concordia. The U-Pb data for these three analyses provide a weighted mean $^{207}Pb/^{206}Pb$ age of 1322 ± 1 Ma (Fig. 16). This age represents the crystallization age for the leuconorite, and is in excellent agreement with the range of ages for other Nain Plutonic Suite troctolitic-anorthositic-noritic-ferrodioritic rocks, known at least to span the range 1330–1295 Ma (Hamilton et al., 1994). From a regional perspective, the Puttuaalu Brook leuconorite seems to have been

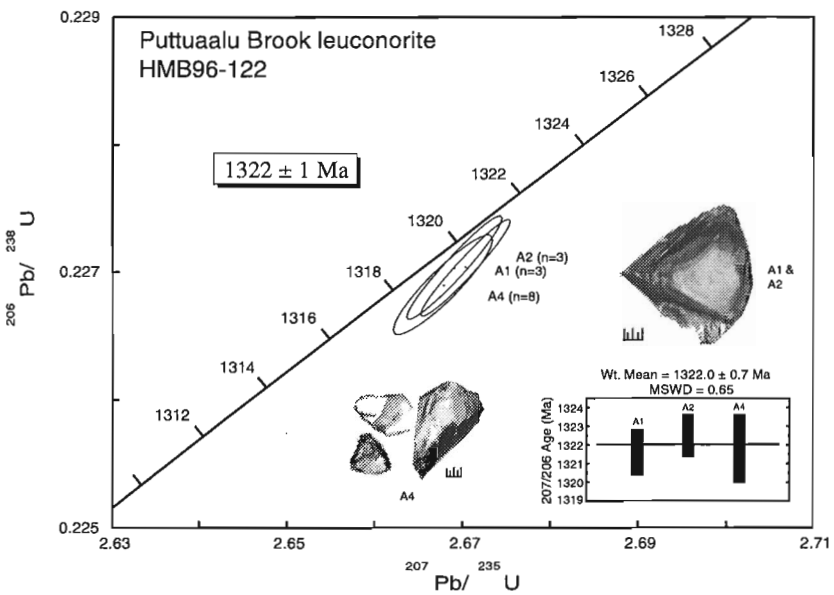

Figure 16.

Concordia diagram showing U-Pb isotopic data for zircon from the leuconorite from Puttuaalu Brook. The age shown is the weighted mean of the $^{207}Pb/^{206}Pb$ ages for the three fractions. Error ellipses are 2σ. Length of scale bar in photographs is 200 μm.

emplaced synchronously with 1322 Ma rapakivi granitoids and leuconorites in the Makhavinekh Lake area, some 100 km to the south (Ryan et al., 1991; Hamilton et al., 1994). As the Puttuaalu Brook unit appears from field relationships to be one of the younger Nain Plutonic Suite anorthositic units in the area, it therefore provides a reasonable minimum age for the remainder of the interior troctolitic and anorthositic intrusions.

DISCUSSION AND CONCLUSIONS

Ryan et al. (1997) argued, on the basis of field relationships and certain morphological characteristics of the rocks, that much of the plutonic terrane between Okak Bay and Webb Bay, traditionally assigned to the Mesoproterozoic Nain Plutonic Suite, is in fact of Paleoproterozoic age. U-Pb geochronological results reported here confirm these rocks to be components of a magmatic suite which crystallized between 2135–2109 Ma. As described by Ryan et al. (1997), the intrusions comprise granitoid (largely monzonitic to granitic) and basic (anorthositic, leuconoritic, leucogabbroic and gabbroic) compositional varieties.

Intrusions of biotite-hornblende granite and quartz monzonite were emplaced at 2128 ± 1 Ma (Halbach granite), 2124 ± 1 Ma (Illuilik quartz monzonite), and 2109 ± 2 Ma (Alliger Lake granite). Gradational to, and emplaced coevally with, the Alliger Lake granitoid was a lens or sheet of associated diorite (Alliger diorite, ~2109 Ma), separating the granite from a large mass of anorthositic and gabbroic rocks to the immediate west (Aupalukitak Mountain-type). The Paleoproterozoic granites dated here form part of a quasi-linear array of presumed crustal melts which include the Wheeler Mountain granites (2137 ± 2 Ma, 2134 +3/-1 Ma) north of Okak Bay as well as the Sheet Hill granite pluton (2110 +5/-2 Ma), immediately southeast of Alliger Lake granite, all of which may be massive to locally strongly foliated (Emslie and Loveridge, 1992; Connelly and Ryan; 1994). Although the proximity and identical age of Sheet Hill and Alliger Lake granites suggests that the two bodies may represent separately exposed lobes of the same pluton, there is enough preliminary geochemical data from representative samples of each to warrant caution in attempting a direct correlation between them (Emslie et al., 1997). A manifest age progression, from 2135 to 2109 Ma, from north to south offers tantalizing evidence towards a spatial migration of Paleoproterozoic granitoid magmatism. Geochemically, this appears to be reflected in a concomitant decrease in light/heavy-rare-earth element fractionation coupled with increasing heavy REE, and may herald either melting in different source regions, differing degrees of fractionation of parent magmas, or a steady rise in degree of melting, with time. The conspicuous southward younging of granitoid emplacement was extrapolated by Ryan and Connelly (1996), based on a smaller data set, to include the relatively small-volume granite and monzonite on Loon and Satok islands (some 60–100 km to the southeast) at roughly 2047 and 2032 Ma, respectively. However, the data presented here suggest that the southern granitoids may represent a discrete, younger, mid-Paleoproterozoic melting event allied possibly with the extension-driven swarm of southeast-trending diabase dykes such as that east of Iglusuataliksuak Lake (HMB96-127; ca. 2045 Ma).

Along the Labrador coast near Tasiuyak Bay, a series of thick, coarse-grained, northeast-trending diabase dykes intruded the Archean gneiss complex at 2121 ± 1.5 Ma. Together with an associated(?) east-southeast-trending set, these dykes bear strong resemblance to, and may correlate with, ca. 2.13–1.86 Ga Napaktok dykes and Domes dykes described north of the map area (Ermanovics and Van Kranendonk, 1990; Ryan, 1990a). Wardle et al. (1992) have described a regional, generally northeast-trending, swarm of diabase dykes (Avayalik dykes) from northernmost Nain Province, Labrador; one such dyke has yielded a preliminary age suggesting magmatic crystallization at ca. 2139 Ma (U-Pb, baddeleyite; Connelly and Mengel, 1996). The Avayalik dyke is therefore only broadly correlative with Tikkigatsiagak diabase dyke intrusion, but rather has better temporal equivalence with the oldest recognized Paleoproterozoic granitoids described above.

We note the similarity in age of the Tikkigatsiagak dyke with quartz tholeiites of the 2121 +14/-7 Ma Marathon diabase dyke swarm of the Lake Superior region (Buchan et al., 1996). Though there is no obvious direct link to be expected between the two regions, it seems reasonable to conclude that the two mafic magmatic events both record a period of finite lithospheric extension and attempted breakup of Archean crustal blocks; whether or not both 2121 Ma melting episodes reflect mantle overturn or plume-driven magmatism, as proposed for the southern margin of the Superior Province (Buchan et al., 1996), remains to be tested.

The U-Pb systematics of zircon from leuconorite at Aupalukitak Mountain establish unambiguously that substantial volumes of anorthositic, leuconoritic, and leucogabbroic magmas were emplaced in the region at approximately 2112 +5/-4 Ma. These magmas therefore, like Nain Plutonic Suite-type basic magmas, also accompanied the intrusion of similar volumes of broadly coeval granitoid melts. By inference, some of these early Paleoproterozoic granites and monzonites may be the products of lower crustal melting as a consequence of underplating by mantle-derived basic magmas which eventually gave rise to the (Paleoproterozoic) anorthositic suite (cf. Emslie et al., 1994). That the Aupalukitak zircons show effects of resetting at ca. 1320 Ma is testimony to the proximity and close spatial association with large volumes of lithologically similar anorthositic intrusions of the Mesoproterozoic Nain Plutonic Suite.

The new ages reported above for the Aupalukitak Mountain leuconorite represent confirmation that Paleoproterozoic basic plutonic rocks coexist with lithologically similar massif-type anorthosites of the Mesoproterozoic Nain Plutonic Suite (cf. Ryan and Connelly, 1996). Recent mapping in the northeast margin of the main composite anorthositic lobe of the Nain Plutonic Suite suggests that a swath of such leucogabbroic, leuconoritic, and anorthositic rocks may extend beyond the Alliger Lake map sheet area northwest

towards Okak Bay and southeast towards Webb Bay (a span of approximately 70 km), and thus represent a regionally significant volume of anorthositic magmatism predating the Nain Plutonic Suite (Ryan et al., 1997). Inasmuch as Connelly and Ryan (1994) have described foliated aplite dykes, emplaced ca. 1871 Ma, which intrude deformed anorthositic and gabbronoritic rocks between Iglusuataliksuak Lake and Webb Bay, it is possible to infer that these plutons may also be Paleoproterozoic (e.g. ca. 2100 Ma) in age.

The basic rocks described here have no known temporal counterparts elsewhere in the early Paleoproterozoic of Laurentia–Baltica. However, a widespread swarm of Jatulian iron-enriched tholeiitic (meta-)diabase dykes and sills occurs in the easternmost Fennoscandian Shield, dated in part at 2114 ± 14 Ma and 2113 ± 4 Ma (U-Pb; summarized by Vuollo et al., 1995). This predominantly northwest-southeast-trending network of continental tholeiites defines one of the most extensive magmatic events to have penetrated the Karelian and Archean domains of the Fennoscandian Shield in northeastern Finland. Events in both regions appear to document post-Archean extensional mafic magmatism followed by tectonic overprinting during Torngat and Svecokarelian Orogeny between 1900–1800 Ma.

Paleoproterozoic plutonic rocks characterized here are further distinguished from their Nain Plutonic Suite counterparts by the observation that they are in many places transected by a swarm of southeast-trending metabasic dykes. This is demonstrable within the Wheeler Mountain granites (ca. 2135 Ma) as well as the younger Alliger Lake granite (2109 Ma). A representative metamorphosed diabase dyke was emplaced at or before ca. 2045 Ma, and constrains the age of its host leucogabbroic rocks east of Iglusuataliksuak Lake to be at least this old. This preliminary age of metabasic dyke intrusion records a period of lithospheric extension heretofore unrecognized but which coincides with a documented time of granitoid magmatism east of Nain, on Loon and Satok islands. Although detailed petrological and geochemical data on these 2047–2032 Ma magmatic rocks are lacking, the U-Pb geochronological data appear to record a period of intracontinental extension as earlier proposed by Ryan and Connelly (1996).

The age of the 140° striking dykes, at ca. 2045 Ma, and their restriction to Archean and Paleoproterozoic gneisses and metaplutonic rocks of the western Nain craton, is reminiscent of Kangâmiut dykes of west Greenland. Zircons from the predominant, late, northeast-trending component of tholeiitic Kangâmiut dykes have recently been dated by SHRIMP ion probe at 2046 ± 8 Ma (Kalsbeek and Nutman, 1996). Together, these data strongly suggest similar processes of lithospheric extension immediately preceding Torngat and Nagssugtoquidian Orogeny on the western and northwestern margin of the North Atlantic craton, respectively. In addition, voluminous extrusion of basaltic lavas of the Mugford Group through continental lithosphere, exposed some 40 km northeast of Okak Bay, suggests that fragmentation was accelerating by approximately 1950 Ma.

The ages presented herein collectively chronicle a period of overlapping anorthositic and granitoid magmatism from ~2135 to 2109 Ma. By analogy with Mesoproterozoic anorthosite-mangerite-charnockite-granite suites, we speculate that the Paleoproterozoic anorthositic and associated monzonitic-granitic magmatism was also dominantly anorogenic in character, occurring during a period of relative tectonic quiescence between late Archean tectonic assembly of western Nain craton (ca. 2550 Ma; e.g. Connelly and Ryan, 1996) and the onset of late Paleoproterozoic Nain–Rae collision during Torngat Orogen (ca. 1860 Ma; Bertrand et al., 1993). Taken together, the evidence of bimodality within the major 2135–2109 Ma magmatic suites, and the profusion of regional diabase dyke swarms (in part dated at 2121 Ma) points towards a model of continental extension and perhaps fragmentation. Consideration of renewed diabase dyke intrusion and coeval granitoid suites at 2047–2030 Ma, and by deposition of supracrustal sequences of Ramah and Mugford groups (Fig. 1) adds further credence to an overall theme involving Paleoproterozoic crustal attenuation.

It bears speculation as to whether deposition during the earliest Proterozoic of Snyder Group sediments, a third supracrustal assemblage in northern Labrador (Fig. 1), in fact coincided with development of local rift basins in Nain Province Archean gneisses during the 2135–2109 Ma magmatic event described here. Conclusions regarding the timing of Ramah Group deposition are possibly improved; intrusion of Napaktok dykes predates Ramah Group quartzite cover sequences and provides a maximum age for Ramah Group if some of the dykes can be correlated with the 2121 Ma Tikkigatsiagak diabase. This constraint is in general agreement with the observation that Napaktok dykes intrude and therefore postdate the ca. 2135 Ma Wheeler Mountain granites north of Okak Bay (Ermanovics and Van Kranendonk, 1990). Tectonic and metamorphic overprinting during ca. 1860 Ma Torngat Orogeny establish a minimum age limit for Napaktok dyke intrusion and Ramah Group deposition.

Figure 17 is a graphic compilation of age data for samples from this study and other published data for rocks of mid-Paleoproterozoic age in central and northern Labrador. The data clearly show the discrete age groupings of semicontinuous ~2137–2109 Ma granitoid, dioritic, anorthositic (leuconorite-leucogabbro) magmatism, and diabase dyke intrusion, and an apparently punctuated repetition of bimodal granitoid-diabase igneous activity between 2047–2032 Ma.

The two age determinations reported here for monzonitic and anorthositic magmatic components of the Mesoproterozoic Nain Plutonic Suite, at 1330 ± 1 Ma and 1322 ± 1 Ma, respectively, represent the first precise dates for plutonic rocks in the northern central batholithic mass of the Nain complex. The age of the Puttuaalu Brook leuconorite significantly predates the emplacement and crystallization of the troctolitic Kiglapait intrusion, some 45 km to the east, dated at 1307 ± 1 Ma (Hamilton, 1997), but is only marginally older than the oldest recognized (fayalite+quartz) monzodiorites of the Umiakovik Lake granitoid batholith , flanking the anorthositic rocks to the northwest (Emslie and Loveridge, 1992). The 1330 Ma quartz monzonite sheet west of Iglusuataliksuak Lake establishes a minimum age for host mesocratic

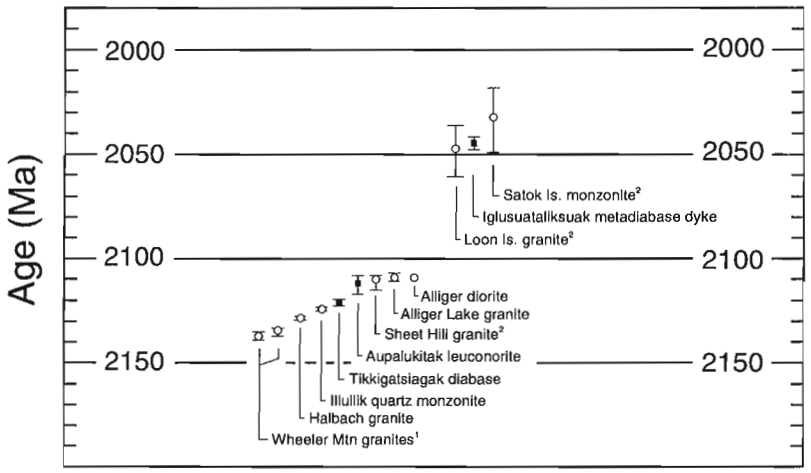

Figure 17.

Summary diagram showing U-Pb isotopic data for Paleoproterozoic intrusive rocks from northern central Labrador. Filled squares represent basic units; open circles are granitoids or related diorite. Published ages: [1]Emslie and Loveridge (1992); [2]Connelly and Ryan (1994).

granulites and thereby also for leucogabbroic and anorthositic blocks carried as xenoliths within the latter; it is possible that the xenolithic material is Paleoproterozoic in age, possibly kindred to anorthositic rocks from Aupalukitak Mountain. Both Mesoproterozoic ages determined here are characteristic of the known range of crystallization ages for Nain Plutonic Suite plutons, and support earlier contentions that the complete span of basic and granitic magmatism during this event was on the order of about 60 Ma.

The recognition of significant volumes of Paleoproterozoic anorthositic rocks within this dominantly Mesoproterozoic magmatic province has important implications for genetic models of massif anorthosite. The Nain Plutonic Suite is for the most part centred on, and intrudes, a significant terrane boundary — namely, the tectonic suture between western Nain and eastern Rae provinces, constructed 400–500 Ma earlier during Torngat Orogeny. The results presented in this paper suggest that the marginal foreland of the Torngat Orogen, interpreted to parallel the rifted west margin of Nain craton was also an earlier site of anorthositic and monzonitic magmatism during the Paleoproterozoic. That this region should be the continued locus of anorthositic and associated granitoid magmatism at ca. 2100 Ma and ca. 1300 Ma is remarkable. Both suites are most likely related to melting driven by lithospheric extension, but it is questionable whether the process was similar in each case. Petrogenetic models invoking special mantle source characteristics are challenged to explain how the same source in each case would survive lithospheric modification through an intervening tectonic reworking at ca. 1860 Ma. General models advocating significant mantle-crust interaction for anorthosite-mangerite-charnockite-granite complexes (e.g. Emslie at al., 1994) may well be applicable to the Paleoproterozoic suite described here; tracer isotopic studies are in progress to aid in evaluating these processes.

An analogous comparison can be made with the Mesoproterozoic (ca. 1435 Ma) Laramie anorthosite complex of Wyoming, recently shown to have intruded adjacent to the strongly recrystallized Paleoproterozoic (ca. 1760 Ma) Horse Creek anorthosite (+granite/monzonite) complex (Scoates and Chamberlain, 1997). In this case, emplacement of the Horse Creek anorthosite complex was synchronous with arc accretion and development of the Cheyenne belt, a crustal-scale shear separating Wyoming Province Archean crust to the north from juvenile Proterozoic rocks to the south. Renewed anorthositic and granitic magmatism of the Laramie anorthosite complex followed approximately 325 Ma later, intruding the terrane boundary. In Labrador, both episodes of anorthositic (and associated granitoid) plutonism can be accommodated in general models of lithospheric thinning, though it is unclear why a spatial-petrological relationship persisted over a considerably longer interim of 800 Ma.

Several Ni-Cu sulphide prospects within the map area appear to be hosted by a variety of plutonic rocks, both Mesoproterozoic *and* possibly Paleoproterozoic in age (Kerr and Smith, 1997; Ryan et al., 1997). If a Voisey's Bay exploration model is sought, then accurate identification of direct Nain Plutonic Suite-related magmatic suites is paramount in establishing whether the showings bear significant analogous economic potential. Alternatively, discovery of notable magmatic sulphide prospects in Paleoproterozoic intrusive equivalents would represent a supplementary new exploration target in the region.

ACKNOWLEDGMENTS

Jack MacRae, Diane Bellerive, and Klaus Santowski of the Geochronology Laboratory are warmly thanked for their expert and invaluable assistance in acquiring the U-Pb data. Mike Villeneuve and Reg Thériault provided thorough and helpful critical comments that resulted in material improvements to the manuscript. Dianne Paul and Katherine Venance are thanked for expert assistance with some of the final figures.

REFERENCES

Berg, J.H.
1974: Further study of the Hettasch intrusion and associated rocks; *in* The Nain Anorthosite Project, Labrador: Field Report 1973, (ed.) S.A. Morse; Department of Geology and Geography, University of Massachusetts, Amherst, Massachusetts, Contribution No. 13, p. 107-119.

Bertrand, J.-M., Roddick, J.C., Van Kranendonk, M.J., and Ermanovics, I.
1993: U-Pb geochronology of deformation and metamorphism across a central transect of the Early Proterozoic Torngat Orogen, North River map area, Labrador; Canadian Journal of Earth Sciences, v. 30, p. 1470-1489.

Buchan, K.L., Halls, H.C., and Mortensen, J.K.
1996: Paleomagnetism, U-Pb geochronology, and geochemistry of Marathon dykes, Superior Province, and comparison with the Fort Frances swarm; Canadian Journal of Earth Sciences, v. 33, p. 1583-1595.

Cadman, A.C., Heaman, L., Tarney, J., Wardle, R.J., and Krogh, T.E.
1993: U-Pb geochronology and geochemical variation within two Proterozoic mafic dyke swarms, Labrador; Canadian Journal of Earth Sciences, v. 30, p. 1490-1504.

Cadman, A.C., Tarney, J., and Hamilton, M.A.
1997: Petrogenetic relationship between Palaeoproterozoic tholeiitic dykes and associated high-Mg noritic dykes, Labrador, Canada; Precambrian Research, v. 82, p. 63-84.

Connelly, J.N.
1993: U-Pb Geochronological Research Agreement: final report for the Newfoundland Department of Mines and Energy, Labrador Mapping Section; Report on file with Newfoundland Geological Survey.

Connelly, J.N. and Mengel, F.C.
1996: The Archean backdrop to Paleoproterozoic tectonism in the Nagssugtoqidian and Torngat orogens: new constraints from U-Pb geochronology; *in* Lithoprobe Eastern Canadian Shield Onshore-Offshore Transect (ECSOOT), Report of 1993 Transect Meeting, (ed.) R.J. Wardle and J. Hall; The University of British Columbia, Lithoprobe Secretariat , Report No. 36, p. 15-24.

Connelly, J.N. and Ryan, B.
1994: Late Archean and Proterozoic events in the central Nain craton; *in* Lithoprobe Eastern Canadian Shield Onshore-Offshore Transect (ECSOOT), Report of 1993 Transect Meeting, (ed.) R.J. Wardle and J. Hall; The University of British Columbia, Lithoprobe Secretariat, Report No. 36, p. 53-61.

Emslie, R.F. and Loveridge, W.D.
1992: Fluorite-bearing Early and Middle Proterozoic granites, Okak Bay area, Labrador: Geochronology, geochemistry and petrogenesis; Lithos, v. 28, p. 87-109.

Emslie, R.F. and Russell, W.J.
1988: Umiakovik Lake batholith and other felsic intrusions, Okak Bay area, Labrador; *in* Current Research, Part C; Geological Survey of Canada, Paper 88-1C, p. 27-32.

Emslie, R.F. and Stirling, J.A.R.
1993: Rapakivi and related granitoids of the Nain Plutonic Suite: geochemistry, mineral assemblages and fluid equilibria; Canadian Mineralogist, v. 31, p. 821-847.

Emslie, R.F., Ermanovics, I.F., and Ryan, A.B.
1997: Geology of the northern Nain Plutonic Suite and its envelope rocks, Labrador; *in* Current Research 1997-C; Geological Survey of Canada, p. 223-234.

Emslie, R.F., Hamilton, M.A., and Thériault, R.J.
1994: Petrogenesis of a mid-Proterozoic anorthosite-mangerite-charnockite-granite (AMCG) complex: isotopic and chemical evidence from the Nain Plutonic Suite; Journal of Geology, v. 102, p. 539-558.

Ermanovics, I.F. and Van Kranendonk, M.J.
1990: The Torngat Orogen in the North River-Nutak transect area of Nain and Churchill Provinces; Geoscience Canada, v. 17, p. 279-283.

Ermanovics, I.F. and Van Kranendonk, M.J.
1998: Geology of the Archean Nain Province and Paleoproterozoic Torngat orogen in a transect of the North River–Nutak map area, Newfoundland and Quebec; Geological Survey of Canada Bulletin 497, 164 p.

Hamilton, M.A.
1993: Contamination of massif anorthosite and Precambrian crustal evolution in central Labrador: a combined trace element and Sr, Nd and Pb isotopic study; PhD thesis, University of Massachusetts, Amherst, Massachusetts, 195 p.
1994: Tholeiitic and weakly alkalic basaltic volcanism of the Mugford Group, northern Labrador: preliminary geochemical results; *in* Current Research 1994-C; Geological Survey of Canada, p. 333-342.
1997: New U-Pb geochronological results from the Mesoproterozoic Nain Plutonic Suite, Labrador, and implications for the origin and emplacement of massif anorthosites and related rocks; *in* Proterozoic Orogenies and Plate Interactions - The North Atlantic Region in Space and Time; COPENA 1997 - IGCP 371 Conference, 18-22 August, 1997, Trondheim, Norway.

Hamilton, M.A., Emslie, R.F. and Roddick, J.C.
1994: Detailed emplacement chronology of basic magmas of the mid-Proterozoic Nain Plutonic Suite, Labrador: insights from U-Pb systematics in zircon and baddeleyite; Eighth International Conference on Geochronology, Cosmochronology and Isotope Geochemistry [Program Abstracts], United States Geological Survey, Circular 1107, p. 124.

Kalsbeek, F. and Nutman, A.P.
1996: Anatomy of the Early Proterozoic Nagssugtoqidian Orogen, West Greenland, explored by reconnaissance SHRIMP U-Pb zircon dating; Geology, v. 24, p. 515-518.

Kerr, A. and Smith, J.L.
1997: The search for magmatic Ni-Cu-Co mineralization in northern Labrador: a summary of active exploration programs; *in* Current Research, Geological Survey Branch, Newfoundland Department of Mines and Energy, Report 97-1, p. 73-91.

Ludwig, K.R.
1991: ISOPLOT: a plotting and regression program for radiogenic-isotope data; version 2.53, U.S. Geological Survey, Open File Report, 91-445, 41 p.

Morse, S.A.
1969: The Kiglapait Layered Intrusion, Labrador; Geological Society of America, Memoir 112, 204 p.
1983: Nain bibliography; *in* Field Report 1981, (ed.) S. A. Morse; Department of Geology and Geography, University of Massachusetts, Amherst, Massachusetts, Contribution No. 40, p. 130-138.

Parrish, R.R., Roddick, J.C., Loveridge, W.D., and Sullivan, R.W.
1987: Uranium-lead analytical techniques at the geochronology laboratory; Geological Survey of Canada; *in* Radiogenic Age and Isotopic Studies: Report 1; Geological Survey of Canada, Paper 87-2, p. 3-7.

Ranson, W.A.
1976: Geology of the Ighlokhsoakhtaliksoakh Lake area; *in* The Nain Anorthosite Project, Labrador: Field Report 1975, (ed.) S.A. Morse; Department of Geology and Geography, University of Massachusetts, Amherst, Massachusetts, Contribution No. 26, p. 35-43.
1977: Anorthositic and monzonitic rocks near Puttuaaluk Lake, Labrador; *in* The Nain Anorthosite Project, Labrador: Field Report 1976, (ed.) S.A. Morse; Department of Geology and Geography, University of Massachusetts, Amherst, Massachusetts, Contribution No. 29, p. 21-32.

Roddick, J.C.
1987: Generalized numerical error analysis with applications to geochronology and thermodynamics; Geochimica et Cosmochimica Acta, v. 51, p. 2129-2135.

Ryan, B.
1990a: Basement-cover relationships and metamorphic patterns in the foreland of the Torngat Orogen in the Saglek-Hebron area, Labrador; Geoscience Canada, v. 17, p. 276-279.
1992: Nain area geology: observations on selected islands, and the area south of Nain Bay (NTS 14C/6, 14; 14D/9); *in* Current Research, Geological Survey Branch, Newfoundland Department of Mines and Energy, Report 92-1, p. 381-398.

Ryan, B. (comp.)
1990b: Preliminary geological map of the Nain Plutonic Suite and surrounding rocks (Nain–Nutak, NTS 14 SW); Newfoundland Department of Mines and Energy, Geological Survey Branch, Map 90-44, Scale 1:500 000.

Ryan, B. and Connelly, J.N.
1996: Paleoproterozoic plutonism in the Nain area: similar rocks (but differing origins?) to the Mesoproterozoic Nain Plutonic Suite; *in* Proterozoic Evolution in the North Atlantic Realm (compiled by C. Gower), COPENA-ECSOOT-IBTA conference, Goose Bay, Labrador, July 29-August 2, 1996, Program and Abstracts, p. 156-157.

Ryan, B., Hynes, A., and Ermanovics, I.
1997: Geology of the Nain Plutonic Suite and its country-rock envelope, Alliger Lake area (NTS 14 E/1), Labrador; *in* Current Research, Geological Survey Branch, Newfoundland Department of Mines and Energy, Report 97-1, p. 29-47.

Ryan, B., Krogh, T.E., Heaman, L., Schärer, U., Philippe, S., and Oliver, G.
1991: On recent geochronological studies in the Nain Province, Churchill Province and Nain Plutonic Suite, north-central Labrador; *in* Current Research, Geological Survey Branch, Newfoundland Department of Mines and Energy, Report 91-1, p. 257-261.

Scoates, J.S. and Chamberlain, K.R.
1997: Orogenic to post-orogenic origin for the 1.76 Ga Horse Creek anorthosite complex, Wyoming, USA; Journal of Geology, v. 105, p. 331-343.

Taylor, F.C.
1979: Reconnaissance geology of a part of the Precambrian Shield, northeastern Quebec, northern Labrador and Northwest Territories; Geological Survey of Canada Memoir 393, 99 p.

Vuollo, J.I., Nykänen, V.M., Liipo, J.P., and Piirainen, T.A.
1995: Palaeoproterozoic mafic dyke swarms in the eastern Fennoscandian Shield, Finland: a review; *in* Physics and Chemistry of Dykes, (eds.) Baer and Heimann; Balkema, Rotterdam, p. 179-192.

Wardle, R.J., Van Kranendonk, M., Mengel, F., and Scott, D.
1992: Geological mapping in the Torngat Orogen, northernmost Labrador: preliminary results; *in* Current Research, Geological Survey Branch, Newfoundland Department of Mines and Energy, Report 92-1, p. 413-429.

Wheeler, E.P., 2nd
1960: Anorthosite-adamellite complex of Nain, Labrador; Geological Society of America Bulletin, v. 71, p. 1755-1762.
1969: Minor intrusives associated with the Nain anorthosite; *in* Origin of Anorthosite and Related Rocks, (ed.) Y. W. Isachsen; New York State Museum and Science Service, Memoir 18, p. 189-206.

Wiebe, R.A.
1988: Structural and magmatic evolution of a magma chamber: the Newark Island layered intrusion, Nain, Labrador; Journal of Petrology, v. 29, p. 383-411.

York, D.
1969: Least-squares fitting of a straight line with correlated errors; Earth and Planetary Science Letters, v. 5, p. 320-324.

U-Pb ages of Archean crust in the southeast arm of the Rae Province, southeastern Ungava Bay, Quebec

David J. Scott[1]

Scott, D.J., 1998: U-Pb ages of Archean crust in the southeast arm of the Rae Province, southeastern Ungava Bay, Quebec; in *Radiogenic Age and Isotopic Studies: Report 11; Geological Survey of Canada, Current Research, 1998-F, p. 41-45.*

Abstract: Two samples from southeastern Ungava Bay have been dated using the U-Pb method on zircon and monazite. A hornblende tonalite from Keglo Bay crystallized at 3019 ± 5 Ma, and was metamorphosed at 1838 ± 2 Ma (monazite). A second tonalite, from Gregson Inlet, crystallized at 2784 ± 9 Ma, and was metamorphosed at ~2666 Ma (zircon overgrowth) and 1834 ± 2 Ma (monazite). These results are the first confirmation of Archean crust in the area between the George River and Abloviak shear zones. The cratonic affinity of these rocks is uncertain.

Résumé : Deux échantillons provenant de la Baie de l'Ungava ont été datés par la méthode U-Pb sur zircon et monazite. Une tonalite à hornblende, provenant de la baie Keglo, a crystallisé à 3 019 ± 5 Ma et a été métamorphisée à 1 838 ± 2 Ma (âge sur monazite). Une deuxième tonalite, provenant de l'anse Gregson, a crystallisé à 2 784 ± 9 Ma, et a été métamorphisée à ~2 666 Ma (âge d'une surcroissance de zircon) et à 1 834 ± 2 Ma (âge sur monazite). Ces résultats confirment pour la première fois la présence d'un socle archéen dans la région entre les zones de cisaillement de la rivière George et du fiord d'Abloviak. L'affinité cratonique de ces roches est incertaine.

[1] Geological Survey of Canada, 601 Booth Street, Ottawa, Ontario K1A 0E8

INTRODUCTION

The Precambrian geology of southeastern Ungava Bay comprises a relatively poorly known assemblage of metaplutonic rocks of assumed Archean age, as well as Paleoproterozoic metaplutonic and metasedimentary rocks (Fig. 1). The bedrock geology of the area was documented at reconnaissance scale in the 1970s by Taylor (1979). More recent investigations in the vicinity include those of Goulet and Ciesielski (1990), Van Kranendonk et al. (1994), and most recently, Bardoux et al. (1996). An outstanding, first-order question is to what extent is Archean crust present in the area, and, if present, what is its cratonic affinity.

The objective of this investigation is to determine the age of crystallization and subsequent metamorphism of metaplutonic rocks of the area that, based on field relationships, have been interpreted as possible tectonostratigraphic 'basement' to Paleoproterozoic units. In this report, results from two samples of representative orthogneiss are presented. This work contributes to the Geological Survey of Canada's northeast Laurentia program and the LITHOPROBE Eastern Canadian Shield Onshore-Offshore Transect (ECSOOT), and will facilitate a first-order comparison of geological events in the Ungava Bay area with those on southern Baffin Island and northernmost Labrador.

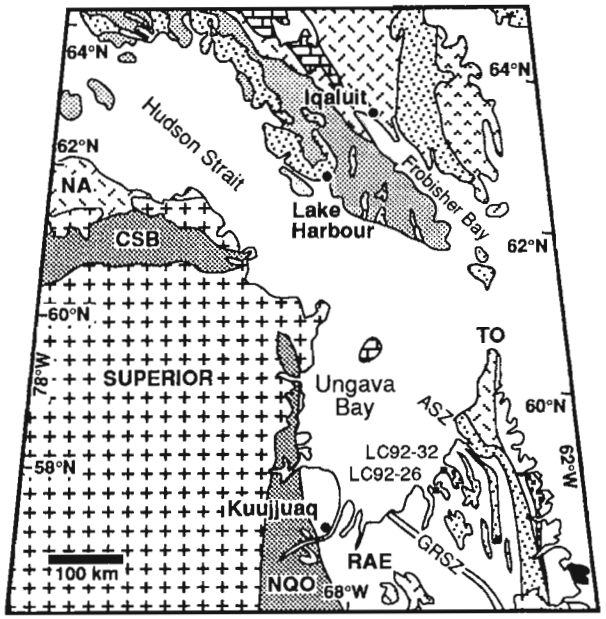

Figure 1. *Location of study area in northeastern Laurentia. ASZ – Abloviak shear zone; CSB – Cape Smith Belt; GRSZ – George River shear zone; NA – Narsajuaq arc; NQO – New Quebec Orogen (Labrador Trough); TO – Torngat Orogen. Paleoproterozoic supracrustal rocks of the Lake Harbour Group and Tasiuyak paragneiss are shown in light stipple; Ramah Group in heavy stipple on the Labrador coast. Ordovician limestone shown in brick pattern. Modified from Hoffman (1988).*

GEOLOGY OF SOUTHEASTERN UNGAVA BAY

Ungava Bay straddles the exposed width of the southeastern Rae Province (Hoffman, 1988), a block of dominantly gneissic rocks that separates the Paleoproterozoic units of the New Quebec Orogen and the underlying Archean Superior craton in the west from rocks of the Torngat Orogen and the Archean Nain craton to the east in Labrador. As such, the geology of southeastern Ungava Bay is a critical element in current attempts to better understand the regional tectonic evolution of northeast Laurentia, but one that remains poorly known relative to the adjacent geological regions.

The rocks between the George River and Abloviak shear zones (GRSZ and ASZ, Fig. 1) consist dominantly of polyphase tonalitic orthogneisses, included mafic and siliciclastic supracrustal rocks, and less-deformed plutonic rocks (Fig. 1). Little is known of the crystallization ages of rocks immediately east of Kuujjuaq; a migmatite sample from the northern de Pas batholith contains zircon with discordant $^{207}Pb/^{206}Pb$ ages between 2.92 and 2.69 Ga and concordant monazite at 1808 ± 2 Ma (Machado et al., 1989). A late-tectonic granite was emplaced at 1805 ± 2 Ma, and contains xenocrysts with $^{207}Pb/^{206}Pb$ ages up to 2.35 Ga (Bardoux et al., 1996). A late granitic vein that is concordant to the main deformation fabric within the George River shear zone crystallized at ~1801–1791 Ma, and places a younger bracket on the timing of movement within the shear zone (Bardoux et al., 1996).

Northeastward, toward Abloviak Fiord, kilometre-scale panels of supracrustal rocks, characterized by marble and siliciclastic units, have been interpreted as correlatives of the <1.93 Ga Lake Harbour Group (Jackson and Taylor, 1972; Scott and Gauthier, 1996). A weakly deformed granite south of the mouth of George River was emplaced at 1853 ± 3 Ma, and contains discordant xenocrystic zircons with $^{207}Pb/^{206}Pb$ ages between 2.80 and 2.63 Ga (Bardoux et al., 1996). Two samples of grey tonalitic gneiss in this vicinity have preliminary U-Pb zircon ages of ~3.03 and 2.95 Ga, respectively (J. David, unpub. data, 1996). At Abloviak Fiord, the polyphase tonalitic orthogneisses, supracrustal rocks of the Lake Harbour Group and the Paleoproterozoic <1.94 Ga Tasiuyak paragneiss (Scott and Gauthier, 1996) are strongly deformed in the ca. 1.84–1.82 Ga Abloviak shear zone (Bertrand et al., 1993; Scott, 1995a) during Torngat orogenesis. To the northeast of the Abloviak shear zone, gneissic rocks of the 1.91–1.86 Ga Burwell plutonic suite (Scott, 1995a; Scott and Machado, 1995) intrude the Archean Nain craton (Scott, 1995b).

Analytical methods

Heavy minerals were separated from two representative samples by standard crushing, grinding, hydrodynamic, and heavy liquid techniques. Sorting of the heavy mineral concentrates was performed using a Frantz isodynamic separator; highest quality monazite was recovered at 0.25–0.5A (10° side slope) and zircon at 1.8A (-0.5° side slope). All zircon

crystals were heavily air-abraded (Krogh, 1982), and only fracture- and inclusion-free crystals were selected for analysis (Table 1). Extraction of Pb and U from zircon and monazite followed the procedure outlined by Parrish et al. (1987). All of the analyses were of single crystals or crystal fragments. Analytical data were reduced using algorithms developed by Roddick (1987), and ages are quoted at 2σ uncertainty.

LC-92-26 Keglo Bay tonalite

On an island in southwestern Keglo Bay, fine-grained tonalite gneiss includes sheets of amphibolite and rare paragneiss, all cut by thin granitic pegmatite veins. Hornblende is the dominant mafic mineral in the tonalite; from regional considerations, it is interpreted as part of a retrograde amphibolite-facies assemblage. Zircon and monazite were recovered from a representative sample of the 'background' fine-grained tonalite phase of the gneiss. This sample has a whole-rock Nd model age (TDM) of 3.07 Ga (L.M. Campbell, pers. comm., 1996).

The zircon population in this sample is relatively homogeneous, consisting of colourless, equant to short prismatic crystals. Most of the diamagnetic zircon grains are of high quality, and few are altered and cracked. Core-overgrowth relationships were not observed by transmitted-light microscopy. Five euhedral zircon crystals were analyzed individually (Fig. 2a), and yielded $^{207}Pb/^{206}Pb$ ages in the range 2987 to 2901 Ma (Table 1). Two fragments of euhedral monazite were analyzed; they are concordant at 1838 ± 2 Ma (Fig. 2a). The seven analyses regress (Davis, 1982) to yield an upper intercept of 3019 ± 5 Ma, interpreted as the age of emplacement of this tonalite. The small difference between the Nd model age (3.07 Ga) and interpreted crystallization age

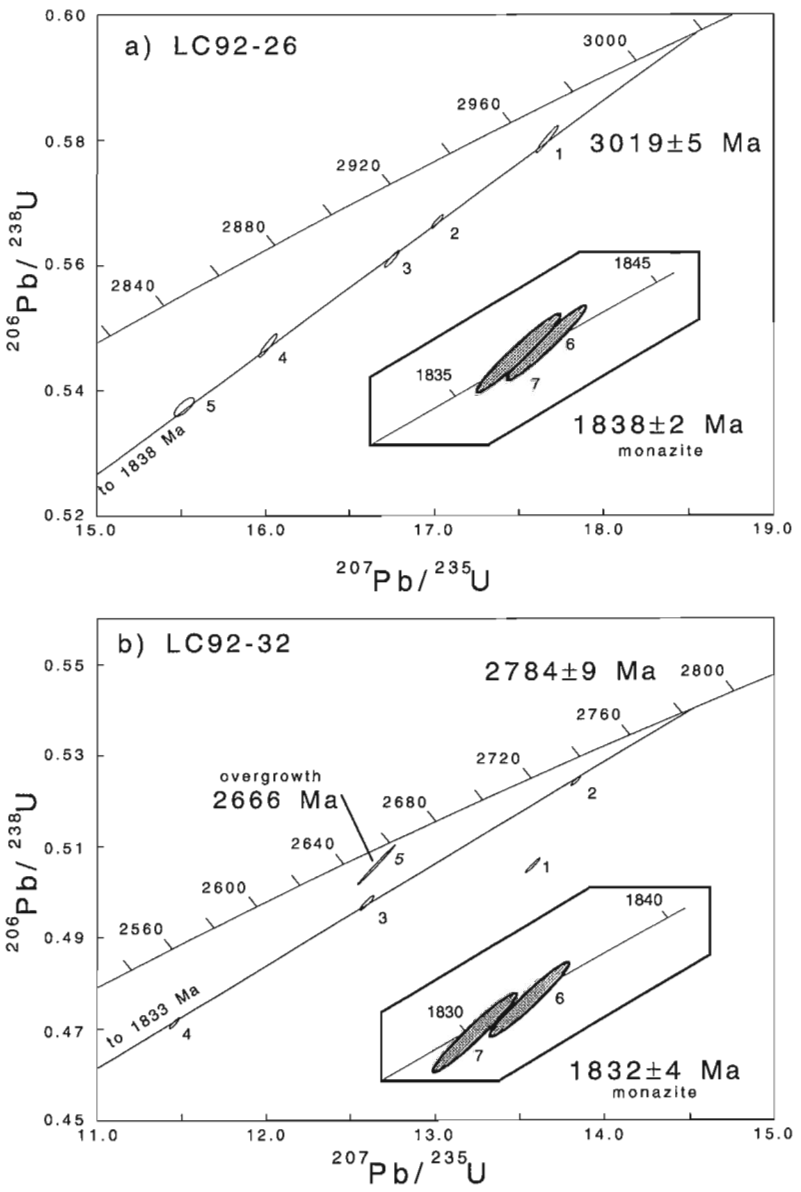

Figure 2.

U-Pb concordia diagrams. Monazite analyses shown as shaded ellipses.

Table 1: U-Pb isotopic data.

Analysis description			Concentrations			Atomic ratios					Age (Ma)
Fraction [1]	No. of grains	Weight (µg)	U (ppm) [2]	Pb (rad) (ppm) [2]	Pb (com) (pg) [3]	$\frac{^{206}Pb}{^{204}Pb}$ [4]	$\frac{^{208}Pb}{^{206}Pb}$ [5]	$\frac{^{206}Pb}{^{238}U}$ (±1σ, %) [5]	$\frac{^{207}Pb}{^{235}U}$ (±1σ, %) [5]	$\frac{^{207}Pb}{^{206}Pb}$ (±1σ, %) [5]	$\frac{^{207}Pb}{^{206}Pb}$
LC92-26, Keglo Bay, (59°05'N; 65°45'W)											
1 z, cl, eu, eq-sp, dia	1	5	42	29	3	2474	0.172	0.5801 ± .19	17.66 ± .19	0.22087 ± .05	2987.0
2 z, cl, eu, eq, dia	1	8	83	57	10	2280	0.171	0.5670 ± .10	17.02 ± .11	0.21766 ± .04	2963.4
3 z, cl, eu, sp, dia	1	6	82	56	12	1532	0.181	0.5602 ± .12	16.74 ± .13	0.21675 ± .05	2956.7
4 z, cl, eu, eq-sp, dia	1	5	53	34	3	2999	0.159	0.5472 ± .17	16.01 ± .17	0.21222 ± .06	2922.6
5 z, cl, eu, eq-sp, dia	1	5	65	49	24	472	0.186	0.5374 ± .13	15.52 ± .19	0.20941 ± .13	2901.0
6 mz, p gr, eu, fr, IF	1	6	7207	4710	5	207800	1.179	0.3302 ± .09	5.119 ± .10	0.11245 ± .03	1839.4
7 mz, p gr, eu, fr, IF	1	7	3703	7299	6	84760	5.782	0.3300 ± .08	5.111 ± .10	0.11233 ± .03	1837.4
LC92-32, Gregson Inlet, (59°15'N; 65°45'W)											
4 z, p br, eu, sp, dia	1	5	88	51	4	3158	0.132	0.5058 ± .17	13.58 ± .17	0.19469 ± .04	2782.2
3 z, p br, eu, sp, dia	1	4	147	85	4	3644	0.098	0.5213 ± .09	13.82 ± .10	0.19128 ± .03	2753.0
3 z, p br, eu, sp, dia	1	4	60	33	7	1260	0.094	0.4977 ± .16	12.60 ± .17	0.18363 ± .06	2685.9
4 z, p br, eu, sp, dia	1	2	176	88	4	3082	0.046	0.4713 ± .13	11.46 ± .13	0.17630 ± .05	2618.4
5 z, cl, eu, og, fr dia	1	3	129	76	4	3619	0.178	0.5063 ± .46	12.70 ± .46	0.18142 ± .04	2665.9
6 mz, p gr, eu, fr, IF	1	11	692	952	3	48560	4.501	0.3286 ± .08	5.078 ± .10	0.11215 ± .03	1834.2
7 mz, p gr, eu, fr, IF	1	5	473	647	4	11300	2.482	0.3279 ± .08	5.061 ± .10	0.11193 ± .03	1831.0

Notes:

[1] Mineral: z=zircon; mz=monazite. Colour: cl=colourless; p=pale; br=brown; gr=green. Form: eu=euhedral; eq=equant; sp=short prism; og=overgrowth; fr=fragment. Magnetic properties: dia=diamagnetic at -0.5° tilt of Frantz magnetic separator; IF=non-magnetic between 0.25 and 0.5A at 10° side slope.

[2] Concentrations are known to 10-20% for weights below 20 µg.

[3] Total common Pb present in analysis corrected for Pb in spike and fractionation (0.09±0.03%/amu).

[4] Measured ratio, corrected for fractionation and spike.

[5] Ratios corrected for spike, fractionation, blank, and initial common Pb. Errors quoted are at the 1-sigma confidence level. U and Pb were loaded separately on Re filaments using the silica gel-phosphoric acid technique, and analyzed on a Finnigan MAT 261 mass spectrometer at the Geological Survey of Canada, Ottawa. Maximum total blanks are 5 pg for Pb and 1 pg for U. Isotopic composition of initial common Pb was calculated at crystallization age using two-stage model of Stacey and Kramers (1975). Decay constants are those recommended by the Geochronology Subcommission, International Union of Geological Sciences (Steiger and Jäger, 1977).

suggests that this tonalite is relatively primitive. The age of the monazite, 1838 ± 2 Ma, is interpreted as the minimum age of a strong thermal disturbance.

LC-92-32 Gregson Inlet tonalite

On the southeast shore of Gregson Inlet, medium-grained tonalite gneiss contains enclaves of layered amphibolite and tonalite, all intruded by thin veins of coarse to pegmatitic granite. Zircon and monazite were recovered from a representative sample of the 'background' medium-grained tonalite component of the gneiss. This sample has a whole-rock Nd model age (TDM) of 3.05 Ga (L.M. Campbell, pers. comm., 1996).

Zircon separated from this sample consists dominantly of colourless to pale brown prismatic crystals that are short to moderately elongate. A subordinate amount of cracked and altered crystals was also recovered. Pale brown to colourless overgrowths were observed only rarely. Four highly abraded, pale brown prisms were analysed individually (Table 1); the first analysis is significantly discordant, whereas the remaining three define a linear array (Fig. 2b). A single colourless overgrowth, removed from a pale brown prism prior to abrasion and analysis, is slightly discordant with a $^{207}Pb/^{206}Pb$ age of 2666 Ma. The two analyzed fragments of euhedral monazite are concordant at 1834 ± 2 Ma. The three most concordant analyses of pale brown prisms and the two monazite analyses regress to yield an upper intercept of 2784 ± 9 Ma, interpreted as the age of the main phase of the tonalite at this location. The difference between the Nd model age (3.05 Ga) and interpreted crystallization age (2.78 Ga) suggests that this tonalite is somewhat more contaminated with older crustal material than the previous sample. Although somewhat discordant, the analysis of the colourless overgrowth suggests that the tonalite may have experienced a significant Archean metamorphic event at ~2666 Ma. The 1834 ± 2 Ma monazite is interpreted as the minimum age of a strong thermal overprint.

DISCUSSION

These U-Pb age determinations clearly demonstrate the presence of Archean crust in the area between George River and Abloviak Fiord. As similar rocks with identical ages are known in both adjacent cratons, the cratonic affinity of the present rocks is not immediately apparent. Both samples show evidence of an important Paleoproterozoic tectonothermal event at ~1.84–1.83 Ga, synchronous with deformation

in the Abloviak shear zone (Torngat Orogen) and magmatism associated with the Narsajuaq arc in northern Quebec and southern Baffin Island (Dunphy and Ludden, 1998; Scott, 1997). The rocks from this study are separated from the Archean gneisses of the Nain craton to the east by the ca. 1.84–1.82 Ga Abloviak shear zone, hence a genetic link to the Nain craton cannot be taken for granted. Similarly, the ca. 1.80 Ga (Bardoux et al., 1996) George River shear zone separates the present rocks from gneisses of the Superior craton to the west. Further, more detailed investigations of the geological evolution of the present block of crust are required in order to more thoroughly document both its Archean and Paleoproterozoic tectonic history, and to facilitate more confident comparisons with the adjacent, better studied cratons.

In the region adjacent to the west of the study area, two samples of grey tonalitic gneiss have preliminary U-Pb zircon ages of ~3.03 and 2.95 Ga, respectively (J. David, unpub. data, 1996). These ages, in addition to those presented here, are a first attempt to characterize the Archean history of this poorly known area. Additional geochronological as well as structural and isotopic studies are ongoing.

ACKNOWLEDGMENTS

These samples were collected by L.M. Campbell during 1992 fieldwork on the GSC's northern Torngat project, and are part of the programme of geochemical and tracer isotopic studies that formed the basis of her doctoral dissertation (University of Colorado, Boulder). Jack MacRae, Diane Bellerive and Klaus Santowski are warmly thanked for the excellence of their technical support. Reviews of this manuscript by T. Skulski and R. Thériault have improved the clarity of the ideas presented. This is Polar Continental Shelf Project contribution 03497.

REFERENCES

Bardoux, M., David, J., Gariépy, C., and Robillard, M.
1996: A progress report on the geology and geochronology of the northeastern Rae Province in southeastern Ungava Bay; *in* Report of 1996 ECSOOT Transect Meetin, (ed.) R.J. Wardle and J. Hall; 57, p. 3-14.

Bertrand, J.-M., Roddick, J.C., Van Kranendonk, M.J., and Ermanovics, I.
1993: U-Pb geochronology of deformation and metamorphism across a central transect of the Early Proterozoic Torngat Orogen, North River map area, Labrador; Canadian Journal of Earth Sciences, v. 30, p. 1470-1489.

Davis, D.W.
1982: Optimum linear regression and error estimation applied to U-Pb data; Canadian Journal of Earth Sciences, v. 19, p. 2141-2149.

Dunphy, J.M. and Ludden, J.N.
1998: Petrological and geochemical characteristics of a Proterozoic magmatic arc (Narsajuaq terrane, Ungava Orogen, Canada) and comparisons to Superior Province granitoids; Precambrian Research, v. 91, p. 109-142.

Goulet, N. and Ciesielski, A.
1990: The Abloviak shear zone and the NW Torngat Orogen, eastern Ungava Bay, Québec; Geoscience Canada, v. 17, p. 269-272.

Hoffman, P.F.
1988: United plates of America, the birth of a craton: Early Proterozoic assembly and growth of Laurentia; Annual Reviews of Earth and Planetary Science, v. 16, p. 543-603.

Jackson, G.D. and Taylor, F.C.
1972: Correlation of major Aphebian rock units in the northeastern Canadian Shield; Canadian Journal of Earth Sciences, v. 9, p. 1650-1669.

Krogh, T.E.
1982: Improved accuracy of U-Pb zircon ages by the creation of more concordant systems using an air abrasion technique; Geochimica et Cosmochimica Acta, v. 46, p. 637-649.

Machado, N., Goulet, N. and Gariépy, C.
1989: U-Pb geochronology of reactivated Archean basement and of Hudsonian metamorphism in the northern Labrador Trough; Canadian Journal of Earth Sciences, v. 26, p. 1-15.

Parrish, R.R., Roddick, J.C., Loveridge, W.D. and Sullivan, R.W.
1987: Uranium-lead analytical techniques at the geochronology laboratory, Geological Survey of Canada; *in* Radiogenic Age and Isotopic Studies: Report 1; Geological Survey of Canada, Paper 87-2, p. 3-7.

Roddick, J.C.
1987: Generalized numerical error analysis with application to geochronology and thermodynamics; Geochimica et Cosmochimica Acta, v. 51, p. 359-362.

Scott, D.J.
1995a: U-Pb geochronology of a Paleoproterozoic continental magmatic arc on the western margin of the Archean Nain craton, northern Labrador, Canada; Canadian Journal of Earth Sciences, v. 32, p. 1870-1882.
1995b: U-Pb geochronology of the Nain craton on the eastern margin of the northern Torngat Orogen, Labrador; Canadian Journal of Earth Sciences, v. 32, p. 1859-1869.
1997: Geology, U-Pb & Pb-Pb geochronology of the Lake Harbour area, southern Baffin Island: implications for the Paleoproterozoic tectonic evolution of NE Laurentia; Canadian Journal of Earth Sciences, v. 34, p. 140-155.

Scott, D.J. and Gauthier, G.
1996: Comparison of TIMS (U-Pb) and Laser Ablation Microprobe ICP-MS (Pb) techniques for age determination of detrital zircons from Paleoproterozoic metasedimentary rocks from northeastern Laurentia, Canada, with tectonic implications; Chemical Geology, v. 131, p. 127-142.

Scott, D.J. and Machado, N.
1995: U-Pb geochronology of the northern Torngat Orogen, Labrador Canada: a record of Paleoproterozoic magmatism and deformation; Precambrian Research, v. 70, p. 169-190.

Stacey, J.S. and Kramers, J.D.
1975: Approximation of terrestrial lead isotope evolution by a two-stage model; Earth and Planetary Science Letters, v. 26, p. 207-221.

Steiger, R.H. and Jäger, E.
1977: Subcommission on geochronology: convention on the use of decay constants in geo- and cosmochronology; Earth and Planetary Science Letters, v. 36, p. 359-362.

Taylor, F.C.
1979: Reconnaissance geology of a part of the Precambrian Shield, northeastern Quebec, northern Labrador, and Northwest Territories; Geological Survey of Canada, Memoir 393, 99 p.

Van Kranendonk, M.J., Wardle, R.J., Mengel, F.C., Campbell, L.M., and Reid, L.
1994: New results and summary of the Archean and Paleoproterozoic geology of the Burwell domain, northern Torngat Orogen, Labrador, Québec, and Northwest Territories; *in* Current Research, 1994-C; Geological Survey of Canada, p. 321-332.

– 5 –

A second report on the U-Pb geochronology of southern Baffin Island, Northwest Territories

David J. Scott[1] and Natasha Wodicka[1]

Scott, D.J. and Wodicka, N., 1998: A second report on the U-Pb geochronology of southern Baffin Island, Northwest Territories; in *Radiogenic Age and Isotopic Studies: Report 11; Geological Survey of Canada, Current Research, 1998-F, p. 47-57.*

Abstract: The geology of the Meta Incognita Peninsula, southern Baffin Island, preserves three principal structural levels: the northern continuation of the Archean Superior craton (Level 1), orthogneisses correlated with the Narsajuaq arc of northern Quebec (Level 2), and orthogneisses and Lake Harbour Group supracrustal rocks intruded by the Cumberland batholith (Level 3). Two Level 2 orthogneisses crystallized at 1830 +5/-3 and 1820 +4/-3 Ma, respectively, and both manifest Archean inheritance. In Level 3, monzogranite orthogneiss is 1950 +6/-4 Ma, and potentially represents the depositional basement to the Lake Harbour Group. A Lake Harbour Group psammite was deposited after 1937 ± 4 Ma. Two monzogranite samples of the Cumberland batholith crystallized at 1865 +4/-2 and 1848 ± 2 Ma, whereas two other monzogranite samples manifest 2.15–2.03 Ga inheritance, compatible with assimilation of Lake Harbour Group material. A monzonite that crosscuts a D_1 thrust fault was emplaced ~1834 -1830 Ma.

Résumé : La géologie de la péninsule Meta Incognita, dans le sud de l'île de Baffin, permet de définir trois niveaux structuraux principaux : le prolongement septentrional de la province archéenne du lac Supérieur (niveau 1), des orthogneiss corrélés avec l'arc de Narsajuaq du nord du Québec (niveau 2), et des roches supracrustales du Groupe de Lake Harbour et des orthogneiss que recoupe le batholite de Cumberland (niveau 3). Deux échantillons d'orthogneiss du niveau 2 ont cristallisé à 1 830 +5/-3 Ma et à 1 820 +4/-3 Ma, respectivement, et montrent un héritage archéen. Un orthogneiss monzogranitique du niveau 3 est daté à 1 950 +6/-4 Ma et pourrait constituer le socle du Groupe de Lake Harbour. Une psammite du Groupe de Lake Harbour a été déposée après 1 937 ± 4 Ma. Deux échantillons de monzogranite du batholite de Cumberland ont cristallisé à 1 865 +4/-2 Ma et à 1 848 ± 2 Ma, respectivement; deux autres témoignent d'un héritage à 2,15–2,03 Ga, ce qui est compatible avec l'assimilation de matière provenant du Groupe de Lake Harbour. Une monzonite qui recoupe une faille de chevauchement D_1 a été mise en place vers 1 834-1 830 Ma.

[1] Geological Survey of Canada, 601 Booth Street, Ottawa, Ontario K1A 0E8

INTRODUCTION

The Precambrian geology of southern Baffin Island comprises Archean metaplutonic rocks as well as Paleoproterozoic metaplutonic and metasedimentary rocks (Fig. 1). The bedrock geology of the area south of 66°N was mapped at reconnaissance scale in 1965 (Blackadar, 1967). In 1995, the Geological Survey of Canada began a three-year multidisciplinary mapping program on the Meta Incognita Peninsula in the Iqaluit–Kimmirut area (Fig. 2); fieldwork has now been completed, and the results are summarized by St-Onge et al. (1996, 1998d; Scott et al., 1997a). Colour Open File maps of the area have been released at 1:100 000 scale (Scott et al., 1996; Hanmer et al., 1996; St-Onge et al., 1997a, b, c, 1998a, b, c). Previous reports of U-Pb geochronology in the area include those of Jackson et al. (1990), Scott and Gauthier (1996), Scott (1997a), and Wodicka and Scott (1997). In this volume, Thériault (1998) reports on the Nd isotopic evolution of the metaplutonic and metasedimentary rocks. Collectively, this work facilitates a more detailed comparison of geological events in southern Baffin Island with those in northernmost Labrador and northern Quebec, and contributes to an improved understanding of the assembly of the North American craton in the Paleoproterozoic.

This report summarizes recent progress in the U-Pb geochronology component of the South Baffin Project, and builds on results reported by Wodicka and Scott (1997). New zircon and monazite results are presented for eight samples of metaplutonic rocks, as well as detrital zircon ages from a metasedimentary rock. These results contribute to the growing analytical database for southern Baffin Island that provides an absolute framework for the timing of magmatic, sedimentary, metamorphic, and deformational events.

GEOLOGY OF THE META INCOGNITA PENINSULA

The geology of the Meta Incognita Peninsula has been divided into three principal structural levels (Wodicka and Scott, 1997; St-Onge et al., 1998d). From lowest to highest, these comprise (Fig. 2) Archean gneisses of the Superior Province and Paleoproterozoic imbricates of lower Povungnituk Group supracrustal rocks (Level 1); ~1.84–1.82 Ga orthogneisses correlated with rocks of the Narsajuaq arc of the Ungava Peninsula (Level 2); and Ramsay River orthogneiss and metasedimentary rocks of the Lake Harbour Group and Blandford Bay assemblage, all of which are intruded by ~1.86–1.85 Ga granitic rocks of the Cumberland batholith (Level 3). These rocks record the development of a southwest-verging thrust-fold belt (D_1–D_2) that imbricated and transported components of structural levels 2 and 3 onto the northern margin of the Superior craton (Level 1). The lithologic assemblages of structural levels 2 and 3 are considered to be

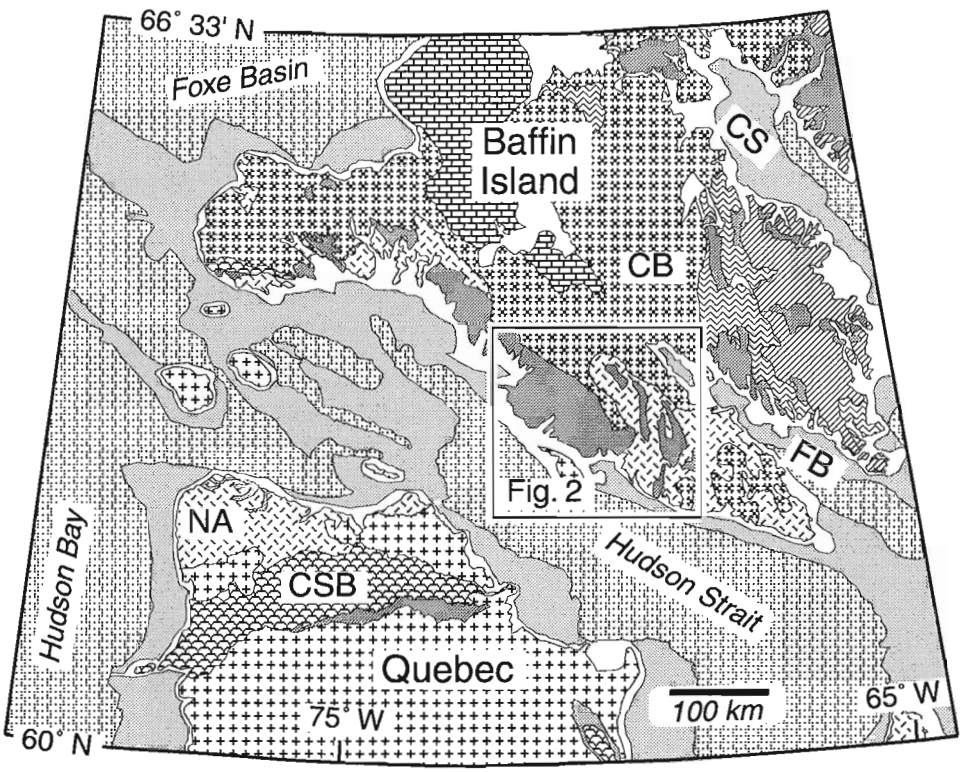

Figure 1. *Location of the project area on Meta Incognita Peninsula (modified after Wheeler et al., 1996; St-Onge et al., 1998d). Abbreviations: CB — Cumberland batholith, CS — Cumberland Sound, CSB — Cape Smith Belt, FB — Frobisher Bay, NA — Narsajuaq arc.*

'exotic' with respect to one another, having undergone separate geological histories prior to their accretion onto the northern margin of the Superior craton after ca. 1.82 Ga. All units of the project area were subsequently deformed by orogen-parallel folding (D_3) and later cross-folding (D_4) (Fig. 2) (St-Onge et al., 1998d).

Structural level 2

Orthopyroxene-bearing, compositionally layered metaplutonic rocks that range from homogeneous monzogranite gneiss to layered monzogranite-granodiorite-tonalite gneiss occur along the northeast coast of Big Island and in the central

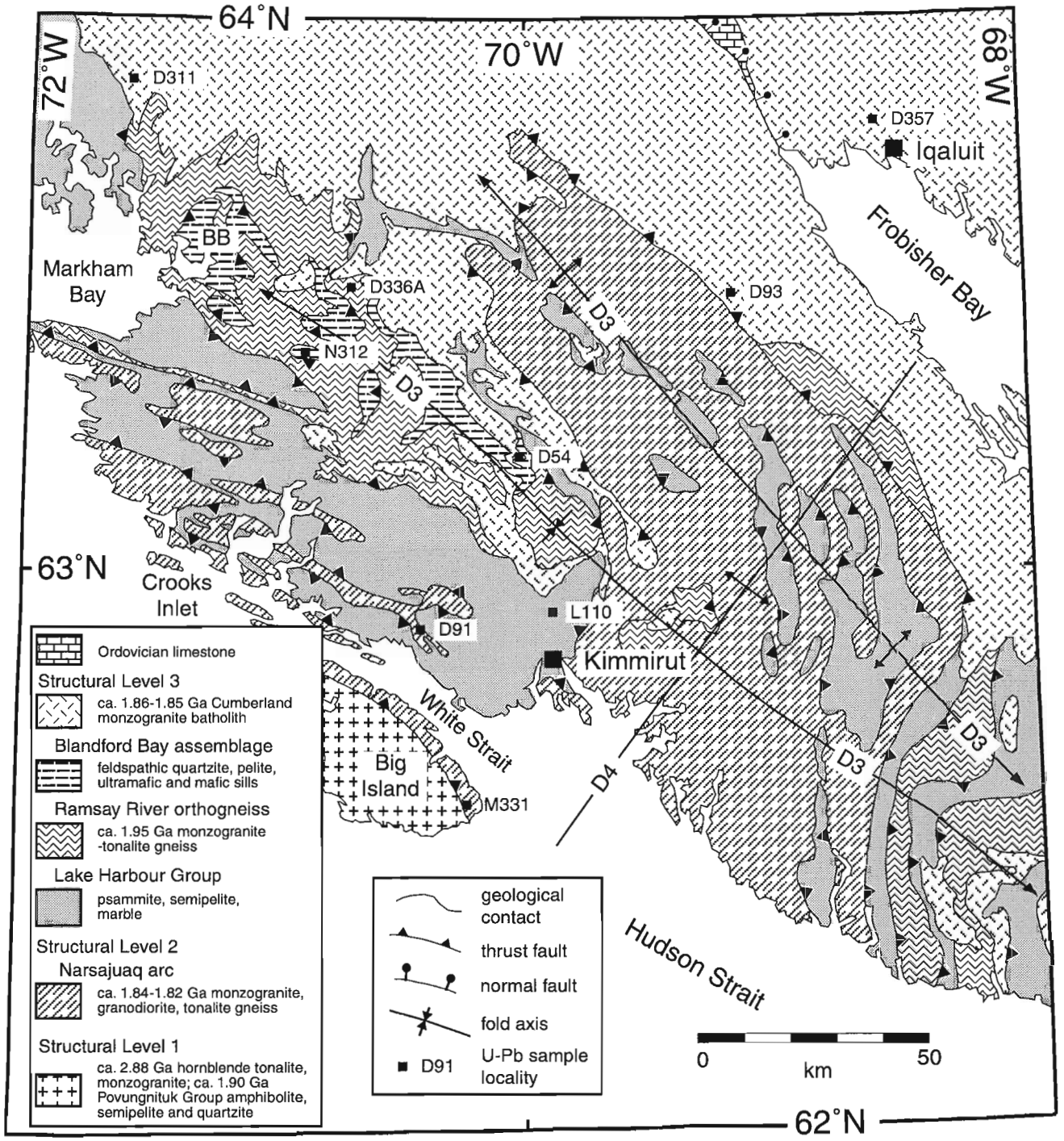

Figure 2. *Summary geological map of the study area, Meta Incognita Peninsula. Locations of samples are shown. Modified from St-Onge et al. (1998d).*

part of the project area (Fig. 2). Previous investigations indicate that the rocks of structural level 2 range in age from 1842 +5/-3 Ma (Scott, 1997a) to as young as 1821 ± 2 Ma (Wodicka and Scott, 1997).

Structural level 3

The oldest rocks of structural level 3 are buff- to pink-weathering, layered orthopyroxene-biotite±hornblende monzogranite-tonalite orthogneiss locally interlayered with subordinate, boudinaged and discontinuous layers of quartz diorite (Fig. 2). Prior to this study, the age(s) of these rocks, referred to as the Ramsay River orthogneisses (St-Onge et al., 1998d), was unknown.

The metasedimentary rocks of the Lake Harbour Group comprise interlayered garnetiferous psammite, semipelite, and pelite with rare orthoquartzite stratigraphically overlain by prominent, laterally continuous to boudinaged bands of pale grey to white marble and calc-silicate rocks. Detrital zircons from samples of the Lake Harbour Group are dominantly Paleoproterozoic (2.2–1.9 Ga), with little to no Archean material (Scott and Gauthier, 1996; Scott, 1997a; Scott et al., 1997b). Deposition of the Lake Harbour Group is younger than 1934 ± 3 Ma, the age of the youngest analyzed detrital zircon (Scott and Gauthier, 1996). Structurally, and possibly stratigraphically, overlying these rocks are the feldspathic quartzites and rusty pelites of the Blandford Bay assemblage. Detrital zircons from a single sample of feldspathic quartzite are exclusively Archean, ~80% of which are older than 2.83 Ga, a smaller proportion older than 3.0 Ga, and one grain is 3.7 Ga (Scott et al., 1997b). Both the Lake Harbour Group and the Blandford Bay assemblage are intruded by generally concordant sheets of mafic to ultramafic rocks.

All units of Level 3 are crosscut by white to pink biotite±orthopyroxene monzogranite and syenogranite veins that range from well foliated to relatively massive, and from a few centimetres to more than ten metres thick; and orthopyroxene monzogranite plutons of the Cumberland batholith. Zircon age determinations on various phases of the batholith range from 1857 +5/-3 Ma to 1850 +3/-2 Ma (Jackson et al., 1990; Scott, 1997b; Wodicka and Scott, 1997). In the following sections, new U-Pb geochronological results from rocks of structural levels 2 and 3 are presented and discussed.

GEOCHRONOLOGY

Analytical methods

Heavy minerals were separated from representative samples by standard crushing, grinding, hydrodynamic, and heavy liquid techniques. Sorting of the heavy mineral concentrates was performed using a Frantz isodynamic separator (Krogh, 1982b); highest-quality monazite was recovered at 0.2 to 0.35A (10° side slope) and zircon at 1.8A (-0.5° side slope). Unless otherwise stated, only fracture- and inclusion-free crystals were selected for analysis (Table 1). Extraction of Pb and U from zircon and monazite followed the procedure outlined by Parrish et al. (1987). Most of the zircon analyses are of single crystals or crystal fragments; multigrain analyses are of restricted populations (n<3), all of which were highly abraded (Krogh, 1982a). Analytical data were reduced using algorithms developed by Roddick (1987), and ages are quoted at 2σ uncertainty.

Structural level 2

Orthopyroxene-biotite tonalite, south shore (D91)

Fine- to medium-grained, orthopyroxene-biotite tonalite was sampled from an outcrop with subordinate sheets of monzogranite and diorite north of White Strait (Fig. 2).

Zircon separated from this sample consists of colourless and pale brown, short, prismatic crystals, most of which display faint concentric (growth?) zoning in plane-polarized light. Most of the diamagnetic grains are of high quality, but some are altered and cracked. Four highly abraded, colourless crystals were analyzed individually (Fig. 3a); the four analyses are highly discordant (3.7-8.1%), with $^{207}Pb/^{206}Pb$ ages that range from 2644 to 2420 Ma, and are interpreted as xenocrysts. Four pale brown prisms were analyzed individually, one of which is concordant at 1831 ± 2 Ma (Fig. 3a, inset). The four analyses regress (Davis, 1982) to yield an upper intercept age of 1830 +5/-3 Ma, interpreted as the age of emplacement of the tonalite. A regression of the four older discordant analyses, pinned at 1830 Ma, yields an upper intercept of 2757 ± 13 Ma; this is interpreted as a minimum crystallization age of the colourless xenocrystic zircons that are interpreted as being derived from Archean crustal material.

Orthopyroxene-biotite monzogranite, Big Island (M331)

Medium- to coarse-grained, orthopyroxene-biotite monzogranite was sampled near the southeast end of Big Island (Fig. 2).

Zircon separated from this sample constitutes a homogeneous population of colourless, short prismatic grains. Concentric zoning is visible in plane-polarized light in many of the highest quality crystals. Five crystals were analyzed individually (Fig. 3b). The oldest is significantly discordant (2.4%), and has a $^{207}Pb/^{206}Pb$ age of 2803 Ma; the other four analyses, two of which are concordant, regress to yield an upper intercept of 1820 +4/-3 Ma, interpreted as the crystallization age of the monzogranite at this location. A reference line from 1820 Ma through the oldest discordant analysis, here interpreted as a xenocryst derived from an Archean crustal component, intersects concordia at 2852 ± 8 Ma, suggesting a minimum primary age of this crystal.

Structural level 3

Monzogranite gneiss, Ramsay River (D336A)

A pinkish-grey-weathering orthopyroxene-biotite±hornblende monzogranite layer of the Ramsay River orthogneiss was sampled in the west-central part of the project area (Fig. 2). At this locality, a massive pink orthopyroxene

Table 1. U-Pb isotopic data.

Fraction				Concentrations			Atomic ratios					Age
	Description [1]	# of grains	Weight (µg)	U (ppm) [2]	Pb (rad) (ppm) [2]	Pb (com) (pg) [3]	$\frac{^{206}Pb}{^{204}Pb}$ [4]	$\frac{^{208}Pb}{^{206}Pb}$ [5]	$\frac{^{206}Pb}{^{238}U}$ (± 1σ, %) [5]	$\frac{^{207}Pb}{^{235}U}$ (± 1σ, %) [5]	$\frac{^{207}Pb}{^{206}Pb}$ (± 1σ, %) [5]	$\frac{^{207}Pb}{^{206}Pb}$ (Ma)
STRUCTURAL LEVEL 2												
Orthopyroxene-biotite tonalite, south shore (D91) 1830 +5/-3 Ma												
1	z, cl, eu, sp, dia	1	6	214	120	4	9061	0.162	0.4886 ± .11	12.07 ± .12	0.17910 ± .03	2644.6
2	z, cl, eu, sp, dia	1	6	111	73	7	2838	0.394	0.4863 ± .13	11.94 ± .14	0.17812 ± .04	2635.5
3	z, cl, eu, sp, dia	1	8	156	81	14	2291	0.198	0.4411 ± .13	10.04 ± .14	0.16519 ± .05	2509.4
4	z, cl, eu, sp, dia	1	10	163	85	14	2868	0.280	0.4189 ± .12	9.051 ± .14	0.15672 ± .07	2420.6
5	z, p br, eu, sp, dia	1	12	26	21	5	1448	0.737	0.3282 ± .30	5.065 ± .31	0.11192 ± .08	1830.9
6	z, p br, eu, sp, dia	1	4	110	55	4	2070	0.680	0.3261 ± .15	5.028 ± .21	0.11183 ± .12	1829.4
7	z, p br, eu, sp, dia	1	10	139	90	4	6998	0.779	0.3254 ± .11	4.999 ± .11	0.11144 ± .05	1823.0
8	z, p br, eu, sp, dia	1	15	40	25	16	786	1.105	0.3201 ± .18	4.902 ± .21	0.11108 ± .11	1817.1
Monzogranite, Big Island (M331) 1820 +4/-3 Ma												
1	z, cl, eu, sp, dia	1	9	75	42	5	5208	0.144	0.5319 ± .13	14.46 ± 14	0.19725 ± .03	2803.6
2	z, cl, eu, sp, dia	1	4	88	28	23	340	0.113	0.3254 ± .16	4.997 ± .34	0.11136 ± .27	1821.6
3	z, cl, eu, sp, dia	1	6	145	45	5	3239	0.148	0.3269 ± .12	5.017 ± .21	0.11131 ± .16	1820.9
4	z, cl, eu, sp, dia	1	8	19	6	5	601	0.142	0.3166 ± .45	4.859 ± .46	0.11131 ± .18	1820.9
5	z, cl, eu, sp, dia	1	4	100	32	4	2497	0.139	0.3241 ± .13	4.969 ± .15	0.11122 ± .08	1819.4
STRUCTURAL LEVEL 3												
Monzogranite gneiss, Ramsay River (D336A) 1950 +6/-4 Ma												
1	z, cl, sb, sp, dia	1	4	74	35	15	445	0.342	0.3550 ± .18	5.860 ± .33	0.11974 ± .26	1952.3
2	z, cl, eu, sp, dia	1	3	135	60	3	2877	0.325	0.3535 ± .13	5.828 ± .14	0.11959 ± .05	1950.1
3	z, cl, eu, sp, dia	1	4	67	29	11	557	0.325	0.3504 ± .18	5.786 ± .25	0.11977 ± .17	1952.7
4	z, cl, eu, sp, dia	1	2	43	20	5	371	0.385	0.3473 ± .50	5.692 ± .54	0.11886 ± .27	1939.2
5	z, cl, sb, sp, dia	1	4	18	6	3	568	0.102	0.3279 ± .53	5.064 ± .52	0.11199 ± .33	1831.9
Psammite, Lake Harbour Group (L110) <1937 ± 4 Ma												
1	z, p br, eu, sp, dia	1	11	247	113	3	25690	0.141	0.4156 ± .09	8.200 ± .10	0.14310 ± .03	2265.1
2	z, p br, eu, sp, dia	1	7	151	51	4	6909	0.013	0.3506 ± .09	5.759 ± .10	0.11914 ± .04	1943.3
3	z, cl, eu, sp, dia	1	4	77	33	10	830	0.251	0.3510 ± .14	5.746 ± .17	0.11873 ± .11	1937.2
4	z, cl, eu, lp, dia	1	8	106	40	15	1219	0.134	0.3475 ± .10	5.682 ± .14	0.11860 ± .08	1935.3
5	z, cl, eu, eq, dia	1	4	79	31	15	516	0.202	0.3399 ± .15	5.464 ± .27	0.11660 ± .21	1904.4
Monzogranite, Cumberland batholith (D357) 1865 +4/-2 Ma												
1	z, cl, eu, sp, dia	1	7	231	81	6	5793	0.103	0.3371 ± .09	5.334 ± .11	0.11475 ± .04	1876.0
2	z, cl, eu, sp, dia	1	14	69	25	4	4933	0.142	0.3351 ± .10	5.269 ± .11	0.11404 ± .04	1864.8
3	z, p br, eu, eq, dia	1	14	116	41	6	5994	0.116	0.3348 ± .10	5.262 ± .11	0.11398 ± .04	1863.8
4	z, p br, eu, sp, dia	1	5	238	80	8	2836	0.165	0.3328 ± .09	5.218 ± .10	0.11370 ± .04	1859.4
Monzogranite vein, Cumberland batholith (D93) 1848 ± 2 Ma												
A	z, br, fr, an, dia	1	7	622	212	122	751	0.074	0.3337 ± .10	5.204 ± .19	0.11311 ± .14	1849.9
B	z, br, ac, eu, dia	3	15	637	215	6	32000	0.076	0.3308 ± .09	5.148 ± .10	0.11287 ± .03	1846.1
C	z, p br, lp, eu, dia	1	6	397	134	13	3859	0.072	0.3314 ± .09	5.163 ± .11	0.11301 ± .04	1848.4
D	z, p br, fr, an, dia	1	10	409	138	2	37130	0.073	0.3311 ± .09	5.157 ± .10	0.11295 ± .03	1847.4
E	z, p br, lp, og, dia	1	9	415	141	3	22630	0.079	0.3306 ± .09	5.154 ± .10	0.11304 ± .03	1848.9
Monzogranite, Cumberland batholith (D311)												
1	z, cl, eu, lp, dia	1	4	49	27	8	163	0.247	0.3917 ± .73	7.227 ± .88	0.13381 ± .49	2148.6
2	z, cl, eu, lp, dia	1	6	226	107	7	794	0.218	0.3917 ± .18	7.201 ± .21	0.13332 ± .11	2142.1
3	z, cl, eu, eq, dia	1	4	54	24	5	1117	0.194	0.3855 ± .20	7.017 ± .20	0.13204 ± .09	2125.3
4	z, cl, eu, lp, dia	1	6	53	23	6	1374	0.195	0.3825 ± .14	6.857 ± .17	0.13002 ± .09	2098.2
5	z, cl, eu, lp, dia	1	5	58	29	18	395	0.225	0.3853 ± .16	6.900 ± .31	0.12986 ± .23	2096.1
6	z, cl, eu, sp, dia	1	3	44	19	4	777	0.189	0.3766 ± .28	6.709 ± .29	0.12921 ± .13	2087.3
7	z, cl, eu, sp, dia	1	3	42	17	6	463	0.161	0.3727 ± .35	6.506 ± .37	0.12661 ± .21	2051.5
Monzogranite, Cumberland batholith (D54)												
8	z, cl, eu, sp, dia	1	5	26	11	8	386	0.188	0.3787 ± .25	6.768 ± .30	0.12961 ± .23	2092.7
9	z, cl, eu, sp, dia	1	6	42	18	6	922	0.192	0.3663 ± .29	6.367 ± .29	0.12609 ± .24	2044.1
10	z, cl, eu, sp, dia	1	4	125	51	3	3620	0.182	0.3652 ± .10	6.302 ± .11	0.12516 ± .05	2031.0
Monzonite, Ramsay River (N312) 1834-1830 Ma												
A1	z, p br, eu, fr	1	132	189	77	4	140000	0.324	0.3280 ± .08	5.069 ± .09	0.11209 ± .03	1833.6
A2	z, p br, eu, fr	1	81	175	71	5	63410	0.325	0.3278 ± .08	5.067 ± .10	0.11210 ± .03	1833.8
A3	z, br, eu, fr, og	1	223	189	75	17	52050	0.285	0.3294 ± .09	5.085 ± .10	0.11195 ± .03	1831.3
B	z, p br, eq, eu, dia	2	11	130	49	5	5855	0.238	0.3241 ± .10	4.957 ± .11	0.11093 ± .06	1814.8
C	z, p br, sp, eu, dia	1	9	92	29	3	6583	0.026	0.3217 ± .12	4.872 ± .12	0.10983 ± .05	1796.5
D	z, p br, fr, dia	1	39	211	86	5	33890	0.325	0.3279 ± .09	5.056 ± .10	0.11183 ± .03	1829.4
MA	mz, p yl, sp, eu, IF	1	6	217	400	3	8057	5.547	0.3203 ± .12	4.832 ± .12	0.10940 ± .05	1789.4
MB	mz, m yl, fr, eu, IF	1	43	343	510	3	84740	4.254	0.3204 ± .09	4.835 ± .10	0.10943 ± .03	1790.0
MC	mz, p yl, rn, IF	1	17	343	1032	4	31570	9.680	0.3215 ± .17	4.916 ± .18	0.11091 ± .03	1814.3
MD	mz, p yl, rn, IF	1	11	422	2065	56	1698	16.266	0.3250 ± .08	4.961 ± .12	0.11073 ± .06	1811.5
ME	mz, p yl, an, IF	1	19	344	3000	4	33920	29.872	0.3249 ± .08	4.974 ± .10	0.11102 ± .03	1816.2

[1] Mineral: z = zircon; mz = monazite. Colour: cl = colourless; br = brown; yl = yellow; p = pale; m = medium. Form: eq = equant; sp = short prism; lp = long prism; ac = acicular; eu = euhedral; sb = subhedral; an = anhedral; rn = rounded; og = overgrowth; fr = fragment.
Magnetic properties: dia = diamagnetic at -0.5° tilt of Frantz magnetic separator; IF = non-magnetic between 0.2 and 0.35 A at 10° side slope.

[2] Concentrations are known to <10% for sample weights above 20 µg, 10-20% for weights below 20 µg.

[3] Total common Pb present in analysis corrected for Pb in spike and fractionation (0.09±0.03%/amu).

[4] Measured ratio, corrected for fractionation and spike.

[5] Ratios corrected for spike, fractionation, blank, and initial common Pb. Errors quoted are at the 1-sigma confidence level. U and Pb were loaded spearately on Re filaments using the silica gel-phosphoric acid technique, and analyzed on a Finnigan MAT 261 mass spectrometer. Maximum total blanks are 5 pg for Pb and 1 pg for U. Isotopic composition of initial common Pb was calculated at crystallization age using two-stage model of Stacey and Kramers (1975). Decay constants recommended by the Geochronology Subcommission, International Union of Geological Sciences (Steiger and Jäger, 1977).

monzogranite phase is clearly discordant to the compositional layering in the host orthogneiss (*see* Fig. 11 *in* Scott et al., 1997a).

Zircon recovered from this sample is of moderate quality, and characterized by dominantly colourless, subhedral to euhedral, short prismatic crystals that are generally less than 100 μm in length. Five highly abraded crystals were analyzed individually (Fig. 4a). The four oldest form a collinear array and regress to yield an upper intercept of 1950 +6/-4 Ma. The most robust analysis (analysis 2, Fig. 4a, $^{206}Pb/^{204}Pb = 2877$) is concordant at 1950 ± 2 Ma. We suggest that 1950 +6/-4 Ma represents the crystallization age of the dominant rock type at this locality. The fifth analysis, although somewhat imprecise, is concordant at 1832 ± 12 Ma. This crystal has a significantly lower U content and a lower Th/U ratio than the other analyzed grains, suggesting that it may have grown during a younger thermal event, most likely related to intrusion of the massive pink monzogranite at this locality. This hypothesis will be tested by U-Pb geochronology on the massive monzogranite.

Psammite, Lake Harbour Group, Soper Lake (L110)

A garnet-biotite psammite of the Lake Harbour Group was sampled north of Kimmirut (Fig. 2).

A wide variety of forms of colourless to pale brown zircon was recovered from this sample. Whereas some of the grains are moderately rounded, presumably as a result of physical transport, the majority of grains display euhedral crystal faces. Five grains were analyzed individually (Fig. 4b). The oldest analysis is discordant, with a $^{207}Pb/^{206}Pb$ age of 2265 Ma. The youngest concordant analysis (analysis 3, Fig. 4b), at 1937 ± 4 Ma, places a maximum age on the time of deposition of this sample. A somewhat younger grain, at

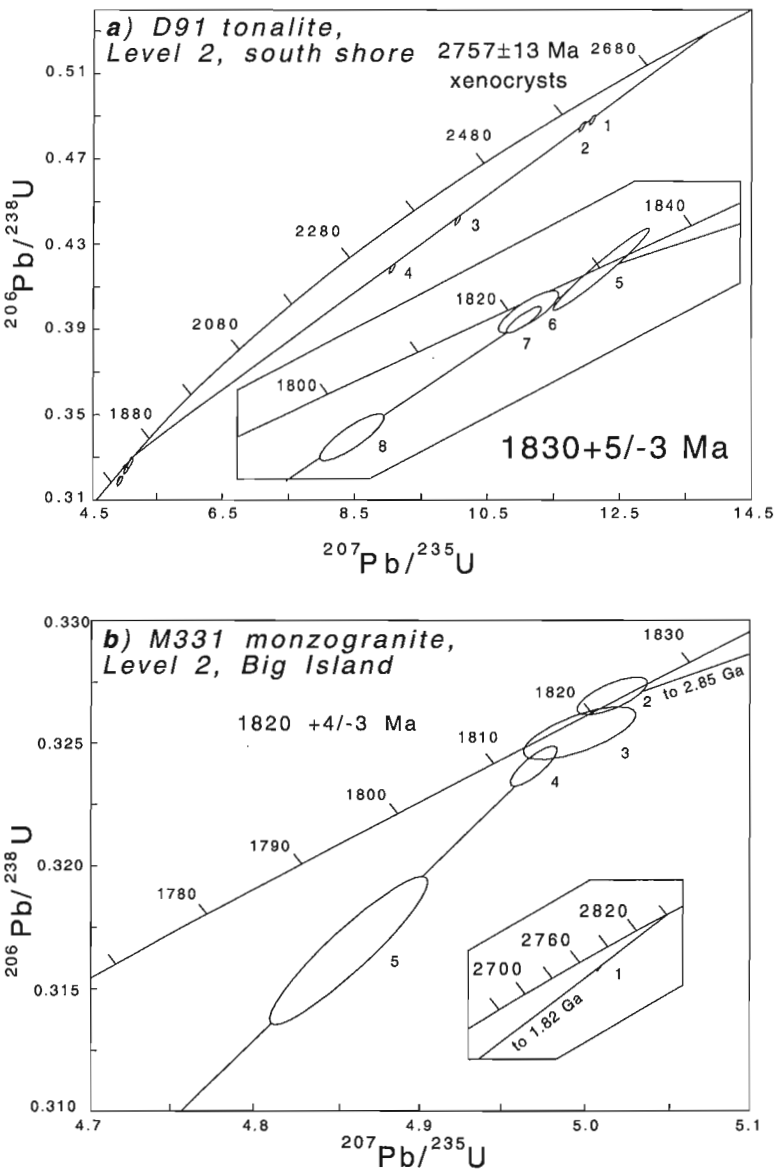

Figure 3.

U-Pb concordia diagrams for two orthogneiss samples (D91 and M331) from structural level 2.

1904 Ma, is too discordant (1.1%) to confidently place an older limit on the timing of deposition. The preferred estimate of the maximum age of deposition is indistinguishable from the 1934 ± 3 Ma upper bracket for a similar Lake Harbour Group psammite from the east shore of Soper Lake (Scott and Gauthier, 1996).

Orthopyroxene monzogranite, northern Cumberland batholith (D357)

Medium-grained, orthopyroxene-biotite monzogranite was sampled in the main body of the Cumberland batholith at the abandoned radar site ~4 km northwest of Iqaluit (Fig. 2).

Zircon recovered from this sample ranges from colourless to pale brown, and from equant to short prismatic crystals. Concentric zoning is visible in plane-polarized light in many of the highest quality crystals, four of which were analyzed individually (Fig. 5a). Two of the analyses are concordant at 1865 ± 2 and 1864 ± 2 Ma; combined with a third analysis, these regress to yield an age of 1865 +4/-2 Ma, interpreted as the age of crystallization of this sample. A slightly older crystal with a $^{207}Pb/^{206}Pb$ age of 1876 ± 2 Ma (analysis 1, Fig. 5a), is interpreted as a xenocryst.

Monzogranite vein, central Cumberland batholith (D93)

An undeformed monzogranite vein, interpreted as related to the Cumberland batholith magmatic system, was sampled west of Frobisher Bay (Fig. 2). The vein truncates the D_1 fabric in monzogranitic Ramsay River orthogneiss (previously interpreted as an older, gneissic component of the Cumberland batholith (Wodicka and Scott, 1997)).

Light brown zircons ranging in shape from spindles and elongate prisms to anhedral fragments were recovered. Four single-grain fractions and one multigrain fraction were

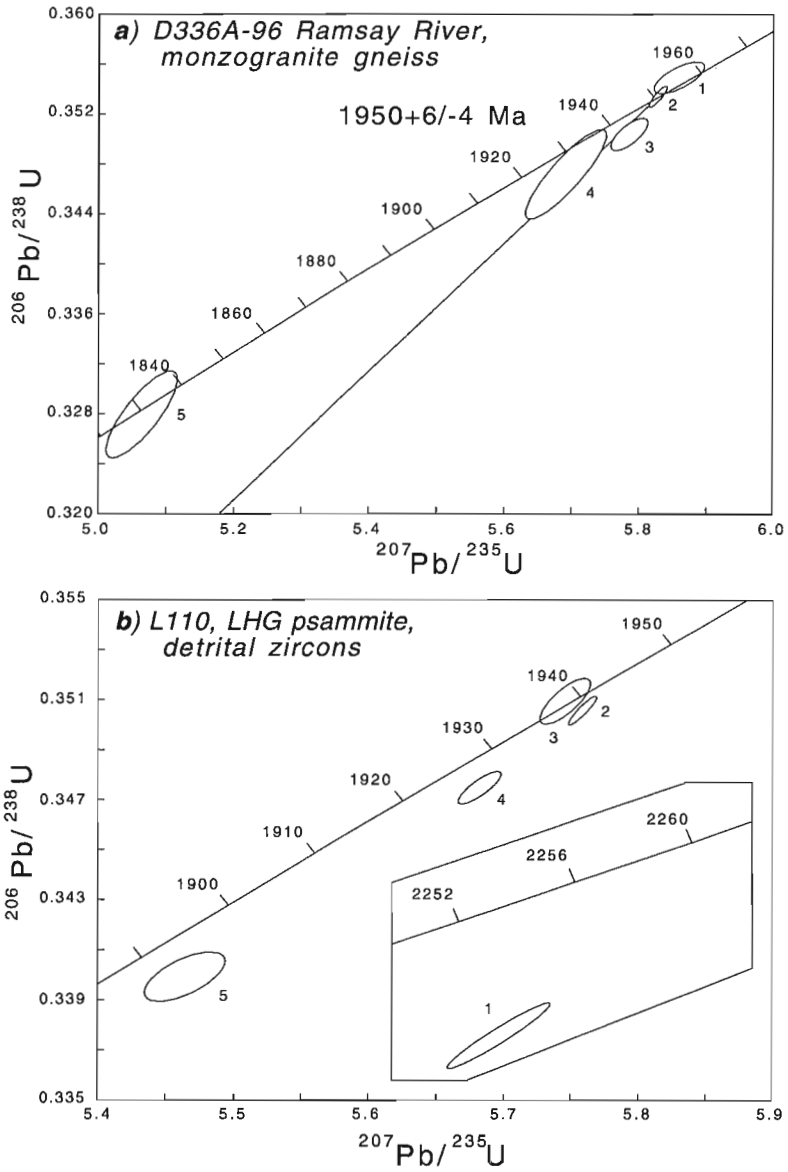

Figure 4.

U-Pb concordia diagrams for a monzogranite orthogneiss sample (D336A) and a Lake Harbour Group psammite (L110) from structural level 3.

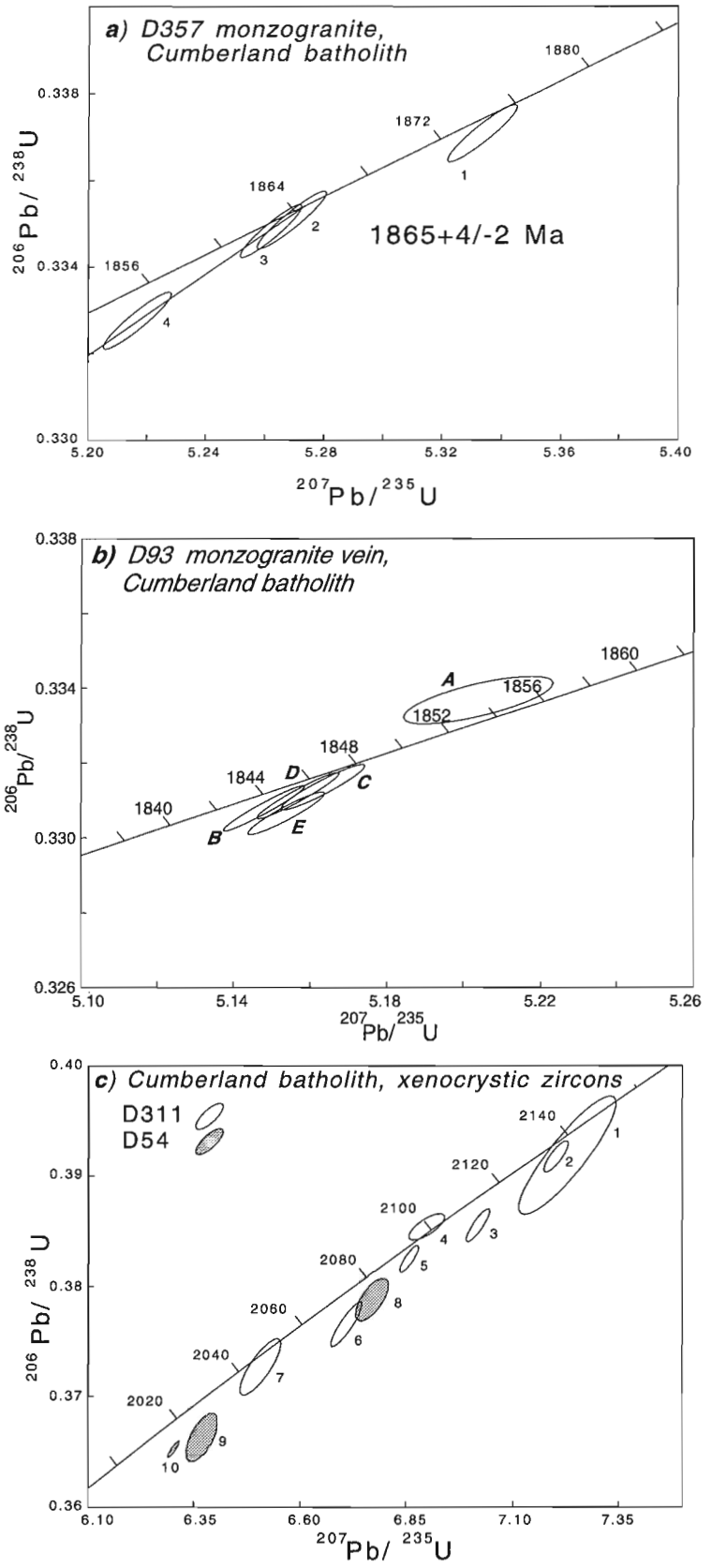

Figure 5. *U-Pb concordia diagrams for four monzogranite samples from the Cumberland batholith (D357, D93, D311 and D54), structural level 3.*

analyzed; four are only slightly discordant (0.2-0.5%) with $^{207}Pb/^{206}Pb$ ages between 1846 and 1849 Ma (Fig. 5b). The fifth analysis is reversely discordant (-0.4%), but yielded a similar $^{207}Pb/^{206}Pb$ age of 1850 Ma. The five analyses give a weighted mean $^{207}Pb/^{206}Pb$ age of 1848 ± 2 Ma. Three of the five analyses (A, C, and E) regress (York, 1969) to yield an upper intercept of 1849 +4/-1 Ma. The average $^{207}Pb/^{206}Pb$ age, 1848 ± 2 Ma, is interpreted as the time of emplacement of this monzogranite vein, and provides a minimum age for D_1 deformation of the host Ramsay River monzogranite gneiss. Monazite from this sample yielded a cooling age of ca. 1843 Ma (Wodicka and Scott, 1997).

Monzogranite, northwest Cumberland batholith (D311)

Medium-grained, orthopyroxene-biotite monzogranite was sampled in the main body of the Cumberland batholith in the northwest corner of the project area (Fig. 2).

The zircon population recovered from this sample is colourless, euhedral, and generally of high quality, with forms that range from equant to prismatic with aspect ratios of 6:1. Seven crystals were analyzed separately (Fig. 5c, analyses 1–7). Most are slightly discordant, with $^{207}Pb/^{206}Pb$ ages that range from 2149 to 2052 Ma. Given that dated samples of the Cumberland batholith range in age from 1865 +4/-2 Ma to 1848 ± 2 Ma (this study; Scott, 1997b; Wodicka and Scott, 1997), and that the host Ramsay River orthogneiss is in part 1950 +6/-4 Ma, we suggest that the seven analyzed crystals from this sample are best interpreted as xenocrysts.

Monzogranite, south-central Cumberland batholith (D54)

Medium-grained, orthopyroxene-biotite monzogranite was sampled from a folded sheet of the Cumberland batholith that intrudes siliciclastic rocks of both the Lake Harbour Group and Blandford Bay assemblage in the central part of the project area (Fig. 2).

Zircon recovered from this sample is dominantly colourless, and ranges from equant through short prismatic to rare elongate grains, with most grains displaying dominantly euhedral habit and, less commonly, faint concentric zoning in plane-polarized light. Three grains were analyzed separately; all are discordant, with $^{207}Pb/^{206}Pb$ ages that range from 2093 to

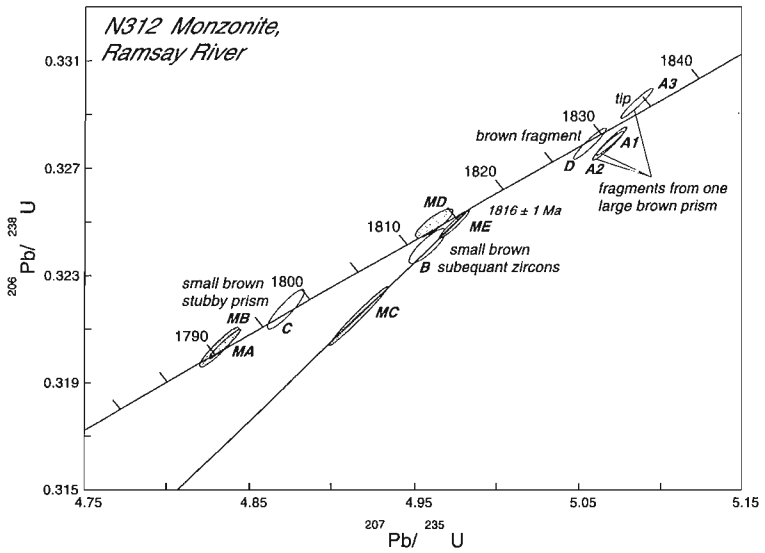

Figure 6.

U-Pb concordia diagram for a monzonite sample (N312) from west of Ramsay River, structural level 3.

2031 Ma (Fig. 5c, analyses 8–10). For reasons outlined for the previous sample, and the additional argument that host-rock psammites of the Lake Harbour Group contain detrital zircons as young as 1934 ± 3 Ma, the three analyzed crystals in this monzogranite sample are interpreted as xenocrysts. It is interesting to note that the range of ages in this and the previous sample — 2.15 to 2.03 Ga — coincides with the most populous ages of detrital grains in siliciclastic rocks of the Lake Harbour Group (Scott and Gauthier, 1996; Scott, 1997a; Scott et al., 1997b).

Monzonite, Ramsay River (N312)

A very coarse-grained, undeformed body of orthopyroxene-bearing monzonite that cuts across a D_1 thrust contact between Ramsay River orthogneiss and metasedimentary rocks of the Blandford Bay assemblage was sampled (Fig. 2).

Zircon separated from this sample is dominated by large, brown prisms up to several millimetres in diameter. A subordinate number of smaller, light brown subequant crystals and stubby prisms is also present. Monazite occurs as well faceted to subrounded crystals and anhedral fragments. Four analyses of broken fragments (including a tip) from large brown zircon prisms are -0.3 to 0.4% discordant and yield the oldest $^{207}Pb/^{206}Pb$ ages, between 1834 and 1829 Ma (Fig. 6). One analysis of small subequant zircons and two analyses of monazite define a linear array with an upper intercept of 1816 ± 1 Ma. A third analysis of monazite is reversely discordant with a slightly younger $^{207}Pb/^{235}U$ age of 1813 ± 2 Ma. A small zircon prism is concordant at 1797 ± 2 Ma. Finally, two analyses of euhedral monazite are concordant at 1791 ± 2 Ma.

Collectively, these data reveal complicated U-Pb systematics and possible evidence for multiple growth events. The oldest zircons display morphologies consistent with a magmatic origin, and are interpreted to record the crystallization age of the monzonite. However, the data are currently insufficient to define a precise age of crystallization, but the monzonite is believed to be no older than ca. 1834 Ma and no younger than ca. 1830 Ma. Concurrently, the younger ages may reflect prolonged (or episodic) zircon and monazite growth over the ca. 1816 to 1791 Ma interval as a result of retrograde fluid flow during regional ductile deformation. Petrographic evidence for minor retrogression in the dated monzonite is consistent with this interpretation.

DISCUSSION

Structural level 2

The two new magmatic ages for the tonalite and monzogranite samples from structural level 2 (D91: 1830 +5/-3 Ma, and M331: 1820 +4/-3 Ma) build on our understanding of the timing of magmatism in southern Baffin Island. The results from this study fall within the previously documented age range for Level 2 orthogneisses, i.e. 1842 +5/-3 Ma to 1821 ± 2 Ma, and corroborate the interpretation that these rocks are correlative with those of the Narsajuaq arc on the Ungava Peninsula, northern Quebec (Dunphy and Ludden, 1998). Evidence for the involvement of Archean crustal material in the petrogenesis of Level 2 orthogneisses is strongly manifest in tonalite D91 (>2757 ± 13 Ma xenocrysts) and to a lesser extent in monzogranite M331 (one ca. 2.85 Ga xenocryst). These observations are consistent with Nd isotopic systematics of Level 2 orthogneisses that demonstrate a significant contribution of older material (Thériault, 1998). The tectonic setting for the formation of these rocks is uncertain, but preliminary whole-rock, major- and trace-element geochemistry suggests formation of these rocks in an arc setting with an important older crustal component (Thériault et al., 1997; Thériault, 1998), consistent with the magmatic arc interpretation advanced by Dunphy and Ludden (1998) for correlative rocks in northern Quebec.

Structural level 3

The results for the sampled monzogranite layer of the Ramsay River orthogneiss (D336A) represent the first age for this lithologic package. At 1950 +6/-4 Ma, this monzogranite orthogneiss predates the more massive monzogranites of the Cumberland batholith by up to 100 million years, and the compositionally similar rocks from the underlying structural level 2 by up to 130 million years. The present data permit that the ca. 1.95 Ga Ramsay River orthogneisses may represent, at least in part, the depositional basement to the metasedimentary rocks of the Lake Harbour Group (<1.93 Ga). Prior to this investigation, suitably old (i.e. >1.93 Ga) rocks were not identified in proximity to the Lake Harbour Group strata. Our understanding of the tectonic history of the Ramsay River orthogneisses is preliminary at this point; isotopic analysis of additional samples is in progress.

The detrital zircons analyses from the Lake Harbour Group psammite (L110) contribute to the growing body of analytical data (isotope dilution TIMS, SHRIMP, and LAM-ICP-MS) that document the dominantly Paleoproterozoic (2.2–1.9 Ga) provenance of these rocks (Scott and Gauthier, 1996; Scott, 1997a; Scott et al., 1997b). Whereas the ca. 1.95 Ga Ramsay River orthogneisses may represent the source of some of the younger detritus in the Lake Harbour Group siliciclastic rocks, the relative absence of Archean material, and the dominance of Paleoproterozoic ages that are uncommon in northeastern Laurentia, is somewhat enigmatic. The extant data require that the provenance of the Lake Harbour Group detritus is dominantly other than Archean material of the nearby Superior or Nain cratons.

The two new magmatic ages for Cumberland batholith-related samples (D357: 1865 +4/-2 Ma, and D93: 1848 ± 2 Ma) solidify our understanding of the timing of its emplacement in southern Baffin Island. These two samples expand the previously known range of ages (ca. 1857–1850 Ma, Jackson et al., 1990; Scott, 1997b; Wodicka and Scott, 1997), and thereby establish new brackets on the timing of Cumberland magmatism. The documentation of 2.15 to 2.03 Ga xenocrystic material in two of the Cumberland monzogranite samples (D311 and D54) provides further information on the petrogenesis of the batholith. The dominant detrital component in the siliciclastic rocks of the Lake Harbour Group is identical in age to these xenocrysts. The widespread occurrence of screens and xenoliths of Lake Harbour Group siliciclastic rocks throughout the batholith, and the coincidence of the 2.15 to 2.03 Ga ages, suggests that the Cumberland magmas assimilated significant volumes of Lake Harbour Group material. This suggestion is supported by similarities in Nd isotopic systematics between rocks of the batholith and siliciclastic rocks of the Lake Harbour Group (Thériault, 1998).

The ca. 1834–1830 Ma emplacement age of the monzonite (N312) that crosscuts a D_1 thrust contact between Ramsay River orthogneiss and metasedimentary rocks of the Blandford Bay assemblage places a minimum age on this phase of deformation at this location. The younger zircon (ca. 1816 Ma, 1797 ± 2 Ma) and monazite (1791 ± 2 Ma) ages in this sample correspond to the known age range for D_2 (accretionary) deformation in this part of the Trans-Hudson Orogen (Scott, 1997a; Wodicka and Scott, 1997).

The new results presented here for samples from structural levels 2 and 3 strengthen arguments based on field relationships (St-Onge et al., 1998d), existing geochronology (Scott, 1997a; Wodicka and Scott, 1997), and Nd isotopic (Thériault, 1998) and whole-rock geochemistry (Thériault et al., 1997) that unique igneous, sedimentological, deformational, and metamorphic events are preserved within each structural level. These data support the overall working hypothesis for this segment of the Trans-Hudson Orogen in which the rocks of levels 2 and 3 are exotic with respect to one another, undergoing separate geological histories prior to their accretion onto the northern margin of the Superior craton (structural level 1) (St-Onge et al., 1997d).

ACKNOWLEDGMENTS

Logistical support for fieldwork provided by the Polar Continental Shelf Project is gratefully acknowledged. Jack MacRae, Diane Bellerive, and Klaus Santowski are warmly thanked for the excellence of their technical support. Discussions and reviews of this manuscript by D. Corrigan, M.R. St-Onge and R.J. Thériault have improved the clarity of the ideas presented. This is Polar Continental Shelf Project contribution 03397.

REFERENCES

Blackadar, R.G.
1967: Geological reconnaissance, southern Baffin Island, District of Franklin; Geological Survey of Canada, Paper 66-47, 32 p.

Davis, D.W.
1982: Optimum linear regression and error estimation applied to U-Pb data; Canadian Journal of Earth Sciences, v. 19, p. 2141-2149.

Dunphy, J.M. and Ludden, J.N.
1998: Petrological and geochemical characteristics of a Proterozoic magmatic arc (Narsajuaq terrane, Ungava Orogen, Canada) and comparisons to Superior Province granitoids; Precambrian Research, v. 91, p. 109-142.

Hanmer, S., St-Onge, M.R., and Scott, D.J.
1996: Geology, White Strait, District of Franklin, Northwest Territories; Geological Survey of Canada, Open File 3192, scale 1:100 000.

Jackson, G.D., Hunt, P.A., Loveridge, W.D., and Parrish, R.R.
1990: Reconnaissance geochronology of Baffin Island, N.W.T.; *in* Radiogenic Age and Isotopic Studies: Report 3; Geological Survey of Canada, Paper 89-2, p. 123-148.

Krogh, T.E.
1982a: Improved accuracy of U-Pb zircon ages by the creation of more concordant systems using an air abrasion technique; Geochimica et Cosmochimica Acta, v. 46, p. 637-649.
1982b: Improved accuracy of U-Pb zircon dating by selection of more concordant fractions using a high gradient magnetic separation technique; Geochimica et Cosmochimica Acta, v. 46, p. 631-635.

Parrish, R.R., Roddick, J.C., Loveridge, W.D., and Sullivan, R.W.
1987: Uranium-lead analytical techniques at the geochronology laboratory, Geological Survey of Canada; *in* Radiogenic Age and Isotopic Studies: Report 1; Geological Survey of Canada, Paper 88-2 p. 3-7.

Roddick, J.C.
1987: Generalized numerical error analysis with application to geochronology and thermodynamics; Geochimica et Cosmochimica Acta, v. 51, p. 359-362.

Scott, D.J.
1997a: Geology, U-Pb & Pb-Pb geochronology of the Lake Harbour area, southern Baffin Island: implications for the Paleoproterozoic tectonic evolution of NE Laurentia; Canadian Journal of Earth Sciences, v. 34, p. 140-155.
1997b: Preliminary U-Pb geochronology of the Hall Peninsula east of Iqaluit, southern Baffin Island; *in* Radiogenic Age and Isotopic Studies: Report 10; Geological Survey of Canada, Current Research 1997-F, p. 67-78.

Scott, D.J. and Gauthier, G.
1996: Comparison of TIMS (U-Pb) and Laser Ablation Microprobe ICP-MS (Pb) techniques for age determination of detrital zircons from Paleoproterozoic metasedimentary rocks from northeastern Laurentia, Canada, with tectonic implications; Chemical Geology, v. 131, p. 127-142.

Scott, D.J., St-Onge, M.R., and Hanmer, S.
1996: Geology, Frobisher Bay, District of Franklin, Northwest Territories; Geological Survey of Canada, Open File 3193, scale 1:100 000.

Scott, D.J., St-Onge, M.R., Wodicka, N., and Hanmer, S.
1997a: Geology of the Markham Bay–Crooks Inlet area, southern Baffin Island, Northwest Territories; *in* Current Research 1997-C; Geological Survey of Canada, p. 157-166.

Scott, D.J., Stern, R., and St-Onge, M.R.
1997b: An overview of the geochronology of detrital zircons in Paleoproterozoic metasedimentary rocks, southern Baffin Island; *in* Report of 1997 ECSOOT Transect Meeting; (ed.) R.J. Wardle and J. Hall; Lithoprobe Report 61, p. 181-185.

St-Onge, M.R., Hanmer, S., and Scott, D.J.
1996: Geology of the Meta Incognita Peninsula, south Baffin Island: tectonostratigraphic units and regional correlations; *in* Current Research 1996-C; Geological Survey of Canada, p. 63-72.

St-Onge, M.R., Hanmer, S., Scott, D.J., and Wodicka, N.
1997a: Geology, Blandford Bay, District of Franklin, Northwest Territories; Geological Survey of Canada, Open File Map 3398, scale 1:100 000.
1997b: Geology, Crooks Inlet, District of Franklin, Northwest Territories; Geological Survey of Canada, Open File Map 3397, scale 1:100 000.
1997c: Geology, Hone River, District of Franklin, Northwest Territories; Geological Survey of Canada, Open File Map 3399, scale 1:100 000.

St-Onge, M.R., Lucas, S.B., Scott, D.J., and Wodicka, N.
1997d: Crustal-scale architecture and tectonostratigraphy of the Quebec–Baffin segment of Trans-Hudson Orogen; *in* Report of 1997 ECSOOT Transect Meeting, (ed.) R.J. Wardle and J. Hall; Lithoprobe Report 61, p. 186-190.

St-Onge, M.R., Scott, D.J., and Wodicka, N.
1998a: Geology, Hidden Bay, District of Franklin, Northwest Territories; Geological Survey of Canada, Open File Map 3536, scale 1:100 000.
1998b: Geology, McKellar Bay, District of Franklin, Northwest Territories; Geological Survey of Canada, Open File Map 3537, scale 1:100 000..
1998c: Geology, Wight Inlet, District of Franklin, Northwest Territories; Geological Survey of Canada, Open File Map 3538, scale 1:100 000.

St-Onge, M.R., Scott, D.J., Wodicka, N., and Lucas, S.B.
1998d: Geology of the McKellar Bay–Wight Inlet–Frobisher Bay area, southern Baffin Island, Northwest Territories; *in* Current Research 1998-C; Geological Survey of Canada, p. 43-54.

Stacey, J.S. and Kramers, J.D.
1975: Approximation of terrestrial lead isotope evolution by a two-stage model; Earth and Planetary Science Letters, v. 26, p. 207-221.

Steiger, R.H. and Jäger, E.
1977: Subcommission on geochronology: convention on the use of decay constants in geo- and cosmochronology; Earth and Planetary Science Letters, v. 36, p. 359-362.

Thériault, R.J.
1998: Nd isotopic and geochemical characteristics of Paleoproterozoic rocks of southern Baffin Island, eastern Trans-Hudson Orogen; *in* Radiogenic Age and Isotopic Studies: Report 11; Geological Survey of Canada.

Thériault, R.J., Scott, D.J., and St-Onge, M.R.
1997: Nd isotopic and geochemical evolution of Paleoproterozoic plutonic rocks, southern Baffin Island; *in* Report of 1997 ECSOOT Transect Meeting; (ed.) R.J. Wardle and J. Hall; Lithoprobe Report 61, p. 203-208.

Wheeler, J.O., Hoffman, P.F., Card, K.D., Davidson, A., Sanford, B.V., Okulitch, A.V., and Roest, W.R.
1996: Geological Map of Canada, Map 1860A; Geological Survey of Canada, scale 1:5 000 000.

Wodicka, N. and Scott, D.J.
1997: A preliminary report on the U-Pb geochronology of the Meta Incognita Peninsula, southern Baffin Island, Northwest Territories; *in* Current Research 1997-C; Geological Survey of Canada, p. 167-178.

York, D.
1969: Least squares fitting of a straight line with correlated errors; Earth and Planetary Science Letters, v. 5, p. 320-324.

– 6 –

Reconnaissance Nd isotopic study of the Paleoproterozoic rocks of Meta Incognita Peninsula, southern Baffin Island, Northwest Territories

R.J. Thériault[1]

Thériault, R.J., 1998: Reconnaissance Nd isotopic study of the Paleoproterozoic rocks of Meta Incognita Peninsula, southern Baffin Island, Northwest Territories; in *Radiogenic Age and Isotopic Studies: Report 11; Geological Survey of Canada, Current Research 1998-F, p. 59-68.*

Abstract: Samarium-neodymium isotopic data are presented for 25 Paleoproterozoic rocks from southern Baffin Island. At structural level 2, the Narsajuaq arc yields ε_{Nd}(1.85 Ga) of -12.6 to -19.1, and $^{147}Sm/^{144}Nd$ of 0.049 to 0.11, suggesting strongly fractionated Archean crustal sources.

At structural level 3, pelitic rocks of the Lake Harbour Group display ε_{Nd}(1.85 Ga) from -4.5 to -7.3 and T_{DM} ages from 2.91 to 2.48 Ga. Metasediments of the Blandford Bay assemblage have ε_{Nd}(1.85 Ga) of -6.0 to -8.5 and T_{DM} ages from 3.13 to 2.83 Ga. The Cumberland batholith yields ε_{Nd}(1.85 Ga) of -2.2 to -7.5, whereas orthogneiss of the Ramsay River suite gives ε_{Nd}(1.85 Ga) of -6.1 to -8.2 and T_{DM} ages of 2.99 to 2.08 Ga. The sharp contrast in Nd isotopic compositions between level 2 and 3 rocks suggests that the two were produced along cratonic margins that were distinct in age and composition.

Résumé : On présente les résultats d'analyses isotopiques Sm-Nd de 25 roches paléoprotérozoïques du sud de l'île de Baffin. Dans le niveau structural 2, l'arc de Narsajuaq montre des valeurs ε_{Nd}(1,85 Ga) allant de -12,6 à -19,1 et des rapports $^{147}Sm/^{144}Nd$ de 0,049 à 0,11, ce qui suggère des sources crustales archéennes intensément fractionnées.

Dans le niveau structural 3, les roches pélitiques du Groupe de Harbour Lake affichent des valeurs ε_{Nd}(1,85 Ga) de -4,5 à -7,3 et des âges T_{DM} de 2,91 à 2,48 Ga. Les roches sédimentaires métamorphisées de l'assemblage de Blandford Bay montrent des valeurs ε_{Nd}(1,85 Ga) de -6,0 à -8,5 et des âges T_{DM} de 3,13 à 2,83 Ga. Le batholite de Cumberland a des valeurs ε_{Nd}(1,85 Ga) de -2,2 à -7,5 et l'orthogneiss de la suite de Ramsay River, des valeurs ε_{Nd}(1,85 Ga) de -6,1 à -8,2 et des âges T_{DM} de 2,99 à 2,08 Ga. Le contraste nette de la composition des isotopes de Nd des roches des niveaux 2 et 3 laisse supposer que les deux niveaux se sont formés le long de marges cratoniques d'âge et de composition différents.

[1] Geological Survey of Canada, 601 Booth Street, Ottawa, Ontario K1A 0E8

INTRODUCTION

A reconnaissance sampling program for geochemical and Sm-Nd isotopic investigations on Meta Incognita Peninsula was conducted in 1996 and 1997. This initiative was undertaken in concert with the systematic geological mapping of southern Baffin Island at 1:100 000 scale by the Continental Geoscience Division, which encompassed an area of approximately 28 000 km^2 of bedrock (St-Onge et al., 1996, 1998; Scott et al., 1997b). The data presented in this report are a representative subset of a broader database, ultimately destined for external publication with complimentary major- and trace-element geochemical data. The samples selected for Sm-Nd isotopic analysis were collected from the 1995 and 1996 field areas, representing the central and western sectors of the project area. The sample set is considered representative of the major lithological types of the project area, as structural repetition of previously mapped units was documented during the 1997 field season (St-Onge et al., 1998).

This reconnaissance isotopic study not only benefits from recently acquired field data, but also from ongoing U-Pb geochronological studies on the ages of crystallization and deposition of the major plutonic and supracrustal units (D. Scott), and on the metamorphic and structural evolution of the area (N. Wodicka), which provide a temporal framework (Scott and Wodicka, 1998; Wodicka and Scott, 1997) for the application of Sm-Nd isotopic data.

GEOLOGICAL SETTING

The Paleoproterozoic rocks of southern Baffin Island represent the northern continuation of the Ungava (northern Quebec) segment of the eastern Trans-Hudson Orogen (Fig. 1). In the Ungava segment, the Trans-Hudson Orogen comprises 3.22–2.74 Ga autochthonous Superior Province basement gneisses, imbricated 2.04–1.92 Ga rift and passive-margin supracrustal rocks of the Povungnituk and Chukotat groups, recording the development of an oceanic basin (St-Onge et al., 1992), the allochthonous Purtuniq ophiolite (Scott et al., 1991; Scott and Helmstaedt, 1992), and the 1.86–1.82 Ga Narsajuaq continental magmatic arc, representing convergence and basin closure (Dunphy, 1995).

On Baffin Island (Fig. 2a) three temporally and lithologically distinct structural levels were juxtaposed by southwest-verging convergence, thrusting, and tectonic stacking of Paleoproterozoic plutonic and supracrustal rocks (structural levels 2 and 3) onto the Archean Superior Province and rift-related rocks of the Povungnituk Group (structural level 1) (St-Onge et al., 1997). Paleoproterozoic thrusting and stacking on southern Baffin Island are the result of two phases of deformation (D_1 and D_2). Post-collision orogen-parallel folding (D_3) and cross-folding (D_4) resulted in exposure of the different structural levels.

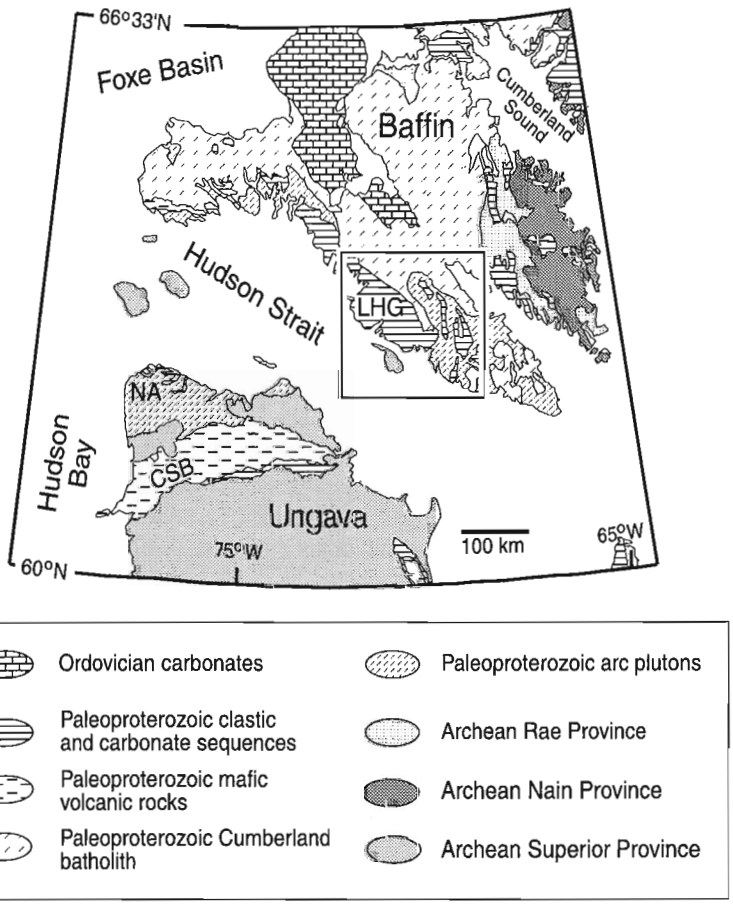

Figure 1.

Generalized geologic map showing major lithotectonic assemblages of southern Baffin Island and the Ungava Peninsula (after St-Onge et al., 1998). Study area is outlined. CSB: Cape Smith belt, LHG: Lake Harbour Group, NA: Narsajuaq arc (Ungava).

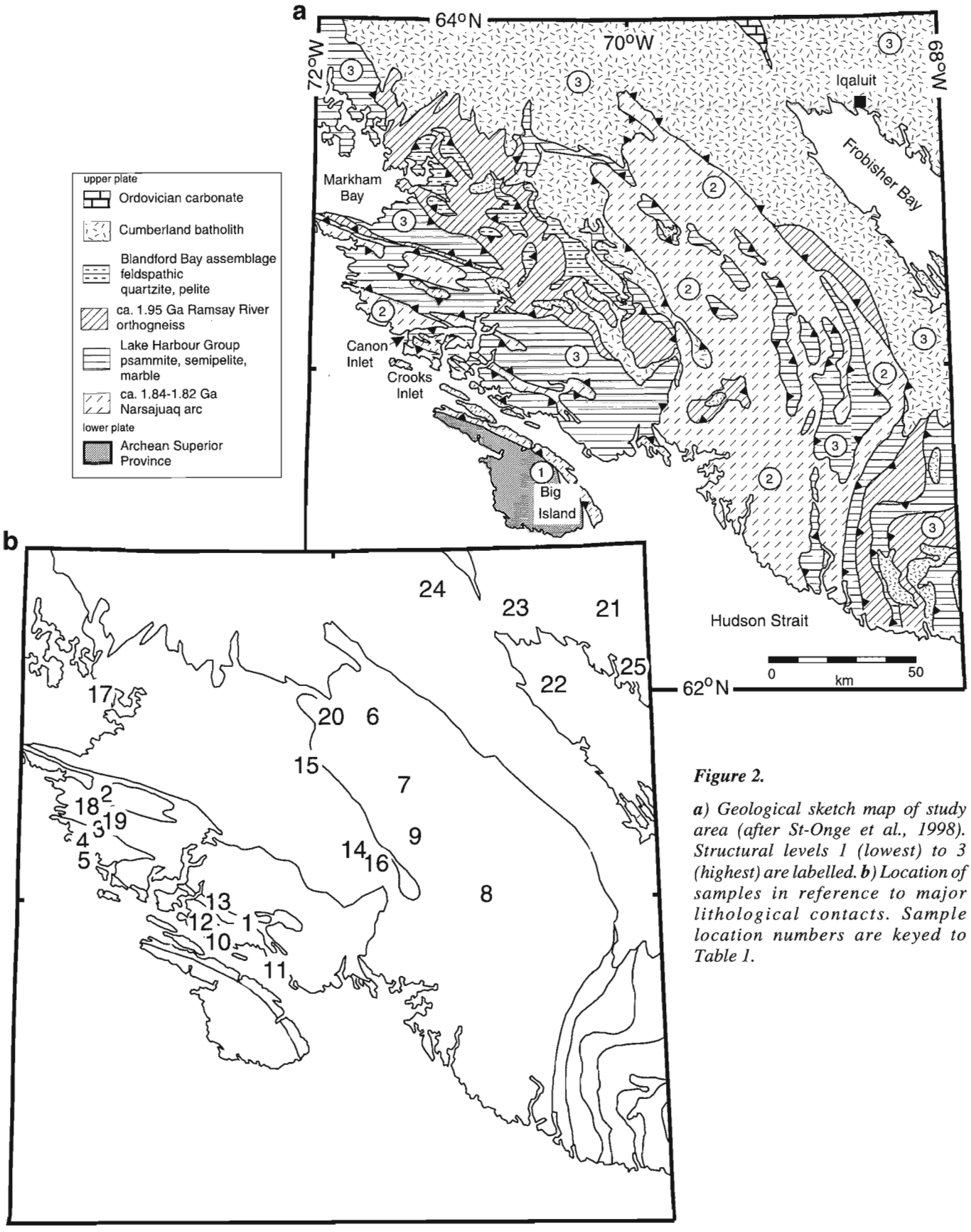

Figure 2.

***a**) Geological sketch map of study area (after St-Onge et al., 1998). Structural levels 1 (lowest) to 3 (highest) are labelled. **b**) Location of samples in reference to major lithological contacts. Sample location numbers are keyed to Table 1.*

Exposure of the structurally lowest rocks (level 1) is restricted to Big Island, off the southern coast of Baffin Island. These rocks are interpreted to constitute the structural basement of levels 2 and 3 throughout the study area (St-Onge et al., 1997). Level 1 rocks consist of late Archean tonalitic and monzogranitic orthogneisses structurally imbricated with quartzite, pelite, semipelite, amphibolite, and ultramafic rocks correlated with the Povungnituk Group of Ungava (St-Onge et al., 1996; Wodicka and Scott, 1997). The Mina mylonite zone, a northeast-dipping belt of ribbon mylonites, separates level 1 from the structurally higher levels 2 and 3.

Structural level 2 comprises foliated hornblende-biotite-orthopyroxene monzogranite-granodiorite-tonalite orthogneisses. These rocks are commonly associated with metre-scale layers of diorite and quartz-diorite gneisses (St-Onge et al., 1996; 1998). Recent U-Pb geochronology suggests that level 2 orthogneisses crystallized between 1842 +5/-3 and 1821 ± 2 Ma and supports correlation with the Narsajuaq arc of Ungava (Scott, 1997; Wodicka and Scott, 1997). Hence, in the remainder of this paper the term Narsajuaq arc is applied to the orthogneisses of structural level 2.

Structurally above level 2, level 3 comprises two supracrustal sequences and metaplutonic suites. Supracrustal rocks of the Lake Harbour Group principally occur in a regional-scale northwest-plunging D_3 synform and as klippen overlying level 2 Narsajuaq orthogneisses (St-Onge et al., 1996; 1997, 1998; Scott et al., 1997b; Wodicka and Scott, 1997). The Lake Harbour Group consists of quartzites, psammites, pelites, marbles, and subordinate mafic and ultramafic rocks. The depositional age of the Lake Harbour Group is bracketed by 1934 ± 3 Ma (Scott and Gauthier, 1996), the youngest age obtained from U-Pb analysis of detrital zircons, and ca. 1865–1850 Ma, the U-Pb crystallization age of the crosscutting Cumberland batholith (Scott, 1997; Scott and Wodicka, 1998). The second supracrustal sequence, the Blandford Bay assemblage (Scott et al., 1997b), structurally overlies the Lake Harbour Group, is characterized by feldspathic quartzite, rusty pelite, and concordant mafic and ultramafic sills, and is intruded by the Cumberland batholith.

The Ramsay River orthogneiss and Cumberland batholith constitiute the plutonic suites of structural level 3. The Ramsay River orthogneiss (St-Onge et al., 1998) consists of orthopyroxene-biotite monzogranite to tonalite gneiss, and subordinate discontinuous layers of quartz diorite. A sample of monzogranite gneiss has been dated at 1950 +6/-4 Ma (Scott and Wodicka, 1998). This age and field considerations have led Scott and Wodicka (1998) to suggest that the Ramsay River orthogneiss may represent the depositional basement to the Lake Harbour Group.

Occupying the northern portion of the study area, the Cumberland batholith (Jackson et al., 1990) comprises dominantly massive to foliated orthopyroxene-biotite monzogranite, with subordinate components that range in composition from tonalite to syenogranite. Bulk rock geochemistry is consistent with emplacement in a continental arc setting (Thériault et al., 1997). The batholith contains numerous dioritic sheets and screens of metasedimentary rocks, the latter likely derived from the Lake Harbour Group.

Table 1. Sm-Nd isotopic data from whole-rock samples from southern Baffin Island.

# on Fig. 2b	Sample	Structural level	Unit	Lithology	Sm(ppm)	Nd(ppm)	$^{147}Sm/^{144}Nd$	$^{143}Nd/^{144}Nd$ (2 s.e.)	ε_{Nd} (1.85 Ga)	T_{DM} (Ga)
1	*95-D091	2	Narsajuaq	tonalite	2.13	23.75	0.0542	0.510042 (8)	-16.9	2.95
2	*96-T030	2	Narsajuaq	granodiorite	2.84	21.87	0.0787	0.510424 (8)	-15.2	3.06
3	*96-T035	2	Narsajuaq	granodiorite	0.81	6.64	0.0734	0.510495 (5)	-12.6	2.87
4	*96-T037	2	Narsajuaq	granodiorite	8.19	54.83	0.0902	0.510534 (4)	-15.8	3.21
5	*96-T038	2	Narsajuaq	monzogranite	0.16	1.99	0.0490	0.510123 (10)	-14.1	2.79
6	96-T044	2	Narsajuaq	monzogranite	5.53	50.81	0.0657	0.510156 (8)	-17.4	3.06
7	96-T050	2	Narsajuaq	monzogranite	8.08	70.82	0.0689	0.510269 (14)	-15.9	3.01
8	96-T053	2	Narsajuaq	granodiorite	1.32	14.35	0.0555	0.509943 (11)	-19.1	3.07
9	96-T055	2	Narsajuaq	granodiorite	4.69	25.75	0.1100	0.510668 (8)	-17.9	3.62
10	95-N016	3	L. Harbour Gp.	grt-psammite	2.54	18.04	0.0850	0.511050 (8)	-4.5	2.48
11	95N019	3	L. Harbour Gp.	grt-sill-pelite	6.60	44.74	0.0892	0.511023 (3)	-6.0	2.59
12	95-D024	3	L. Harbour Gp.	grt-sill pelite	4.06	28.22	0.0869	0.511065 (5)	-4.6	2.50
13	95-I-030	3	L. Harbour Gp.	grt-sill pelite	2.68	13.77	0.1176	0.511305 (4)	-7.3	2.91
14	D055A	3	Blandford Bay	quartzite	0.81	4.93	0.0990	0.511013 (10)	-8.5	2.83
15	95-C221	3	Blandford Bay	gt. semipelite	4.12	20.34	0.1223	0.511420 (7)	-6.1	2.87
16	95-I051E	3	Blandford Bay	psammite	7.36	31.30	0.1420	0.511668 (10)	-6.0	3.13
17	96-D331A	3	Ramsay River	tonalite	1.77	8.69	0.1229	0.511428 (10)	-6.1	2.88
18	*96-T031	3	Ramsay River	granodiorite	2.79	13.25	0.1272	0.511456 (8)	-6.6	2.97
19	*96-T032	3	Ramsay River	monzogranite	4.93	25.40	0.1173	0.511249 (8)	-8.2	2.99
20	96-T046	3	Ramsay River	monzogranite	9.13	55.13	0.1001	0.511050 (11)	-8.1	2.80
21	95-D078B	3	Cumberland	opx-biot monzogranite	2.80	22.82	0.0741	0.510989 (8)	-3.1	2.35
22	95-I114	3	Cumberland	opx-cpx monzogranite	11.43	67.40	0.1025	0.511355 (4)	-2.7	2.45
23	95-J033	3	Cumberland	biot monzogranite	3.55	16.54	0.1297	0.511443 (8)	-7.4	3.08
24	95-N065	3	Cumberland	granodiorite	5.04	39.41	0.0773	0.510864 (10)	-6.3	2.55
25	95-D100	3	Cumberland	qtz. diorite	1.32	8.36	0.0959	0.511299 (8)	-2.2	2.39

$^{143}Nd/^{144}Nd$ ratios normalized to $^{146}Nd/^{144}Nd + 0.7219$. Individual 2s error on individual $^{143}Nd/^{144}Nd$ determinations are 10^{-6} of reported values. Uncertainty on ε_{Nd} values approximately 0.5 ε_{Nd} unit. Uncertainty on Sm and Nd concentrations is better than 1%. T_{DM} model ages are calculated according to the depleted mantle parameters of Goldstein et al. (1984). * denotes samples from the imbricated thrust sheets near the Canon Inlet area.

Along the south coast of Meta Incognita Peninsula, in the Crooks Inlet and Canon Inlet areas (Fig. 2a), northwest-striking thrust sheets of levels 2 and 3 rocks are structurally imbricated, thus often rendering difficult the unambiguous field identification of level 2 and 3 orthogneisses.

SAMARIUM-NEODYMIUM ISOTOPE GEOCHEMISTRY

Data are presented in Table 1 and Figures 3, 4 and 5 for 25 whole-rock samples representative of the principal lithologies of structural levels 2 and 3. Although the samples represent Paleoproterozoic ages from ca. 1.95 Ga to ca. 1.82 Ga, all ε_{Nd} values were calculated for 1.85 Ga. This allows direct comparison of Nd isotopic compositions of all samples, and interpretation of the data based on equivalent time-integrated ε_{Nd} values.

Analytical methods

Kilogram-size samples were crushed and powdered in a W-carbide ring mill for Sm-Nd isotope analysis. Sample powders, spiked with a mixed ^{148}Nd-^{149}Sm solution, were dissolved in an HF-HNO_3 mixture. Extraction of rare earth elements (REE) was done by cation exchange chromatography on TruSpec™ resin optimized for REE separation, or on Biorad™ AG50W-x12 resin. Separation of Sm and Nd from other REEs followed HDEHP (Di (2-ethylexyl) orthophosphoric acid)- teflon powder chromatography. Total procedure blanks were less than 100 pg for Nd and 50 pg for Sm. Mass analysis was carried out on a MAT-261 solid-source mass spectrometer in static multicollection mode for Nd and Sm. Nd isotopic compositions were normalized to $^{146}Nd/^{144}Nd = 0.7219$. The $^{143}Nd/^{144}Nd$ ratios were corrected to LaJolla $^{143}Nd/^{144}Nd = 0.511860$. External precision for ε_{Nd} values is estimated to be within ±0.5 ε unit. The

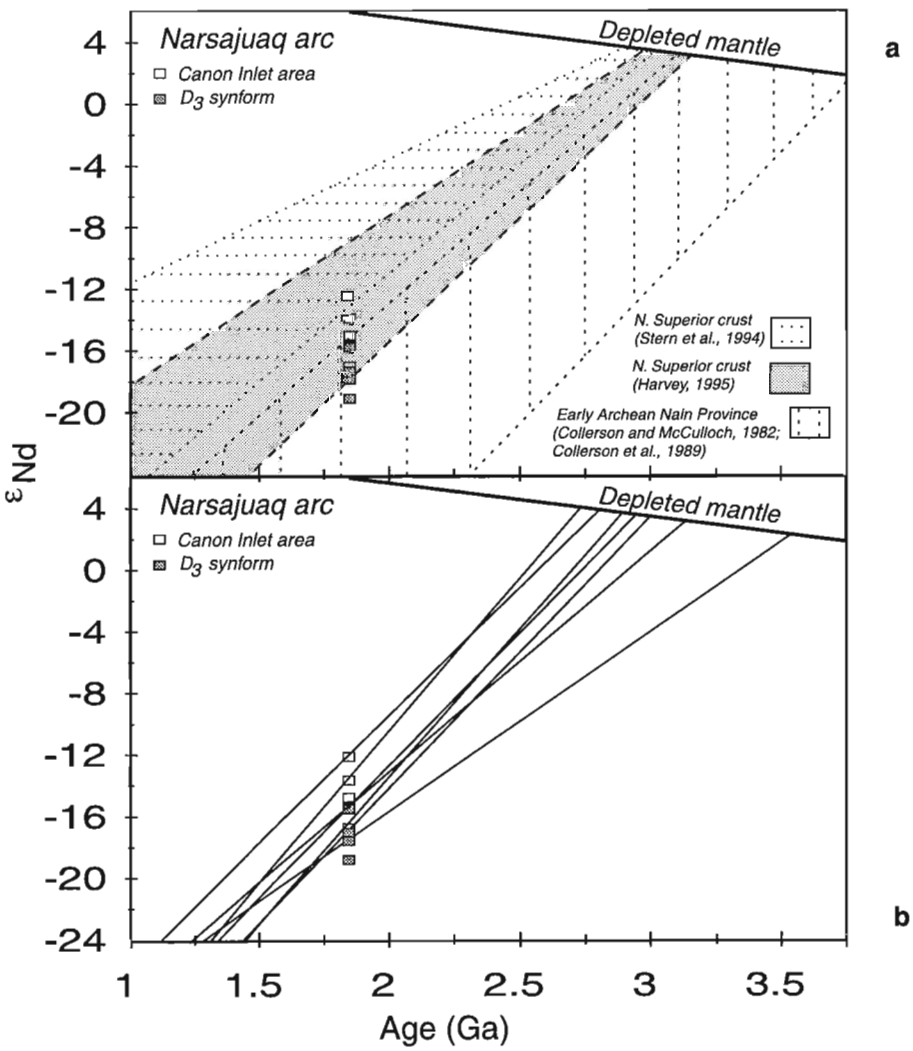

Figure 3. *ε_{Nd} against time plots for Narsajuaq arc orthogneisses of structural level 2 showing* ***a****) evolution fields for Archean crust presently exposed in northeast Laurentia, and* ***b****) showing evolution lines for individual samples.*

$^{147}Sm/^{144}Nd$ values are reproducible to 0.5%. The ε_{Nd} values were calculated assuming CHUR $^{147}Sm/^{144}Nd = 0.1967$ and present-day $^{143}Nd/^{144}Nd = 0.512638$ (Jacobsen and Wasserburg, 1980). Depleted mantle (T_{DM}) model ages were calculated according to the model of Goldstein et al. (1984), whereby the depleted mantle has evolved linearly since 4.6 Ga to a present-day ε_{Nd} value of +10.

Structural level 2

A total of nine samples of Narsajuaq arc granodiorites and monzogranites were analyzed. Five of the samples are from imbricated thrust sheets in the vicinity of Canon Inlet, and the remaining four samples are from a regional-scale D_3 antiform in the eastern part of the study area, where most of structural level 2 is exposed (Fig. 2b). The five samples from the thrust sheets in the Canon Inlet area yielded ε_{Nd} values ranging from -12.6 to -16.9, $^{147}Sm/^{144}Nd$ ratios of 0.0490 to 0.0902, and T_{DM} model ages ranging from 3.21 to 2.87 Ga (Fig. 3). The samples from the regional-scale antiform have ε_{Nd} values of -15.9 to -19.1, $^{147}Sm/^{144}Nd$ ratios of 0.0555 to 0.1100, and T_{DM} ages of 3.01 to 3.62 Ga. The isotopic signatures suggest dominance of an Archean crustal precursor in the petrogenesis of these orthogneisses. The unusually low $^{147}Sm/^{144}Nd$ ratios are indicative of unusually strong light-rare-earth-element enrichment. No correlation exists between $^{147}Sm/^{144}Nd$ ratios and whole-rock geochemistry (Thériault, unpub. data).

Structural level 3

Lake Harbour Group

Four pelitic rocks from the Lake Harbour Group yielded ε_{Nd} values of -4.5 to -7.3, and T_{DM} model ages of 2.91 to 2.48 Ga, indicative of early Paleoproterozoic to late Archean crustal

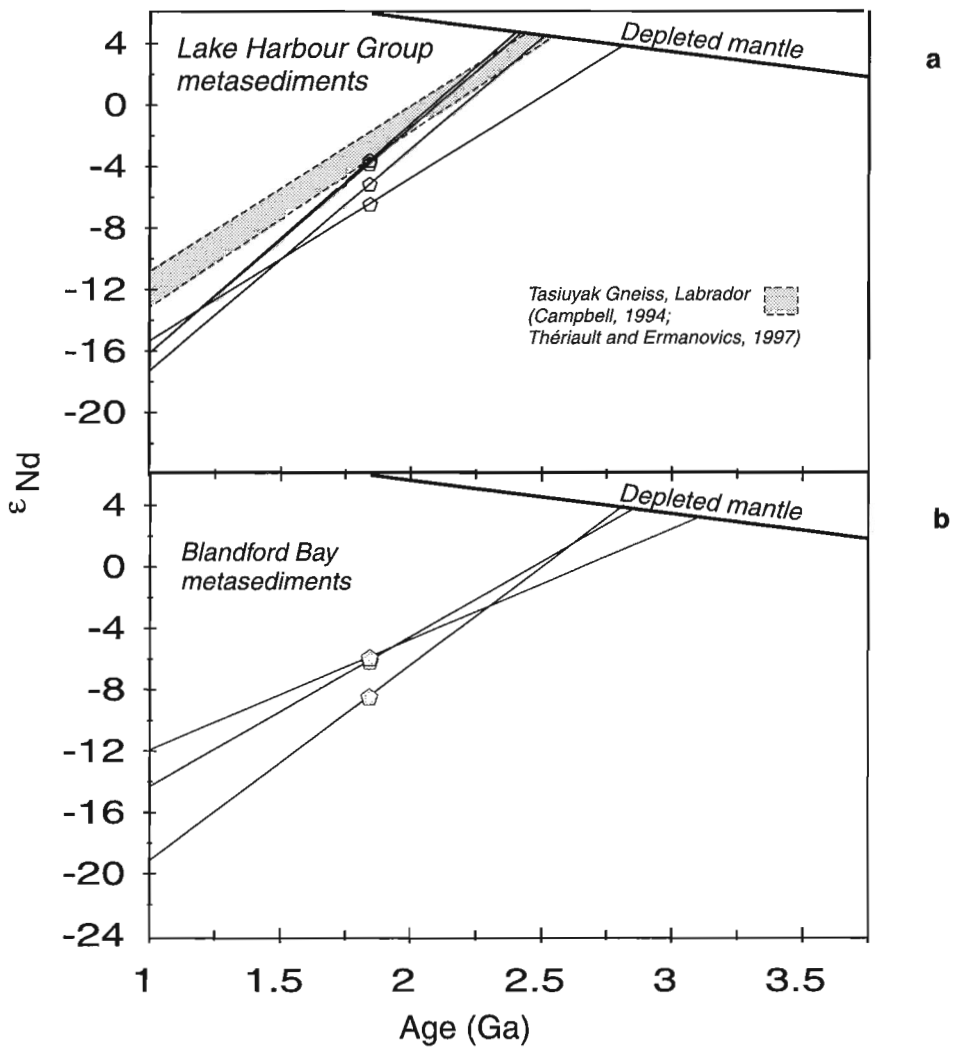

Figure 4. *ε_{Nd} against time plots for **a**) Lake Harbour Group metasediments, showing field for evolution of Tasiuyak gneiss, and **b**) for Blandford Bay assemblage metasediments.*

sources (Fig. 4a). The $^{147}Sm/^{144}Nd$ ratios of 0.0850 to 0.1176 suggest a degree of light-rare-earth-element enrichment that is common in many upper to mid-crustal rocks (Taylor and McClennan, 1985).

Blandford Bay assemblage

Three samples of semipelite, psammite, and feldspathic quartzite from the Blandford Bay assemblage have ε_{Nd} of -6.0 to -8.5, $^{147}Sm/^{144}Nd$ ratios of 0.0990 to 0.1420, and T_{DM} of 3.13 to 2.83 Ga (Fig. 4b). The tendency to lower ε_{Nd} values and older T_{DM} ages for the Blandford Bay metasedimentary rocks relative to those of the Lake Harbour Group values suggests older sources may have contributed detritus to the Blandford Bay assemblage.

Ramsay River orthogneiss

Four samples from the Ramsay River orthogneiss that range in composition from tonalite to granite were collected from the northwestern part of the study area near Markham Bay, from imbricated thrust sheets northwest of Canon Inlet, and from a structural basin overlying level 2 in the eastern portion of the area (Fig. 2). The ε_{Nd} values range from -6.1 to -8.2 (Fig. 5a). The $^{147}Sm/^{144}Nd$ ratios span from 0.1001 to 0.1229, and T_{DM} model ages from 2.99 to 2.80 Ga.

Cumberland batholith

Five Cumberland batholith rocks, ranging in composition from quartz diorite to monzogranite, display ε_{Nd} values of -2.2 to -7.4 and $^{147}Sm/^{144}Nd$ ratios spanning from 0.0741 and 0.1297, indicative of derivation from evolved, light-rare-earth-element-enriched crustal components (Fig. 5b). T_{DM} ages ranging from 3.08 to 2.35 Ga suggest Paleoproterozoic to Archean crustal sources for Cumberland batholith

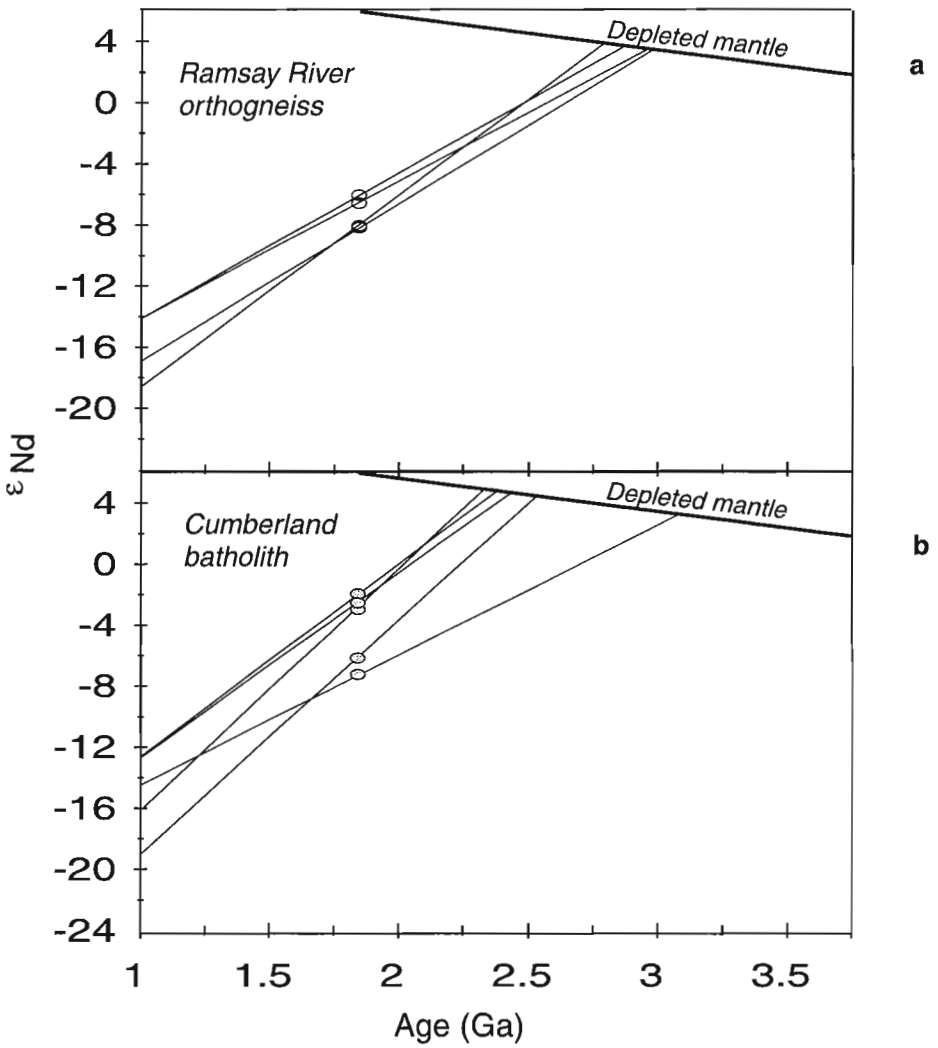

Figure 5. *ε_{Nd} against time plots for **a**) Ramsay River orthogneiss and **b**) Cumberland batholith granitoids.*

magmas. The overlapping Sm-Nd isotopic compositions of the Cumberland batholith and older metasedimentary rocks of Lake Harbour Group, which are engulfed by the batholith, suggests a genetic relationship between these two structural level 3 units.

DISCUSSION

The Sm-Nd isotopic compositions presented here underscore fundamental differences in the age and composition of the crustal precursors of levels 2 and 3. Discussion of the significance of these differences follows assessment of the data for individual lithologies.

The Narsajuaq arc orthogneisses of structural level 2 are characterized by their low ε_{Nd} values (-12.6 to -19.1) and unusually low $^{147}Sm/^{144}Nd$ ratios (0.0490 to 0.1100). These $^{147}Sm/^{144}Nd$ ratios are a reflection of profound chemical fractionation, and may be a feature resulting from melting and extreme differentiation of a more primitive magma during the Paleoproterozoic, or a geochemical imprint of an Archean crustal component. If the low $^{147}Sm/^{144}Nd$ ratios resulted from Paleoproterozoic fractionation, a clear relationship would exist between whole rock composition and $^{147}Sm/^{144}Nd$. However, the absence of such a correlation implies that the low $^{147}Sm/^{144}Nd$ ratios are a geochemical feature inherited from an earlier crustal component which was assimilated by the source magmas of Narsajuaq rocks.

In an attempt to identify the crustal component in level 2 orthogneisses, Archean rocks of northeast Laurentia with similar $^{147}Sm/^{144}Nd$ ratios and $\varepsilon_{Nd}(1.85\ Ga)$ values were compared with the data for level 2 orthogneisses. These include early Archean gneisses of the Nain Province in Labrador (Collerson and McCulloch, 1982; Collerson et al., 1989) and some of the late Archean orthogneisses of the northern Superior Province exposed in northern Ungava Peninsula (Harvey, 1995) (Fig. 3a). Most of the Archean rocks of the northern Superior Province generally have $\varepsilon_{Nd}(1.85\ Ga)$ and $^{147}Sm/^{144}Nd$ ratios (Stern et al., 1994) which are too elevated to be considered as crustal components to the Narsajuaq orthogneisses of level 2. However, considerable overlap exists between the $\varepsilon_{Nd}(1.85\ Ga)$ values displayed by the Narsajuaq arc and the northern Superior Province rocks from Ungava Peninsula studied by Harvey (1995) (Fig. 3a). Furthermore, $\varepsilon_{Nd}(1.85\ Ga)$ values for the Narsajuaq arc coincide with the range of values obtained from Early Archean gneisses from the Nain Province of Labrador (Collerson and McCulloch, 1982; Collerson et al., 1989) (Fig 2a). Although similarities exist between the Sm-Nd isotopic composition of the Narsajuaq arc on Baffin Island and Archean rocks of parts of the northern Superior and Nain Provinces, the current Nd isotopic data set does not allow unequivocal identification of the Archean crustal component present in the Narsajuaq arc orthogneisses.

The Narsajuaq arc rocks exposed on southern Baffin Island bear dramatically different Sm-Nd isotopic signatures from the Narsajuaq rocks of the Ungava Peninsula (Fig. 3b). There, Dunphy (1995) documented $\varepsilon_{Nd}(1.85\ Ga)$ of +4.0 to -18.5, with only six of nineteen samples yielding $\varepsilon_{Nd}(1.85\ Ga)$ less than -10, and the remaining thirteen samples having $\varepsilon_{Nd}(1.85\ Ga)$ greater than -6.6. The north-south disparity in the Nd isotopic composition of correlated Narsajuaq arc rocks from Ungava to Meta Incognita Peninsula may be explained by a north-dipping subduction zone, resulting in continental arc magmas being intruded into or produced in a northward-thickening Archean crustal block. This hypothesis is consistent with a subduction polarity away from the Superior Province, as postulated by workers in the various segments of the eastern Trans-Hudson Orogen (St-Onge et al., 1992, 1997; Scott, 1995; Scott and Machado, 1995). Alternatively, the differences in ε_{Nd} and $^{147}Sm/^{144}Nd$ between the Narsajuaq arc of Ungava and Meta Incognita peninsulas may document the relic of a fundamental age boundary in the Archean cratonic margin into which the Narsajuaq arc was built. In such a scenario, the Archean margin would have comprised older, more fractionated rocks in the north, and more juvenile rocks near its southern edge.

As noted above, rocks from structural level 3 yield Sm-Nd isotopic signatures that are distinct from level 2. The metasedimentary rocks of the Lake Harbour Group have ε_{Nd} of -4.5 to -7.3 and $^{147}Sm/^{144}Nd$ ratios of 0.085 to 0.1176, which unequivocally suggest younger and less fractionated crustal sources relative to the metaplutonic rocks of level 2 rocks. The ε_{Nd} values of three Blandford Bay assemblage metasedimentary rocks (-6.0 to -8.5) overlap with many of the ε_{Nd} values for the Lake Harbour Group samples, and may indicate derivation of detritus of sources of similar Nd isotopic composition. However, the $\varepsilon_{Nd}(1.85\ Ga)$ values and T_{DM} ages of the Blandford Bay assemblage range as low as -8.5 and 3.13 Ga respectively, suggesting contribution of an older sedimentary source which is not recognized in the Lake Harbour Group samples. Older sources are suggested by U-Pb SHRIMP analysis of detrital zircons from Blandford Bay assemblage metasedimentary rocks, which have yielded ages greater than 2.8 Ga. A small proportion of zircon grains produced ages greater than 3.0 Ga, and one grain yielded an age of ca. 3.7 Ga (Scott et al., 1997a).

Detrital zircons from the Lake Harbour Group and Tasiuyak paragneiss of Labrador and southeastern Baffin Island have yielded U-Pb ages mostly in the 1.9–2.2 Ga range, with few Archean ages (Scott and Gauthier, 1996; Scott, 1997), leading to speculation that the two metasedimentary units had received detritus from a common Paleoproterozoic source (Scott et al., 1997a). However, the Lake Harbour Group samples show ε_{Nd} values (-4.5 to -7.3) that are more negative than the -2 to -3.8 values reported for the Tasiuyak paragneiss (Campbell, 1994; Thériault and Ermanovics, 1997), suggesting slightly older crustal components in Lake Harbour Group samples relative to Tasiuyak paragneiss for which Sm-Nd data exist. Nonetheless, the ε_{Nd} values and T_{DM} ages of the Lake Harbour Group do support derivation from Paleoproterozoic sources. A potential source for some of the Lake Harbour Group metasediments may be the Ramsay River orthogneisses, which yield $\varepsilon_{Nd}(1.85\ Ga)$ values ranging from -6.1 to -8.2, overlapping with the Lake

Harbour Group values of -4.5 to -7.3. The possibility that the Ramsay River orthogneiss represents depositional basement to the Lake Harbour Group (Scott and Wodicka, 1998) reinforces the hypothesis that the former may have contributed detritus to the latter.

The ε_{Nd} values of the Cumberland batholith (-2.2 to -7.4) overlap the range of values for Lake Harbour Group metasedimentary rocks, commonly included in the batholith. The most likely interpretation of the Cumberland batholith ε_{Nd} values is pervasive assimilation of Lake Harbour Group material by the Cumberland source magmas. The Cumberland batholith ε_{Nd} values contrast with the ε_{Nd} values of -6.1 to -8.2 displayed by the Ramsay River orthogneiss. The more negative values, as well as older T_{DM} ages, reflect the presence of slightly older crustal component in the Ramsay River orthogneiss not evident in the Cumberland batholith. The presence of an older crustal component in the Ramsay River orthogneiss is consistent with preliminary U-Pb ages suggesting that the latter predates the Cumberland batholith by approximately 100 Ma (St-Onge et al., 1998).

Although notable differences in Sm-Nd isotopic signatures exist between the various rock units of structural level 3, none of these display Nd isotopic compositions as evolved as those of level 2. The dramatic contrast between levels 2 and 3 points to the involvement of fundamentally differing crusts, both in terms of age and bulk composition. It is difficult to reconcile this difference in fundamental characteristics within the context of a single subduction system, where continental arc magmas would have been generated in the mantle wedge beneath, and within, a single cratonic margin. The stark contrast in Sm-Nd isotopic compositions between rocks of levels 2 and 3 supports the existence of at least two distinct Paleoproterozoic subduction zones. One subduction zone would have produced the Narsajuaq arc by pervasive assimilation or melting of crustal rocks with low $^{147}Sm/^{144}Nd$ ratios and ε_{Nd}(1.85 Ga) values less than -12.6 (upper limit of Narsajuaq values). A second subduction zone involving a cratonic margin with more elevated $^{147}Sm/^{144}Nd$ ratios and ε_{Nd}(1.85 Ga) values would have produced the magmatic rocks of structural level 3. Although the Cumberland batholith and Ramsay River orthogneiss vary in age by approximately 100 Ma, it is conceivable that both of these level 3 metaplutonic suites represent separate episodes of magmatism along a same continental margin. Such a scenario would be consistent with the occurrence of temporally distinct magmatic rocks with similar Sm-Nd isotopic signatures on structural level 3.

ACKNOWLEDGMENTS

Sample collection would not have been possible without the enthusiastic help of Ian Russell, Dave Copeland, Liz Turner, Greg Brown, and Jasen Robillard, and the expert flying skills of Nancy Laforest and Tom McMahon. Marc St-Onge, Dave Scott, and Natasha Wodicka are warmly thanked for their constructive criticism of an earlier version of this manuscript.

REFERENCES

Campbell, L.M.
1994: Preliminary results from an Sm-Nd isotopic study of Proterozoic crustal formation and accretion in the Torngat orogen, northen Labrador; *in* Eastern Canadian Shield Onshore-Offshore Transect (ECSOOT), Transect Meeting (December 10-11, 1993), (comp.) R.J. Wardle and J. Hall; The University of British Columbia, LITHOPROBE Secretariat, Report No. 36, p. 100-107.

Collerson, K.D. and McCulloch, M.T.
1982: The origin and evolution of Archean crust as inferred from Nd, Sr and Pb isotopic studies in Labrador; *in* 5th International Conference on Geochronology, Cosmochronology and Isotope Geology, extended Abstracts, p. 61-62.

Collerson, K.D., McCulloch, M.T., and Nutman, A.P.
1989: Sr and Nd isotope systematics of polymetamorphic Archean gneisses from southern West Greenland and Northern Labrador; Canadian Journal of Earth Sciences, v. 26, p. 446-466.

Dunphy, J.M.
1995: Magmatic evolution and crustal accretion in the early Proterozoic: the geology and geochemistry of the Narsajuaq terrane, Ungava Orogen, northern Quebec; Ph.D. thesis, Université de Montréal, Montréal, Quebec, 333 p.

Goldstein, S.L., O'Nions, R.K., and Hamilton, P.J.
1984: A Sm-Nd study of atmospheric dusts and particulates from major river systems; Earth and Planetary Science Letters, v. 70, p. 221-236.

Harvey, D.
1995: Géochimie et traceur isotopique du néodyme dans les intrusifs Archéens de la parite nord-est de la péninsule d'Ungava; M.Sc. thesis, Université de Montréal, Montréal, Quebec, 133 p.

Jackson, G.D., Hunt, P.A., Loveridge, W.D., and Parrish, R.R.
1990: Reconnaissance geology of Baffin Island, N.W.T.; *in* Radiogenic Age and Isotopic Studies: Report 3; Geological Survey of Canada, Paper 89-2, p. 123-148.

Jacobsen, S.B. and Wasserburg, G.J.
1980: Sm-Nd evolution of chondrites; Earth and Planetary Science Letters, v. 50, p. 139-155.

Scott, D.J.
1995: U-Pb geochronology of a Paleoproterozoic continental magmatic arc on the western margin of the Archean Nain craton, northern Labrador, Canada; Canadian Journal of Earth Sciences, v. 32, p. 1870-1882.
1997: Geology, U-Pb, and Pb-Pb geochronology of the Lake Harbour area, southern Baffin Island: implications for the Paleoproterozoic tectonic evolution of northeastern Laurentia; Canadian Journal of Earth Sciences, v. 34, p. 140-155.

Scott, D.J. and Gauthier, G.
1996: Comparison of TIMS (U-Pb) and laser ablation microprobe ICP-MS (Pb) techniques for age determination of detrital zircons from Paleoproterozoic metasedimentary rocks from northeastern Laurentia, Canada, with tectonic implications; Chemical Geology, v. 131, p. 127-142.

Scott, D.J. and Helmstaedt, H.
1992: Purtuniq ophiolite, Cape Smith belt, northern Quebec, Canada: a reconstructed section of early Proterozoic oceanic crust; Geology, v. 20, p. 173-176.

Scott, D.J. and Machado, N.
1995: U-Pb geochronology of the northen Torngat orogen, Labrador, Canada: a record of Palaeoproterozoic magmatism and deformation; Precambrian Research, v. 70, p. 169-190.

Scott, D.J. and Wodicka, N.
1998: A second report on the U-Pb geochronology of southern Baffin Island; *in* Radiogenic Age and Isotopic Studies: Report 11, Geological Survey of Canada, Current Research, 1998-F.

Scott, D.J., Stern, R.A., and St-Onge, M.R.
1997a: An overview of the geochronology of detrital zircons in Paleoproterozoic metasedimentary rocks, southern Baffin Island; *in* Eastern Canadian Shield Onshore-Offshore Transect (ECSOOT), Transect Meeting (April 14-15, 1997), (comp.) R.J. Wardle and J. Hall; The University of British Columbia, LITHOPROBE Secretariat, Report No. 61, p. 181-185.

Scott, D.J., St-Onge, M.R., Lucas, S.B., and Helmstaedt, H.
1991: Geology and chemistry of the early Proterozoic Purtuniq ophiolite, Cape Smith Belt, northern Quebec, Canada; *in* Ophiolite genesis and evolution of the oceanic lithosphere, (ed.) T. Peters; Kluwer Academic Publishers, Amsterdam, p. 825-857.

Scott, D.J., St-Onge, M.R., Wodicka, N., and Hanmer, S.
1997b: Geology of the Markham Bay–Crooks Inlet area, southern Baffin Island, Northwest Territories; *in* Current Research 1997-C; Geological Survey of Canada, p. 157-166.

Stern, R.A., Percival, J.A., and Mortensen, J.K.
1994: Geochemical evolution of the Minto block: a 2.7 Ga continental arc built on the Superior craton; Precambrian Research, v. 65, p. 115-153.

St-Onge, M.R., Hanmer, S., and Scott, D.J.
1996: Geology of the Meta Incognita Peninsula, south Baffin Island, Northwest Territories: tectonostratigraphic units and regional correlations; *in* Current Research 1996-C; Geological Survey of Canada, p. 63-72.

St-Onge, M.R., Lucas, S.B., and Parrish, R.R.
1992: Terrane accretion in the internal zone of the Ungava orogen, northern Quebec. Part I: tectonostratigraphic assemblages and their tectonic implications; Canadian Journal of Earth Sciences, v. 29, p. 746-764.

St-Onge, M.R., Lucas, S.B., Scott, D.J., and Wodicka, N.
1997: Crustal-scale architecture and tectonostratigraphy of the Quebec–Baffin segment of the Trans-Hudson Orogen; *in* Eastern Canadian Shield Onshore-Offshore Transect (ECSOOT), Transect Meeting (April 14-15, 1997), (comp.) R.J. Wardle and J. Hall; The University of British Columbia, LITHOPROBE Secretariat, Report No. 61, p. 186-192.

St-Onge, M.R., Scott, D.J., Wodicka, N., and Lucas, S.B.
1998: Geology of the McKellar Bay–Wight Inlet–Frobisher Bay area, southern Baffin Island, Northwest Territories; *in* Current Research 1998-C; Geological Survey of Canada, p. 43-54.

Taylor, S.R. and McLennan, S.M.
1985: The continental crust: its composition and evolution; Blackwell Scientific Publications, Oxford, 312 p.

Thériault, R.J. and Ermanovics, I.
1997: Sm-Nd and geochemical characterization of the Torngat Orogen, Labrador, Canada; Precambrian Research, v. 81, p. 15-35.

Thériault, R.J., Scott, D.J., and St-Onge, M.R.
1997: Nd isotopic and geochemical evolution of Paleoproterozoic plutonic rocks, southern Baffin Island; *in* Eastern Canadian Shield Onshore-Offshore Transect (ECSOOT), Transect Meeting (April 14-15, 1997), (comp.) R.J. Wardle and J. Hall; The University of British Columbia, LITHOPROBE Secretariat, Report No. 61, p. 203-208.

Wodicka, N., and Scott, D.J.
1997: A preliminary report on the U-Pb geochronology of the Meta Incognita Peninsula, southern Baffin Island, Northwest Territories; *in* Current Research 1997-C; Geological Survey of Canada, p. 167-178.

– 7 –

Tectonic setting and U-Pb zircon age of the Poulin-de-Courval Mangerite, Saguenay–Lac Saint-Jean area, Grenville Province, Quebec

C. Hébert[1], O. van Breemen[2], and P. Lacoste[1]

Hébert, C., van Breemen, O., and Lacoste, P., 1998: Tectonic setting and U-Pb zircon age of the Poulin-de-Courval Mangerite, Saguenay–Lac Saint-Jean area, Grenville Province, Quebec; in *Radiogenic Age and Isotopic Studies: Report 11; Geological Survey of Canada, Current Research 1998-F, p. 69-76.*

Abstract: A U-Pb zircon age of 1068 ± 3 Ma has been obtained for the Poulin-de-Courval Mangerite. This mangerite, as all the other Precambrian intrusions of the region, is affected by syn- to late-Grenvillian deformations represented by at least two well preserved fabrics. The east-west- to east-southeast-trending fabric is related to a thrusting movement which is overprinted by a major northeast-southwest-trending dextral-oblique reverse shear zone called Saint-Fulgence shear zone. This shear zone has tectonized the contacts between the Poulin-de-Courval Mangerite and its host rocks the Lac Saint-Jean anorthositic suite (1160–1140 Ma) and the Cap à l'Est gneiss complex. The Poulin-de-Courval Mangerite is part of a regionally occurring, 1082–1050 Ma plutonic suite which includes the Chicoutimi Mangerite and the La Baie Granite. The age obtained represent late movement attributed to the Grenvillian regional deformation along the St-Fulgence shear zone following the development of the east-west fabric.

Résumé : Un âge U-Pb sur zircon de 1 068 ± 3 Ma a été obtenu pour la Mangérite de Poulin-de-Courval. Cette mangérite, comme toutes les autres intrusions précambriennes de la région, a été touchée par des déformations syn-grenvilliennes à tardi-grenvilliennes que représentent au moins deux fabriques bien conservées. La fabrique de direction est-ouest à est-sud-ouest est apparentée à un mouvement chevauchant auquel se superpose la zone de cisaillement de Saint-Fulgence, zone de cisaillement majeure à mouvement inverse dextre-oblique et à direction nord-est–sud-ouest. Cette zone de cisaillement a tectonisé les contacts de la Mangérite de Poulin-de-Crouval et de ses encaissants, la suite anorthositique du Lac Saint-Jean (1 160–1 140 Ma) et le complexe gneissique de Cap à l'Est. La Mangérite de Poulin-de-Courval fait partie d'une suite plutonique (1 082–1 050 Ma) de distribution régionale qui comprend la Mangérite de Chicoutimi et le Granite de La Baie. L'âge obtenu représente un mouvement tardif attribuée à la déformation régionale grenvillienne survenue le long de la zone de cisaillement de St-Fulgence après la formation de la fabrique est-ouest.

[1] Ministère des Ressources naturelles du Québec, 5700 4e avenue Ouest Charlesbourg, Québec G1H 6R1
[2] Geological Survey of Canada, 601 Booth Street, Ottawa, Ontario K1A 0E8

INTRODUCTION

U-Pb age dating in the Saguenay–Lac Saint-Jean area has hitherto demonstrated three major magmatic episodes that are in the 1160–1140 Ma, 1082–1050 Ma, and 1020–1010 Ma ranges (Higgins and van Breemen, 1996). The oldest episode marks the emplacement of the 1157 ± 3 Ma Lac Saint-Jean anorthositic suite (Hébert and Lacoste, 1998f) (Fig. 1) which outcrops over 20 000 km^2 (Higgins and van Breemen, 1992). The anorthositic member of this plutonic suite is dominated by anorthosite, norite, leuconorite, and, in part by troctolite. The Lac Saint-Jean anorthositic suite is partially enveloped by younger mangeritic, charnockitic, and granitic masses which, together with the anorthositic and gabbroic rocks, define a typical anorthosite-mangerite-charnockite-granite suite that is generally associated with extensional cratonic conditions (Emslie and Hunt, 1990). Among the granitoid bodies typical of this suite is the Lac Labrecque Granite, which has yielded a crystallization age of 1146 ± 3 Ma (Higgins and van Breemen, 1996).

While plutons of the Lac Saint-Jean anorthositic suite do not appear to be linked to a particular structural feature, granitoid plutons of the 1082–1050 Ma episode outcrop along a major shear zone. This shear zone extends for more than 100 km along the southeast flank of the anorthosite suite. The presence of a major tectonic break along the southeastern margin of the Lac Saint-Jean anorthositic suite has long been proposed (Rondot, 1986) (Fig. 2). This break is easily recognizable on aeromagnetic and reconnaissance-scale geological maps; it has recently been examined over a strike length of 100 km and is herein referred to as the Saint-Fulgence shear zone (Fig. 3) (Hébert and Lacoste, 1998e, f). North of the Saguenay River, it juxtaposes gabbroic rocks (units lsj2, lsj3) on the northwest with the Cap à l'Est gneiss complex (units cpe1, cpe2) on the southeast (Fig. 3). Further north, it branches and separates the Lac Saint-Jean anorthositic suite, the Poulin-de-Courval Mangerite, and the Cap à l'Est gneiss complex.

The 1082–1050 Ma felsic plutons include the 1067 ± 3 Ma La Baie Granite (Higgins and van Breemen, 1996), the 1082 ± 3 Ma Chicoutimi Mangerite (Hervet et al., 1994), and the coeval Chicoutimi Syenite (Higgins and van Breemen, 1996). Mafic rocks appear to be restricted to a few small bodies such as the 1076 ± 3 Ma Canton Taché Leucogabbro (Higgins and van Breemen, 1992) and to post-tectonic 1050 ± 10 Ma diabase dykes (Hervet et al., 1994). These intrusive

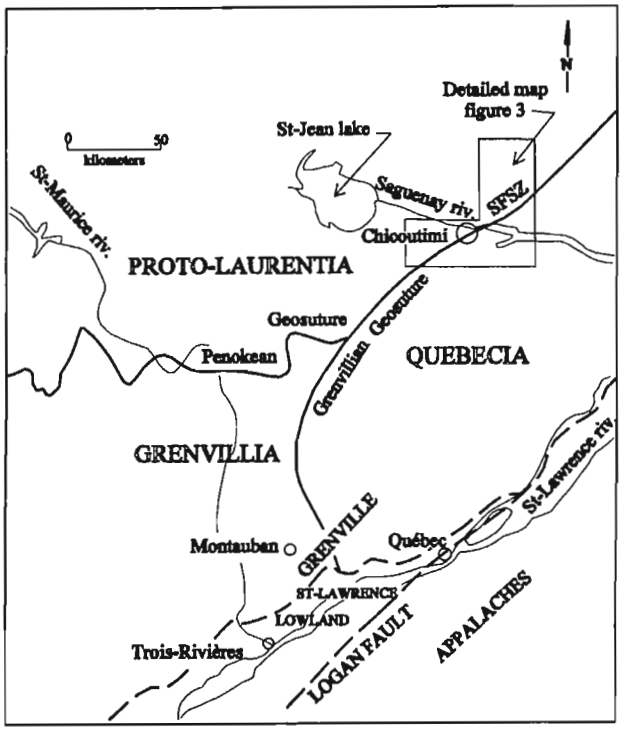

Figure 2. *Location of geosutures and proto-continent boundaries in the central Grenville Province, proposed by Rondot (1986), SFSZ — Saint-Fulgence shear zone.*

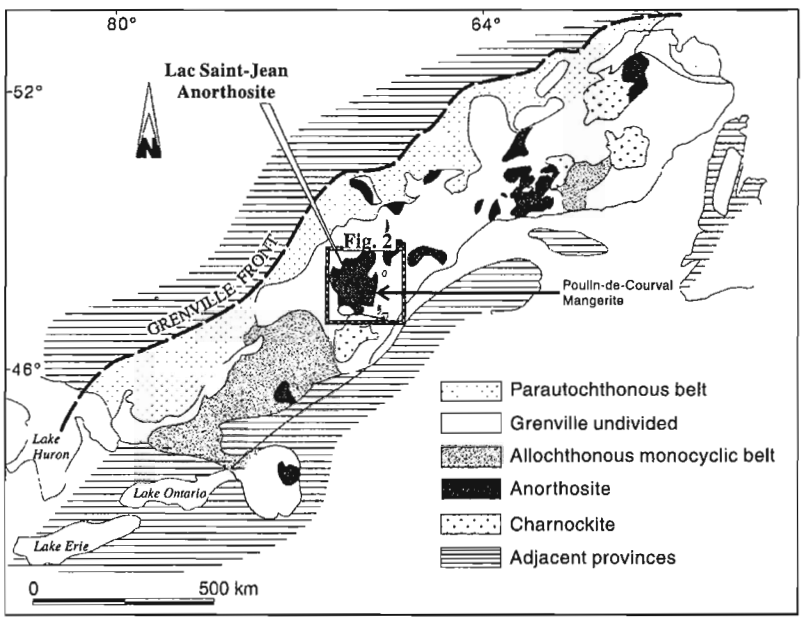

Figure 1.

Location of the Lac Saint-Jean Anorthositic Complex in the Grenville Province. Figure modified from Hervet et al (1994).

bodies and the time-correlative, but distant, Saint-Urbain Anorthosite Complex have been recently interpreted (Higgins and van Breemen,1996) as part of an anorthosite-mangerite-charnockite-granite suite younger than the Lac Saint-Jean anorthositic suite. A third and final anorthosite-mangerite-charnokite-granite suite is constrained at 1020–1010 Ma and includes the Saint-Ambroise Granite and the Labrieville Anorthosite Complex (Higgins and van Breemen, 1996).

This paper focuses on the emplacement age and structural setting of the Poulin-de-Courval Mangerite, a major granitoid intrusion of the second plutonic suite. The study shows that the emplacement of this body occurred in the final stages of Grenvillian deformation in the area. The paper sheds additional light on the nature and structural setting of the 1082–1050 Ma plutonism in the Saguenay–Lac Saint-Jean area and discusses its linkage to anorthosite-mangerite-charnokite-granite-type plutonism.

REGIONAL GEOLOGY

The Poulin-de-Courval Mangerite outcrops between two segments of the Saint-Fulgence shear zone which separates the Lac Saint-Jean anorthositic suite (1160–1140 Ma) from the Cap à L'Est (unit cpe) gneiss complex, whose age is unknown (Fig. 3).

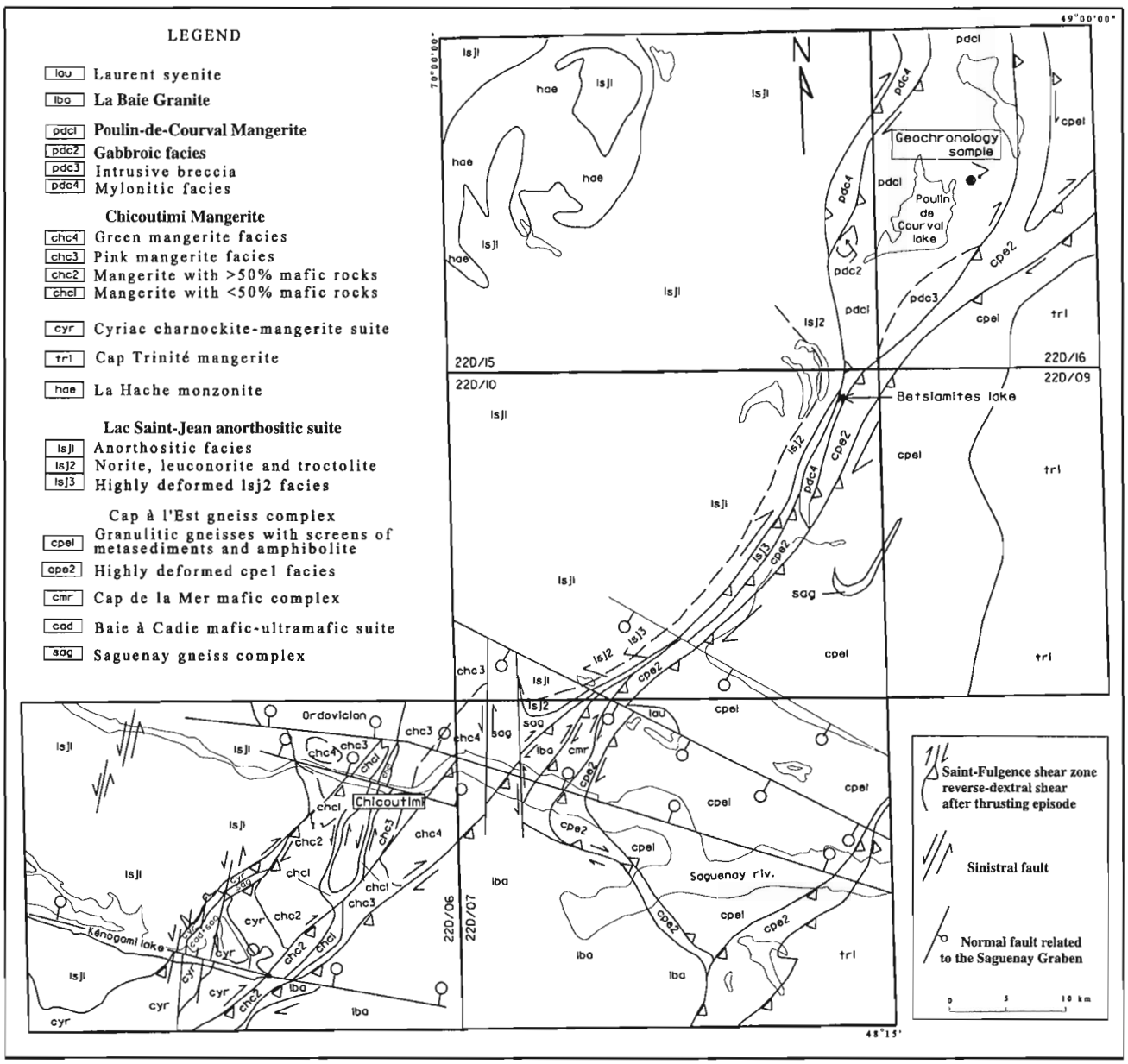

Figure 3. *Regional geology schematic map from Poulin-de-Courval Mangerite (NE) to the Chicoutimi Mangerite (SW).*

Cap à l'Est gneiss complex

The region east and southeast of the Lac Saint-Jean anorthositic suite is underlain by the Cap à l'Est gneiss complex (Fig. 3; Hébert and Lacoste, 1994, 1998b, c, d, e). This granulitic domain is largely composed of monotonous, granoblastic gneisses and/or gneissic granitoid rocks with locally preserved augen textures. The overall homogeneity, the lack of evidence for primary layering, and the sporadic preservation of augen textures are taken as indicative of a plutonic origin. These gneisses enclose mappable screens of amphibolite, marble, quartzite, and sillimanite-graphite-garnet-biotite paragneisses, as well as small and rare masses of anorthositic (Fig. 4) and gabbroic rocks. It is suggested that these supracrustal rocks are related to the supracrustal facies of the Saguenay gneiss complex (unit sag) (Fig. 3) (Hébert and Lacoste, 1998e, f). Screens of amphibolite and supracrustal rocks are more abundant structurally down the section, towards the Poulin-de-Courval Mangerite and the Lac Saint-Jean anorthositic suite.

In the Cap à l'Est gneiss complex, two important fabrics of Grenvillian age are easily identifiable. The older fabric is an east-southeast- to east-west-trending foliation or gneissosity, whereas the younger is a very penetrative northeast-southwest-trending mylonitic foliation related to the Saint-Fulgence shear zone.

Lac Saint-Jean anorthositic suite

The Lac Saint-Jean anorthositic suite is one of the largest anorthosite massifs in the Grenville Province. It is a composite intrusion where the anorthositic member of its anorthosite-mangerite-charnokite-granite suite is chiefly composed of anorthosite with subordinate norite, leuconorite, and some troctolite. Immediately west of the Poulin-de-Courval Mangerite, the Lac Saint-Jean anorthositic suite is composed of mafic rocks with gabbro, norite, leuconorite, and troctolite as the main constituents (units lsj2, lsj3). Megacrystic and recrystallized anorthosite is dominant further west (unit lsj1) (Fig. 3, 5).

Figure 4. *Screen of anorthosite in the cpe2 facies of the Cap à l'Est gneiss complex. Outcrop located near the southeastern contact of the Poulin-de-Courval Mangerite (Fig. 3).*

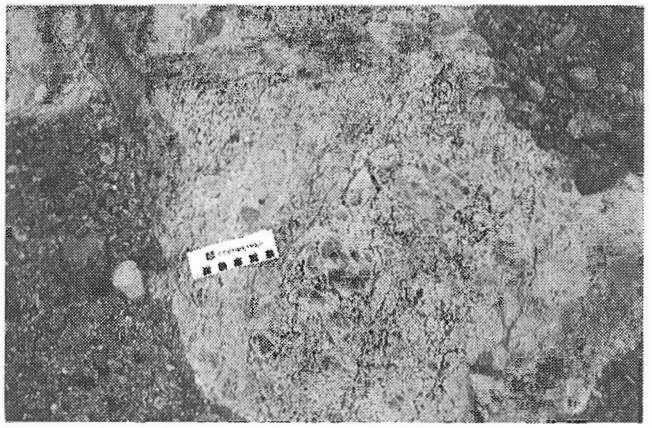

Figure 5. *Megacrystic and recrystallized anorthosite. Facies lsj1 in Fig. 3.*

There is some geochronological evidence that the crystallization of the Lac Saint-Jean anorthositic suite continued, at least in part, from 1157 ± 3 Ma to 1142 ± 3 Ma (Higgins and van Breemen, 1992). This multiphase intrusion is also spatially associated with a number of younger granitoid bodies including the 1146 ± 3 Ma Lac Labrecque granite so that the Lac Saint-Jean anorthositic suite as a whole defines a typical anorthosite-mangerite-charnokite-granite suite (Higgins and van Breemen, 1996). These bodies are distinctly older than other granitoid bodies such as the 1082 ± 3 Ma Chicoutimi Mangerite and the ca. 1067 ± 3 Ma La Baie Granite, which are also spatially associated with the Lac Saint-Jean anorthositic suite and believed to be part of an anorthosite-mangerite-charnokite-granite suite (Emslie and Hunt, 1990; Higgins and van Breemen, 1996). The rocks of the anorthosite suite have been variably recrystallized, deformed, and metamorphosed during the Grenvillian Orogeny. The Lac Saint-Jean anorthositic suite also contains the same east-west- to east-southeast-trending fabric identified in the Cap à l'Est gneiss complex and is also overprinted by the Saint-Fulgence shear zone and its northeast-southwest fabric which is represented by the lsj3 facies along the contact with the host rocks.

Poulin-de-Courval Mangerite

The Poulin-de-Courval Mangerite outcrops between two segments of the Saint-Fulgence shear zone, separating the Lac Saint-Jean anorthositic suite and the Cap à l'Est gneiss complex (Fig. 3). The main mass (unit pdc1) of the body, centred on Poulin-de-Courval lake, is more than 10 km wide by 30 km long. Sheared mangeritic rocks (unit pdc4) of the main body also extend as a thin and conformable tail within the shear zone for more than 10 km towards the southwest (Hébert and Lacoste, 1998a, b, c).

The Poulin-de-Courval Mangerite is a composite body mainly composed of hypersthene-monzonite with subordinate hypersthene-granite and syenite. The rocks are generally porphyritic with K-feldspar crystals up to 2.5 cm long, some with rapakivi texture (Fig. 6). Monzodiorite, jotunite, and gabbro occur locally as minor mafic phases of this composite intrusion. The western margin of the small gabbro-jotunite

Figure 6. *Rapakivi texture in the Poulin-de-Courval Mangerite.*

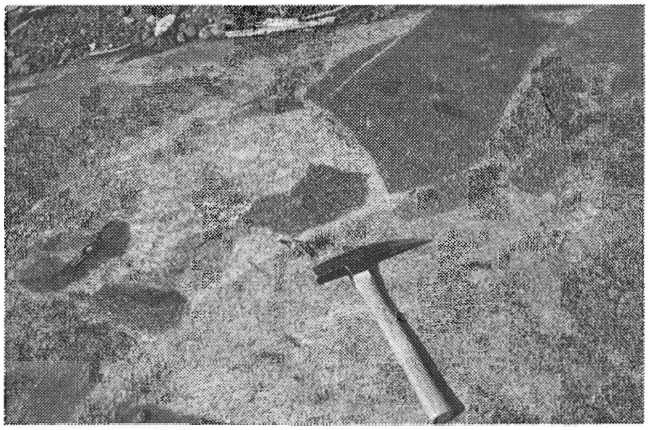

Figure 7. *Western intrusive breccia in the Poulin-de-Courval Mangerite. Note the angular mafic fragments in the phenocrystic monzonitic to syenitic matrix.*

mass (unit pdc2), on the west side of the mangeritic intrusion, is in contact with a mylonitic phase (unit pdc4) of the monzonitic to syenitic rocks of the main intrusion (unit pdc1). At the southern margin of the jotunite-gabbro mass, there is an undeformed intrusive breccia with mafic fragments in a matrix of porphyritic monzonite and syenite (Fig. 7). Gradational passage between these two phases demonstrates common origin. Moreover, the massive porphyritic monzonite in the breccia is identical in mineralogy and modal composition to the immediately adjacent mylonitic facies (unit pdc4) of the augen monzonite. Accordingly, the latter is also interpreted to be part of the Poulin-de-Courval intrusion. Another intrusive breccia (unit pdc3) with mafic fragments also outcrops near the southern contact of the mangeritic body.

Rocks in the interior of the body range from massive to weakly foliated. But, in contrast, the rocks near the margin are generally well foliated and include augen gneiss, straight gneiss, and mylonite, some derived from the intrusion itself. This is well documented by the pdc4 facies of the Poulin-de-Courval Mangerite, which outcrops along the western contact between the Poulin-de-Courval Mangerite and the Lac Saint-Jean anorthositic suite (Fig. 3). These deformed rocks carry a strong east-southeast-trending, steeply plunging, stretching lineation and reverse-sense kinematic indicators. Gneissic, mylonitic, and straight gneiss fabrics of the wall rocks in the opposite sides of the intrusion are also conformable to its outline.

In the intrusive breccia (unit pdc3), the mafic fragments and the felsic matrix carry a well developed east-west- to east-southeast-striking foliation and gneissosity overprinted by a steep northeast-southwest-trending foliation with a slightly oblique southwest-plunging lineation which is conformable with the Saint-Fulgence shear zone.

STRUCTURE

East-west to east-southeast fabric

Fieldwork near Chicoutimi in 1995 and 1996 (Hébert and Lacoste, 1998e, f) (Hébert et al., 1998), has documented an east-southeast- to east-west-trending foliation and gneissosity in the intrusive breccia (unit pdc3) of the Poulin-de-Courval Mangerite, which is also present in the Lac Saint-Jean anorthosite (1160–1140 Ma), the Chicoutimi Mangerite (1082 ± 3 Ma) and the La Baie Granite (1067 ± 3 Ma). The fabric, which dips 10–20° north-northeast or south-southwest is related to the Grenvillian thrusting event.

Saint-Fulgence shear zone

The thrusting phase was followed by another episode of shortening which caused intense tight folding at outcrop scale (Fig. 8). This deformation is associated with regional-scale, spoon-shaped folds as shown by unit sag within the Cap à l'Est gneiss complex, in the NTS areas 22 D/10 and 22 D/9 (Fig. 3). This late Grenvillian episode of shortening was the first stage of a major deformation, which involved intense shearing and caused a highly penetrative mylonitic foliation. This intense deformation is recorded in the Saint-Fulgence shear zone where it resulted in a 2–5 km wide zone of straight gneisses (Fig. 9). It comprises a number of southeasterly

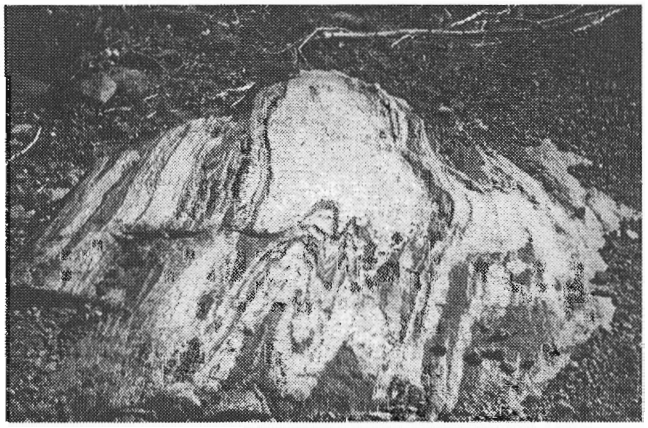

Figure 8. *Example of shortening by folding within a thrust sheet in the Cap à l'Est gneiss complex.*

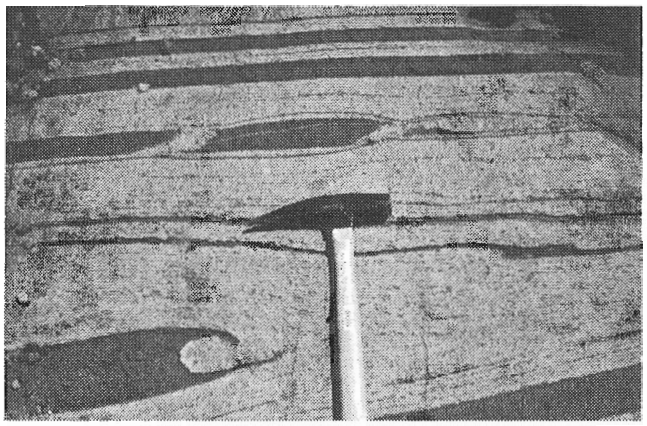

Figure 9. Straight gneiss in the Saint-Fulgence shear zone (SFSZ). Photo from the highly deformed Cap à l'Est gneiss complex facies (cpe2) (Fig. 3).

moderately to steeply dipping anastomosing zones of mylonites and straight gneisses with strong and steeply plunging mineral and stretching lineations. The shear zones cut across and transpose anorthositic rocks of the Lac Saint-Jean anorthositic suite in the immediate footwall (unit lsj3). Kinematic indicators suggest a reverse dextral-oblique sense of displacement (Hébert and Lacoste, 1998c).

GEOCHRONOLOGY

A sample of mangerite from the Poulin-de-Courval intrusion was selected for U-Pb zircon geochronology from a quarry test site located east of Poulin-de-Courval lake (Fig. 3). This mangerite has a pale green colour on fresh surface, and is homogeneous and massive with large phenocrysts of K-feldspar up to 3 cm long, with some rapakivi and antirapakivi textures. Orthoclase phenocrysts are mainly perthitic, and the plagioclase shows good twinning and is locally saussuritized. In the matrix, quartz and mafic minerals such as pyroxene and amphibole are interstitial to the phenocrysts. Accessory minerals are titanite, apatite, zircon, and iron

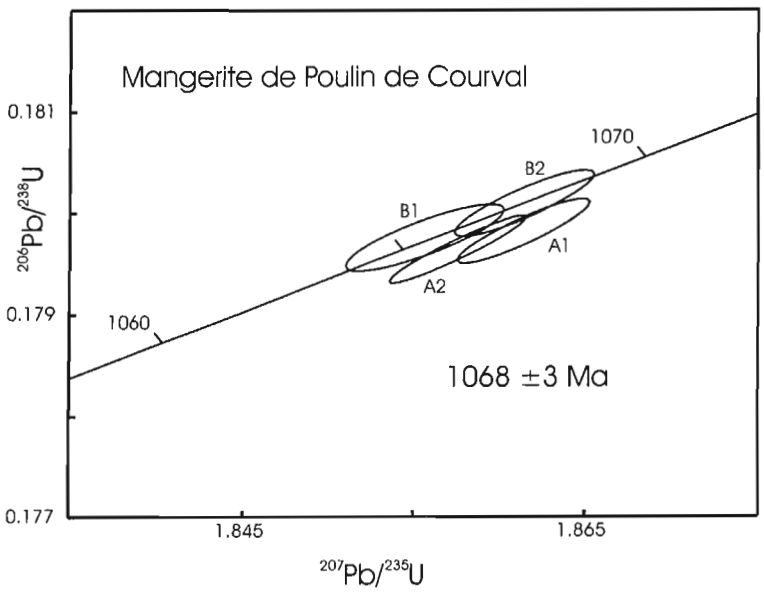

Figure 10.

U-Pb concordia diagram of zircon. Error ellipses reflect the 2 sigma uncertainty.

Table 1. U-Pb isotopic data.

Fraction[1] Size	Wt. (µg)	U (ppm)	Pb[2] (ppm)	$^{206}Pb/^{204}Pb$[3]	$^{206}Pb_c$[4]	^{208}Pb (%)	$^{206}Pb/^{238}U$[5]	$^{207}Pb/^{238}U$[5]	R	$^{207}Pb/^{206}Pb$[5]	Age Ma[6]
Poulin-de-Courval Mangerite (95-HEB-1; z4095) Easting 399150 Northing 5413800 Zone 19											
A2, +105-149 N0	76	68	14	6436	9	0.24	0.1796 ± .09	1.858 ± .11	0.95	0.07500 ± .03	1068.4 ± 1.4
B1, +149 N0	45	67	14	1914	17	0.23	0.1798 ± .09	1.856 ± .12	0.84	0.07487 ± .07	1065.0 ± 2.8
B2, +149 N0	81	65	13	3533	17	0.24	0.1801 ± .09	1.861 ± .11	0.87	0.07496 ± .05	1067.5 ± 2.1
A1, +105-149 N0	53	65	13	6096	6	0.24	0.1798 ± .09	1.861 ± .10	0.9	0.07508 ± .04	1070.5 ± 1.8

Notes: [1]sizes in microns before abrasion (e.g. +149); N refers to non-magnetic at side slope indicated in degrees and 1.8 Amp current in Frantz isodynamic separator; [2]radiogenic Pb; [3]measured ratio, corrected for spike and fractionation; [4]total common Pb in analysis corrected for fractionation and spike; [5]corrected for blank Pb and U, common Pb, errors quoted are one sigma in percent; R correlation of errors in isotope ratios; [6] $^{207}Pb/^{206}Pb$ model age.

oxide. Zircons are clear, prismatic, subhedral with length-to-breadth ratios of 2:1 to 3:1. There is no evidence of metamorphic overgrowths.

The zircons were strongly abraded following the method of Krogh (1982). Techniques of U-Pb isotope dilution are detailed in Parrish et al. (1987), which includes a modified version of the regression analysis procedure of York (1969). U-Pb isotopic data are presented in Table 1. Age uncertainties are quoted at the 2 sigma level. Zircons have consistently low U concentrations of 65 ppm to 68 ppm. On a concordia plot, four data points plot on or near the concordia and have overlapping uncertainties (Fig. 10). A mean $^{207}Pb/^{206}Pb$ age of 1068 ± 3 Ma is assigned to the data and is interpreted to represent the time of crystallization based on the igneous morphology of the zircons.

DISCUSSION

Field relationships suggest that emplacement of the Poulin-de-Courval Mangerite occurred during a late stage of thrusting which was followed by intensive shearing represented by the Saint-Fulgence shear zone. While some parts of the intrusion are mylonitized and sheared within the shear zone, other parts are undeformed, suggesting that the igneous textures have been preserved during the regional deformation. Accordingly, the ca. 1068 ± 3 Ma U-Pb zircon crystallization age reported here for the Poulin-de-Courval Mangerite is considered to represent late movements attributed to the Grenvillian regional deformation along the Saint-Fulgence shear zone.

To the southwest, in the Chicoutimi area (Fig. 3), recent mapping has shown that the (1160–1140 Ma) Lac Saint-Jean anorthosite, the 1082 ± 3 Ma Chicoutimi Mangerite (Hervet et al., 1994), and the 1067 ± 3 Ma La Baie Granite (Higgins and van Breemen, 1996) have similar structural-intrusive relationships, with respect to the east-west to east-southeast thrust deformation and the Saint-Fulgence shear zone, to the Poulin-de-Courval Mangerite (Hébert and Lacoste, 1998e, f). Accordingly, magmatic emplacement of all these bodies is considered syn- to late tectonic with respect to the Grenvillian thrusting deformation and the later regional movements along the Saint-Fulgence shear zone. It is also important to note that the Chicoutimi Mangerite is more deformed by the shear zone than the younger granitoids of the 1082–1050 Ma suite. These relationships show that most of the deformation along the Saint-Fulgence shear zone and the earlier thrusting movement outlined by the east-west- to south-southeast-trending fabric, occurred between 1082 Ma and 1067 Ma. It is not known whether the deformations were continuous or episodic during this interval.

It is notable that a time gap of more than 60 Ma separates the 1160–1140 Ma emplacement of the Lac Saint-Jean anorthositic suite and the 1082–1050 emplacement of granitoid bodies. It is also striking that while anorthositic and gabbroic rocks dominate in the Lac Saint-Jean anorthositic suite, the younger suite is composed chiefly of granitoid rocks, with a few small masses of mafic rocks and the 1050 ± 10 Ma post-tectonic diabase dykes. The time gap and the contrasting nature of the plutonic products do not support a direct genetic link between these two plutonic suites. In addition, the association, in the area, of 1082–1068 Ma granitoid magmatism with a regional-scale shear zone suggests an orogenic, rather than an anorogenic, anorthosite-mangerite-charnokite-granite-type setting.

CONCLUSIONS

- The igneous crystallization age of the Poulin-de-Courval Mangerite is 1068 ± 3 Ma. This body is part of a regionally distributed, 1082–1050 Ma plutonic suite chiefly composed of granitoid rocks. The suite comprises the Chicoutimi Mangerite and the La Baie Granite dated 1082 ± 3 Ma and 1067 ± 3 Ma, respectively, and postdates the emplacement of the Lac Saint-Jean anorthositic suite by over 60 Ma.
- Field intrusive and structural relationships of the Poulin-de-Courval Mangerite, as well as four other granitoid bodies of the 1082–1050 Ma suite, indicate that intrusion occurred during a late stage of thrusting that was followed by an intensive period of shearing related to the Saint-Fulgence shear zone. Accordingly, the ca. 1068–1067 Ma ages obtained for the Poulin-de-Courval Mangerite and the La Baie Granite represent a maximum age limit for the final stages of Grenvillian deformation along the Saint-Fulgence shear zone in the region.
- Granitoid plutonism along the Saint-Fulgence shear zone cannot be linked to emplacement of the Lac Saint-Jean anorthositic suite. The contacts between these granitoids and the Lac Saint-Jean anorthositic suite are not tectonic in nature, but have undergone strong deformation. Spatial association of the 1082–1050 Ma igneous suite with the regional shear zone suggests an orogenic, rather than an anorogenic, anorthosite-mangerite-charnokite-granite-type setting for granitoid plutonism in the Saint-Fulgence shear zone.

ACKNOWLEDGMENTS

We thank Dr. Leopold Nadeau (CGQ-CGC) for critically reading and improving the manuscript. The manuscript also benefitted from critical reviews by Dr. Natasha Wodicka and Dr. Kamal N.M. Sharma.

REFERENCES

Emslie, R.F. and Hunt, P.A.
1990: Age and petrogenetic significance of igneous mangerite-charnockite suites associated with massif anorthosite, Grenville Province; Journal of Geology, v. 98, p. 213- 231.

Hébert, C. et Lacoste, P.
1994: Linéament de St-Fulgence-Poulin-de-Courval; *dans* Séminaire d'information sur la recherche géologique, Programme et résumés, ministère des Ressources naturelles du Québec, DV 94-09, p. 56.
1998a: Géologie de la région du lac Moncouche 22 D/15; ministère des Ressources naturelles du Québec, Annotated map: SI-22D15-C3G-98H.

Hébert, C. et Lacoste, P. (cont.)
1998b: Géologie de la région du lac Poulin-de-Courval 22 D/16; ministère des Ressources naturelles du Québec, 13 p.
1998c: Géologie de la région du lac Jalobert, 22 D/10; ministère des Ressources naturelles du Québec, Map: SI-22D10-C3G-98J.
1998d: Géologie de la région du lac Savanes, 22 D/09; ministère des Ressources naturelles du Québec, Annotated map: SI-22D09-C3G-98H.
1998e: Géologie de la région de Bagotville, 22 D/07; ministère des Ressources naturelles du Québec, Map: SI-22D07-C3G-98I.
1998f: Géologie de la région de Jonquière–Chicoutimi, 22D/06; ministère des Ressources naturelles du Québec, Map: SI-22D06-C3G-98I.

Hébert, C., Daigneault, R., and Chown, E.H.
1998: Tectono-magmatic history of the Saguenay area, GAC-MAC-1998, Quebec city, Pre-congress field trip guide, A-06, 67 p.

Hervet, M., van Breemen, O., and Higgins, M.D.
1994: U-Pb crystallization age near the southeast margin of the Lac-St-Jean anorthositic complex, Grenville Province, Quebec; *in* Radiogenic Age and Isotopic Studies; Report 8; Geological Survey of Canada, Current Research 1994-F, p. 114-124.

Higgins, M.D. and van Breemen, O.
1992: The age of the Lac-Saint-Jean Anorthosite Complex and associated mafic rocks, Grenville Province, Canada; Canadian Journal of Earth Sciences, v. 29, p. 1412-1423.
1996: Three generations of anorthosite-mangerite-charnockite-granite(AMC) magmatism, contact metamorphism and tectonism in the Saguenay–Lac-St-Jean region of the Grenville Province, Canada; Precambrian Research, v. 79, p. 327-346.

Krogh, TE
1982: Improved accuracy of U-Pb zircon ages by the creation of more concordant systems using an air abrasion technique: Geochemical et Cosmochimica Acta, v. 46, p. 637-649.

Parrish, R.R., Roddick, J.C., Loveridge, W.D., and Sullivan, R.W.
1987: Uranium-lead analytical techniques at the geochronological laboratory, Geological Survey of Canada; in Radiogenic age and Isotopic Studies: Report 1; Geological Survey of Canada, Paper 87-2, p. 3-7.

Rondot, J.
1986: Geosutures dans le Grenville; *in* The Grenville Province, (ed.) J.M. Moore, A. Davidson and A.J. Baer; Geological Association of Canada, Special Paper 31, p. 313-325.

York, D.
1969: Least squares fitting of a straight line with correlated errors; Earth and Planetary Science Letters, v. 5, p. 320-324.

– 8 –

Strontium isotopic composition of modern walrus teeth from Hudson Bay and Arctic Islands, Quebec and Northwest Territories

W.J. Davis[1], P. Outridge[1], and R.E.A. Stewart[2]

Davis, W.J., Outridge, P., and Stewart, R.E.A., 1998: Strontium isotopic composition of modern walrus teeth, Hudson Bay and Arctic Islands, Quebec and Northwest Territories; in *Radiogenic Age and Isotopic Studies: Report 11; Geological Survey of Canada, Current Research 98-F, p. 77-80.*

Abstract: Sr isotopic data are reported for modern walrus teeth collected from various sites in the Canadian Arctic Islands and Hudson Bay. Initial $^{87}Sr/^{86}Sr$ ratios of the teeth are similar to modern seawater values and show no geographical correlation with local coastal geology, nor with other chemical signatures in the teeth.

Résumé : On a présenté des données isotopiques Sr portant sur des dents de morse prélevées à divers endroits dans l'archipel Arctique canadien et dans la baie d'Hudson. Les rapports initiaux $^{87}Sr/^{86}Sr$ de ces dents sont semblables aux rapports actuels obtenus pour l'eau de mer et ne montrent aucune corrélation géographique avec la géologie du littoral local ni avec les autres signatures chimiques des dents.

[1] Geological Survey of Canada, 601 Booth Street, Ottawa, Ontario K1A 0E8
[2] Department of Fisheries and Oceans, 501 University Crescent, Winnipeg, Manitoba R3T 2N6

INTRODUCTION

A new and rapidly evolving field in environmental geochemistry involves using the elemental or isotopic composition of animal tissues to determine the geographical provenance of the animals. This so-called 'element signature analysis' makes use of natural differences in tissue chemistry, which may be characteristic of different geographical areas, to address several key issues in wildlife biology such as the geographical origin of individual animals, the approximate boundaries of animal 'stocks' (subpopulations with distinctly different ranges), and identifying migrants within stocks (van der Merwe et al., 1990; Vogel et al., 1990). Information of this sort, which is often difficult or impossible to obtain with other techniques, has several important applications in wildlife management, including enforcement of hunting quotas, determination of stock intermix rates, and the reconstruction of individual life-history details.

An ongoing collaborative project between the Department of Fisheries and Oceans and the Analytical Chemistry Laboratories of the Geological Survey of Canada is exploring the use of element signature analysis for stock identification in Atlantic walrus (*Odobenus rosmarus rosmarus*) in the Canadian Arctic, the first application of the technique to a marine mammal species. Work to date has shown that Pb isotope ratios (ICP-MS) and trace-element concentrations, particularly those of Co, are key diagnostics for walrus stock identification (Outridge and Stewart, unpub. data).

In this note, we report data on the Sr isotope composition of walrus teeth from different regions of the eastern Canadian Arctic (Fig. 1). Although Sr is well mixed in seawater and its isotopic composition shows little regional variability in the oceans (Burke et al., 1982; Payton et al., 1993; Faure, 1986), terrestrial Sr isotope ratios vary over a broad range (0.706 to 0.728; Faure 1986), in relation to age and composition of underlying geology. Because walrus are nearshore dwellers, feeding on marine bivalves in coastal seas usually less than 80 m deep, the possible influence of varying terrestrial Sr input into the coastal environment may produce geographical differences in Sr isotopes in walrus tissues. The walrus communities are located within coastal areas of dominantly Archean crust, with characteristic, high terrestrial $^{87}Sr/^{86}Sr$ values (0.72; Faure, 1986), and in areas of Paleozoic carbonate and clastic sedimentary sequences with low $^{87}Sr/^{86}Sr$ values (<0.709; Fig 1).

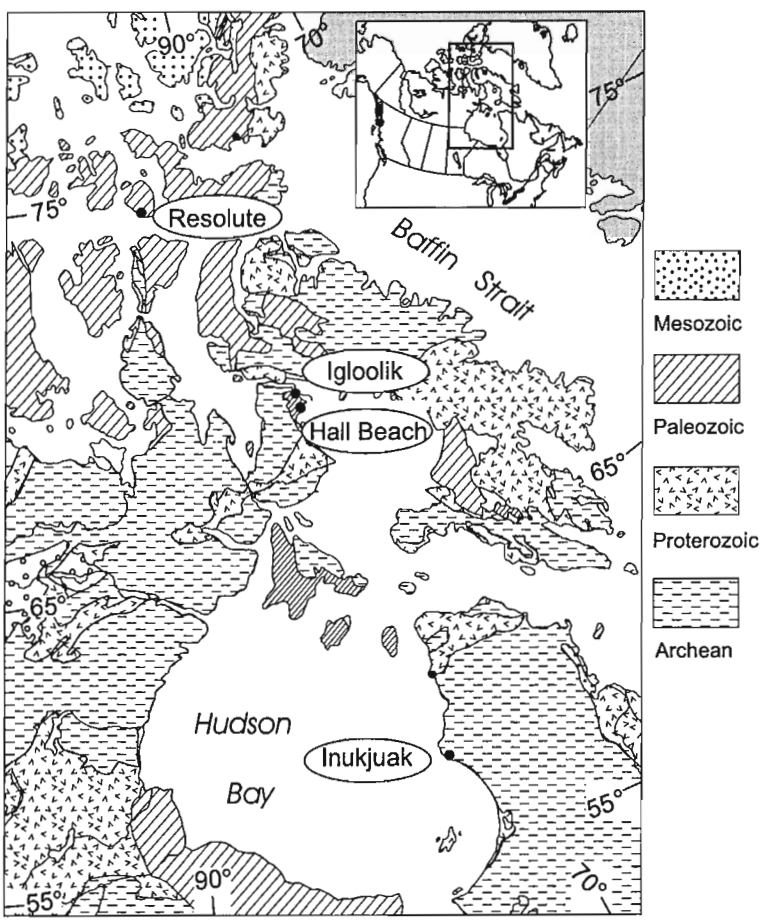

Figure 1.

Location map showing communities from which walrus were sampled, and simplified bedrock geology.

METHODS AND MATERIALS

Sample collection

Walrus teeth were collected by Fisheries and Oceans biologists or Inuit hunters during Inuit subsistence hunts in the period 1988–96 at communities in Foxe Basin, eastern Hudson Bay, and the High Arctic (Fig. 1). Sex, body size, date, and approximate capture location were recorded, and a lower right canine tooth, or the intact mandible, collected. Samples of the lower right canines were used in this study, because they accumulate relatively high (>100 μg/g) concentrations of Sr, and permanently incorporate Sr into the apatite crystal lattice. Teeth were mounted in epoxy resin and cross-sectioned for age estimation based on enumeration of cementum growth layers (Garlich-Miller et al., 1993). For this study, 11 tooth samples exhibiting a range of trace-element and Pb isotopic compositions were analyzed from four sites: Inukjuak, Igloolik, Hall Beach, and Resolute (Fig. 1). Those from Hall Beach included two individuals (HB88-01, HB88-14) whose Pb isotope ratios identified them as significant outliers from the majority of animals landed at that site (Outridge and Stewart, unpub. data).

Sample preparation

Tooth cementum samples for Sr analysis (0.05–0.35 g) were excised from the cross-sections or from unsectioned teeth with a Dremel hand tool equipped with a rotary cutting blade. Cementum is deposited in incremental layers below the gum line on the outside of the pre-existing tooth, commencing in the first year with a layer adjacent to the dentine boundary. Care was taken to ensure that whole cementum sections were removed from crown to root, and so the cementum analysed was deposited throughout the entire life of the individual. Any dentine and adhering organic matter, alveolar bone, or epoxy on the sample was removed with a rotary grinding tool.

Subsequent preparation occurred in a Class 100 HEPA-filtered work area, using ultra-pure HNO_3. The excised samples were ultrasonically washed in 3N HNO_3 at room temperature, rinsed in de-ionized water (MilliQ™) to remove surface contamination, dried with acetone, and weighed. Samples were spiked with ^{84}Sr isotope, digested over heat in 2 mL 3N HNO_3 to dryness, and finally brought back into solution with 1 mL 3N HNO_3 over gentle heat.

Strontium was separated from other cations by ion-exchange chromatography using Sr-Spec™ resin (EIChrom Industries, Darien, Ill., USA), in Teflon™ columns with a 250 μL resin bed. The columns were cleaned with three alternating washes of 3 mL 3N HNO_3 and water, and conditioned with 1 mL 3N HNO_3. Sample solutions (1 mL) were added to the columns, and eluated with 6 mL 3.2N HNO_3. The Sr was eluated from the column with 4 mL water. Total Sr in the procedural blank was 220 pg, which represented 0.001–0.004% of the total Sr in the tooth samples.

Thermal ionization mass spectrometry

Strontium isotopes were measured in static multicollection mode on a Finnigan-Mat 261 mass spectrometer. The Sr was loaded with H_3PO_4 onto a single Ta filament. Measured isotopic ratios were corrected for mass fractionation to a $^{88}Sr/^{86}Sr$ value of 8.37521. Repeated analysis of NBS 987 standard solution yielded a $^{87}Sr/^{86}Sr$ value of 0.710288 ± 0.000025 (2 sigma), and all ratios have been bias corrected to a value of 0.710250. Errors for unknowns in Table 1 are given as the external precision determined for NBS 987 standard solution, except for those analysis where the internal analytical precision exceeds the external, in which case the within-run standard error (95% confidence) is quoted.

RESULTS AND DISCUSSION

There are no consistent geographical differences, within analytical error, in the $^{87}Sr/^{86}Sr$ ratio in walrus teeth across the eastern Canadian Arctic and Hudson Bay (Table 1; Fig. 1). The teeth show a large variation in Sr concentration, which does not correlate with geographical location. Nine of the eleven samples are indistinguishable, and give an average $^{87}Sr/^{86}Sr$ value of 0.709151 ± 29 (MSWD = 1.21). This value

Table 1. $^{87}Sr/^{86}Sr$ isotopic ratios and Sr concentrations in walrus teeth from the eastern Canadian Arctic.

Animal ID No.	Harvest Date	Locality/Region	Sr (μg/g)	$^{87}Sr/^{86}Sr$[1]
HB88_01	1988	Hall Beach, Foxe Basin	134.6	0.709128 ± 25
HB88_03	1988	Hall Beach, Foxe Basin	138.8	0.709133 ± 35
HB88_14	1988	Hall Beach, Foxe Basin	191.3	0.709167 ±57
HB96_04	1996	Hall Beach, Foxe Basin	136.7	0.709100 ±25
IG88_45	1988	Igloolik, Foxe Basin	119.4	0.709162 ±25
IG96_40	1996	Igloolik, Foxe Basin	195.1	0.709150 ±28
IG96_47	1996	Igloolik, Foxe Basin	111.7	0.709090 ±25
IN90_127	1990	Inukjuak, Hudson Bay	114.8	0.709135 ±30
IN92_151	1992	Inukjuak, Hudson Bay	255.3	0.709165 ±25
RB96_03	1996	Resolute, High Arctic	154.5	0.709165 ±25
RB96_11	1996	Resolute, High Arctic	158.1	0.709154 ±25

[1] $^{87}Sr/^{86}Sr$ reported relative to $^{88}Sr/^{86}Sr$ = 8.37521 and $^{87}Sr/^{86}Sr$ = 0.710250 for NBS 987 standard solution. Absolute errors are given as two sigma external errors from replicate analyses of NBS 987, or within-run standard error if greater than ±0.000025

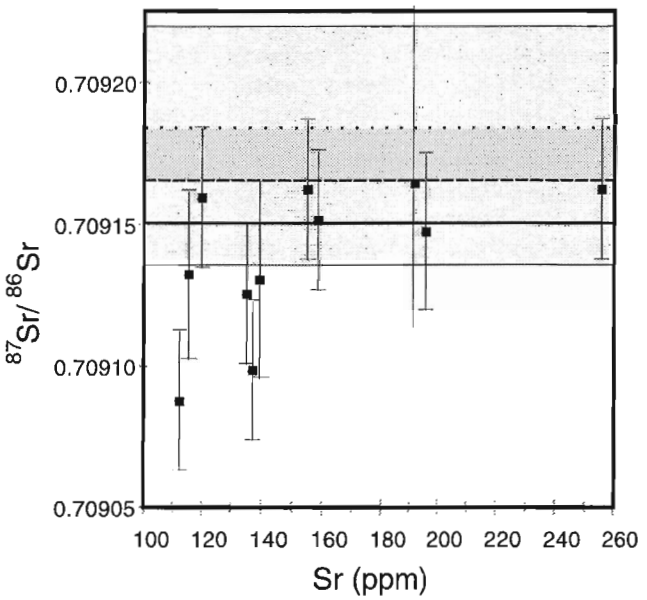

Figure 2. *Plot of Sr content vs. $^{87}Sr/^{86}Sr$ for walrus teeth. Weighted mean value of nine analyses indicated by heavy solid line. Estimates of modern seawater values bracket dark stippled area (dotted line = 0.709165 ± 24 - Payton et al., 1993; dashed line = 0.70918 ± 4 - Burke et al., 1982; normalized to NBS 987 = 0.710250), two sigma error range indicated by pale stipple.*

is slightly lower, but within error of the modern seawater ratio of 0.709165 ± 24 (Payton et al. 1993) to 0.719180 ± 40 (Fig. 2; Burke et al., 1982). None of the samples yielded $^{87}Sr/^{86}Sr$ values higher than modern seawater values, as might be expected if a significant terrestrial Sr component of Archean age were present. Two samples have slightly lower $^{87}Sr/^{86}Sr$ values, and low Sr concentrations. If significant, one explanation could be that these animals contain a Sr input from the Paleozoic sedimentary sequences which have $^{87}Sr/^{86}Sr$ values less than modern seawater.

In conclusion, Sr isotope ratios in walrus teeth have seawater values and are not of use for walrus stock identification work. Further, since most other marine mammals and fish are more pelagic in distribution than walrus, it is unlikely that Sr isotopic compositions will be useful for stock identification with many other marine species.

ACKNOWLEDGEMENTS

We would like to thank Reg Thériault and Jen Doherty for their work in developing and establishing the Sr-Spec column chemistry used in this paper. Reg Thériault is thanked for his constructive comments on an earlier version of the manuscript.

REFERENCES

Burke, W.H., Densison, R.E., Hetherington, E.A., Koepncik, R.B., Nelson, H.F., and Otto, J.B.
1982: Variation of seawater $^{87}Sr/^{86}Sr$ throughout Phanerozoic time; Geology, v. 10, p. 516-519.

Faure, G.
1986: Principles of Isotope Geology, second edition; John Wiley and Sons, Inc. New York.

Garlich-Miller, J.L., Stewart, R.E.A., Stewart, B.E., and Hiltz, E.A.
1993: Comparison of mandibular with cemental growth-layer counts for ageing Atlantic walrus (Odobenus rosmarus); Canadian Journal of Zoology, v. 71, p. 163-167.

Payton A, Kastner M, Martin E.E, Macdougall J.D, and Hebert T.
1993: Marine barite as a monitor of seawater strontium isotope composition; Nature, v. 366, p. 445-449.

van der Merwe N.J., Lee-Thorp J.A., Thackery J.F., Hall-Martin A., Kruger F.J., Coetzee H., Bell R.H.V, and Lindeque M..
1990: Source-area determination of elephant ivory by isotopic analysis; Nature, v. 346, p. 744-746.

Vogel J.C., Eglington, B., and Auret J.M.
1990: Isotope fingerprints in elephant bone and ivory; Nature, v. 346, p. 747-749.

– 9 –

New geochronological results for the Tavani area (55 K), eastern Kaminak greenstone belt, District of Keewatin, Northwest Territories

W.J. Davis[1] and T. Peterson[1]

Davis, W.J. and Peterson, T., 1998: New geochronological results for the Tavani area (55 K), eastern Kaminak greenstone belt, District of Keewatin, Northwest Territories; in *Radiogenic Age and Isotopic Studies: Report 11; Geological Survey of Canada, Current Research 1998-F, p. 81-88.*

Abstract: Two felsic volcanic rocks of the Akliqnaktuk Formation in the Tavani area have yielded zircon ages of 2700 ± 1 Ma and 2695 ± 3 Ma, similar to ages reported for volcanic rocks from the Kaminak Lake area. The Last Lake pluton and associated dykes intrude foliated volcanic rocks, and the 2686 ± 4 and 2686 ± 2 Ma ages for the pluton and a dyke, provide a minimum age of deformation of the volcanic rocks in that area. Detrital zircons from an interbedded polymictic conglomerate and arkose unit within the Akliqnaktuk Formation have ages from 2700 to 2657 ± 2 Ma, indicating that this unit is significantly younger than the volcanic rocks, and not part of the Akliqnaktuk Formation. The unit may be correlative to similar sedimentary units reported elsewhere in the Kaminak belt, for example, the Spi Lake conglomerate.

Résumé : La datation de zircons provenant de deux roches volcanofelsiques de la Formation d'Akliqnaktuk dans la région de Tavani a donné des âges (2 700 ±1 Ma et 2 695 ± 3 Ma) similaires aux âges des roches volcaniques de la région du lac Kaminak. Le pluton du lac Last et les dykes associés recoupent des roches volcaniques feuilletées; les âges de 2 686 ± 4 Ma et 2 686 ± 2 Ma du pluton et d'un dyke donne l'âge minimal de la déformation des roches volcaniques dans la région. Des zircons détritiques provenant d'une unité de conglomérat polygénique et d'arkose interstratifiés dans la Formation d'Akliqnaktuk donnent des âges de 2 700 à 2 657 ± 2 Ma, ce qui indique que l'unité est considérablement plus jeune que les roches volcaniques et qu'elle ne fait pas partie de la Formation d'Akliqnaktuk. Elle pourrait être corrélative avec des unités sédimentaires similaires observées ailleurs dans la ceinture de Kaminak, comme le conglomérat du lac Spi.

[1] Geological Survey of Canada, 601 Booth Street, Ottawa, Ontario K1A 0E8

INTRODUCTION

In this paper we report new U-Pb zircon ages for volcanic, plutonic, and sedimentary rocks from the Tavani area in the eastern Kaminak greenstone belt (southwest corner of NTS 55 K), western Churchill Province. The Kaminak belt is a large, Neoarchean, volcanic-dominated, supracrustal domain that extends 300 km west-southwest from Hudson Bay. The bedrock geology of the Tavani area was most recently mapped at 1:100 000 scale by Park and Ralser (1992), but the area, in particular the supracrustal rocks, has received very little geochronological study. Geochronological studies were initiated in conjunction with targeted mapping in the area by Peterson (1997) with the following objectives: 1) to establish the age of volcanic units for local tectono-stratigraphic, as well as regional, correlations; 2) to determine the age of regional deformational events by dating crosscutting intrusive rocks; and 3) to provide a maximum age estimate and characterize the provenance of a distinctive polymictic conglomerate and arkose unit within the volcanic tectono-stratigraphy.

GEOLOGICAL SETTING

The eastern portion of the Kaminak greenstone belt (Tavani area) is dominated by pillowed mafic volcanic rocks, with subordinate breccias and felsic flows and tuffs, all intruded by syn- to post-tectonic granitoids (Fig. 1; Park and Ralser, 1992; Peterson, 1997). The Archean rocks are overlain by Proterozoic epicontinental clastic rocks (lower Hurwitz Group), exposed in northeast-oriented synclines that parallel the dominant fabric in adjacent Archean rocks (Park and Ralser, 1992). Park and Ralser (1992) divided the Archean supracrustal rocks into two sequences: the volcanic-dominated Kasigialik Group (equivalent to the Kaminak Group of Davidson (1970) to the west), and the sediment-dominated Tagiulik Formation. The lower Kasigialik Group consists of the Atungag Formation, an older(?) series of greenschist- to amphibolite-facies, mafic, pillowed flows and iron-formation with few intercalated clastic sediments or tuffs. It is overlain by the Akliqnaktuk Formation, a mafic to felsic series rich in tuffs and volcanic breccias, and by the Evitaruktuk Formation composed of quartzofeldspathic turbidites and conglomerates (Park and Ralser, 1992). The Tagiulik Formation, which Park and Ralser (1992) considered allochthonous with respect to the Kasigialik Group, consists of quartz-poor turbidites with magnetite-chert iron-formation, conglomerate, and arkose.

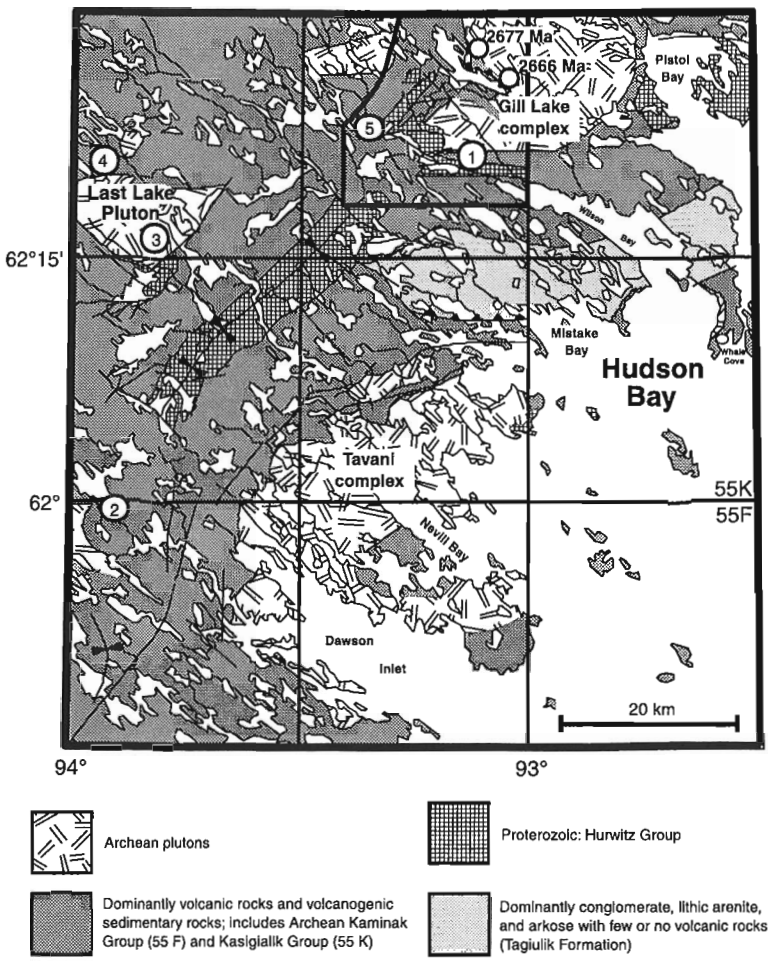

Figure 1.

Simplified geology of the Kaminak greenstone belt east of 94° W. See text for references. The truncated rectangle (top, center) outlines the area of Figure 2. Age data reported in Park and Ralser (1992). Sample location sites are as follows: 1) felsic volcanic PHA-96-395; 2) felsic tuff PHA-96-337c; 3) Last Lake tonalite pluton PHA-96-31b; 4) tonalite dyke PHA-96-58; 5) Wilson River conglomerate PHA-96-2001.

U-Pb GEOCHRONOLOGY

Previous work

Previous U-Pb geochronological work in the Tavani area is limited to ages for plutonic rocks from the Gill Lake area reported in Park and Ralser (1992). These include an age of 2677 ± 2 Ma for the Gill Lake pluton and 2666 ± 2 and 2663 ± 3 Ma for two samples of the east Gill Lake pluton (Fig. 1, 2). The plutons are interpreted to span a period of deformation of the area (Park and Ralser, 1992). The age of Archean supracrustal rocks in the Tavani area is not known. Mortensen and Thorpe (1987) reported ages of 2692 ± 1 and 2697.5 ± 1.4 Ma for felsic volcanic rocks of the Kaminak Group from the Kaminak Lake area, 100 km to the west of the Tavani area. Patterson and Heaman (1990) reported a younger age of 2681 ± 3 Ma for a felsic volcanic rock at Quartzite Lake. Cavell et al. (1992) determined SHRIMP ion microprobe ages of 2700 ± 11 Ma for a tonalite phase of the Kaminak batholith and a 2659 ± 5 Ma age for an ijolite-carbonatite intrusion at Kaminak Lake.

Analytical methods

Heavy-mineral concentrates were prepared by standard techniques (crushing, grinding, Wilfley^{TM} table, heavy liquids), and sorted by magnetic susceptibility using a Frantz^{TM} isodynamic separator. All zircon fractions were air abraded (Krogh, 1982). Analytical methods for U-Pb analyses of zircon are summarized in Parrish et al. (1987), and for titanite in Davis et al. (1997). Analytical errors are determined based on error propagation methods of Roddick (1987), and reproducibility of standard zircon solutions. Analytical results are presented in Table 1.

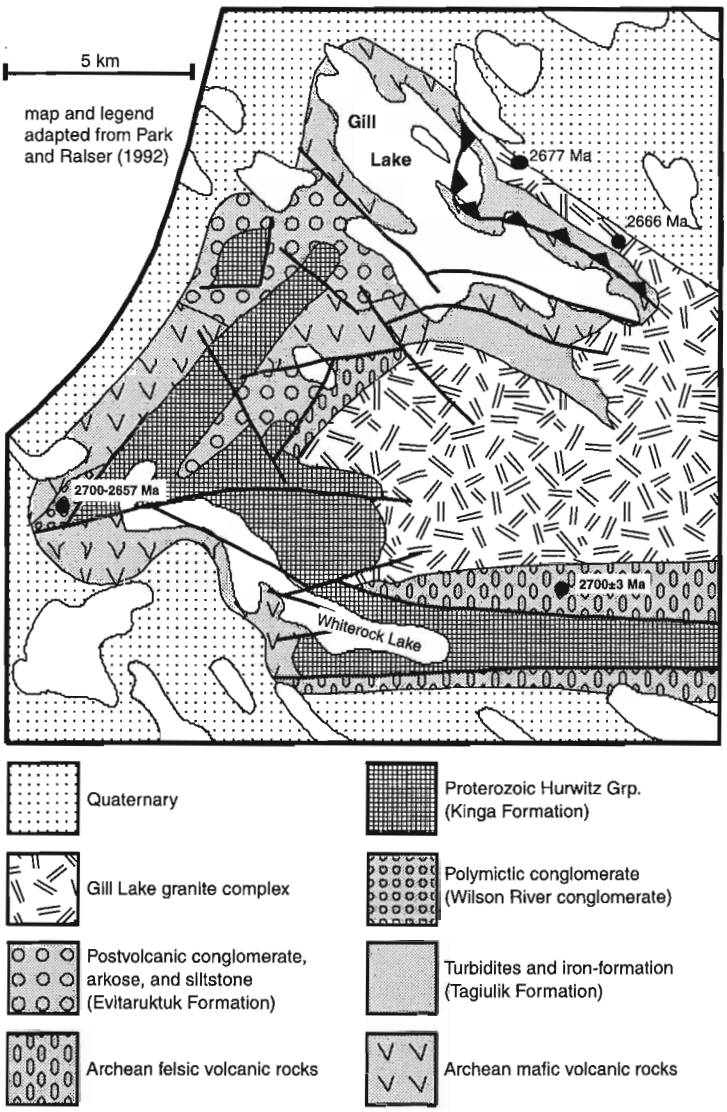

Figure 2.

Geology of the Gill Lake–Whiterock Lake area, after Park and Ralser (1992) (see Fig. 1 for location). The Wilson River (not indicated) enters the northwestern end of Whiterock Lake.

Table 1. U-Pb analytical data.

Fraction[1]				Concentrations[2]			Atomic Ratios[3]					Age (Ma)[4]
ID	Description	#gr	Wt. (µg)	U (ppm)	Pb* (ppm)	Pb_c (pg)	$\frac{^{206}Pb}{^{204}Pb}$	$\frac{^{208}Pb}{^{206}Pb}$	$\frac{^{206}Pb}{^{238}U}$	$\frac{^{207}Pb}{^{235}U}$	$\frac{^{207}Pb}{^{206}Pb}$	$\frac{^{207}Pb}{^{206}Pb}$
1. PHA-96-395 Z4510	***UTM 490510, 6913220 (14)***											
1 Z	dia,e,cl,c,pr	5	12	88	53	8	3923	0.1554	0.5194 ± .16%	13.272 ± .17%	0.18533 ± .06%	2701.1 ± 1.8
2 Z	dia,e,cl,c,pr	10	23	30	18	5	4101	0.1752	0.5199 ± .16%	13.281 ± .17%	0.18527 ± .06%	2700.7 ± 1.8
3 Z	dia,e,cl,c,eq	3	5	126	74	3	8465	0.1284	0.5198 ± .16%	13.266 ± .17%	0.18511 ± .06%	2699.2 ± 1.8
2. PHA-96-337C z4512	***UTM 447101, 6873700 (14)***											
4 Z	-0.5,fg,s,pb,ro	3	4	40	24	6	923	0.1342	0.5345 ± .28%	13.619 ± .28%	0.18479 ± .08%	2696.4 ± 2.6
5 Z	0°ss,s,cl,pb,eq,ro	3	1	70	42	4	603	0.1202	0.5339 ± .53%	13.577 ± .51%	0.18444 ± .17%	2693.2 ± 5.7
6 Z	0° ss,e,cl,pb,eq,ro	4	1	63	37	4	571	0.1401	0.5216 ± .60%	13.275 ± .58%	0.18461 ± .20%	2694.7 ± 6.6
7 Z	-0.5° ss,e,cl,pb,eq	4	1	62	36	8	266	0.1244	0.5133 ± .72%	13.078 ± .70%	0.18479 ± .26%	2696.4 ± 8.7
8 Z	dia, fg,b,ro?	2	4	22	13	11	239	0.2257	0.4672 ± .96%	11.788 ± .92%	0.18298 ± .30%	2680.0 ± 9.9
3. PHA-96-31B z4572	***UTM 458624, 6903820 (15)***											
9 Z	dia,e,cl,pp,eq	2	12	50	30	5	3867	0.1485	0.5160 ± .16%	13.084 ± .17%	0.18390 ± .06%	2688.4 ± 1.8
10 Z	dia,e,cl,pp,pr	5	20	45	27	3	8421	0.1611	0.5153 ± .16%	13.045 ± .17%	0.18360 ± .06%	2685.7 ± 1.8
11 Z	dia,e,cl,pp,eq	4	38	38	23	4	10277	0.1599	0.5156 ± .16%	13.047 ± .17%	0.18351 ± .06%	2684.9 ± 1.8
12 T	0.75,s,b	15	219	69	43	686	634	0.2162	0.5200 ± .09%	13.158 ± .17%	0.18351 ± .12%	2684.8 ± 4.0
13 T	0.75,a,b	15	286	15	14	446	278	0.914	0.5025 ± .11%	12.613 ± .34%	0.18206 ± .27%	2671.7 ± 9.1
4. PHA-96-58 z4556	***UTM 448201, 6911369 (15)***											
14 Z	dia,e,cl,pb,pr	4	8	44	27	8	1284	0.2179	0.5115 ± .22%	12.976 ± .23%	0.18398 ± .06%	2689.0 ± 2.0
15 Z	dia,e,cl,co,t	2	17	36	22	12	1599	0.1858	0.5160 ± .16%	13.065 ± .17%	0.18366 ± .06%	2686.2 ± 1.8
16 Z	dia,e,cl,co,t	5	20	33	20	4	4853	0.1643	0.5157 ± .16%	13.052 ± .17%	0.18355 ± .06%	2685.2 ± 1.8
17 Z	dia,e,cl,b,eq	1	8	38	21	4	2199	0.0832	0.5123 ± .16%	12.943 ± .17%	0.18325 ± .06%	2682.5 ± 1.9
18 T	0.75A, s,pb,fr	15	54	69	36	244	432	0.0197	0.5057 ± .16%	12.515 ± .22%	0.17948 ± .17%	2648.1 ± 5.7
19 T	0.75A,a,b,fr	15	66	64	36	936	141	0.0897	0.5133 ± .17%	12.710 ± .68%	0.17957 ± .57%	2648.9 ± 19.0
5. PHA-96-2001 z4529	***UTM 481600, 6916200 (15)***											
20 Z	dia,fg,cl,pb	1	5	40	24	6	974	0.1462	0.5181 ± .22%	13.241 ± .22%	0.18536 ± .07%	2701.4 ± 2.2
21 Z	dia,eu,cl,co,pr	1	2	25	16	5	325	0.1849	0.5213 ± .82%	13.292 ± .82%	0.18493 ± .25%	2697.6 ± 8.2
22 Z	dia,eu,cl,co,pr	1	2	28	17	7	294	0.2038	0.5172 ± .63%	13.176 ± .62%	0.18476 ± .20%	2696.1 ± 6.6
23 Z	dia,fg,cl,pb	1	8	42	25	12	905	0.1529	0.5182 ± .18%	13.163 ± .19%	0.18422 ± .08%	2691.3 ± 2.7
24 Z	dia,eu,cl,pp,eq	1	3	69	39	3	2271	0.0958	0.5165 ± .17%	13.116 ± .17%	0.18417 ± .06%	2690.7 ± 1.8
25 Z	dia,eu,cl,co,eq	1	2	66	40	4	913	0.1698	0.5177 ± .31%	13.135 ± .33%	0.18403 ± .14%	2689.5 ± 4.6
26 Z	dia,eu,cl,pp,eq	1	2	49	31	5	599	0.2493	0.5076 ± .47%	12.712 ± .49%	0.18165 ± .23%	2668.0 ± 7.5
27 Z	dia,eu,cl,co,eq,ro	1	2	88	55	2	2999	0.2562	0.5061 ± .20%	12.618 ± .20%	0.18081 ± .06%	2660.3 ± 1.8
28 Z	dia,eu/fg,cl,pb	1	3	99	59	4	2722	0.176	0.5104 ± .16%	12.694 ± .17%	0.18039 ± .06%	2656.5 ± 1.8

[1] Legend: Mineral: Z = zircon, T = titanite; Magnetic properties: dia - diamagnetic @ 1.8 A; , nm 0° - non-magnetic at indicated side slope of Frantz™; 0.75A - non-magnetic at given amperage (10° side slope). Grain characteristics: eu=euhedral, s=subhedral, a= anhedral, fg= fragment, cl=clear, co= colourless, b=brown, pp=pale pink, pb=pale brown, eq= equant, t=tabular, pr=prismatic (>3:1), ro=rounded or poorly developed facets, fr= fractured. #gr - number of individual grains included in fraction; uncertainty in sample weight estimated at ±1 µg.

[2] Concentration uncertainty varies with sample weight: >10% for sample weights <10 µg, <10% for sample weights above 10 µg. * = Radiogenic Pb; P_c = total common Pb in analysis corrected for spike and fractionation.

[3] Ratios corrected for spike, fractionation, blank and initial common Pb, except $^{206}Pb/^{204}Pb$ ratio corrected for spike and fractionation only. Errors are one sigma in %

[4] $^{207}Pb/^{206}Pb$ age with 2 sigma absolute error in Ma.

Akliqnaktuk Formation: felsic volcanic - PHA-96-395

Sample PHA-96-395 was taken from a weakly quartz-phyric, massive, felsic volcanic rock within the Akliqnaktuk Formation, north of Whiterock Lake (Fig. 2). Abundant clear, euhedral, prismatic, zircon crystals were recovered. Two multigrain fractions of the dominant, elongate (3:1 to 4:1) population of zircons (fractions 1 and 2, Table 1) yield concordant ages of 2701 ± 2 Ma. A third fraction (fraction 3) of more equant crystals (2:1) yielded a concordant age of 2699 ± 2. The age of the volcanic rock is given by the weighted mean of the three analyses at 2700 ± 1 Ma (Fig. 3a).

Akliqnaktuk Formation: felsic tuff - PHA-96-337c

Sample PHA-96-337c is from a 80 cm thick, flinty, buff- to pale-orange-weathering felsic tuff layer within mafic volcanic rocks of the Akliqnaktuk Formation (Fig. 1, 2). Several felsic horizons, ranging in width from 10 cm to 1 m, occur in the outcrop, along with graded, pebbly to silty beds that may be epiclastic rocks. Zircons consist of colourless to pale brown crystals with subhedral morphologies. Many grains are fragments of larger crystals and generally have poorly developed crystal faces. Five analyses of small multigrain fractions (fractions 4–8, Table 1) yield variably discordant ages that define a discordia line with an upper intercept age of

2695 ± 3 Ma (Fig. 3b). The zircons apparently represent a single age population, with no indication of inherited or detrital grains of different origin. This is consistent with a primary igneous origin for this tuff layer. However, the morphology of the zircons, and the high proportion of fractured grains, are not inconsistent with an epiclastic origin. If the tuff layer had an epiclastic origin then 2695 ± 3 Ma represents a maximum age for the adjacent mafic volcanic rocks.

Last Lake pluton - PHA-96-31b

Sample PHA-96-31b is from the Last Lake pluton, a weakly foliated, homogenous biotite ± hornblende tonalite. The pluton intrudes strongly deformed mafic volcanic rocks, and includes metre- to kilometre-scale mafic volcanic rafts that contain a bedding-parallel, east-west foliation (S_1) parallel to that in the country rock. This fabric is not developed in the pluton; therefore, the intrusion age provides a minimum age for the development of the dominant east-west foliation in the host volcanic rocks. The pluton contains a weak, steep foliation subparallel (045°) to a variably developed cleavage in the host volcanic rocks.

Zircons in this sample consist of clear, colourless to pale pink, euhedral grains ranging from equant to prismatic morphologies. Two fractions of multifaceted equant grains (fractions 9, 11) yielded concordant ages of 2688 ± 2 and 2685 ± 2 Ma. A third fraction (fraction10) of more prismatic zircons yielded an age of 2686 ± 2 Ma. The age of the pluton is determined by the weighted mean age of the three analyses at 2686 ± 4 Ma.

Titanite was also recovered from this sample. A fraction of dark brown, blocky fragments yielded a reversely discordant result with a $^{207}Pb/^{206}Pb$ age of 2685 ± 4 Ma (fraction 12); similar to the age determined for zircon. A second titanite fraction consisting of paler brown, clear, subhedral crystals yielded a 2% discordant result with a $^{207}Pb/^{206}Pb$ age of 2672 ± 10 Ma (fraction 13).

Tonalite dyke - PHA-96-58

Sample PHA-96-58 is from a metre-wide, white-weathering, tonalite dyke that intrudes mafic volcanic rocks about 1 km north of the Last Lake pluton. The trace-element composition of this dyke (and of all analyzed dykes and stocks from this area)

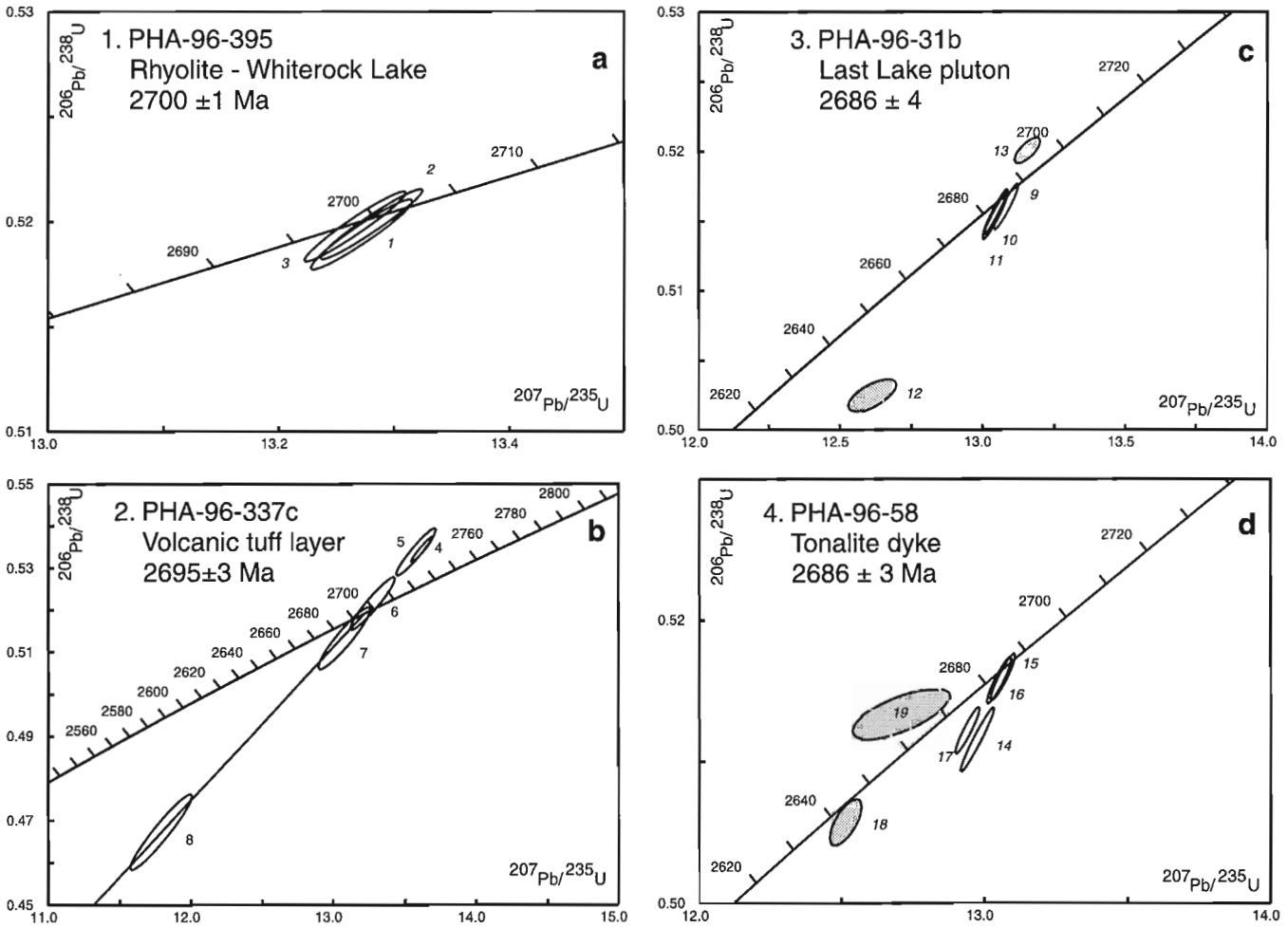

*Figure 3. U-Pb concordia diagrams: **a**) PHA-96-395; **b**) PHA-96-337c; **c**) PHA-96-31b; **d**) PHA-96-58. Zircon = open ellipse; titanite = shaded ellipse. Ellipse is 95% confidence interval.*

is similar to the Last Lake pluton (Peterson, unpub. data), consistent with the field interpretation that the dyke is genetically related to the pluton. Like the Last Lake pluton, the dyke cuts the dominant east-west S_1 foliation in the country rocks. The dyke is openly folded and contains a weakly developed axial planar foliation striking 045°.

The sample contained abundant euhedral to subhedral zircon crystals. The grains are typically clear and pale brown in colour. Morphologies of the grains range from tabular to elongate prismatic grains. A fraction consisting of two large euhedral tabular grains yielded a concordant age of 2686 ± 2 Ma (fraction 15, Figure 3d). Five smaller tabular grains yielded a similar, concordant age of 2685 ± 2 Ma (fraction 16). A discordant (1%) age of 2689 Ma was determined for a group of four elongate, prismatic crystals (fraction 14). A fourth fraction of equant to slightly rounded brown coloured grains yielded a discordant (0.6%) age of 2683 Ma (fraction 17). The best age estimate is provided by the average of the two concordant analyses at 2686 ± 2 Ma. Pale brown to brown, anhedral to subhedral, titanite grains yielded discordant ages of 2648 and 2649 Ma, significantly younger than the crystallization age of the dyke.

Conglomerate-arkose unit - PHA-96-2001

Park and Ralser (1992) included a distinctive, polymictic conglomerate and interbedded arkose unit exposed along the Wilson River within the Akliqnaktuk Formation (Fig. 2). The conglomerate contains a wide variety of clast types, including volcanic rocks and granitoids, some of which contain a pre-existing foliation (Fig. 4). The unit itself is penetratively foliated (Fig. 4). The nature of the contact with the underlying volcanic rocks (conformity/unconformity/fault) was not determined. The character of this sedimentary unit is similar to the Spi Lake conglomerate (Beavon, 1976; Patterson, 1991) which unconformably overlies the Kaminak Group and intrusive rocks west of Kaminak Lake.

A sample of an arkose layer within the conglomerate sequence from near the Wilson River yielded a range of detrital zircon ages from 2657 to 2702 Ma (Fig. 5). The zircons are euhedral and well faceted, showing minimal abrasion or rounding. The older grains overlap the ages of volcanic rocks in the area (2690–2700 Ma), and the younger grains are similar to, or younger than, the age of local syn- to post-tectonic plutonic rocks (2677–2663 Ma; Park and Ralser, 1992). The youngest grain provides a maximum depositional age of 2657 ± 2 Ma for this unit, at least 30 million years younger than the Akliqnaktuk Formation volcanic rocks, and less than 5 to 20 million years younger than adjacent plutons. Deposition postdates early deformation (before 2685 Ma) of the belt determined by the age of the Last Lake pluton. The youngest zircon grain is younger than rocks from the Tavani area, but is similar in age to the ijolite-carbonatite complex at Kaminak Lake (2659 Ma: Cavell et al., 1992).

DISCUSSION AND CONCLUSIONS

The new zircon ages document a span of at least 5 million years for felsic volcanism within the Akliqnaktuk Formation in the Tavani area. The age of the mafic volcanic-dominated Atungag Formation and equivalent rocks remains unknown. Volcanic ages in the Tavani area are similar to ages of felsic volcanic rocks within the Kaminak belt to the west, at Spi Lake (2697.5 ± 1.4 Ma) and Kaminak Lake (2692 ± 1 Ma; Mortensen and Thorpe, 1987). Although the data set remains small (n = 5), much of the felsic volcanism within the Kaminak belt over a strike length of more than 150 km occurred over a brief time interval of less than 10 million years. Deformation of the volcanic rocks in the Tavani area occurred less than 10 million years after their formation. An exception is a rhyolite at Quartzite Lake (2681 ± 3 Ma; Patterson and Heaman, 1991), which is significantly younger than other felsic volcanic rocks dated from the Kaminak belt. Deposition of this rhyolite postdates the deformation (occurring before 2686 ± 2 Ma) in the Tavani area, bracketed by intrusion of the Last

Figure 4.

River-polished outcrop of the Wilson River conglomerate, showing dark volcanic (V) and light tonalite clasts (T), both deformed with the matrix. Hammer handle for scale.

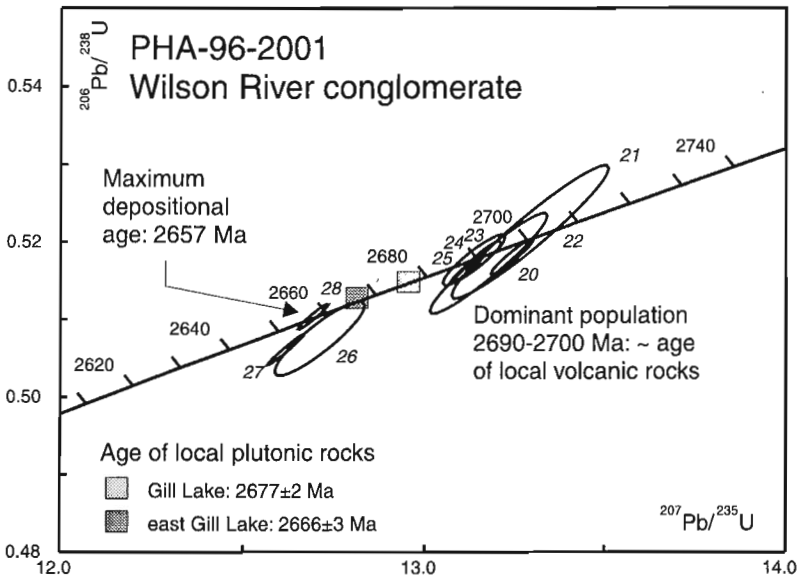

Figure 5.

U-Pb concordia diagram for PHA-96-2001. Gill Lake pluton data from Park and Ralser (1992).

Lake pluton. This suggests that at least two volcanic (± intrusive) sequences are represented in the Kaminak belt, separated by a deformational event.

The maximum depositional age of 2657 ± 2 Ma determined for the Wilson River conglomerate and arkose indicates that this unit is not part of the Akliqnaktuk Formation as originally proposed by Park and Ralser (1992). Rather, these sediments postdate the intrusion of late to postdeformational granitoids, but predate deposition of the Hurwitz group. The sedimentalogical characteristics of the conglomerate, along with its age relationships, are similar to Timiskaming-type deposits of the southern Abitibi belt (Mueller and Donaldson, 1992; Corfu et al., 1991), and it may have a similar tectonic origin. The Timiskaming Group sediments postdate early deformation of the southern Abitibi volcanic belt and intrusion of calc-alkaline plutonic rocks, and are associated with contemporaneous alkaline magmatic rocks (Corfu et al., 1991). Timiskaming Group sedimentary rocks contain detrital zircons with ages similar to local volcanic and plutonic rocks, as well as zircons similar in age to the associated alkaline igneous rocks. Interestingly, the youngest zircon found in the Wilson River conglomerate (2657 ± 2 Ma) is close in age to the 2659 ± 5 Ma, ijolite-carbonatite complex at Kaminak Lake (Cavell et al., 1992), which lies 75 km west-southwest of the Wilson River.

The conglomerate at the Wilson River is similar to some units of the Evitaruktuk Formation described by Park and Ralser (1992), and it is possible that the Evitaruktuk Formation is correlative, and therefore significantly younger than the volcanic formations of the Kasigiliak Group. Another potential correlative unit in the Kaminak belt is the Spi Lake conglomerate, which unconformably overlies the Kaminak Group (Beavon, 1976; Patterson, 1991). If this correlation can be substantiated this would constitute a sedimentary unit of regional significance.

REFERENCES

Beavon, R.V.
1976: Early Aphebian basaltic volcanism in the southern District of Keewatin, Northwest Territories; Canadian Journal of Earth Sciences, v. 13, p. 1003-1005.

Cavell, P.A., Wijbrans, J.R., and Baadsgaard, H.
1992: Archean magmatism in the Kaminak Lake area, District of Keewatin, Northwest Territories: ages of the carbonatite-bearing alkaline complex and some host granitoid rocks; Canadian Journal of Earth Sciences, v. 29, p. 896-908

Corfu, F., Jackson, S.L., and Sutcliffe, R.H.
1991: U-Pb ages and tectonic significance of late Archean alkalic magmatism and non-marine sedimentation: Timiskaming Group, southern Abitibi belt, Ontario; Canadian Journal of Earth Sciences, v. 28, p. 489-503 Canadian Journal of Earth Sciences, v. 29.

Davidson, A.
1970: Precambrian geology, Kaminak Lake map area, District of Keewatin; Geological Survey of Canada, Paper 69-51.

Davis, W.J., McNicoll, V., Bellerive, D., Santowski, K., and Scott, D.J.
1997: Modified chemical procedures for the extraction and purification of uranium from titanite, allanite, and rutile in the Geochronology Laboratory, Geological Survey of Canada; *in* Radiogenic Age and Isotopic Studies: Report 10; Geological Survey of Canada, Current Research 1997-F, p. 33-36.

Mueller, W. and Donaldson, A.
1992: Development of sedimentary basins in the Archean Abitibi belt, Canada: an overview; Canadian Journal of Earth Sciences, v. 29, p. 2249-2265.

Krogh, T.E.
1982: Improved accuracy of U-Pb zircon ages by the creation of more concordant systems using an air abrasion technique; Geochimica et Cosmochimica Acta, v. 46, p. 637-649.

Mortensen, J.K. and Thorpe, R.I.
1987: U-Pb zircon ages of felsic volcanic rocks in the Kaminak Lake area, District of Keewatin; *in* Radiogenic Age and Isotope Studies: Report 1; Geological Survey of Canada, Paper 87-2, p. 123-128.

Park, A.F. and Ralser, S.
1992: Precambrian geology of the southwestern part of the Tavani map area, District of Keewatin, Northwest Territories; Geological Survey of Canada Bulletin 416.

Parrish, R.R., Roddick, J.C., Loveridge, W.D., and Sullivan, R.W.
1987: Uranium-lead analytical techniques at the geochronology laboratory, Geological Survey of Canada; *in* Radiogenic Age and Isotopic Studies: Report 1; Geological Survey of Canada, Paper 87-2, p. 3-7.

Patterson J. and Heaman L.
1990: Geochronological constraints on the depositional age of the Hurwitz Group, N.W.T.; Geological Association of Canada, Program with Abstracts, v. 15, p. A102.

Patterson, J.G.
1991: The Spi Group: a post-Archean, pre-2.1 Ga rift succession, Trans-Hudson hinterland; Canadian Journal of Earth Sciences, v. 28, p. 1863-1872.

Peterson, T.D.
1997: New mapping of Archean supracrustal rocks in the Kaminak Belt, District of Keewatin, Northwest Territories; *in* Current Research 1997-C; Geological Survey of Canada, p. 111-121.

Roddick, J.C.
1987: Generalized numerical error analysis with applications to geochronology and thermodynamics; Geochimica et Cosmochimica Acta, v. 51, p. 2129-2135.

– 10 –

Geochronological investigations of the Woodburn Lake group, western Churchill Province, Northwest Territories: preliminary results[1]

W.J. Davis[2] and E. Zaleski[2]

Davis, W.J. and Zaleski, E., 1998: Geochronological investigations of the Woodburn Lake group, western Churchill Province, Northwest Territories: preliminary results; in *Radiogenic Age and Isotopic Studies: Report 11; Geological Survey of Canada, Current Research 1998-F, p. 89-97.*

Abstract: U-Pb dating of zircon from a felsic volcanic rock in the Woodburn Lake group results in an age of 2710 +3.5/-2.1 Ma, significantly younger than previously dated volcanic rocks (2.75–2.80 Ga). The new result suggests that the Woodburn Lake group comprises two volcanic sequences separated in age by up to 90 million years. Detrital zircons in an orthoquartzite range from 2.81 to 3.0 Ga, with the majority of the grains having ages of ca. 2.96 Ga. The euhedral prismatic morphology of the zircons implies textural immaturity in chemically mature quartzite and, hence, intense chemical weathering, and deposition in a low-energy environment. The supracrustal rocks were intruded by quartz-feldspar porphyry at 2620 +3/-2 Ma and granite at 2610 +3/-2 Ma. The porphyry has an S_1 foliation, whereas the relative timing of the foliation in the granite is uncertain. This suggests that D_1 deformation, at least in part, occurred after 2620 Ma, and that significant deformation of the belt occurred after 2610 Ma.

Résumé : La datation U-Pb sur zircons d'une roche volcanofelsique du groupe de Woodburn Lake a donné un âge de 2 710 +3,5/-2,1 Ma, sensiblement plus jeune que celui des roches volcaniques antérieurement datées (2,75–2,80 Ga). Ce nouvel âge semble indiquer que le groupe du Woodburn Lake comprend deux séquences volcaniques espacées chronologiquement de jusqu'à 90 Ma. L'âge de zircons détritiques dans un orthoquartzite varie de 2,81 à 3,0 Ga, la plupart des grains remontant à environ 2,96 Ga. La morphologie prismatique automorphe des zircons suggère une immaturité texturale du quartzite chimiquement mature et, donc, une intense altération chimique et une sédimentation dans un milieu à faible énergie. Les roches supracrustales ont été recoupées par du porphyre quartzofeldspathique à 2 620 +3/-2 Ma et par du granite à 2 610 +3/-2 Ma. Le porphyre montre une schistosité S_1, alors que la chronologie relative de la schistosité du granite est incertaine. Cela laisse supposer que la déformation D_1 est au moins en partie postérieure à 2 620 Ma et qu'une déformation importante de la ceinture a eu lieu après 2 610 Ma.

[1] Contribution to the Western Churchill NATMAP Project

[2] Geological Survey of Canada, 601 Booth Street, Ottawa, Ontario K1A 0E8

INTRODUCTION

A new bedrock mapping project was initiated in the Woodburn Lake group in 1996 (Zaleski et al., 1997a, b), following up on previous work by Fraser (1988), Ashton (1988), Annesley (1989), Henderson et al. (1991), Roddick et al. (1992), and Henderson and Henderson (1994), among others. The Woodburn project is a component of the ongoing Western Churchill NATMAP initiative which encompasses a broad area of Archean and Proterozoic supracrustal, plutonic, and gneissic rocks in the Rae and Hearne provinces. In this report, we present the initial results of U-Pb zircon geochronological studies in the Woodburn Lake group designed to establish the ages of supracrustal and plutonic rocks, determine the ages of major deformational events, and contribute to regional correlations and understanding of the tectonic setting of the supracrustal belts.

The Woodburn Lake group lies in the Rae province, north of the Snowbird tectonic zone (Fig. 1). It comprises Archean quartzites, komatiites, iron-formation, felsic to mafic volcanic rocks, and derived sedimentary rocks. Similar Archean assemblages define a discontinuous, northeasterly trending zone from the Woodburn Lake group through the Prince Albert group in the Committee Fold Belt (Frisch, 1982; Schau, 1982) to the Mary River group on northern Baffin Island (Bethune and Scammell, 1997). Correlations among these groups have been proposed by Jackson and Taylor (1972), Taylor (1985), Fraser (1988), and Ashton (1988). Few high-precision U-Pb zircon ages are available for the volcanic rocks, with the exception of felsic to intermediate rocks of the Mary River group, which have been precisely dated at 2730–2715 Ma (Jackson et al., 1990; Bethune and Scammell, 1997). A single felsic volcanic rock from the Prince Albert group has an imprecise age of ca. 2.8 Ga, and felsic volcanic rocks of the Woodburn Lake group, north and south of the present study area, have ages of greater than 2.75 to 2.80 Ga (Tella et al., 1985; Roddick et al., 1992).

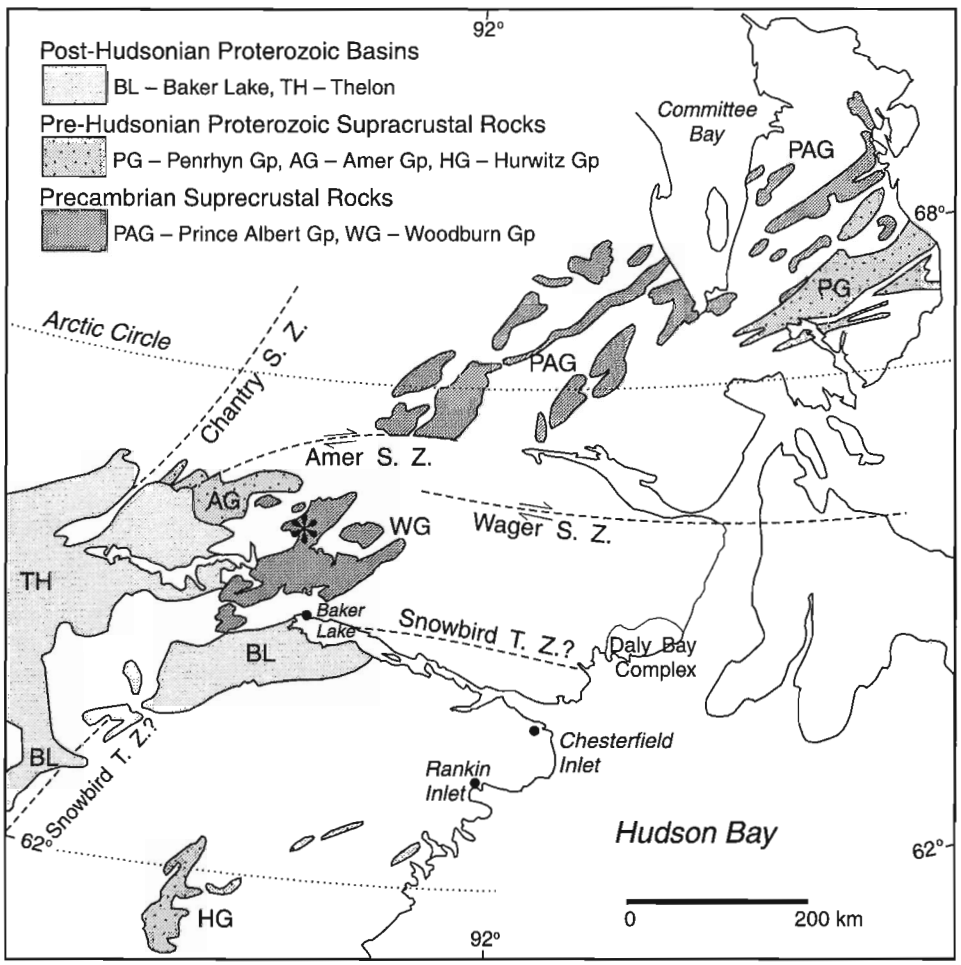

Figure 1. *Regional geology northwest of Hudson Bay showing the distribution of Archean supracrustal rocks of the Woodburn Lake group and the Prince Albert group, as well as the Paleoproterozoic Amer group and crustal-scale shear zones (S.Z.). The location of the study area is shown by an asterisk. Adapted from Henderson et al. (1991) with the Snowbird tectonic zone (Snowbird T.Z.) from Hoffman (1988).*

The Woodburn Lake group lies in an area of the western Churchill Province variably affected by Archean and Paleoproterozoic deformation. Patterson (1986) proposed that Archean rocks south of the Amer belt (Tella, 1994), formed the metamorphic and plutonic internides to the Paleoproterozic Amer fold and thrust belt, 25 km to the north of the present study area. Attempts to determine the age of deformation in the Woodburn Lake group have largely relied on dating the massive and foliated plutons that intrude the supracrustal rocks, and have resulted in conflicting interpretations. Ashton (1988) obtained an age of 2621 ± 2 Ma on massive granite, and a younger age of 2599 ± 5 Ma on foliated granite (Fig. 2). He concluded that strain partitioning played a role in the development of tectonic fabrics in the granitoid rocks, and suggested that significant deformation, possibly of Paleoproterozoic age, postdated the emplacement of granites. In contrast, Roddick et al. (1992) obtained a composite age of 2612 ± 4 Ma on massive granites and concluded that major deformation in the Woodburn Lake group was of Archean age.

GEOLOGY OF THE WOODBURN LAKE GROUP

The Woodburn Lake group can be broadly subdivided into mature sedimentary rocks (orthoquartzite and oligomictic conglomerate), ultramafic to mafic flows and derived schists, chemical sedimentary rocks (iron-formation), and felsic to intermediate volcano-sedimentary rocks comprising pyroclastic and volcanogenic sedimentary lithofacies (Fig. 2). The stratigraphic succession is uncertain. Ashton (1988), Fraser (1988), and Annesley (1989) proposed that the quartzite unconformably overlies volcanic rocks and interbedded

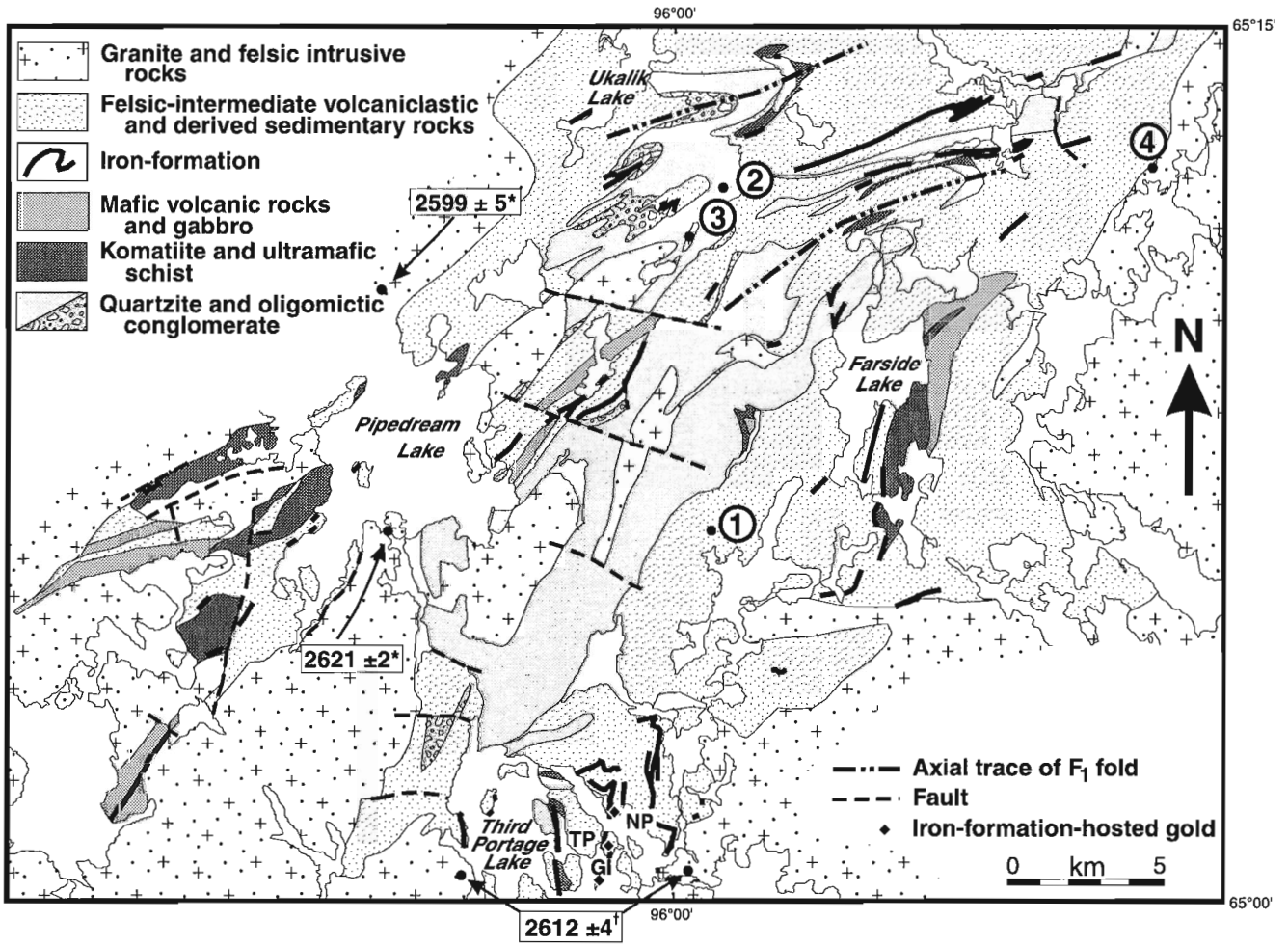

Figure 2. *Generalized geology of part of the Woodburn Lake group, with numbered locations of sample sites. 1 = felsic lapilli tuff (ZB96-223AZ), 2 = orthoquarztite (ZB96-186AZ), 3 = foliated quartz-feldspar porphyry dyke (ZB96-128AZ), 4 = foliated granite (ZB96-204AZ). Additional U-Pb zircon ages of foliated (2599 ± 5 Ma) and massive (2612 ± 4 and 2621 ± 2 Ma) granites are from (*) Ashton (1988) and (†) Roddick et al. (1992). Iron-formation-hosted gold deposits of the Meadowbank camp are abbreviated as follows: NP = North Portage, TP = Third Portage, GI = Goose Island.*

iron-formation, and they considered oligomictic conglomerate to be a basal conglomerate underneath quartzite. The presence of fuchsite in the quartzite, and high Cr and Ni contents, suggests a detrital component from mafic or ultramafic sources (Ashton, 1988). In contrast, Kjarsgaard et al. (1997) suggested that quartzite is the basal unit, overlain by an upward-younging sequence from komatiites to komatiitic basalt, to felsic and intermediate volcanic and sedimentary rocks. The presence of quartzite(?) clasts in volcanic debris-flow deposits, implies that at least some volcano-sedimentary rocks stratigraphically overlie quartzites (Zaleski et al., 1997a, b).

Three generations of ductile tectonic fabrics were recognized in the field (Zaleski et al., 1997a, b) including mineral foliation, mylonitic layering, and clast flattening (S_1); mineral lineation and clast elongation (L_1); crenulation cleavage (S_2)

Table 1. U-Pb analytical data.

Fraction[1]				Concentrations[2]			Atomic Ratios[3]					Age (Ma)[4]
ID	Description	#gr	Wt. (µg)	U (ppm)	Pb* (ppm)	Pb_c (pg)	$\frac{^{206}Pb}{^{204}Pb}$	$\frac{^{208}Pb}{^{206}Pb}$	$\frac{^{206}Pb}{^{238}U}$	$\frac{^{207}Pb}{^{235}U}$	$\frac{^{207}Pb}{^{206}Pb}$	$\frac{^{207}Pb}{^{206}Pb}$
1. Felsic Lapilli Tuff - ZB96-223AZ					***95.987W, 65.105E***							
1	Z nm0°,eu,cl,pb,pr,fr	5	7	92	62	6	3633	0.3379	0.5175 ± .17%	13.298 ± .17%	0.18637 ± .06%	2710.4 ± 1.8
2	Z nm0°,eu,cl,pb,pr,fr	6	10¶	62	40	5	4188	0.2729	0.5151 ± .21%	13.235 ± .22%	0.18634 ± .06%	2710.2 ± 1.8
3	Z nm0°,eu,cl,pb,pr,fr	9	6	102	69	3	7158	0.3368	0.5161 ± .16%	13.252 ± .17%	0.18624 ± .06%	2709.2 ± 1.8
4	Z nm0°,eu,cl,pb,eu	15	9	26	16	7	1111	0.2228	0.5204 ± .16%	13.366 ± .17%	0.18627 ± .06%	2709.5 ± 2.0
5	Z nm0°,eu,cl,pb,eu	7	7¶	9	5	6	360	0.2329	0.5136 ± 1.1%	13.188 ± 1.1%	0.18621 ± .21%	2709.0 ± 7.0
2. Orthoquartzite - ZB96-186AZ					***95.979W, 65.200N***							
6	Z nm0°,eu,cl,co,pr,ro	1	3¶	59	38	11	543	0.1189	0.5526 ± .54%	16.494 ± .55%	0.21647 ± .21%	2954.6 ± 6.7
7	Z nm0°,eu,cl,pb,eq	1	3¶	98	63	3	2697	0.0650	0.5851 ± .28%	17.922 ± .33%	0.22214 ± .06%	2996.3 ± 1.9
8	Z nm0°,eu,cl,co,eq	1	4¶	95	57	20	544	0.1323	0.5173 ± .55%	15.526 ± .54%	0.21767 ± .17%	2963.5 ± 5.3
9	Z nm0°,eu,cl,co,eq	1	3¶	45	24	17	267	0.1236	0.4634 ± .85%	13.766 ± .86%	0.21545 ± .32%	2947. ± 10
10	Z nm0°,eu,cl,co,eq	1	3¶	58	34	16	389	0.1041	0.5252 ± .63%	14.301 ± .70%	0.19750 ± .35%	2806. ± 11
11	Z nm0°,eu,cl,co,spr	1	1¶	63	40	5	420	0.1260	0.5479 ± .64%	15.488 ± .62%	0.20502 ± .14%	2866.6 ± 4.7
12	Z nm0°,eu,cl,co,spr	1	1¶	94	65	34	118	0.1803	0.5765 ± 1.5%	16.916 ± 1.4%	0.21281 ± .54%	2927.0 ± 17
13	Z nm0°,eu,cl,co,spr	1	1¶	108	71	9	416	0.1301	0.5699 ± .37%	17.039 ± .35%	0.21685 ± .18%	2957.5 ± 5.7
14	Z nm0°,eu,cl,co,spr	1	1¶	90	59	19	188	0.1092	0.5776 ± .90%	17.344 ± .80%	0.21776 ± .31%	2964.2 ± 10
15	Z nm0°,eu,cl,co,spr	1	1¶	59	38	5	456	0.1271	0.5648 ± .45%	16.960 ± .43%	0.21780 ± .12%	2964.5 ± 4.0
16	Z nm0°,eu,cl,co,spr	1	1¶	94	66	6	569	0.1826	0.5813 ± .34%	17.661 ± .31%	0.22037 ± .16%	2983.4 ± 5.1
3. Quartz-Feldspar Porphyry - ZB96-128AZ					***95.989W, 65.189N***							
17	Z dia,fg,cl,co,og?	2	2¶	75	44	8	563	0.2327	0.4829 ± .50%	11.783 ± .51%	0.17697 ± .23%	2625. ± 8.
18	Z dia,eu,cl,pb,eq	3	3¶	102	62	11	835	0.2471	0.4981 ± .21%	12.145 ± .20%	0.17685 ± .09%	2623.5 ± 2.9
19	Z dia,eu,cl,pb,eq	5	3¶	76	47	15	496	0.2516	0.4996 ± .35%	12.177 ± .36%	0.17677 ± .22%	2622.8 ± 7.2
20	Z dia,eu,cl,pb,eq	5	4	176	105	12	1779	0.2243	0.4961 ± .16%	12.072 ± .17%	0.17649 ± .06%	2620.2 ± 1.8
21	Z dia,eu,cl,pb,eq	8	5	68	42	5	2250	0.2616	0.4996 ± .16%	12.147 ± .17%	0.17633 ± .06%	2618.7 ± 1.8
22	Z dia,fg,cl,co,og	3	5¶	14	8	6	381	0.2656	0.5011 ± .57%	12.170 ± .55%	0.17616 ± .18%	2617.0 ± 5.9
23	Z dia,fg,cl,co,og?	4	4¶	33	18	29	149	0.2107	0.4630 ± 1.2%	11.227 ± 1.2%	0.17587 ± .74%	2614. ± 25
24	Z dia,fg,cl,co,og?	1	1¶	72	44	7	335	0.2468	0.4949 ± .97%	11.912 ± .98%	0.17456 ± .32%	2602. ± 11
4. Foliated Granite - ZB96-204AZ					***95.679W, 65.211N***							
25	Z nm0°,eu,cl,pp,eq	7	6	112	69	3	7510	0.2284	0.5060 ± .16%	12.582 ± .17%	0.18035 ± .06%	2656.1 ± 1.8
26	Z -0.5°,eu,cl,pp,eq	6	7	37	22	3	2497	0.2216	0.4974 ± .16%	12.017 ± .17%	0.17522 ± .06%	2608.2 ± 1.8
27	Z nm0°,eu,cl,pp,spr	4	5	155	92	9	2824	0.2154	0.4977 ± .16%	12.020 ± .17%	0.17517 ± .06%	2607.7 ± 1.8
28	Z dia,eu,cl,pp,spr	9	8	137	82	7	4478	0.2243	0.4958 ± .16%	11.971 ± .17%	0.17510 ± .06%	2607.0 ± 1.8
29	Z nm0°,eu,cl,pp,spr	5	4	86	52	2	4319	0.2317	0.4963 ± .16%	11.979 ± .17%	0.17506 ± .06%	2606.6 ± 1.8
30	Z -0.5°,eu,cl,pp,spr	5	8	74	44	5	3620	0.2240	0.4951 ± .16%	11.934 ± .17%	0.17483 ± .06%	2604.4 ± 1.8
31	Z nm0°,eu,cl,pp,eq	4	6	127	75	3	7228	0.2115	0.4944 ± .16%	11.896 ± .17%	0.17452 ± .06%	2601.5 ± 1.8
32	Z -0.5°,eu,cl,pp,spr	5	5	80	46	16	784	0.2036	0.4916 ± .20%	11.821 ± .19%	0.17440 ± .09%	2600.3 ± 3.1
33	Z dia,eu,cl,pp,spr	8	7	103	61	6	3831	0.2405	0.4878 ± .16%	11.699 ± .17%	0.17395 ± .06%	2596.0 ± 1.8
34	T 0.5A,a,fg,pb,fr	16	37	111	85	58	1913	0.6385	0.4904 ± .08%	11.783 ± .11%	0.17425 ± .05%	2598.9 ± 1.6
35	T 0.5A,a,fg,pb,fr	18	27	107	79	50	1551	0.6526	0.4690 ± .10%	10.905 ± .12%	0.16863 ± .05%	2544.1 ± 1.8

[1] Legend: Mineral: Z = zircon, T = titanite; Magnetic properties: dia - diamagnetic @ 1.8 A, nm0° - non-magnetic on Frantz™ at indicated side slope in degrees; 0.5A indicates magnetic at indicated amperage (10° side slope). Grain characteristics: eu=euhedral, a= anhedral, fg= fragment, fr = fractured, og= overgrowth, cl=clear, co= colourless, pp=pale pink, pb=pale brown, eq= equant, pr=prismatic (>3:1), spr= prismatic (<3:1), ro=rounded or poorly developed facets. #gr - number of individual grains included in fraction; ¶ indicates fraction not weighed, weight estimated from grain size, concentration data are qualitative only; all others, uncertainty in sample weight estimated at ±1 µg.

[2] Concentration uncertainty varies with sample weight: >10% for sample weights <10 µg, <10% for sample weights above 10 µg. * = Radiogenic Pb. P_c = total common Pb in analysis corrected for spike and fractionation.

[3] Ratios corrected for spike, fractionation, blank and initial common Pb, except $^{206}Pb/^{204}Pb$ ratio corrected for spike and fractionation only. Errors are one sigma in %.

[4] $^{207}Pb/^{206}Pb$ age with 2 sigma absolute error in Ma.

and crenulation axes (F_2); kink bands and fracture cleavage (S_3) and kink axes (F_3). In addition, tight to isoclinal F_1 folds, and tight to open F_2 folds were observed. The map pattern in the northern part of the area is dominated by northeasterly trending D_1 structures and, north of Farside Lake, the S_1 schistosity is axial planar to outcrop-scale and map-scale F_1 folds (Fig. 2). In the structurally complex area east of Third Portage Lake, contacts and S_1 schistosity are deformed by several generations of map-scale folds with associated crenulations and crenulation cleavage. Despite the apparent lack of large-scale D_2 and D_3 structures in the northern area, D_2 crenulation microfolds and D_3 kink folds are common and widely distributed. In many cases, the presence of microfolds on schistosity surfaces, for example in high-strain zones and foliated granitoids, was useful as supporting evidence in the correlation of D_1 fabrics between lithological units. In the northern area, high-strain zones parallel to the S_1 schistosity were interpreted as D_1 structures, in part based on the presence of F_2 crenulations superimposed on the high-strain fabrics. Preliminary structural analysis shows that the orientations of D_1 planar and linear fabrics in the high-strain zones are similar to those reported by Patterson (1986) for fabrics associated with folds in the Amer group. However, in the Woodburn Lake group, preliminary petrographic observations suggest that the S_1 schistosity visible on the outcrop may represent a reworked earlier cleavage, hence raising the possibility of pre-D_1, and thus far, cryptic deformation. These interpretations and relationships are the subject of continuing investigations.

U-Pb GEOCHRONOLOGY

Analytical methods

Heavy mineral concentrates were prepared by standard techniques (crushing, grinding, Wilfley™ table, heavy liquids), and sorted by magnetic susceptibility using a Frantz™ isodynamic separator. Mineral fractions were carefully selected under a binocular microscope. All zircon fractions were air abraded (Krogh, 1982). Analytical methods for U-Pb analyses of zircon are summarized in Parrish et al. (1987) and for titanite in Davis et al. (1997). Analytical errors are determined based on error propagation methods of Roddick (1987), and reproducibility of standard zircon solutions. The U-Pb analytical data are presented in Table 1.

Felsic lapilli tuff - ZB96-223AZ

A northeasterly trending package of felsic to intermediate volcanic rocks, volcaniclastic sedimentary rocks, and interbedded iron-formation extends from the Meadowbank gold prospect to Farside Lake and beyond (Fig. 2). The zone is host to many gold, polymetallic, and base-metal occurrences (Kjarsgaard et al., 1997; Zaleski et al., 1997b; Kerswill et al., 1998). Quartzite structurally underlies the volcanosedimentary package along its northwestern contact. Rare quartzite clasts were observed in volcanic debris-flow deposits, suggesting the volcanic package stratigraphically overlies the quartzite. However, an intervening sliver of ultramafic rocks and pillow basalt implies additional structural complications.

A sample of buff-weathering, felsic, lapilli tuff with quartz and plagioclase phenocrysts was collected from a site 6 km southwest of Farside Lake (location 1, Fig. 2). Bedding in the area is defined by interlayered fine tuff, crystal tuff, and lapilli tuff, as well as by local thin iron-formation. Zircons in the sample are euhedral, doubly terminated, prismatic grains with square cross-sections, and smaller, equant multifaceted crystals. The grains are clear and range in colour from pale yellow to pale brown. Prismatic grains typically have c-axis-parallel fractures and many grains are crystal fragments. Three analyses of multigrain fractions of prismatic zircon yielded discordant results (1.4–1.0%) with identical $^{207}Pb/^{206}Pb$ ages of 2710 Ma (fractions 1–3; Fig. 3). An analysis of 15 small, equant brown zircons yielded a similar, discordant (0.4%) age of 2609 ± 2 Ma (fraction 4). A second fraction of

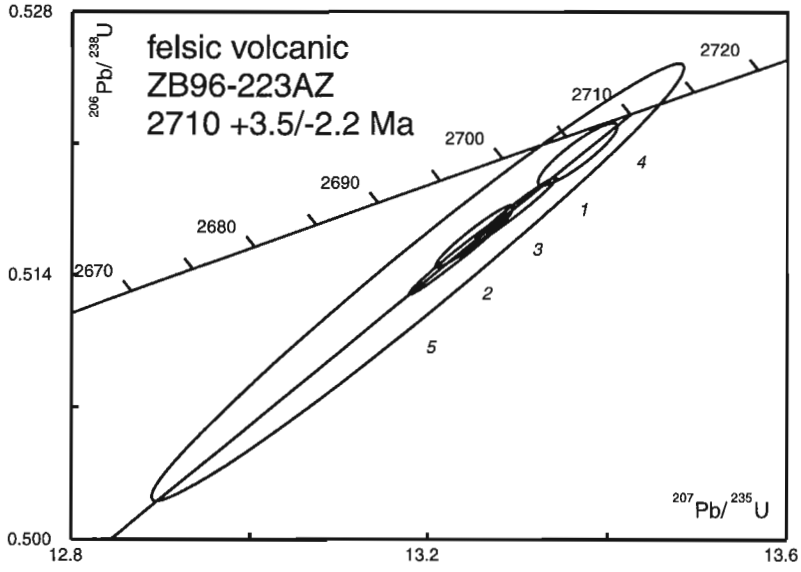

Figure 3.

U-Pb concordia diagram for sample ZB96-223AZ.

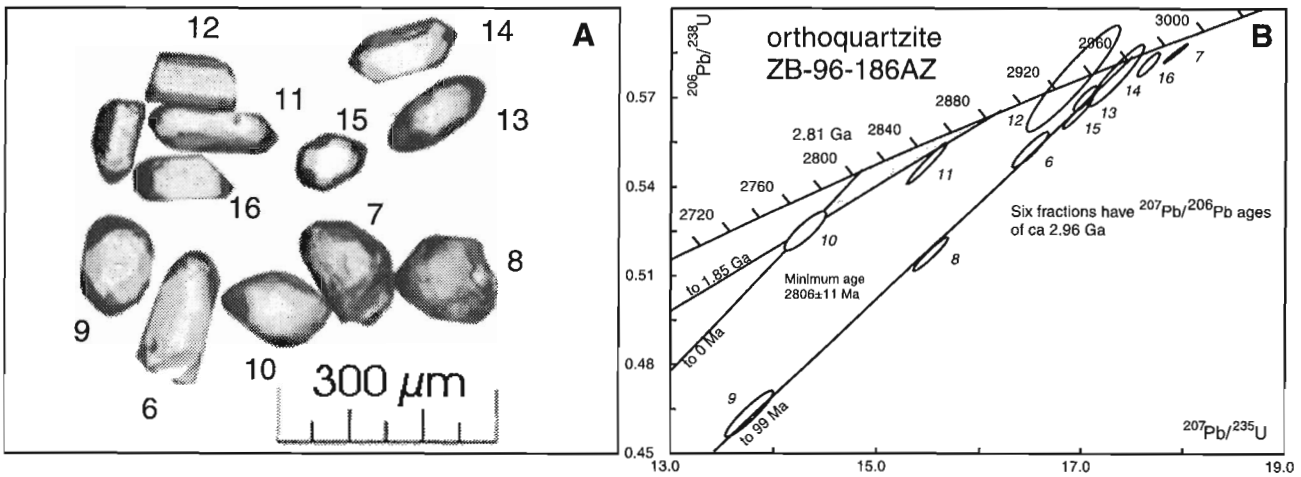

Figure 4. *A) Photograph (transmitted light) of zircons from orthoquartzite sample ZB96-186AZ. Note the sharp crystal terminations in many of the grains. Numbers are cross-referenced to Table 1 and Figure 4b.* ***B****) U-Pb concordia diagram for sample ZB96-186AZ. Lines through discordant fraction E are forced through 1.85 Ma and 0 Ma, with shaded region indicating range of possible ages for the fraction.*

equant grains yielded a very imprecise result due to a large correction for blank Pb (fraction 5). All five analyses have identical $^{207}Pb/^{206}Pb$ ages and regression of the data yields an upper intercept age of 2710 + 3.5/-2.2 Ma (MSWD = 0.6).

The 2710 + 3.5/-2.2 Ma age is significantly younger than the 2798 +24/-21 Ma age reported for a dacite porphyry northwest of the Meadowbank River (Tella et al., 1985), and the greater than 2750 to less than 2800 Ma age estimate for a dacite porphyry north of Whitehills Lake, approximately 30 km to the south (Roddick et al., 1992). The new data indicate that there are at least two ages of felsic volcanic rocks in the Woodburn Lake group, separated by as much as 90 million years. The geological relationship between these two felsic volcanic packages is not known at present, nor is it clear which, if either, is temporally related to the komatiite succession.

Orthoquartzite - ZB96-186AZ

Orthoquartzite is part of a chloritoid-kyanite slate, quartzite, and oligomictic conglomerate sequence, forming a well defined map-scale F_1 fold in the northern part of the map area (Fig. 2). At the sample location, 4 km southeast of Ukalik Lake (location 2, Fig. 2), the quartzite has a grey-blue colour which distinguishes it from the more typical white orthoquartzite of the area. At the sample site, the quartzite contains an east-northeasterly striking, bedding-parallel S_1 schistosity, and a mineral lineation (tourmaline?), plunging moderately to the east-southeast. A pink-weathering, medium-grained monzonite apparently intrudes (contacts covered) the quartzite near the sample site, and may be the extension of a well exposed quartz-feldspar porphyry dyke in quartzite 1 km to the southwest. The dyke was also sampled for dating (location 3, Fig. 2).

Zircon recovered from the orthoquartzite consists of a variety of morphological types, dominated by short prisms with length to breadth ratios of 2:1 or 3:1 (Fig 4a). Tabular and equant grains are also common. The zircons show little or no evidence of pitting, rounding or abrasion. Most grains have sharp, well developed crystal edges and smooth flat faces (Fig. 4a). Some grains, for example grain 6 (Fig. 4a), have rounded terminations, possibly as a result of abrasion in a sedimentary environment. Eleven single grains, selected to sample the range of types observed in the total population, were analyzed (Table 1). All of the analyses are discordant and have $^{207}Pb/^{206}Pb$ ages ranging from 2806 Ma to 2996 Ma (Fig 4b). There is no obvious correlation between grain type and age. Six of the eleven fractions have $^{207}Pb/^{206}Pb$ ages of ca. 2.96 Ga, and this may represent the age of important source rocks to the quartzite (Fig. 4b). The analysis with the youngest $^{207}Pb/^{206}Pb$ age (fraction 10) is discordant, precluding a precise estimate of the maximum depositional age for the sediment. The minimum estimate is 2806 ± 11 Ma. However, if significant Pb loss occurred in the Paleoproterozoic (e.g. ca. 1.85 Ga) then the maximum limit could be as old as 2.89 Ga (Figure 4b). Lead-loss patterns for zircon in two of the other three samples studied so far in the Woodburn area have near-zero age lower intercepts (e.g. ZB96-223AZ, ZB96-128AZ), the third has a 1.2 Ga lower intercept. If sample ZB96-186AZ has a similar, near-zero lead-loss pattern, then the maximum depositional age is probably close to 2.81 Ga.

The euhedral prismatic morphology of the zircons suggests that the quartzite represents a chemically mature, but texturally immature, sediment, such as might be derived from intense chemical weathering in the source area. These features also imply deposition in a low-energy environment, rather than on a shelf (e.g. Chandler, 1988).

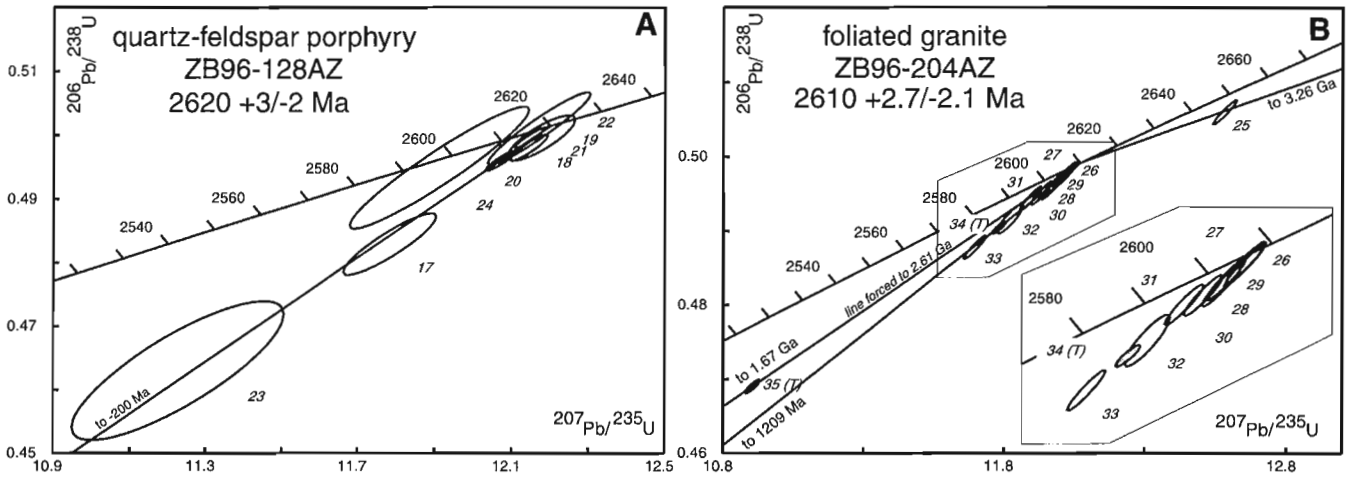

***Figure 5.** U-Pb concordia diagram for samples ZB96-128AZ (**A**) and ZB96-204AZ (**B**).*

The results thus far do not definitively distinguish the relative ages of the quartzite and the older volcanic rocks northwest of the Meadowbank River (2798 +24/-21 Ma; Tella et al., 1985), and south of Tehek Lake (>2750 to <2800 Ma; Roddick et al., 1992). The age of the older volcanic units statistically overlap the 2806 ± 11 Ma age for the youngest detrital zircon in the orthoquartzite, and it is possible that the ca. 2.8 Ga volcanic rocks predate, or are contemporaneous with, the orthoquartzite. Thus far, there is no evidence of detrital zircons with ages similar to or younger than the 2710 Ma volcanic rock in the area, consistent with field observations that the felsic volcanic package stratigraphically overlies quartzites.

Foliated quartz-feldspar porphyry - ZB96-128AZ

A 30 m wide, quartz-feldspar porphyry dyke intrudes quartzite (location 3, Fig. 2), approximately 1 km southwest of the quartzite sample location. The dyke trends about 020° and is oblique to the northeasterly trending, S_1 schistosity in the quartzite. Weak deflection of the schistosity suggests some sinistral movement along the dyke contacts. Apophyses of the dyke, up to several metres in width, are concordant to the S_1 schistosity in the quartzite. A schistosity defined by micaceous partings and lamellae in the apophyses is parallel to S_1 in the host quartzite. Crenulations of the schistosity in the porphyry have subhorizontal axes, typical of F_2 meso- and microfolds in the area. These relationships suggest that the porphyry dyke contains at least late D_1 fabric elements and, hence, its emplacement occurred before, or during D_1 deformation.

Zircons recovered from a sample of the porphyry are dominantly of two morphological types: pale brown, euhedral, equant to short prisms; and colourless, anhedral, platy fragments. The latter were interpreted as overgrowth fragments. Four analyses of colourless zircon plates (fractions 17, 22-24) yielded imprecise results owing to the combination of low U contents, small sample weights, and high relative proportions of blank Pb (Table 1). Fraction 22 gave a concordant age of 2617 ± 6 Ma and fraction 24 a concordant age of 2602 ± 11 Ma (Fig. 5a). The other two analyses (fractions 17 and 23) are discordant with $^{207}Pb/^{206}Pb$ ages of 2602 to 2625 Ma. Four analyses of strongly abraded, euhedral, equant grains yielded variably discordant results with $^{207}Pb/^{206}Pb$ ages of 2617 to 2624 Ma. Seven of the eight fractions (17–23) define a discordia line with an upper intercept age of 2620 +3/-2 Ma (MSWD = 2.0; Fig. 5a). This is interpreted as the crystallization age of the porphyry.

The 2620 +3/-2 Ma age of the foliated porphyry dyke is within error of a 2621 ± 2 Ma age for a massive granite on the southern shore of Pipedream Lake (Ashton, 1988). The age of the deformed porphyry suggests that significant D_1 deformation occurred after 2620 +3/-2 Ma, and the absence of a foliation in similar-aged intrusions elsewhere in the area (Fig. 2) supports the contention of Ashton (1988) that strain partitioning was a major factor in determining the local strain state of granites.

Foliated granite - ZB96-204AZ

To help resolve the question of the age and significance of deformed granites, we sampled a foliated augen granite that intrudes the eastern margin of the Woodburn Lake group (location 4, Fig. 2). Locally, the granite grades over about 5 m to quartz-feldspar porphyry adjacent to the contact. At the sample location, the granite contact is locally oblique to the schistosity (interpreted as S_1) in the intermediate volcanic host, while small granitic apophyses are concordant to the fabric in the host rock. The foliation in the granite is parallel to that in the host rock. The granite contains some small (<0.5 m) inclusions of intermediate volcanic rock, with foliation parallel to that in the granite. Crenulations and mesoscale folds characteristic of D_2 structures were not observed and, hence, the relative timing of foliation development is uncertain.

Zircons recovered from the sample consist dominantly of clear, colourless to pale pink, euhedral, short prisms with length to breadth ratios of 2:1 to 3:1. Equant multifaceted types are less common. Some equant grains have rounded terminations. Analyses of eight multigrain fractions of the short

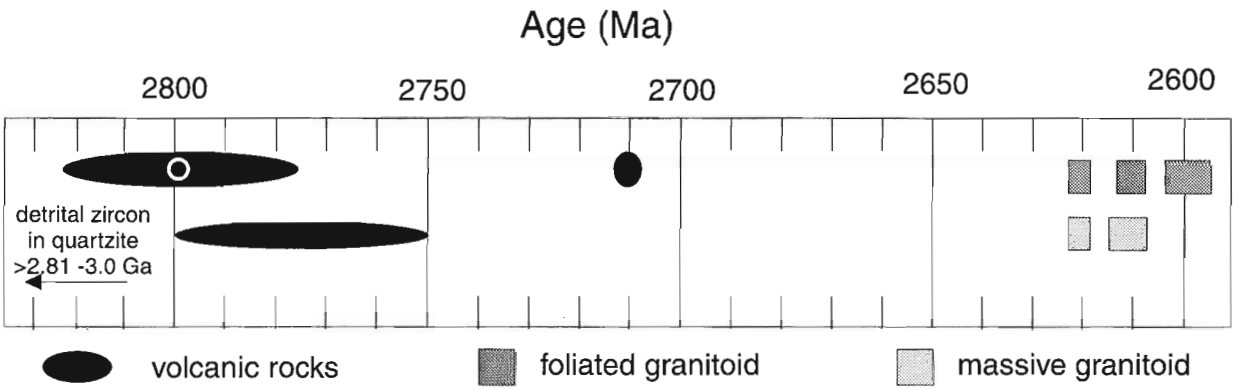

Figure 6. *Summary of U-Pb geochronology for the Woodburn Lake group. Data sources referenced in text.*

prisms or equant grains (fractions 26–33) yielded variably discordant results (Fig. 5b). The eight analyses define a discordia line with an upper intercept age of 2610 +3/-2 Ma (MSWD = 0.73; Fig. 5b). A single analysis of the equant, slightly rounded grains (fractions 25) yielded an older, discordant age of 2656 Ma, indicating inherited zircon in the sample.

In addition to zircon, the sample contained anhedral to subhedral fragments of titanite that range in colour from dark brown to almost colourless. The grains all contain fractures. A collection of medium to dark brown titanite (fraction 34) yielded a discordant age of 2599 Ma that plots on the discordia line defined by the zircon. A second fraction of colourless to paler brown titanite (fraction 35) is more discordant and plots to the left of the zircon discordia, indicating an disturbance of the U-Pb system in the second fraction older than that defined by the discordant zircons (Fig. 5b). A line defined by the crystallization age of 2610 Ma and the discordant titanite (fraction 35) intersects concordia at ca. 1.7 Ga.

The 2610 +3/-2 Ma age of the foliated granite is within error of the 2612 ± 4 Ma composite age of two massive granites dated by Roddick et al. (1992) near Third Portage Lake. The massive nature of the Third Portage Lake granites led Roddick et al. (1992) to suggest that the major deformation in the Woodburn Lake group predated ca. 2.61 Ga. In contrast, Ashton (1988) documented older, massive granites (2621 ± 2 Ma), and younger foliated granites (2599 ± 5 Ma), and argued that the deformation state of the granites was a function of strain partitioning, permitting significant deformation after 2.6 Ga. The 2610 +3/-2 Ma age for a foliated granite reported here further implies that at least some deformation, possibly including D_1 deformation, was synchronous with, or postdated the emplacement of ca. 2.60–2.61 Ga granitoids. The lower age bracket for D_1 deformation is open, and it is possible that it could be as young as the Paleoproterozoic deformation of the Amer group (Patterson, 1986). In the Deep Rose Lake area, 130 km to the west-northwest, the Amer group unconformably overlies ca. 2610 Ma massive to weakly foliated basement granite in which the foliation is thought to predate the unconformity (Tella, pers. comm. 1997; Tella et al., 1984; LeCheminant and Roddick, 1991). This suggests a syn- or post-2.61 Ga, but pre-Amer deformation, at least in the Deep Rose Lake area. The extent and significance of the Paleoproterozoic deformation of Archean rocks remains a major question throughout this region of the Churchill Province.

CONCLUSIONS

1. The age of 2710 +3.5/-2.1 Ma for a felsic volcanic rock in the Woodburn Lake group is significantly younger than previous estimates of greater than 2.75 to less than 2.80 Ga (Fig. 6; Roddick et al., 1992; Tella et al., 1985). This suggests that the Woodburn Lake group comprises two volcanic sequences separated in time by up to 90 million years.

2. Orthoquartzite contains detrital zircons which are well faceted and show minimal abrasion, features consistent with a chemically mature, but texturally immature sediment deposited in a low-energy environment. Detrital zircon ages are discordant and range from 2.81 to 3.0 Ga with the majority of the grains having ages of ca. 2.96 Ga. The maximum depositional age is poorly constrained between 2.81 and 2.89 Ga, depending on the systematics of Pb loss for the youngest, discordant grain.

3. Supracrustal rocks of the Woodburn Lake group were intruded by a quartz-feldspar porphyry at 2620 +3/-2 Ma and granite at 2610 +3/-2 Ma. The quartz-feldspar porphyry has an S_1 foliation, whereas the relative timing of foliation in the granite is uncertain. This suggests that D_1 deformation occurred, at least in part, during or after dyke emplacement at 2620 +3/-2 Ma, and that some deformation of the belt occurred after 2610 Ma. This is consistent with earlier results of Ashton (1988) who suggested a deformation occurring after 2599 ± 5 Ma. Granites of similar age show different development of tectonic fabrics as a consequence of strain partitioning. The identification of clear crosscutting relationships with respect to tectonic fabrics is critical to the use of granites in precisely bracketing the age of deformational events in the Woodburn Lake group.

ACKNOWLEDGMENTS

Dianne Bellerive, Jack Macrae, and Klaus Santowski are thanked for technical assistance in chemistry and mass spectrometry. A.N. LeCheminant and S. Tella are thanked for critical reviews of the manuscript, and Reg Thériault for editorial comments.

REFERENCES

Annesley, I.R.
1989: Petrochemistry of the Woodburn Lake Group komatiite suite, Amer Lake, N.W.T., Canada; Ph.D. Thesis, University of Ottawa, Ottawa, Ontario, 406 p.

Ashton, K.E.
1988: Precambrian geology of the southeastern Amer Lake area (66 H/1), near Baker Lake, N.W.T.; Ph.D. Thesis, Queen's University, Kingston, Ontario, 335 p.

Bethune, K.M. and Scammell, R.J.
1997: Koch Island area, District of Franklin, Northwest Territories, (part of NTS 37 C); Geological Survey of Canada, Open File 3391, scale 1:50 000.

Chandler, F.W.
1988: Quartz arenites: review and interpretation; Sedimentary Geology, v. 58, p. 105-126.

Davis, W.J., McNicoll, V., Bellerive, D., Santowski, K., and Scott, D.J.
1997: Modified chemical procedures for the extraction and purification of uranium from titanite, allanite, and rutile in the Geochronology Laboratory, Geological Survey of Canada; *in* Radiogenic Age and Isotopic Studies: Report 10; Geological Survey of Canada, Current Research 1997-F, p. 33-36.

Fraser, J.A.
1988: Geology of the Woodburn Lake map area, District of Keewatin; Geological Survey of Canada, Paper 87-11, 12 p.

Frisch, T.
1982: Precambrian geology of the Prince Albert hills, western Melville Peninsula, Northwest Territories; Geological Survey of Canada, Bulletin 346, 70 p.

Henderson, J.R. and Henderson, M.N.
1994: Geology of the Whitehills–Tehek Lakes area, District of Keewatin, Northwest Territories (parts of 56 D, 56 E, 66 A, and 66 H); Geological Survey of Canada, Open File 2923, scale 1:100 000.

Henderson, J.R., Henderson, M.N., Pryer, L.L., and Cresswell, R.G.
1991: Geology of the Whitehills–Tehek Lakes area, District of Keewatin: an Archean supracrustal belt with iron-formation-hosted gold mineralization in the central Churchill Province; *in* Current Research, Geological Survey of Canada, Paper 91-1C, p. 149-156.

Hoffman, P.F.
1988: United plates of America, the birth of a craton: Early Proterozoic assembly and growth of Laurentia; Annual Reviews of Earth and Planetary Sciences, v. 16, p. 543-603.

Jackson, G.D. and Taylor, F.D.
1972: Correlation of major Aphebian rock units in the northeastern Canadian Shield; Canadian Journal of Earth Sciences, v. 9, p. 1650-1669.

Jackson, G.D., Hunt, P.A., Loveridge, W.D., and Parrish, R.R.
1990: Reconnaissance geology of Baffin Island, N.W.T.; *in* Radiogenic Age and Isotopic Studies: Report 3, Geological Survey of Canada, Paper 89-2, p. 123-148.

Kerswill, J.A., Goff, S.P., Wilkinson, L., Jenner, G.A., Kjarsgaard, B.A., Bretzlaff, R., and Samaris, C.
1998: An update on the metallogeny of the Woodburn Lake group, western Churchill Province, Northwest Territories; *in* Current Research 1998-C, Geological Survey of Canada, p. 29-42

Kjarsgaard, B.A., Kerswill, J.A., and Jenner, G.A.
1997: Lithostratigraphy and metallogenic implications of komatiite - banded iron-formation - felsic volcanic rocks of the Archean Woodburn Lake group, Pipedream lake, central Churchill Province, Northwest Territories; *in* Current Research 1997-C, Geological Survey of Canada, p. 101-110.

Krogh, T.E.
1982: Improved accuracy of U-Pb zircon ages by the creation of more concordant systems using an air abrasion technique; Geochimica et Cosmochimica Acta, v. 46, p. 637-649.

LeCheminant, A.N. and Roddick, J.C.
1991: U-Pb zircon evidence for widespread 2.6 Ga felsic magmatism in the central District of Keewatin, N.W.T.; *in* Radiogenic Age and Isotopic Studies: Report 4, Geological Survey of Canada, Paper 90-2, p. 91-99.

Parrish, R.R., Roddick, J.C., Loveridge, W.D., and Sullivan, R.W.
1987: Uranium-lead analytical techniques at the geochronology laboratory, Geological Survey of Canada; *in* Radiogenic Age and Isotopic Studies: Report 1, Geological Survey of Canada, Paper 87-2, p. 3-7.

Patterson, J.G.
1986: The Amer belt: remnant of an Aphebian foreland fold and thrust belt; Canadian Journal of Earth Sciences, v. 23, p. 2012-2023.

Roddick, J.C.
1987: Generalized numerical error analysis with applications to geochronology and thermodynamics; Geochimica et Cosmochimica Acta, v. 51, p. 2129-2135.

Roddick, J.C., Henderson, J.R., and Chapman, H.J.
1992: U-Pb ages from the Archean Whitehills–Tehek lakes supracrustal belt, Churchill Province, District of Keewatin, Northwest Territories; *in* Radiogenic Age and Isotopic Studies: Report 6, Geological Survey of Canada, Paper 92-2, p. 31-40.

Schau, M.
1982: Geology of the Prince Albert group in parts of Walker Lake and Laughland Lake map areas, District of Keewatin; Geological Survey of Canada, Bulletin 337, 62 p.

Taylor, F.C.
1985: Precambrian geology of the Half Way Hills area, District of Keewatin; Geological Survey of Canada, Memoir 415, 19 p.

Tella, S.
1994: Geology, Amer Lake (66 H), Deep Rose Lake (66 G), and parts of Pelly Lake (66 F), District of Keewatin, Northwest Territories, Geological Survey of Canada, Open File 2969, scale 1:250 000.

Tella, S., Heywood, W.W., and Loveridge, W.D.
1985: A U-Pb age on zircon from a dacite porphyry, Amer Lake map area, District of Keewatin, NWT; *in* Current Research, Part B, Geological Survey of Canada, Paper 85-1B, p. 371-374.

Tella, S., Thompson, D.L., and James, D.T.
1984: Geology of parts of the Deep Rose Lake and Pelly Lake map areas, District of Keewatin; *in* Current Research, Part A, Geological Survey of Canada, Paper 84-1A, p. 313-322.

Zaleski, E., Corrigan, D., Kjarsgaard, B.A., Jenner, G.A., Kerswill, J.A., and Henderson, J.R.
1997a: Preliminary results of mapping and structural interpretation from the Woodburn project, western Churchill Province, Northwest Territories; in Current Research 1997-C, Geological Survey of Canada, p. 91-100.

Zaleski, E., Corrigan, D., Kjarsgaard, B.A., Kerswill, J.A., Jenner, G.A., and Henderson, J.R.
1997b: Geology, Woodburn Lake group, Meadowbank River to Tehek Lake (66 H/1, 56 E/4), District of Keewatin (Nunavut), Northwest Territories; Geological Survey of Canada, Open File 3461, scale 1:50 000.

– 11 –

U-Pb geochronology of Wijinnedi Lake area, Slave Province, District of Mackenzie, Northwest Territories

M.E. Villeneuve[1] and J.B. Henderson[1]

Villeneuve, M.E. and Henderson, J.B., 1998: U-Pb geochronology of Wijinnedi Lake area, Slave Province, District of Mackenzie, Northwest Territories; in *Radiogenic Age and Isotopic Studies: Report 11; Geological Survey of Canada, Current Research 1998-F, p. 99-106.*

Abstract: U-Pb ages from the Wijinnedi Lake area of the southwestern Slave Province are presented. A volcaniclastic breccia from the Wijinnedi domain gives an age of 2673.3 ± 1.4 Ma. Granitoids from the Ghost domain have ages between 2605 Ma and 2589 Ma. A sample of K-feldspar-megacrystic granite that cores the northeasterly trending antiformal structure gives a zircon age of 2598 ± 2 Ma and a monazite age of 2589 ± 2 Ma, identical to the crystallization age of an orthopyroxene-bearing granite. These data provide a maximum age for post-granulite facies uplift of the Ghost domain. A ca. 2605 Ma age on granodiorite suggests that granulite-facies metamorphism may have lasted at least 15 Ma.

Least deformed trondhjemite from Hinscliffe domain gives a zircon age of 2654 ± 4 Ma and titanite age of approximately 2610 Ma. The difference between the monazite age in the Ghost domain and titanite age in the Hinscliffe domain suggests differential uplift within the region during the latter stages of Slave Province tectonism.

Résumé : Des échantillons prélevés dans la région du lac Wijinnedi, dans le sud-ouest de la Province des Esclaves, ont été datés par la méthode U-Pb. Une brèche volcanoclastique du domaine de Wijinnedi donne un âge de 2 673,3 ± 1,4 Ma. Des roches granitoïdes du domaine de Ghost donnent des âges entre 2 605 Ma et 2 589 Ma. Un échantillon de granite à phénocristaux de feldspath qui forme le coeur de la structure anticlinale de direction nord-est a un âge de 2 598 ± 2 Ma (zircon) et de 2 589 ± 2 Ma (monazite), ce qui est identique à l'âge de la cristallisation d'un granite à orthopyroxène. Ces données révèlent l'âge maximal maximal du soulèvement du domaine de Ghost qui est postérieur au métamorphisme de faciès des granulites. Un âge d'environ 2 605 Ma attribué à un granodiorite semble indiquer que ce métamorphisme a duré au moins 15 Ma.

Un échantillon de trondhjémite peu déformée du domaine de Hinscliffe date de 2 654 ± 4 Ma (zircon) et d'environ 2 610 Ma (titanite). La différence entre l'âge de la monazite du domaine de Ghost et celui de la titanite du domaine de Hinscliffe traduit un soulèvement différentiel de la région au cours des derniers stades du diatrophisme de la Province des Esclaves.

[1] Geological Survey of Canada, 601 Booth Street, Ottawa, Ontario K1A 0E8

INTRODUCTION

The Wijinnedi Lake area is located near the southwestern margin of the Slave Province, 160 km north-northwest of Yellowknife, at the north end of a 100 km long asymmetric Paleoproterozoic uplift cored by granulite-grade mid-crustal rocks (Henderson and Chacko, 1995). On the basis of 1:50 000 scale geological mapping of the map area, the uplift terrane was divided into three structurally bound, lithologically distinct domains that increase in metamorphic grade and degree of deformation from north to south (Fig. 1; Henderson and Schaan, 1993; Henderson, 1994). Geochronological data from each of these three domains is presented in this paper. Rocks from a fourth domain, along the east side of the map area outside the uplift, are not considered in this study.

The Wijinnedi domain is dominated by a Yellowknife Supergroup, intermediate to felsic, volcaniclastic dome that is mantled by more mafic volcanic rocks. They are conformably overlain by a major unit of interlayered mudstones and thin siltstones that lacks the greywacke turbidites that so commonly characterize the Yellowknife Supergroup metasedimentary rocks elsewhere. Metamorphic grade varies from sub-biotite greenschist to a migmatite zone to the east and south.

The Hinscliffe domain is separated from the Wijinnedi domain to the north and the Ghost domain to the south by major mylonite zones. It consists of trondhjemitic to granodioritic rocks and minor pegmatite that are extensively recrystallized. The granitoid rocks contain highly variable proportions of amphibolite inclusions that are crosscut by several generations of granitoid veins. The mafic inclusions are considered to represent synplutonic mafic dykes. Most of the complex is highly deformed with many of the rocks having a gneissic aspect that increases towards the margins.

The Ghost domain underlies the southeastern half of the map area within the uplift and is by far the most lithologically heterogeneous of the domains. The rocks occur about a northeasterly trending antiformal structure that is cored by a massive, very coarse-grained, megacrystic syenogranite. The dominant plutonic phase of the domain is tonalite and its gneissic equivalents. Other volumetrically less abundant intrusions range in composition from diorite and quartz diorite, through granodiorite, to granite, in places intimately mixed on a scale difficult to resolve at the mapping scale of 1:50 000. Supracrustal rocks are also present throughout the domain, but are most abundant remote from the antiformal axis. They are dominated by metasedimentary migmatite to diatexite, although a major migmatitic unit in the northern part of the domain is considered to be derived from an intermediate volcanic protolith. The rocks throughout the domain are at high metamorphic grade, with the eastern and southeastern two-thirds of the domain at granulite grade. Pressure-temperature estimates, from a series of granulite-grade rocks throughout the domain, range between 6 and 7 Kbars and 825 and 900°C (Chacko et al., 1995a, b). Many of the plutonic bodies contain igneous textures, and the intrusions are considered to have been emplaced and crystallized under granulite-grade conditions. Five intrusive units from this domain were analyzed in the course of this study.

The Dauphinee domain occurs along the east side of the map area and is separated from the Ghost domain by an extensive cataclastic shear zone along which much of the Paleoproterozoic uplift of the western three domains took place. This domain is characterized by massive to weakly foliated granitoid rocks, metamorphosed melanocratic granitoids, and migmatitic Yellowknife Supergroup metasedimentary rocks. No rocks from this domain were dated, although the large quartz diorite to diorite body in the northern part of the domain is similar to a quartz diorite in the Ghost domain that was analyzed.

METHODS

Following the separation of heavy minerals using heavy liquids, samples were passed through a Frantz LB-1™ magnetic separator to purify zircon with the least magnetic susceptibility. Crystals were then hand picked for analysis based on criteria that optimized for their clarity, lack of cloudiness, and lack of fracture. All zircons were abraded prior to analysis to increase concordance by removing the outer portions of the grains where much of the Pb loss and alteration take place (Krogh, 1982). Following abrasion, photography, and final mineral selection, mineral fractions were analyzed according to methods summarized in Parrish et al. (1987). Data have been reduced and errors have been propagated using software written by J.C. Roddick; error propagation was done by numerical methods (Roddick, 1987, Parrish et al., 1987). Error ellipses on concordia diagrams are shown at the 2-sigma (95% confidence) level of uncertainty. Final errors are indicated on Table 1. Linear regressions on discordant arrays of data use a modified York (1969) method that takes into account the scatter of the points about the line (*see* discussion in Parrish et al., 1987). Fraction letters shown on concordia diagrams are keyed to the fraction letters in Table 1.

U/Pb RESULTS

Sample 1: Yellowknife Supergroup metadacite, Wijinnedi domain

The intermediate to felsic volcanic dome that dominates the Wijinnedi domain consists mainly of thick units of deformed volcaniclastic breccia with finer grained units that are less abundant. The sample from the northern margin of the dome is a grey to greenish grey, fine-grained, volcaniclastic metadacite, and is both feldspar- and quartz-phyric (Fig. 1). A small yield of less than 20 zircons from this sample consisted of a population of large, clear, pink, euhedral grains with smooth surfaces and a population of small, equant, colourless zircons with a slight frosting on the crystal faces. One fraction of a single clear zircon and two multigrain frosted zircon fractions give nearly identical concordant results and overlap at an average $^{207}Pb/^{206}Pb$ age of 2673.3 ± 1.4 Ma (Fig. 2a). A fraction (B), consisting of one small frosted zircon, resulted in an analysis with a $^{207}Pb/^{206}Pb$ age of 2791 Ma and a large error of ± 35 Ma, indicating that this volcaniclastic sample may contain xenocrysts of older inherited material.

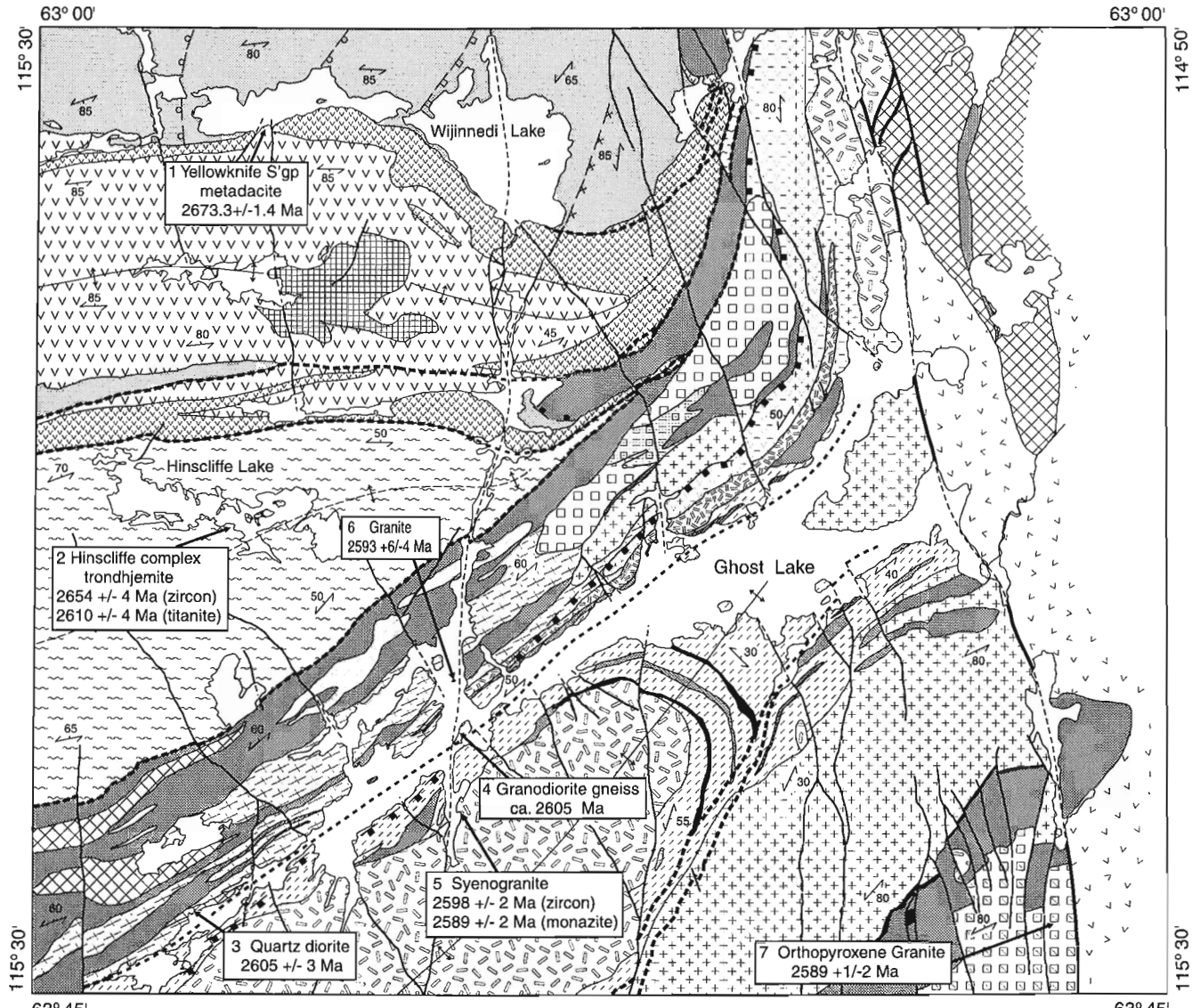

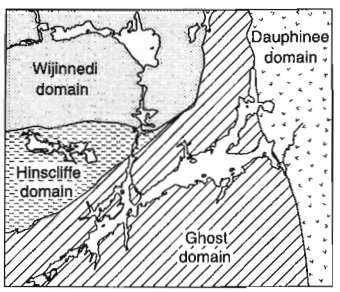

1 0 1 2 3 4 5 km

Granite, granodiorite; orthopyroxene bearing (2589 Ma)
Granite, granodiorite (2593 Ma)
Syenogranite; megacrystic (2598 Ma)
Tonalite to megacrystic granite
Granodiorite
Tonalite
Granodiorite to tonalite gneiss (ca. 2605 Ma)
Quartz diorite, diorite (2605 Ma)
Granitoid rocks of the Ghost domain, undivided
Granitoid rocks of the Dauphinee domain, undivided
Granitoid rocks and metasedimentary migmatite
Amphibolite
Metagabbro

HINSCLIFFE COMPLEX
Trondhjemite, granodiorite; gneissic to massive (2654 Ma)

Paleoproterozoic faults; defined, assumed
Archean shear zones; defined, assumed
Anticline / antiform; defined, assumed
Foliation, generalized
Orthopyroxene zone boundary

YELLOWKNIFE SUPERGROUP
Mudstone, minor siltstone, greywacke and metamorphosed equivalents:
chlorite zone
biotite zone
cordierite zone
sillimanite zone
migmatite and diatexite zone
Paragneiss, migmatitic; ortho and clino pyroxene, biotite and hornblende bearing
Intermediate to felsic volcanic rocks, metamorphosed (2673 Ma)
Mafic to intermediate volcanic rocks, metamorphosed

Figure 1. *Geological map of the Wijinnedi Lake area showing location of samples analyzed.*

Sample 2: trondhjemite, Hinscliffe domain

A sample trondhjemite was collected from the south shore of Hinscliffe Lake (Fig. 1) from a least deformed window in this otherwise highly deformed igneous complex. This sample represents the best preserved, central part of the complex and is the oldest of three granitoid phases present at the locality (Fig. 1) based on crosscutting relationships. Zircons from the sample are elongate to subspherical with poorly developed crystal faces and blunted terminations. They are extremely clear, crack-free, with a slight pinkish tint. Some have a few small, spherical blebs within the crystal. Three single-grain, low-uranium fractions plot on concordia with a weighted average $^{207}Pb/^{206}Pb$ age of 2654 ± 4 Ma (Fig. 2b). This age is interpreted as the crystallization age of trondhjemite.

A single fraction of large, light brown, anhedral titanite was analyzed and gave a 0.5% discordant $^{207}Pb/^{206}Pb$ age of 2610 ± 4 Ma (Fig. 2b). This age is interpreted to be an estimate of resetting of the U-Pb system due to cooling below ca 600°C, the approximate closure temperature of titanite (Heaman and Parrish, 1991).

Sample 3: quartz diorite, Ghost Domain

Two large bodies and several smaller sills to lenses of weakly to moderately foliated, medium-grained, hornblende- and biotite-bearing quartz diorite to diorite occur north of Ghost Lake, near the western boundary of the area. A large, lithologically identical intrusion also occurs northeast of Ghost Lake in the Dauphinee domain. The sample comes from one of the smaller lenses in the Ghost domain (Fig. 1). A heterogeneous population of large (+105 μm diameter) rounded, subspherical, pink, clear zircons was recovered and analyzed as single grains. Three analyses (B, E, F) agree within error and overlap concordia at 2605 ± 3 Ma (weighted average of $^{207}Pb/^{206}Pb$ age; Fig. 2c). Fraction F has a large error due to the low U content and small sample size, leading to a high common Pb:radiogenic Pb ratio. A single analysis (A) plots near concordia at 2691 ± 1 Ma, illustrating that xenocrysts coeval with Yellowknife Supergroup volcanic rocks are present. These may have been derived by incorporation of partial melts or xenoliths, in the magma source region.

Sample 4: granodiorite gneiss, Ghost domain

The most abundant phase in the domain is tonalite with associated tonalite-granodiorite gneisses. Sample 4 was taken from a granodioritic phase of this unit (Fig. 1) and consists of grey, well layered and foliated, fine-grained granodiorite. Minor, thin, amphibolitic layers and pinkish, more leucocratic, coarser grained granitoid layers are also prevalent, but were avoided during sampling. Zircons from this sample fall into two populations: 1) rounded, pink, smooth-surfaced

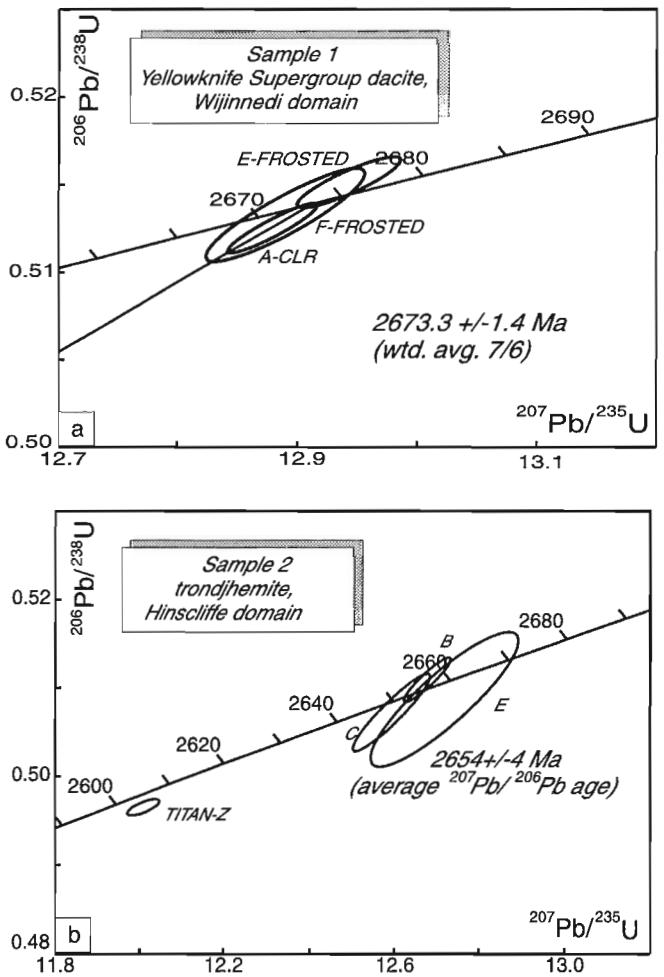

Figure 2.

Concordia diagrams for samples analyzed. Error ellipses are shown at 2σ.

grains with relict crystal faces and severely blunted terminations, and 2) a small group of elongate to stubby, clear, colourless prismatic fragments with no rounding of terminations. Visible cores are evident in grains of both populations and were avoided during hand picking of the grains to be analyzed. Fractions B, E, and F belong to the first population group. The scatter in the data from these fractions points to the presence of cryptic inherited cores within the zircons and, unfortunately, prevents an unambiguous determination of the crystallization age (Fig. 2d). However, the near concordance of fraction B, coupled with a similar $^{207}Pb/^{206}Pb$ age for the more discordant fraction E, suggests that an age of ca. 2605 Ma is a reasonable estimate for the maximum age of at least one of the gneissic components. Fraction D is a single-grain analysis of a large, elongate, clear zircon belonging to the second population and yields an analysis that plots slightly above concordia, with a $^{207}Pb/^{206}Pb$ age of 2640 ± 1 Ma. This result can be interpreted as the age of a xenocrystic component, or alternatively, it may be one age of the various components making up the gneissic layers.

Sample 5: megacrystic syenogranite, Ghost domain

One of the major units in the southern Ghost domain is the large undeformed K-feldspar-megacrystic syenogranite intrusion that forms the core of the northeast-plunging antiform. The sample is dark pink to red, massive, homogeneous, and contains abundant biotite between the very coarse microcline megacrysts. Although the surrounding rocks are at granulite grade, the sample, and indeed most specimens examined, does not contain orthopyroxene, although it is present in rare cases (T. Chacko, pers. comm., 1994). Chacko et al. (1995b) suggested the syenogranite was emplaced under granulite-grade conditions, but underwent autoregression due to the progressive increase in the water content of the magma as it crystallized.

Zircons range from extremely elongate (length:width >4:1) to stubby, equant grains. All grains show a rounding of the terminations and edges that is common in other units throughout the area. Four single-grain analyses range from 0.2% to 1.8% discordant and have similar $^{207}Pb/^{206}Pb$ ages, although fraction A may contain a minor component of inherited Pb (Fig. 2e). A regression through all four fractions results in an upper intercept age of 2598 ± 2 Ma (lower intercept = 127 ± 400 Ma, MSWD = 4).

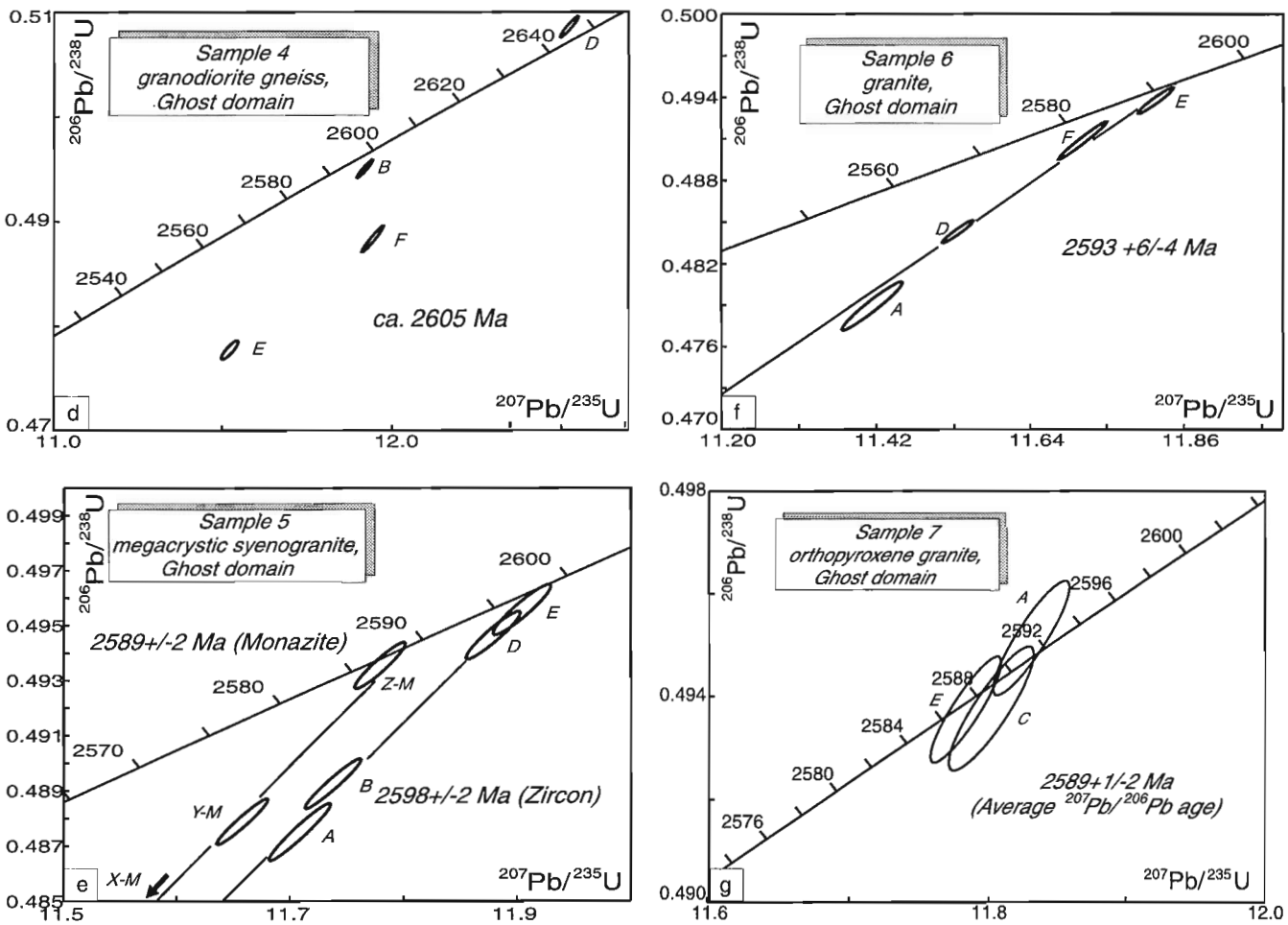

***Figure 2** (cont.).*

In addition to zircon, the sample contains abundant, large euhedral to subhedral crystals of monazite. Analysis of three single-grain fractions resulted in one extremely discordant fraction (X), one concordant fraction (Z), and one slightly discordant fraction (Y). Regression of all three fractions gives an age of 2589 ± 2 Ma (lower intercept = 40 ± 3 6 Ma; MSWD = 9), with the good precision being defined by the fractions nearest to concordia.

Sample 6: undeformed granite, Ghost domain

A large body of generally massive granite to granodiorite with minor pegmatite occurs on the northwest limb of the domain antiform, north of the main part of Ghost Lake. Numerous, 10 m scale or less dykes, sills, and irregular intrusions of similar granite and pegmatite occur elsewhere in the domain, particularly along the north shore of Ghost Lake where their massive aspect contrasts with the much more strongly foliated rocks in which they are emplaced. The sample, a pink, evenly fine-grained, homogeneous, biotite granite was taken from one of these smaller bodies.

Zircons constitute a surprisingly heterogeneous population displaying a range of morphologies from highly elongate to large, equant, clear grains with fractures, to brown grains with sharp to rounded terminations. Many of the grains show a system of radiating fractures emanating from rounded cores, indicative of high-uranium inherited components. All analyses were carried out on single grains in order to highlight any effects of cryptic inherited material. Four fractions form a poorly defined discordia (MSWD = 15) away from a near-concordant fraction E (Fig. 2f) that has an upper intercept age of 2593 +6/-4 Ma (lower intercept = 741 ± 410 Ma).

Table 1. U-Pb data and sample locations.

Fraction[a]	Wt.[b] µg	U ppm	Pb[c] ppm	$^{206}Pb/^{204}Pb$[d]	Pb[e] pg	$^{208}Pb/^{206}Pb$[f]	Radiogenic ratios (± 1σ, %)[f] $^{207}Pb/^{235}U$	$^{206}Pb/^{238}U$	$^{207}Pb/^{206}Pb$	$^{207}Pb/^{206}Pb$ Age (Ma)[g]	Discord.[h] %
1. Yellowknife Supergroup metadacite, Wijinnedi domain (Z2915; 63.9750°N 115.3667°E)											
A-CLR (Z)	8	121	71	512	42	0.149	12.890 ± 0.26	0.5133 ± 0.26	0.18214 ± 0.12	2673 ± 4	0.09
B-CLR (Z)	2	106	68	203	27	0.196	14.461 ± 1.46	0.5358 ± 0.77	0.19576 ± 1.09	2791 ± 35	1.13
E-FROST (Z)	6	113	69	847	25	0.197	12.943 ± 0.17	0.5151 ± 0.14	0.18222 ± 0.08	2673 ± 3	-0.24
F-FROST (Z)	7	121	72	2469	11	0.172	12.879 ± 0.14	0.5125 ± 0.14	0.18226 ± 0.06	2674 ± 2	0.28
2. Trondjhemite, Hinscliffe domain (Z2914; 63.8981°N 115.4953°E)											
B (Z)	16	51	29	928	1	0.123	12.677 ± 0.22	0.5109 ± 0.25	0.17997 ± 0.09	2653 ± 3	-0.36
C (Z)	6	131	72	471	23	0.083	12.592 ± 0.36	0.5072 ± 0.43	0.18007 ± 0.16	2654 ± 5	0.41
E (Z)	5	55	30	249	33	0.077	12.717 ± 0.69	0.5087 ± 0.75	0.18131 ± 0.36	2665 ± 12	0.63
Z (T)	1288	30	18	700	1743	0.207	12.009 ± 0.16	0.4965 ± 0.09	0.17542 ± 0.11	2610 ± 4	0.53
3. Quartz diorite, Ghost domain (Z2991; 63.7717°N 115.4060°E)											
A (Z)	5	221	143	5331	7	0.269	13.119 ± 0.11	0.5165 ± 0.10	0.18421 ± 0.03	2691 ± 1	0.31
B (Z)	15	103	62	4283	11	0.229	11.989 ± 0.11	0.4969 ± 0.10	0.17498 ± 0.03	2606 ± 1	0.25
E (Z)	6	137	79	945	26	0.169	12.006 ± 0.15	0.4982 ± 0.12	0.17478 ± 0.07	2604 ± 2	-0.10
F (Z)	5	50	28	285	12	0.156	11.899 ± 0.64	0.4966 ± 0.52	0.17377 ± 0.40	2594 ± 13	-0.24
4. Granodiorite gneiss, Ghost domain (Z2993; 63.8164°N 115.2512°E)											
B (Z)	4	808	413	10507	10	0.027	11.919 ± 0.10	0.4951 ± 0.09	0.17462 ± 0.03	2602 ± 1	0.46
D (Z)	4	177	108	5175	2	0.219	12.524 ± 0.11	0.5086 ± 0.10	0.17859 ± 0.03	2640 ± 1	-0.49
E (Z)	10	162	83	8129	6	0.077	11.522 ± 0.11	0.4777 ± 0.09	0.17492 ± 0.05	2605 ± 2	4.08
F (Z)	8	196	102	6066	8	0.058	11.943 ± 0.14	0.4884 ± 0.13	0.17736 ± 0.03	2628 ± 1	2.98
5. Megacrystic yenogranite, Ghost domain (Z3220; 63.7971°N 115.2506°E)											
A (Z)	10	140	79	8574	4	0.179	11.709 ± 0.12	0.4875 ± 0.11	0.17419 ± 0.03	2598 ± 1	1.80
B (Z)	7	278	147	8384	7	0.084	11.738 ± 0.10	0.4893 ± 0.09	0.17400 ± 0.03	2597 ± 1	1.36
D (Z)	5	231	127	4718	7	0.120	11.879 ± 0.10	0.4946 ± 0.09	0.17418 ± 0.04	2598 ± 1	0.35
E (Z)	4	200	108	2382	11	0.098	11.904 ± 0.11	0.4956 ± 0.09	0.17422 ± 0.04	2599 ± 1	0.18
X (M)	18	1792	14525	33717	24	22.497	9.411 ± 0.11	0.3950 ± 0.10	0.17281 ± 0.03	2585 ± 1	19.94
Y (M)	5	1165	9442	19864	8	17.992	11.658 ± 0.10	0.4879 ± 0.09	0.17330 ± 0.03	2590 ± 1	1.32
Z (M)	4	659	5044	9225	9	16.718	11.779 ± 0.10	0.4935 ± 0.09	0.17309 ± 0.03	2588 ± 1	0.08
6. Undeformed granite, Ghost domain (Z2992; 63.7555°N 115.2585°E)											
A (Z)	3	226	118	2223	9	0.098	11.414 ± 0.19	0.4789 ± 0.18	0.17285 ± 0.05	2585 ± 2	2.93
D (Z)	8	744	412	9611	19	0.156	11.535 ± 0.10	0.4843 ± 0.08	0.17275 ± 0.03	2584 ± 1	1.80
E (Z)	5	370	197	8054	7	0.083	11.822 ± 0.11	0.4939 ± 0.10	0.17361 ± 0.03	2593 ± 1	0.26
F (Z)	2	424	222	6683	4	0.066	11.715 ± 0.15	0.4909 ± 0.14	0.17310 ± 0.03	2588 ± 1	0.63
7. Orthopyroxene granite, Ghost domain (Z3371; 63.7664°N 114.9041°E)											
A (Z)	3	153	84	2579	5	0.118	11.832 ± 0.12	0.4951 ± 0.11	0.17331 ± 0.05	2590 ± 2	-0.14
C (Z)	5	109	59	1373	11	0.105	11.802 ± 0.13	0.4938 ± 0.12	0.17336 ± 0.06	2590 ± 2	0.16
E (Z)	6	129	70	6120	1	0.096	11.784 ± 0.11	0.4937 ± 0.10	0.17310 ± 0.05	2588 ± 2	0.04

[a]All zircon fractions are abraded; (Z)=Zircon, (M)=Monazite, (T)=Titanite, [b]Error on weight =±0.001 mg, [c]Radiogenic Pb, [d]Measured ratio corrected for spike and Pb fractionation of 0.09 ± 0.03%/AMU, [e]Total common Pb on analysis corrected for fractionation and spike, of blank model Pb composition, [f]Corrected for blank and spike Pb and U and common Pb (Stacey-Kramers model Pb equal to the $^{207}Pb/^{206}Pb$ age), [g]Age error is ±2SE in Ma, [h]Discordance along a discordia to origin.

Although the scatter about the line indicates effects of inheritance, the near concordance of fractions E and F, coupled with the less than10 Ma differential in $^{207}Pb/^{206}Pb$ ages for all fractions suggests that the upper intercept age is a reasonable estimate for the age of intrusion.

Sample 7: orthopyroxene granite, Ghost domain

In the southeast corner of the map area is the third major granite body of the domain, a yellow to greenish-brown, massive to weakly foliated, medium- to coarse-grained, equigranular to locally weakly megacrystic granite that contains clinopyroxene, orthopyroxene, and biotite.

The sample analyzed contains stubby, euhedral, clear, colourless zircons that yield ages overlapping concordia (Fig. 2g). The average $^{207}Pb/^{206}Pb$ age of the zircons is 2589 +2/-1 Ma, which is regarded as the age of crystallization of the granite and also a point in time when the host rocks were at granulite-grade conditions.

DISCUSSION

The Wijinnedi Lake area is located far to the west of the line (defined by Nd and Pb isotope data: Davis and Hegner, 1992; Thorpe et al., 1992; Davis et al., 1996) that separates crust with evidence of protracted history to the west from more juvenile crust to the east. None of the granitic or gneissic samples dated from the Wijinnedi Lake area contain inherited zircon older than 2.69 Ga, perhaps indicative of a lack of involvement of significantly older crust in the generation of these melts. This apparent lack of a major ancient component is supported by the Nd and Pb data of Yamashita (pers. comm., 1996) on the same samples. The relatively juvenile $\varepsilon_{Nd(2600)}$ values range between of 0 and +1.4 and the Pb isotopic values are among the most juvenile in the Slave Province, having smaller radiogenic ratios than material from the Yellowknife area, in accord with the regional differences outlined in Davis et al. (1996).

The oldest unit dated in the Wijinnedi Lake area is represented by the 2673.3 ± 1.4 Ma dacite from the intermediate to felsic volcanic dome in the Wijinnedi domain. This age is close to the young end of the Yellowknife Supergroup volcanic age spectrum for the Slave Province as a whole (Villeneuve and van Breemen, 1994). It is similar to the 2667 ± 4 Ma age of the Banting Formation at Yellowknife (Isachsen et al., 1991) but somewhat older than the 2658–2660 Ma ages of the felsic volcanic centres at Russell Lake to the south of the area, and Clan Lake to the north of Yellowknife (Mortensen et al, 1992).

The oldest granitoid unit is represented by the 2654 ± 4 Ma trondhjemite at Hinscliffe Lake. Whereas the age is somewhat younger than that from the intermediate-felsic volcanic dome to the north, its close physical and temporal proximity to the volcanic centre suggests the trondhjemitic complex may be a deeper and more prolonged expression of the surface magmatic event. The age of titanite closure, about 2.61 Ga, tentatively places constraints on the timing of metamorphic cooling of this domain.

The five dates on granitoid bodies in the high metamorphic grade Ghost domain range between 2605 Ma and 2589 Ma, which fall towards the young end of plutonic events in the Slave Province. Like similar intrusive bodies elsewhere in the Slave Province, the more mafic compositions are older than their more granitic counterparts. Most of the domain is at granulite grade and, on the basis of textural evidence, most of the intrusive units in the central and southeastern part of the domain were emplaced and crystallized under granulite-grade conditions. This is clearly the case for the orthopyroxene granite at 2589 ± 2 Ma (sample 7), and probably for the 2598 ± 2 Ma syenogranite (sample 5) that contains textural evidence for retrogression from granulite grade (T. Chacko, pers. comm., 1994).

Tonalite and the associated tonalite gneisses represent the dominant intrusive phases of the Ghost domain and appear to have been emplaced at granulite grade. These units can be tentatively correlated, on the basis of field evidence, with the granodiorite gneiss sample dated at about 2605 Ma (sample 4). If such a correlation is correct, this would suggest a minimum estimate of 15 Ma for the length of time that the rocks of the south and east Ghost domain were exposed to granulite-grade conditions. On the basis of both geothermobarometric and textural evidence, Farquhar et al. (1993) have suggested the rocks from the southeastern part of the domain may have undergone relatively quick decompression from granulite conditions. The syenogranite monazite age at 2589 ± 2 (sample 5), if interpreted as either retrogressive metamorphic growth of secondary monazite or the time of U-Pb system closure from primary igneous monazite (approximately 700°C, Heaman and Parrish, 1991), dates the decompression event, which took place synchronously with the intrusion of the orthopyroxene granite (sample 7). Also coeval (within error) with these units, is the 2593 +6/-4 Ma granite-granodiorite-pegmatite unit (sample 6) that occurs within the domain, but outside the present day extent of granulite grade rocks. This granite postdates most of the deformation associated with the Ghost domain. Coupled with the older 2.61 Ga titanite cooling age within the Hinscliffe domain, the undeformed nature of the granite is perhaps suggestive of earlier uplift of that domain and multiple reactivation of the bounding shear zones between the adjacent domains.

ACKNOWLEDGMENTS

The authors would like to thank the technical staff of the Geochronology Laboratory, Jack MacRae, Diane Bellerive, and Klaus Santowski for their efficient and careful analysis of the mineral fractions. Reviews by Otto van Breemen and Reg Thériault were particularly helpful.

REFERENCES

Chacko, T., Creaser, R.A., Farquhar, J., and Muehlenbachs, K.
1995a: The deep crust of the western Slave Province — initial petrologic and isotopic data from the high-grade rocks of the Ghost Domain; Lithoprobe Slave/Northern Cordillera Lithospheric Evolution Workshop, Lithoprobe Report 44, p. 4-7.
1995b: A petrologic study of granulites and associated rocks from the Ghost Lake area, southwestern Slave Province; Geological Association of Canada–Mineralogical Association of Canada Annual Meeting, Program with Abstracts, v. 20, p. A-15.

Davis, W.J. and Hegner, E.
1992: Neodymium isotopic evidence for the tectonic assembly of Late Archean crust in the Slave Province, northwest Canada; Contributions to Mineralogy and Petrology, v. 111, p. 493-504.

Davis, D.W., Gariepy, C., and van Breemen, O.
1996: Pb isotopic recycling of late Archaean granites and the extent of recycling early Archaean crust in the Slave Province, northwest Canada; Chemical Geology, v. 130, p. 255-269.

Farquhar, J., Snavely, J.A., and Chacko, T.
1993: Granulite facies metamorphism near Ghost Lake, Slave Province, NWT; Geological Association of Canada–Mineralogical Association of Canada Joint Annual Meeting, Program and Abstracts, v. 18, p. A-28.

Heaman, L. and Parrish, R.
1991: U-Pb geochronology of accessory minerals; *in* Short Course Handbook on Applications of Radiogenic Isotope Systematics to Problems in Geology, Mineral Association of Canada, v. 19 p. 59-102

Henderson, J.B.
1994: Geology of the Wijinnedi Lake area — a Paleoproterozoic (?) asymmetric uplift of Archean rocks on the southwestern Slave Province, District of Mackenzie; *in* Current Research 1994-C, Geological Survey of Canada, p.71-79.

Henderson, J.B. and Chako, T.
1995: A reconnaissance of the high grade metamorphic terrane south of Ghost Lake, southwestern Slave Province, Northwest Territories; *in* Current Research 1995-C, Geological Survey of Canada, p.77-85.

Henderson, J.B. and Schaan, S.E.
1993: Geology of the Wijinnedi Lake area: a transect into mid crustal levels in the western Slave Province, District of Mackenzie, Northwest Territories; *in* Current Research 1993-C, Geological Survey of Canada, p.83-91.

Isachsen, C.E., Bowring, S.A., and Padgham, W.A.
1991: U-Pb zircon geochronology of the Yellowknife volcanic belt, NWT, Canada: new constraints on the timing and duration of greenstone belt magmatism; Journal of Geology, v. 99, p. 55-67.

Krogh, T.E.
1982: Improved accuracy of U-Pb zircon ages by the creation of more concordant systems using an air abrasion technique; Geochimica et Cosmochimica Acta, v. 46, p. 637-649.

Mortensen, J.K., Henderson, J.B., Jackson, V.A., and Padgham, W.A.
1992: U-Pb geochronology of the Yellowknife Supergroup felsic volcanic rocks in the Russell Lake and Clan Lake areas, southwestern Slave Province; *in* Radiogenic Age and Isotopic Studies: Report 5; Geological Survey of Canada, Paper 92-2, p. 1-7

Parrish, R.R., Roddick, J.C., Loveridge, W.D. and Sullivan, R.W.
1987: Uranium-lead analytical techniques at the Geochronology Laboratory, Geological Survey of Canada; *in* Radiogenic Age and Isotopic Studies: Report 1; Geological Survey of Canada, Paper 87-2, p.3-7.

Roddick, J.C.
1987: Generalized numerical error analysis with application to geochronology and thermodynamics; Geochimica et Cosmochimica Acta, v. 51, p.359-362.

Thorpe, R., Cummings, G.L., and Mortensen, J.K.
1992: A significant Pb isotopic boundary in the Slave Province and its probable relationship to ancient basement in the western Slave Province; *in* Project Summaries, Canada–Northwest Territories Mineral Development Agreement 1987-91, Geological Survey of Canada, Open File Report 2484, p.179-184.

Villeneuve, M.E. and van Breemen, O.
1994: A compilation of U-Pb age data from the Slave Province; Geological Survey of Canada, Open File 2972, 53 p.

York, D.
1969: Least squares fitting of a straight line with correlated errors; Earth and Planetary Science Letters, v. 5, p. 320-324.

– 12 –

Detrital zircon geochronology of sequence 'C' grits, Dorsey Terrane (Thirtymile Range, Southern Yukon): provenance and stratigraphic correlation

G.M. Ross[1] and T.A. Harms[2]

Ross, G.M. and Harms, T.A., 1998: Detrital zircon geochronology of sequence 'C' grits, Dorsey Terrane (Thirtymile Range, Southern Yukon): provenance and stratigraphic correlation; in *Radiogenic Age and Isotopic Studies: Report 11; Geological Survey of Canada, Current Research 1998-F, p. 107-115.*

Abstract: Detrital zircons analyzed from coarse grits within the eastern Dorsey Terrane of the Thirtymile Range, southern Yukon Territory, yield Proterozoic and Archean $^{207}Pb/^{206}Pb$ ages that range from ca. 1777 Ma to 2600 Ma, similar to the range of crystallization ages of basement in the Peace River Arch area of northern Alberta and northeastern British Columbia. This suggests that the source of these grits was crystalline basement of western Canada, thus confirming a North American affinity for these sedimentary rocks and their correlation with the Cassiar Terrane of northern British Columbia. The western Canadian provenance documented in the detrital zircons is consistent with models that suggest approximately 450 km of right-lateral displacement along the Tintina–Northern Rocky Mountain Trench fault, rather than recent suggestions of a western Montana provenance for the Cassiar Terrane that require greater than 2000 km displacement.

Résumé : L'analyse de zircons détritiques provenant de sables grossiers dans la partie est du terrane de Dorsey dans la chaîne de Thirtymile, dans le sud du territoire du Yukon, a donné des âges $^{207}Pb/^{206}Pb$ du Protérozoïque et de l'Archéen s'échelonnant entre environ 1 777 Ma à 2 600 Ma, semblables aux âges de cristallisation du socle de la région de l'arche de Peace River dans le nord de l'Alberta et le nord-est de la Colombie-Britannique. Ces sables tireraient donc leur origine du socle cristallin de l'Ouest du Canada, ce qui confirmerait l'affinité nord-américaine pour ces roches sédimentaires et leur corrélation avec le terrane de Cassiar dans le nord de la Colombie-Britannique. Cette origine révélée par les zircons détritiques est conforme aux modèles selon lesquels un déplacement dextre d'environ 450 km se serait produit le long de la faille de Tintina–sillon des Rocheuses du nord, et infirme les suggestions récentes selon lesquelles l'origine du terrane de Cassiar se situerait dans l'ouest du Montana, ce qui supposerait un déplacement de plus de 2 000 km.

[1] Geological Survey of Canada, 3303 33rd Street, Calgary, Alberta T2L 2A7
[2] Department of Geology, Amherst College, Amherst, Massachusetts 01002

INTRODUCTION

U-Pb geochronology of detrital mineral phases offers an important tool in deciphering the age and provenance of sedimentary strata. Technical improvements that have led to the ability to analyze smaller amounts of Pb, which allows for analysis of younger zircons and smaller sample sizes including individual mineral grains, such as zircon and monazite. Additionally, the understanding of the geological framework for western Canada has undergone considerable evolution over the last decade as a consequence of greater understanding of the geochronology of both authochthonous and allochthonous basement (Villeneuve et al., 1993; Ross, 1991 and related papers, respectively) and the proliferation of detrital mineral geochronology data (Ross and Bowring, 1990; Ross and Parrish, 1991; Smith and Gehrels, 1991; Gehrels et al., 1991; Ross et al., 1992, 1993, 1997; Gehrels et al.,1995; Rainbird et al., 1992, 1997; Ross and Villeneuve, 1997). Collectively, these data sets have characterized both the provenance and potential source areas of much of the Cordilleran margin of the southern Canadian Cordillera (south of 60°) from Mesoproterozoic through Triassic time. Given this framework, detrital mineral geochronology provides an excellent technique for establishing the tectonic affinity of suspect terranes that lie outboard of rocks of demonstrable western Canadian affinity.

This paper reports on new data collected from sedimentary strata in the southern Yukon assigned to the Dorsey Terrane by Wheeler et al., (1991). These rocks are symptomatic of some of the problems geologists face in attempting to decipher the stratigraphic and structural setting of lithologically similar, structurally complex rocks with poor age constraints. Our results, based on detrital zircon geochronology, offer some constraints concerning provenance, stratigraphic correlation, and displacement along the Tintina–Northern Rocky Mountain Trench fault, a major dextral fault in the northern Canadian Cordillera.

GEOLOGICAL SETTING

In a very general way, the Canadian Cordillera consists of two parts: the imbricated and metamorphosed rocks that are the deformed continental-margin wedge of western North America, and to the west, terranes that may represent either displaced fragments of the North American margin or exotic terranes that have been accreted to the margin. The deformation and metamorphism of these outboard terranes makes recognition of their tectonic affinities difficult, particularly if there are poor biostratigraphic constraints, and hence they are referred to as 'suspect' until their affinities can be established (Coney et al., 1980). In the northern Canadian Cordillera, most of the imbricated wedge of demonstrable North American affinity lies inboard (east) of a major strike-slip structure (Tintina–Northern Rocky Mountain Trench; Fig. 1). Structural relationships between inboard North American and outboard suspect terranes are complex in the vicinity of this fault and include the presence of a major nappe of allochthonous accreted rocks (Anvil allochthon) and the strike-slip displacement of a fragment of the margin, the Cassiar Terrane. Throughout much of the area where it is recognized, the Cassiar Terrane consists of sedimentary rocks of Neoproterozoic (ca. 728 Ma; Evenchick et al., 1984) to Paleozoic ages with clear ties and similarities to western Canadian miogeoclinal strata (Wheeler et al., 1991). In the southern Yukon, the northern continuation of the Cassiar Terrane exhibits complex and poorly defined structural relationships with pericratonic and marginal basin rocks (Kootenay, Dorsey, and Slide Mountain terranes). The similarity of some of the lithologies of these different terranes, in combination with poor biostratigraphic control and structural complexities, have made unraveling stratigraphies and assignment of terrane affinities difficult.

In the Thirtymile Range, in the area covered by the Teslin map sheet (105 C), southern Yukon (Fig. 1), rocks on the western flank of Cassiar Terrane and inboard of demonstrably non-North American terranes such as Stikinia, Quesnellia, and Cache Creek are a complexly deformed succession of strata that have been assigned to the Dorsey Terrane (Wheeler et al., 1991). There, the Dorsey Terrane includes rocks of probable affinity with North American units of late Neoproterozoic through Paleozoic age (Gordey, 1992; 1995; Harms, 1992; Fig. 1). These consist of a sequence of marble, overlain by a thick unit of arkosic grit, topped by basalt flows and minor purple shale and green chert, juxtaposed by faults against interbedded chert-pebble conglomerate, black shale, and black chert (informally named 'sequences C and D/E', respectively, by Harms, 1992). No paleontological age constraints have been determined for these strata. It is their close lithologic similarity to distinctive units of the Cassiar Terrane — the grit to clastics of Windermere age (Ingenika Group) and the chert-pebble conglomerate to the Earn Group — that suggests a correlation to North American stratigraphy. In the Thirtymile Range, these sequences are flanked to the west structurally by Carboniferous limestone (Mulligan, 1963) and thick accumulations of mafic flows and volcaniclastic rocks; because of their present separation by faults it is unclear whether they represent part of the same or different tectonostratigraphic assemblages. Proposals that clastic rocks of the Dorsey Terrane in the Thirtymile Range should be correlated with North American lithologic counterparts east of the Tintina–Northern Rocky Mountain Trench fault (Gordey et al., 1991; Gordey and Stevens, 1994; Gordey, 1995; Harms, 1992; Harms et al., 1997) can be tested by sedimentary provenance studies and, in particular, by detrital zircon geochronology.

Sample description

The samples investigated in this study are from coarse arkosic sandstones ('grits') exposed in the Thirtymile Range. The samples were collected from a ridge section (approximately 60°37′30″N/132°24′15″W) within informally named unit C3 of Harms (1992). Unit C3 is dominated by silicified grit with minor quartz-feldspar crystal clast conglomerate horizons. The grits are characterized by massive, lenticular bedding with rare graded beds suggesting deposition by submarine processes, likely a turbidite environment. The grits are

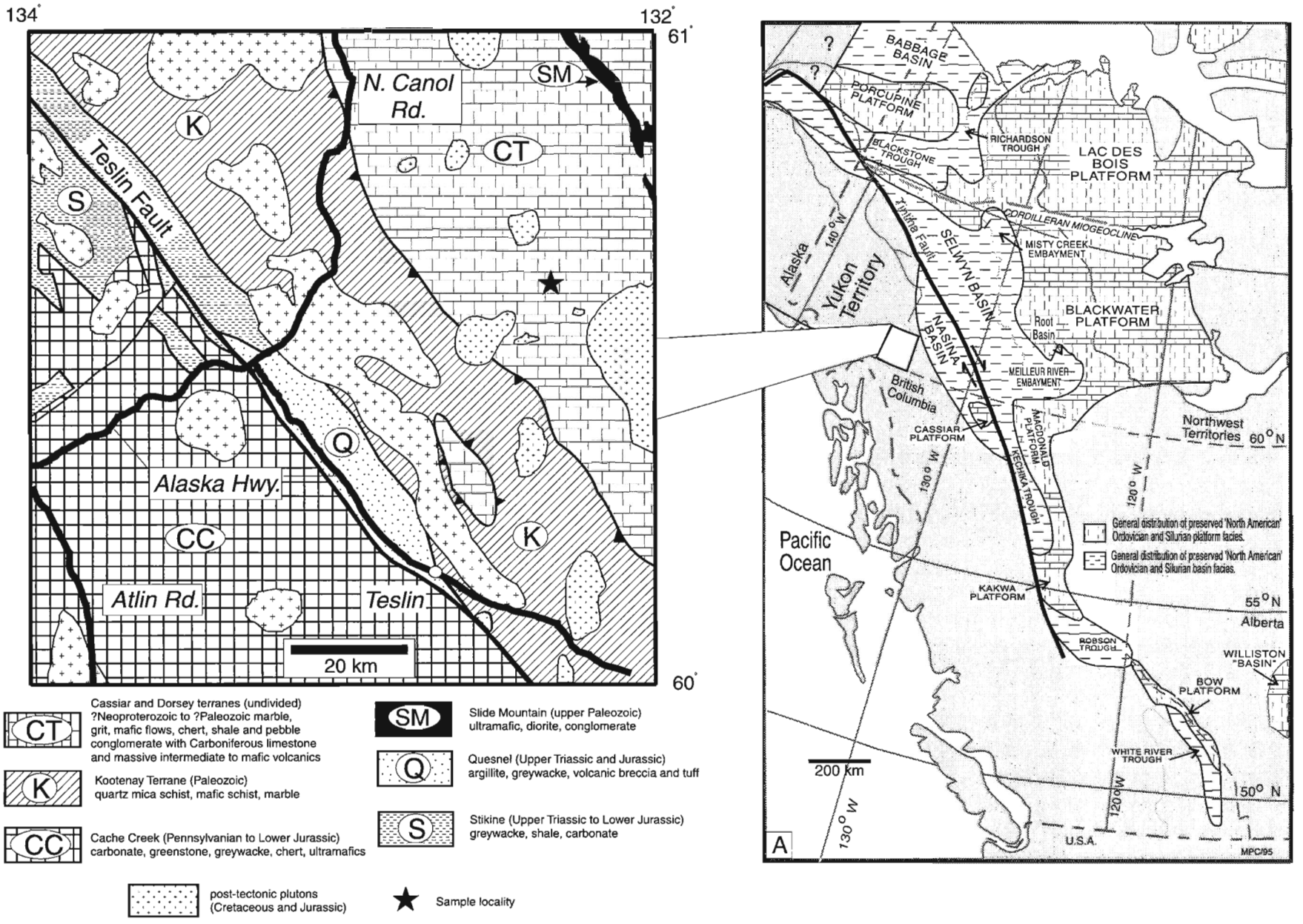

Figure 1. *Location map showing the general configuration of the platform-to-basin geometry of the miogeocline (from Cecile et al., 1997). Inset shows the location and general geology of the Teslin map area and the location of the grit samples (from Gordey, 1995).*

associated with minor interbedded argillite, tuffaceous argillite, and chert. No measured stratigraphic sections of this unit have been attempted due to the structurally fragmented nature of the sequences in the Thirtymile Range (Harms, 1992) which have been included in the Ingenika Group(?) of Gordey and Stevens (1994) and the Thirtymile assemblage of Harms and Stevens (1996). The two samples analyzed here both consist of coarse, poorly sorted, matrix-supported, granular quartz sandstones with subordinate feldspar in a greenish matrix of argillaceous and micaceous material. Sample 91-DY-38a comes from the lower part of Unit C3, and sample 91-DY-41 comes from several hundred metres above it, near the top of this grit unit.

ANALYTICAL TECHNIQUES

The two, small, fist-sized hand samples of grits were crushed using standard techniques and passed directly through heavy liquids. Both samples resulted in a relatively small yield of zircons, about 100 grains or less. Because of the small sample size, the zircon separate was passed only once through a Frantz magnetic separator at relatively low magnetic field (10° sidetilt and 1.4 A) to remove only the most magnetic grains. Grains were then hand-picked on the basis of morphology, and those grains with the best optical properties (and hence best chances of yielding concordant data) were chosen for abrasion and analysis. The grains were abraded to enhance concordance (Krogh, 1982) and their weight was calculated on the basis of dimensional measurement with the microscope and known density of zircon (4.5 g/cc). After abrasion, photography and final mineral selection, individual fractions were analyzed following the methods of Parrish et al. (1987). Data were reduced and errors propagated after the methods of Roddick (1987) and Parrish et al. (1987); analyses plotted on concordia diagrams are shown at 2-sigma (95% confidence) level of uncertainty (Fig. 2). Final errors are indicated on Table 1. Fraction letters shown on concordia plots are keyed to fraction letters in Table 1.

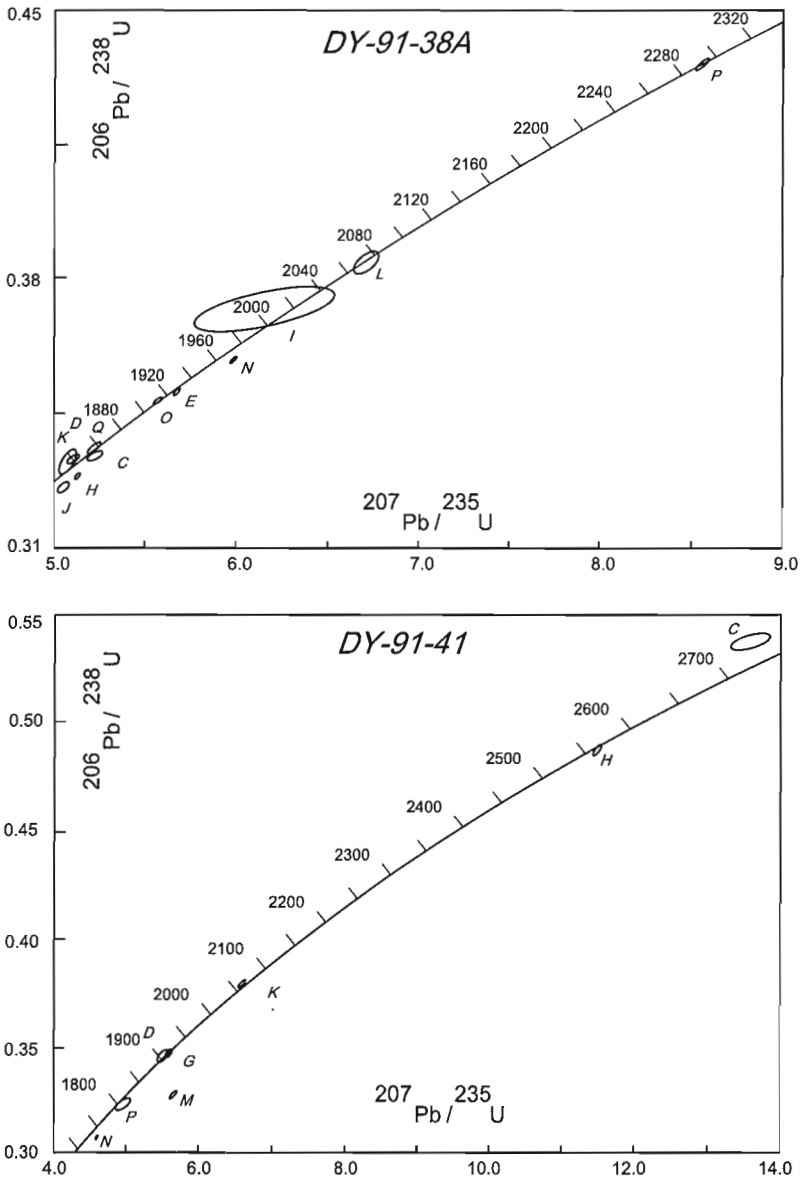

Figure 2.

Concordia plots for U-Pb data for samples DY-91-38a and DY-91-41.

RESULTS

Sample 91-DY-38a

Three populations of zircons were recognized in this sample: 1) rounded purple grains that are pale pink to purple in colour and range from grains that are well rounded to grains that contain approximately 50% of original crystal facets. Most of the rounded purple grains are cloudy. The results from the analyses of 4 of the purple grains (grains C–H; Table 1) show similar uranium contents (152–190 ppm) and yielded Paleoproterozoic $^{207}Pb/^{206}Pb$ ages (1827–1932 Ma) (Fig. 2). The analytical precision and concordance (<2%) of the zircons suggest that these are real age differences and that the zircons are derived from rocks with distinctly different ages. 2) A population of clear grains (I–L; Table 1) consists of subequant, elliptical grains that lack any crystal faces. They have moderate U contents, minor discordance, and result in $^{207}Pb/^{206}Pb$ ages that range from 1820–2076 Ma (Fig. 2). 3) The euhedral population consists of sharply faceted prismatic crystals with 3:1 elongation ratios. The crystals are very clear and inclusion-free with a pale purple colour. Their similar morphologies and well preserved crystal faces suggested that they may have been derived from similar, relatively proximal, sources. However, such inferences are not borne out by the $^{207}Pb/^{206}Pb$ ages which range from 1853–2292 Ma for the four analyzed grains (Fig. 2).

Sample 91-DY-41

Zircons were not abundant in this sample and consisted of a heterogeneous suite of subhedral to rounded grains that included simple, clear, colourless, rounded subhedra, slightly rounded prismatic grains, and large (+149 μm) multifaceted crystals. Smaller grains (<149 μm) were mostly moderately rounded. A range of ages was determined from the 9 analyzed grains and showed no correlation between morphology and age. With the exception of grain M, which is 12% discordant (Table 1), most grains are close to concordia (Fig. 2). A larger error is associated with grain C, which has a low U content and lower $^{206}Pb/^{204}Pb$ ratio, which leads to greater uncertainty in the $^{207}Pb/^{206}Pb$ age. The range of $^{207}Pb/^{206}Pb$ ages is similar to those obtained from sample 38a.

DISCUSSION

The detrital zircon suite in sequence C of the Thirtymile Range has its ultimate derivation from Precambrian crystalline sources. The distribution of ages is similar to the range of known crystallization ages for the crust of western Canada. Comparison of the suite of ages from the Thirtymile Range sandstones with those from the crystalline basement of western Canada and several detrital suites from sandstones of western Canada offers a useful perspective on provenance, correlation and ultimate sediment sources (Fig. 3). The distribution of ages in the Thirtymile Range sandstones is very similar to the distribution of crystallization ages from the basement of

Table 1. U-Pb analytical data, Dorsey grits.

Fraction[a]	Wt.[b] μg	U ppm	Pb[c] ppm	$\frac{^{206}Pb}{^{204}Pb}$[d]	Pb[e] pg	$\frac{^{208}Pb}{^{206}Pb}$[f]	Radiogenic ratios (± 1σ, %)[f] $\frac{^{207}Pb}{^{235}U}$	$\frac{^{206}Pb}{^{238}U}$	$\frac{^{207}Pb}{^{206}Pb}$	$\frac{^{207}Pb}{^{206}Pb}$ Age (Ma)[g]	Discord.[h] %
91-DY-38A Dorsey Terrane (Z3365; 60.6305°N 138.4131° E)											
C (Z, p, r)	3	152	56	355	25	0.160	5.225 ± 0.41	0.3323 ± 0.17	0.11404 ± 0.33	1865 ± 12	0.94
D (Z, r, p)	2	170	61	546	15	0.140	5.106 ± 0.33	0.3316 ± 0.17	0.11168 ± 0.24	1827 ± 9	-1.20
E (Z, r, p)	2	173	70	1108	5	0.230	5.678 ± 0.15	0.3478 ± 0.13	0.11839 ± 0.09	1932 ± 3	0.47
H (Z, r, p)	2	194	67	2385	4	0.120	5.129 ± 0.15	0.3274 ± 0.12	0.11361 ± 0.10	1858 ± 4	1.98
I (Z, cl, r)	1	65	30	52	36	0.330	6.152 ± 3.11	0.3678 ± 0.74	0.12133 ± 2.70	1976 ± 93	-2.54
J (Z, cl, r)	1	196	70	396	11	0.170	5.052 ± 0.31	0.3247 ± 0.20	0.11285 ± 0.24	1846 ± 9	2.05
K (Z, cl, r)	1	136	49	574	0	0.150	5.076 ± 0.47	0.3309 ± 0.45	0.11126 ± 0.37	1820 ± 13	-1.43
L (Zcl, r)	1	72	33	325	3	0.270	6.709 ± 0.53	0.3790 ± 0.36	0.12838 ± 0.42	2076 ± 15	0.24
N (Z, p, e)	1	709	273	1348	12	0.140	5.986 ± 0.15	0.3555 ± 0.11	0.12211 ± 0.08	1987 ± 3	1.54
O (Z, p, e)	1	404	171	617	15	0.300	5.575 ± 0.22	0.3456 ± 0.12	0.11698 ± 0.14	1911 ± 5	-0.20
P (Z, p, e)	1	247	114	854	8	0.110	8.557 ± 0.22	0.4269 ± 0.17	0.14537 ± 0.11	2292 ± 4	0.02
Q (Z, p, e)	1	177	68	552	7	0.230	5.221 ± 0.36	0.3343 ± 0.20	0.11329 ± 0.22	1853 ± 8	-0.38
DY-91-41 (Z3656; 60.6305° N 138.4131° E)											
B (Z, p; sh)	3	174	84	288	45	0.180	8.567 ± 2.25	0.4230 ± 1.43	0.14689 ± 1.72	2310 ± 58	1.85
C (Z, p, e)	2	34	24	97	32	0.330	13.586 ± 1 00	0.5375 ± 0.37	0.18332 ± 0.83	2683 ± 27	-4.11
D (Z, cl, r)	1	52	21	188	6	0.250	5.515 ± 0.68	0.3446 ± 0.41	0.11607 ± 0.53	1897 ± 19	-0.75
G (Z, p,sh)	1	108	48	267	9	0.380	5.597 ± 0.40	0.3459 ± 0.28	0.11736 ± 0.31	1917 ± 11	0.10
H (Z, cl, r)	1	115	61	528	7	0.090	11.486 ± 0.25	0.4869 ± 0.25	0.17110 ± 0.17	2569 ± 6	0.53
K (Z, p, r)	1	142	60	590	5	0.170	6.590 ± 0.38	0.3780 ± 0.24	0.12643 ± 0.21	2049 ± 8	-1.04
M (Z, p, e)	1	139	50	355	9	0.150	5.659 ± 0.44	0.3267 ± 0.27	0.12562 ± 0.25	2038 ± 9	12.10
N (Z, p, r)	1	291	96	1641	4	0.140	4.599 ± 0.18	0.3069 ± 0.14	0.10867 ± 0.11	1777 ± 4	3.32
P (Z, p, r)	1	125	47	162	18	0.240	4.963 ± 1.08	0.3222 ± 0.43	0.11172 ± 0.84	1828 ± 30	1.70

[a]All zircon fractions are abraded (Z=Zircon; cl=clear; p=purple; r=rounded; e=euhedral; sh=subhedral), [b]Weights determined by measuring a:b:c axes of grain and multiplying by density of zircon (4.5 g/cc), [c]Radiogenic Pb, [d]Measured ratio corrected for spike and Pb fractionation of 0.09±0.03%/AMU, [e]Total common Pb on analysis corrected for fractionation and spike, of blank model Pb composition, [f]Corrected for blank and spike Pb and U and common Pb (Stacey-Kramers model Pb composition equivalent to the $^{207}Pb/^{206}Pb$ age), [g]Age error is ±2SE in Ma, [h]Discordance along a discordia to origin.

northern Alberta and British Columbia. Importantly, the common occurrence of zircons in the age range of ca. 2.0–2.4 Ga is considered a distinctive element of the basement of northern Alberta, where such ages are widespread in the basement and less common in the exposed shield regions (Villeneuve et al., 1993). Specific domains of western Canada that may have contributed zircons include Nova Domain (ca. 2600 Ma grains); Buffalo Head, Chinchaga, and Wabamun domains (2076–2310 Ma), Ksituan, Taltson, and Hottah domains (1917–1987 Ma); and Great Bear and Fort Simpson domains (1820–1865 Ma) (Fig. 4). Importantly, ca. 1750–1850 Ma zircons, typical of sediments derived from crystalline basement of southern Alberta, including the Windermere Supergroup south of 54°N, are lacking (Ross and Parrish, 1991; Gehrels et al., 1995). Although grain N from DY-41 ($^{207}Pb/^{206}Pb$ age of 1777 Ma) might be considered a candidate for derivation from the southern Alberta basement, it is important to note that this analysis is 3% discordant, which prevents a confident age assignment. The distribution of ages can be further compared with suites of detrital grains from Siluro-Devonian sandstones of northeastern British Columbia that are inferred to have been derived from the crystalline basement of the Peace River Arch, an important positive paleotopographic element that provided sediment to the Cordilleran margin from late Proterozoic through Devonian time (O'Connell et. al., 1990; Ross et al.,1993; Gehrels et al., 1995; Ross and Villeneuve, 1997). This exercise shows that there is a strong similarity between the suite of detrital grains dated in the Thirtymile Range grits and those derived from the Peace River Arch (Fig. 3). We suggest that the ultimate source of these grits is the crystalline basement of the Peace River Arch region.

Implications for age, stratigraphic correlation, and displacement along Tintina–Northern Rocky Mountain Trench

The geochronology of the detrital zircons from the Thirtymile Range grits demonstrates clearly a North American, and in particular a western Canadian, provenance. This conclusion can be used to demonstrate that 1) the Thirtymile grits, if North American, are most likely Ingenika Group equivalents

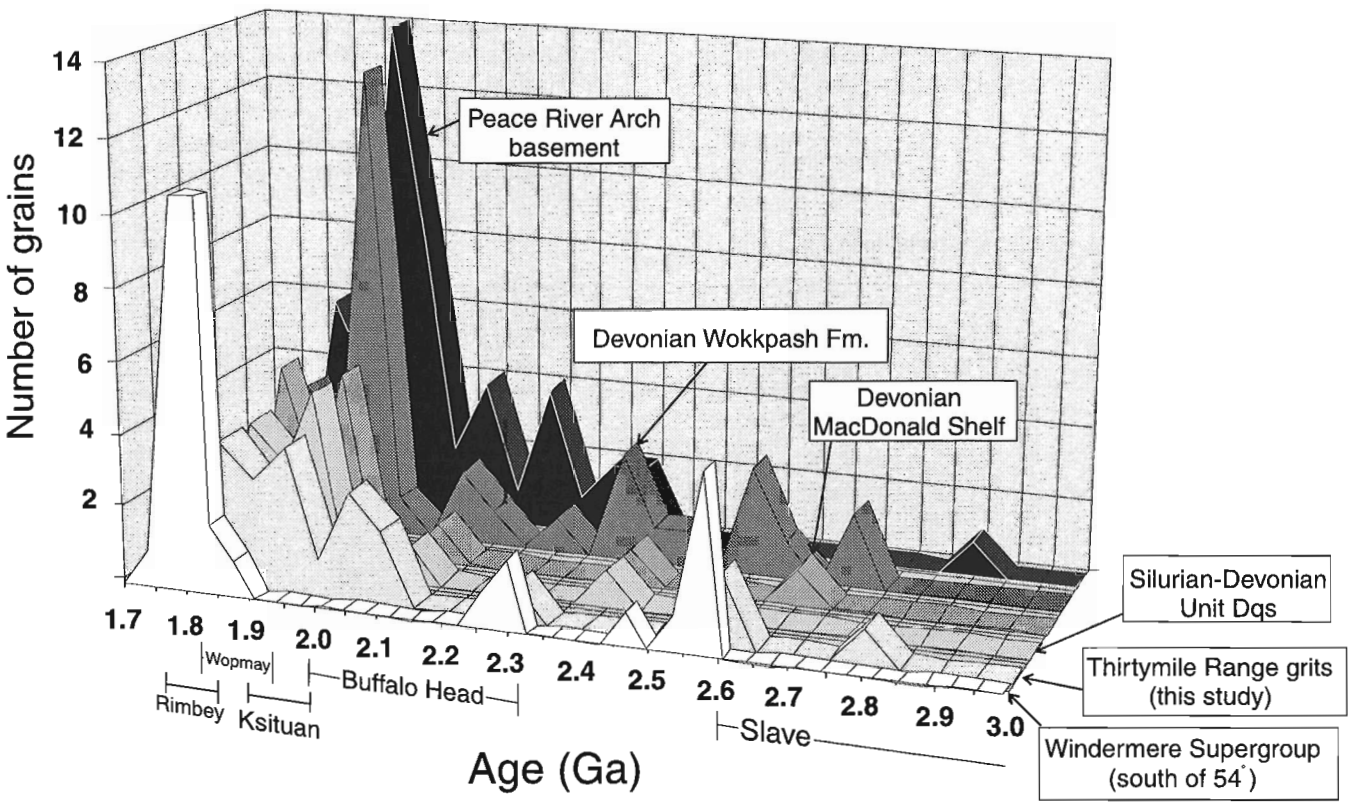

Figure 3. *Histogram plot comparing the detrital zircon ages from the Thirtymile Range grits with the ages of basement of northern Alberta (Peace River Arch) and with ages of detrital zircons from miogeoclinal sedimentary rocks (data from Ross and Parrish, 1991 (Windermere Supergroup); Ross et al., 1993 (Silurian-Devonian Unit Dqs and Devonian MacDonald shelf sandstones); G. Gehrels (unpublished, Devonian Wokkpash Formation); and Villeneuve et al., 1993 (Peace River Arch basement)). Note the similarity of the range of ages between the Peace River Arch basement, Devonian sandstones, and Thirtymile grits (particularly the presence of zircons >2.0 Ga), which contrast with the bimodal pattern characteristic of the Windermere south of 54°N.*

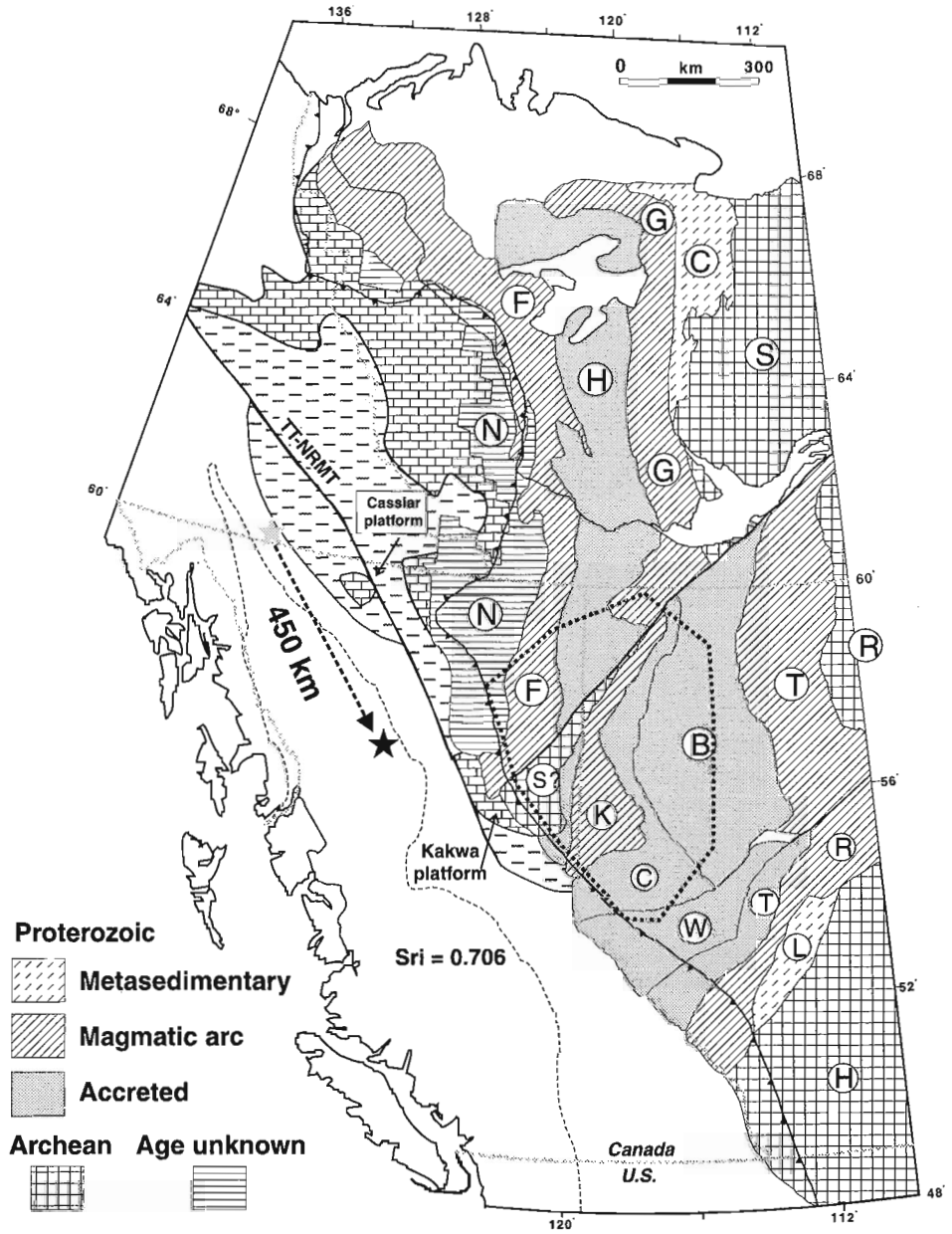

Figure 4. *Simplified map of the Cordilleran miogeocline plotted with the U-Pb ages of adjacent autochthonous basement.The Cassiar Terrane, which lies west of Tintina–Northern Rocky Mountain Trench fault, is here defined on the basis of Lower Paleozoic facies (shelf = brick pattern; basin = dash pattern; from Cecile et al., 1997) and is composed of Cassiar platform and Nasina basin, would restore 450 km southeast along the fault according to Gabrielse (1985). Note that restoration of displacement along the Tintina–Northern Rocky Mountain Trench (dashed line) would place the Thirtymile Range grits (dark star) in the vicinity of basement in northern Alberta and northeastern British Columbia. Dashed polygon in the basement shows postulated source areas represented in the Thirtymile Range grits. Restoration into northern Montana and Idaho (Pope and Sears, 1997) would place these grits adjacent to crust composed predominantly of Archean age rocks, inconsistent with the ages of detrital zircons in this study. Abbreviations for basement domains: Archean: S -Slave Province; R - Rae Province; H - Hearne Province; S? - Nova domain (Slave Province?); Proterozoic accreted terranes: H - Hottah Terrane; C - Chinchaga; B - Buffalo Head; W - Wabamun; T - Thorsby; Proterozoic magmatic terranes: G - Great Bear; F - Fort Simpson; K - Ksituan; T - Taltson; R - Rimbey; Proterozoic metasedimentary terranes: C -Coronation; L - Lacombe. N - Nahanni domain (Hoffman, 1989), age unknown. GSL -Great Slave Lake; GBL - Great Bear Lake. Sr initial ratio = 0.706, which approximates the edge of Precambrian crust is taken from Armstrong (1988).*

of late Neoproterozoic, not Paleozoic, age; and 2) that the latitudinal displacement of the Thirtymile grits, since the Neoproterozoic, is probably from around the Peace River arch region and not more.

According to Gordey (1992,1995) and Gordey and Stevens (1994) the strata examined in this study are considered to have stratigraphic ties to North America and may be correlative with Neoproterozoic to Cambrian grits of the Ingenika Group. A plausible explanation based on the detrital zircon data from the Thirtymile Range, implies a clear tie to western Canadian basement. The zircon data do not offer any direct age constraints, except that the age of the grits must be less than 1830 Ma, the youngest and least discordant $^{207}Pb/^{206}Pb$ age. However, comparison with demonstrable Paleozoic sandstones derived from the Peace River Arch offers some additional, albeit indirect, constraints (Fig. 3). The Thirtymile Range detrital zircons match the age of crystalline basement as well as the ages of detrital grains from Silurian to Devonian sandstones of the outer part of the continental shelf in northern British Columbia. This might be suggestive of correlation and assignment of a Paleozoic age to the sequence C grits of the Thirtymile Range. However, each of the sandstones shown on Figure 3 is a clean, well sorted, quartz arenite that contrasts with the immature and poorly sorted composition of the Thirtymile Range sandstones. The Windermere Supergroup, of which the Ingenika Group is the local correlative, is characterized by coarse conglomeratic lithologies and it is suggested that the zircon data, in combination with the grain size of the analyzed grits, are consistent with the suggestion that the unit C3 grits are part of the Ingenika Group (Gordey, 1995). The range of ages in the Thirtymile Range grits contrasts with those that typify the Windermere Supergroup south of 54° (Fig. 3), suggesting that there may be an important change in the provenance of the Windermere Supergroup of the southern Cordillera compared to the northern Cordillera. This may be a reflection of first-order differences in the geometry of the Cordilleran margin, such as a change from upper-plate to lower-plate passive margin, as suggested by Cecile et al. (1997). Further geochronologic studies are underway to examine this possibility.

The position of the Thirtymile Range grits within North American strata west of the Tintina–Northern Rocky Mountain Trench suggest that they can be considered part of the Cassiar Terrane. The correlation of the detrital zircon patterns in the Thirtymile Range grits with the crystalline ages of basement in northern Alberta places additional constraints on the displacement history of the Cassiar Terrane since the Neoproterozoic. The displacement of the Cassiar Terrane along the right-lateral Tintina–Northern Rocky Mountain Trench is at least 450 km (Gabrielse, 1985) (Fig. 4), but could be as much as 600 km (Butler et al., 1988). According to a recent hypothesis (Pope and Sears, 1997) displacement could be approximately 2000 km, based on offset faunal and stratigraphic patterns in Cambrian strata. These latter authors noted the lack of a Paleozoic passive-margin succession in western Montana across the Salmon River suture and suggested that the Cassiar Terrane is the displaced fragment of that margin. This would predict that the provenance of sedimentary strata of the Cassiar Terrane should reflect a western Montana–southern Alberta provenance which would consist of Archean and Proterozoic (<1850 Ma) crust (Hoffman, 1989; Ross et al., 1991). It is clear from the histogram plots that the Thirtymile Range grits of the Cassiar Terrane analyzed in this study (Fig. 3) were derived from northern Alberta, in clear contrast to the detrital zircon signature typical of coeval Neoproterozoic (Windermere Supergroup) strata in the southern Cordillera. The provenance link between northern Alberta and the Cassiar Terrane is consistent with approximately 450 km of post-Cretaceous displacement suggested by Gabrielse (1985) (Fig. 4) and is strong evidence that the Cassiar Terrane is not far-travelled.

CONCLUSIONS

Detrital zircons analyzed from coarse grits within the Thirtymile Range of the southern Yukon Territory yield Proterozoic and Archean $^{207}Pb/^{206}Pb$ ages. The range of ages, from ca. 1800 Ma to 2600 Ma can be connected to the ages of basement in the Peace River Arch area of northern Alberta and northeastern British Columbia. This suggests that the source of these grits was crystalline basement of western Canada and confirms a North American affinity for these sedimentary rocks and their correlation with the Cassiar Terrane of northern British Columbia. The western Canadian provenance documented in the detrital zircon ages is consistent with models that suggest ca. 450 km of right lateral displacement along the Tintina–Northern Rocky Mountain Trench, and argues against suggestions of a western Montanan provenance for the Cassiar Terrane.

ACKNOWLEDGMENTS

Laboratory assistance of Randy Parrish, Jack MacRae, and Klaus Santowski is gratefully acknowledged. George Gehrels is thanked for supplying unpublished zircon data from the Wokkpash Formation. Discussions and written commentary by JoAnne Nelson, Mike Cecile, Mike Villeneuve, Reg Thériault, Jim Mortensen, and Steve Gordey helped clarify the ideas and data presented herein.

REFERENCES

Armstrong, R.L.
1988: Mesozoic and early Cenozoic magmatic evolution of the Canadian Cordillera; *in* Processes of Continental Lithospheric Deformation, (ed.) S.P. Clark, Jr., B.C. Burchfiel, and J. Suppe; Geological Society of America, Special Publication 218, p. 55-92.

Butler, R.F., Harms, T.A., and Gabrielse, H.
1988: Cretaceous remagnetization of the Sylvester allochthon: limits to post-105 Ma northward displacement of north-central British Columbia; Canadian Journal of Earth Sciences, v. 25, p. 1316-1325.

Cecile, M.P., Morrow, D.W., and Williams, G.K.
1997: Early Paleozoic (Cambrian to Devonian) tectonic framework, Canadian Cordillera; Bulletin of Canadian Petroleum Geology, v. 45, p. 54-74.

Coney, P.J., Jones, D.L., and Monger, J.W.H.
1980: Cordilleran suspect terranes; Nature, v. 288, p. 329-333.

Evenchick, C.A., Parrish, R.R., and Gabrielse, H.
1984: Precambrian gneiss and Late Proterozoic sedimentation in north-central British Columbia; Geology, v. 12, p. 233-237.

Gabrielse, H.
1985: Major dextral displacements along the Northern Rocky Mountain Trench and related lineaments in north-central British Columbia; Geological Society of America Bulletin, v. 96, p. 1-14.

Gehrels, G.E., Dickinson, W.R., Ross, G.M., Stewart, J.H., and Howell, D.H.
1995: Detrital zircon reference for Cambrian to Triassic strata of western North America; Geology, v. 23, p. 831-834.

Gehrels, G.E., McClelland, W.C., Samson, S.D., and Patchett, P.J.
1991: U-Pb geochronology of detrital zircons from a continental margin assemblage in the northern Coast Mountains, Alaska; Canadian Journal of Earth Sciences, v. 28, p. 1285-1300.

Gordey, S.P.
1992: Geological fieldwork in Teslin map area, southern Yukon Territory; *in* Current Research, Part A; Geological Survey of Canada, Paper 92-1A, p. 279-286.
1995: Structure and terrane relationships of Cassiar and Kootenay (Yukon–Tanana) terranes, Teslin map area, southern Yukon Territory; *in* Current Research 1995-A; Geological Survey of Canada, p. 135-140.

Gordey, S.P. and Stevens, R.A.
1994: Preliminary interpretation of bedrock geology of the Teslin map area (105 C), southern Yukon Territory; Geological Survey of Canada, Open File 2886, scale 1:250 000.

Gordey, S.P., Geldsetzer, H.H.J., Morrow, D.W., Bamber, E.W., Henderson, S.C.M., Richards, B.C., McGugan, A., Gibson, D.W., and Poulton, T.P.
1991: Part A. Ancestral North America; *in* Upper Devonian to Middle Jurassic assemblages, Chapter 8 of Geology of the Cordilleran Orogen in Canada; (ed.) H. Gabrielse and C.J. Yorath, Geology of Canada, no. 4, p. 219-327.

Harms, T.A.
1992: Stratigraphy of the southern Thirtymile Range, Teslin map area, southern Yukon Territory; *in* Current Research, Part A; Geological Survey of Canada, Paper 92-1A, p. 297-302.

Harms, T.A. and Stevens, R.A.
1996: A working hypothesis for the tectonostratigraphic affinity of the Stikine Ranges and a portion of the Dorsey Terrane; *in* (comp.) Cook, F.A. and Erdmer; Slave–Northern Cordilleran Lithospheric Evolution (SNORCLE) Transect and Cordilleran Tectonics Workshop meeting, March 1-3, University of Calgary, Lithoprobe Report #50, p. 93-95.

Harms, T.A., Stevens, R.A., and Creaser, R.A.
1997: Assemblage analysis and tectonostratigraphic affinity of Dorsey Terrane and adjacent areas — northern British Columbia and southern Yukon; Geological Association of Canada, Abstracts with Program, v. 22, p. A64.

Hoffman, P. F.
1989: Precambrian geology and tectonic history of North America, *in* The Geology of North America — An Overview; (ed.) A.W. Bally and A.R.Palmer; Geological Society of America, The Geology of North America, v. A, p. 447-512.

Krogh, T.E.
1982: Improved accuracy of U-Pb zircon ages by the creation of more concordant systems using an air abrasion technique; Geochimica et Cosmochimica Acta, v. 46, p. 637-649.

Mulligan, R.
1963: Geology of the Teslin map area, Yukon Territory (105 C): Geological Survey of Canada, Memoir 326, 96 p.

O'Connell, S.C., Dix, G.R., and Barclay, J.E.
1990: The origin, history, and regional structural development of the Peace River Arch, western Canada; Canadian Society of Petroleum Geologists Bulletin, 38A, p. 4-24.

Parrish, R.R., Roddick, J.C., Loveridge, W.D., and Sullivan, R.W.
1987: Uranium-lead analytical techniques at the geochronology laboratory, Geological Survey of Canada; *in* Radiogenic Age and Isotope Studies: Report 1; Geological Survey of Canada, Paper 87-2, p. 3-7.

Pope, M.C. and Sears, J.W.
1997: Cassiar platform, north-central British Columbia: A miogeoclinal fragment from Idaho; Geology, v. 25, p. 515-518.

Rainbird, R.H., Heaman, L.M., and Young, G.M.
1992: Sampling Laurentia: detrital zircon geochronology offers evidence for an extensive Neoproterozoic river system originating from the Grenville orogen; Geology, v. 20, p. 351-354.

Rainbird, R.H., McNicoll, V.J., Thériault, R.J., Heaman, L.M., Abbott, J.G., Long, D.G.F., and Thorkelson, D.J.
1997: Pan-continental river system draining Grenville orogen recorded by U-Pb and Sm-Nd geochronology of Neoproterozoic quartz arenites and mudrocks, northwest Canada; Journal of Geology, v. 105, p. 1-17.

Roddick, J.C.
1987: Generalized numerical error analysis with applications to geochronology and thermodynamics; Geochimica et Cosmochimica Acta, v. 51, p. 2129-2135.

Ross, G.M.
1991: Precambrian basement in the Canadian Cordillera: an introduction; Canadian Journal of Earth Sciences, v. 28, p. 1133-1139.

Ross, G.M., and Bowring, S.A.
1990: Detrital zircon geochronology of the Windermere Supergroup and the tectonic assembly of the southern Canadian Cordillera; Journal of Geology, v. 98, p. 879-893.

Ross, G.M., and Parrish, R.R.
1991: U-Pb detrital zircon geochronology of metasedimentary rocks in the Canadian Cordillera and the age of continental basement; Canadian Journal of Earth Sciences, v. 28, p. 1254-1270.

Ross, G.M., and Villeneuve, M.E.
1997: U-Pb geochronology of stranger stones in Neoproterozoic diamictites, Canadian Cordillera: implications for provenance and ages of deposition; *in* Radiogenic Age and Isotopic Studies: Report 10; Geological Survey of Canada, Current Research 1997-F, p. 141-155.

Ross, G.M., Gehrels, G.E., and Patchett, P.J.
1997: Provenance of Triassic strata in the Cordilleran miogeocline, western Canada; Bulletin of Canadian Petroleum Geology, v. 45, p. 461-473.

Ross, G.M., McNicoll, V.J. Geldsetzer, H.H.J., Parrish, R.R., Carr, S.D., and Kinsman, A.
1993: Detrital zircon geochronology of Siluro-Devonian sandstones, Rocky Mountains, northeast British Columbia; Bulletin of Canadian Petroleum Geology, v. 41, p. 349-357.

Ross, G.M., Parrish, R.R., Villeneuve, M.E., and Bowring, S.A.
1991: Geophysics and geochronology of the crystalline basement of the Alberta Basin, western Canada; Canadian Journal of Earth Sciences, v. 28, p. 512-522.

Ross, G.M., Parrish, R.R., and Winston, D.
1992: Provenance and U-Pb geochronology of the Mesoproterozoic Belt Supergroup (northwestern United States): implications for the age of deposition and pre-Panthalassa plate reconstructions. Earth and Planetary Science Letters, v. 113, p. 57-76.

Smith, M.T. and Gehrels, G.E.
1991: Detrital zircon geochronology of Upper Proterozoic and Lower Paleozoic continental margin strata of Kootenay Arc: implications for early Paleozoic tectonic development of the eastern Canadian Cordillera; Canadian Journal of Earth Sciences, v. 28, p. 1271-1284.

Villeneuve, M.E., Ross, G.M., Parrish, R.R., Thériault, R.J., Miles, W., and Broome, J.
1993: Geophysical subdivision, U-Pb geochronology and Sm-Nd isotope geochemistry of the crystalline basement of the Western Canada Sedimentary Basin; Geological Survey of Canada, Bulletin 447, 86 p.

Wheeler, J.O., Brookfield, A.J., Gabrielse, H., Monger, J.W.H., Tipper, H.W., and Woodsworth, G.J.
1991: Terrane map of the Canadian Cordillera; Geological Survey of Canada, Map 1713A, scale 1:2 000 000.

Age of the Cap Mountain (Northwest Territories) Proterozoic section, sequence B, based on detrital zircon ages

M.E. Villeneuve[1], N.J. Butterfield[2], D.G. Cook[3], B.C. MacLean[3], and R.H. Rainbird[1]

Villeneuve, M.E., Butterfield.,N.J., Cook, D.G., MacLean, B.C., and Rainbird, R.H., 1998: Age of the Cap Mountain (Northwest Territories) Proterozoic section, sequence B, based on detrital zircon ages; in *Radiogenic Age and Isotopic Studies: Report 11; Geological Survey of Canada, Current Research 1998-F, p. 117-127.*

Abstract: Grenville-age zircons (ca. 1 Ga) have been extracted from the lowermost two units of the Proterozoic sedimentary section exposed on Cap Mountain, Interior Plains, Northwest Territories, thus necessitating a major change in our understanding of the correlation of these rocks. The strata were previously considered to correlate with the Paleoproterozoic, 1.84–1.27 Ga Hornby Bay Group (sequence A) of Coppermine Homocline, but, because they are younger than ca. 1 Ga they clearly belong to sequence B and correlate in a general way with Mackenzie Mountains Supergroup to the west and Shaler Supergroup to the northeast. Specific unit-to-unit correlations within the groups cannot as yet be made.

Résumé : Des zircons d'âge grenvillien (environ 1 Ga) ont été prélevés dans les deux unités inférieures des roches sédimentaires protérozoïques qui affleurent sur le mont Cap, dans les plaines Intérieures, dans les Territoires du Nord-Ouest, ce qui nous oblige à modifier de façon significative notre compréhension de la corrélation de ces roches. On pensait que les strates étaient en corrélation avec le Groupe de Hornby Bay (séquence A) du Paléoprotérozïque de l'homoclinale de Coppermine, dont l'âge se situe entre 1,84 Ga à 1,27 Ga, mais, puisque leur âge est inférieur à environ 1 Ga, ces strates appartiennent incontestablement à la séquence B et sont, en général, en corrélation avec le Supergroupe de Mackenzie Mountains à l'ouest et le Supergroupe de Shaler au nord-est. On ne peut pas encore établir de corrélations précises entre les unités au sein des groupes.

[1] Geological Survey of Canada, 601 Booth Street, Ottawa, Ontario K1A 0E8
[2] Department of Earth Sciences, The University of Western Ontario, London, Ontario, Canada N6A 5B7
[3] Geological Survey of Canada, 3303-33rd Street, Calgary, Alberta T2L 2A7

INTRODUCTION

It is convenient to discuss post-Wopmay Orogen Proterozoic stratigraphy of northwestern Canada in terms of the three major sequences, A, B, and C (Fig. 1) of Young et al. (1979). The Paleo/Mesoproterozoic sequence A is represented in Coppermine Homocline by the Hornby Bay, Dismal Lakes, and Coppermine River groups, and in the Cordillera by the Wernecke Supergroup. The age of sequence A is constrained by underlying 1.84 Ga and older basement rocks of the Wopmay Orogen (Hoffman and Bowring, 1984), and by the 1267 Ma Coppermine basalts (LeCheminant and Heaman, 1989) at the

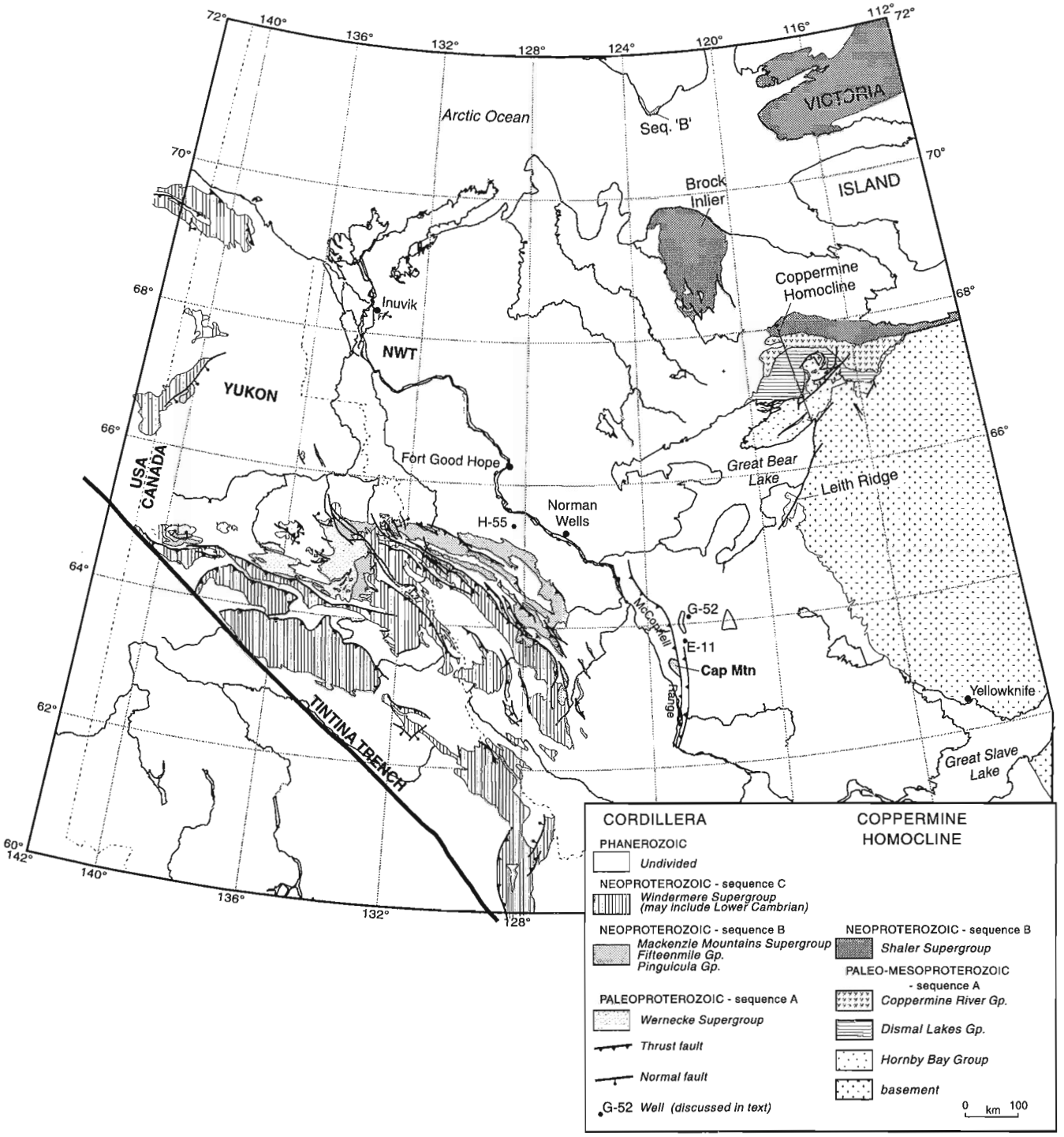

Figure 1. *Location of Cap Mountain Proterozoic section relative to other Proterozoic outcrops in the Cordillera, Coppermine Homocline, Brock Inlier, and Victoria Island. Modified from Cook and MacLean, (1996, Fig.1).*

top of the sequence. Neoproterozoic sequence B comprises the Shaler Supergroup in Coppermine Homocline, Brock Inlier, and Victoria Island, and Mackenzie Mountains Supergroup, Pinguicula, and Fifteenmile groups in the Cordillera. Sequence B ranges in age from 1.00 Ga to 0.78 Ga (Rainbird et al., 1997). Sequence C comprises the Windermere Supergroup and is confined to the Cordillera; its age ranges from 0.78 Ga to 0.54 Ga (Rainbird et al., 1996a).

Most Proterozoic sedimentary rocks in northwestern Canada have been reasonably assigned to one or the other of these major sequences. However, correlation has been problematic for a section greater than 1800 m thick, of unmetamorphosed Proterozoic strata (Aitken et al., 1973b), exposed in the northeast-facing scarp of Cap Mountain (NTS 95-O; 63°26′N; 123°14′W) in the McConnell Range, Northwest Territories (Fig. 1). The closest outcropping Proterozoic units (Fig. 1) are the sequence B, Neoproterozoic, Mackenzie Mountains Supergroup about 125 km to the west in the Mackenzie Mountains (Douglas and Norris, 1974), and sequence A, Paleoproterozoic, Hornby Bay Group about 250 km to the northeast in Leith Ridge (Ross and Kerans, 1989). Correlation of the section has been difficult partly due to its isolation and partly due to the lack of specific age control.

CORRELATION HISTORY

On Cap Mountain, Hume (1924) mapped the Mount Clark and Lone Land formations as an undivided unit. His map and legend imply that the Lone Land Formation included the entire Precambrian section. Douglas and Norris (1963) mapped four Proterozoic units overlain by a "strong angular unconformity" at the base of the Mount Clark Formation (Fig. 2). They restricted the term 'Lone Land Formation' to the uppermost unit (identified on their map as unit 4), which they considered to be unconformable on unit 3. On the basis of that supposed unconformity, Douglas and Norris (1974) considered the lower three units to be Helikian (1640–880 Ma) and the uppermost (Lone Land Formation) to be Hadrynian (880–600).

Aitken et al. (1973a, b) confirmed the sub-Cambrian unconformity (Fig. 3), but found no unconformity at the base of the Lone Land, and considered all four Precambrian units to be Helikian. At that time they considered the Mackenzie Mountains Supergroup also to be Helikian, but made no specific correlations to Mackenzie Mountains Supergroup units. In fact, they rejected such correlation stating that "the strata do not belong to any formation recognized in the Mackenzie Mountains" (1973a, p. 243). They did, however, note lithologic similarities between map unit 1 and the Tsezotene

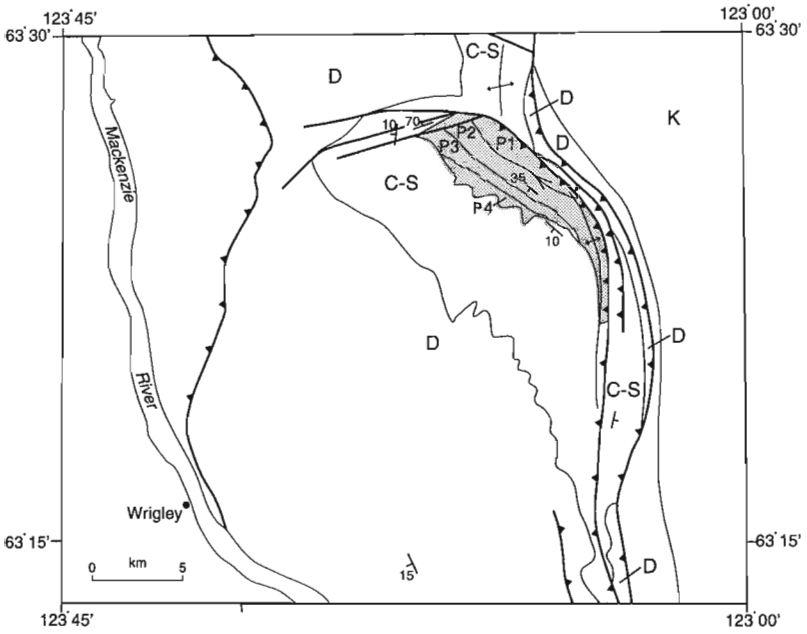

Figure 2.

Map of Cap Mountain showing four Proterozoic units and sub-Cambrian unconformity. Extracted from Douglas and Norris (1974).

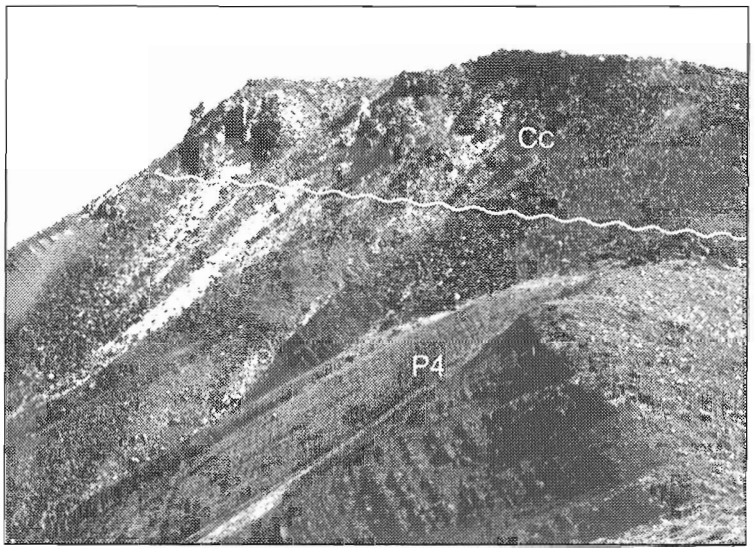

Figure 3.

Angular unconformity beneath Mount Clark Formation at Cap Mountain; P4 - Proterozoic Lone Land Formation, Cc - Lower Cambrian Mount Clark Formation. View southeastward along strike of Proterozoic strata. From Aitken et al. (1973b, plate 21). GSC 1990-20

Formation of Mackenzie Mountains Supergroup, but rejected that possible correlation because of the absence of an overlying, thick, quartzite-dominated sequence that could correspond to the Katherine Group.

Meijer Drees (1975), correlated the Cap Mountain section with adjacent subsurface strata penetrated in exploration wells drilled to the east, and suggested that the Cap Mountain units correlated with the much older (sequence A) formations of the Hornby Bay and Dismal Lakes groups exposed on Coppermine Homocline. Aitken and Pugh (1984) supported Meijer Drees' correlations with the Hornby Bay Group and, moreover, specifically identified map unit 1 in two wells, Shell Blackwater Lake G-52, and Union Japex et al. Blackwater E-11 (*see* Fig. 1 for location).

Palynological preparation of shales from outcrop of the Lone Land Formation and drill cuttings from Blackwater Lake G-52 at depths between 6320 and 6380 feet have yielded a moderate diversity of well preserved acritarchs and cyanobacterial microfossils. Notably, the Lone Land assemblage includes the large sphaeromorphic acritarch *Chuaria*, which has previously been reported from both the Mackenzie Mountains and Shaler supergroups (Hoffman and Rainbird, 1995), although it also occurs in Hector Formation (Windermere Supergroup) further south in the Cordillera; worldwide, *Chuaria* ranges through the whole of the Neoproterozoic. In Blackwater Lake G-52, the distinctive acanthomorphic acritarch *Trachyhystrichosphaera* has been recovered at depths of 6330 and 6350 feet. *Trachyhystrichosphaera* occurs worldwide in ca. 1000–700 Ma rocks (including the Grassy Bay, Wynniatt, and Kilian formations in the Shaler Supergroup) and appears to be an excellent index fossil for the sequence B interval (Butterfield et al., 1994). Other aspects of the G-52 fossil assemblage compare closely with the Wynniatt assemblage on Victoria Island and clearly establish the sequence B status of the borehole samples. *Trachyhystrichosphaera* has not yet been detected in the Lone Land Formation and, indeed, the overall fossil assemblage there is not particularly comparable to G-52 despite the proximity of the two sections. Map unit 1 on Cap Mountain has not been examined for microfossils, so the possibility that it may correlate more closely with G-52, as suggested on lithostratigraphic grounds by Aitken and Pugh (1984), has not been tested. In any event, acritarchs from both the Lone Land Formation and pre-Paleozoic horizons in Blackwater Lake G-52 confirm a Neoproterozoic age for their respective host sediments.

Rainbird et al. (1997) report a persistent and wide-spread occurrence of 'Grenville-age' detrital zircons from quartz-arenite units of sequence B and consequently the Cap Mountain uncertainties had potential for resolution by geochronological analysis. Aitken's samples from the Cap Mountain section are curated at Geological Survey of Canada, Calgary; these were examined and samples were selected by Rainbird, and analyzed by Villeneuve at the GSC geochronology laboratory in Ottawa.

STRATIGRAPHY

Detailed lithologic description of the Cap Mountain section can be found in Aitken et al. (1973b). The following summary descriptions are quoted from Aitken et al. (1973a, p. 244):

Map unit 1

"...the Mount Cap section consists of a lowermost unit (map-unit 1 of Douglas and Norris 1963), 1670 feet thick and consisting of purple to purple-red and minor green, extensively mudcracked mudstones and shales, interbedded with either greenish grey to pale green, dense argillaceous and silty yellow-weathering laminated dolomite; or very fine grained, greyish green to greyish purple, laminated, crosslaminated and ripple-marked sandstone or siltstone; or both. Contortion and various dolomite breccias suggest an evaporitic environment."

It was this unit that Aitken et al. (1973a) considered to be lithologically similar to Tsezotene Formation in the Mackenzie Mountains, but they found no correspondence between overlying units. Aitken and Pugh (1984) considered that this unit

was penetrated by two wells, Blackwater Lake G-52, and Blackwater E-11. Butterfield extracted *Trachyhystrichosphaera* from G-52.

Map unit 2

"Map-unit 1 is overlain, apparently conformably, by map-unit 2, which is 1720 feet thick and consists mainly of brick-red to purplish red mudcracked mudstone, commonly with hematite-coated fracture surfaces and subordinate amounts of greyish purple, mostly very fine grained, rarely coarse grained, generally crosslaminated or crossbedded muddy sandstone, with abundant rip-up clasts of purple shale and local ripple-marks. A zone 400-500 feet below the top contains two intervals composed of dolomite, partly stromatolitic, and minor amounts of pale grey to greenish grey quartzose sandstone."

Map unit 3

"Map-unit 2 is overlain apparently conformably, by map-unit 3, a succession of shales, siltstones and sandstones 1700 feet thick. The upper and lower thirds of the unit are relatively poor in sandstones and slightly recessive, and the middle third is dominated by resistant sandstones. The shales and siltstones are green or greenish grey to purple or purplish grey and lack the reddish colour of underlying units. They are mainly thin bedded to laminated. The sandstones are clean orthoquartzites, mainly very fine and fine grained, but medium to very coarse grained in isolated beds, with a few jasper-bearing grit beds. Crossbedding is generally, and in some beds spectacularly, developed.

In the basal 200 feet of map-unit 3, structures suggestive of shallow-water deposition are lacking, and contorted beds suggest deposition on a slope. Higher beds are partly mudcracked, and the bases of sandstone beds are commonly erosional, indicating a return to prevailing shallow-water deposition which characterizes most of the Proterozoic at this locality. The basal 260 feet of the upper, relatively shaly third of the formation is characterized, however, by lenticular and interrupted bedding with a few sedimentary over-folds. These beds are considered to be the product of slope deposition."

Lone Land Formation

"Map-unit 3 is overlain by the 850-foot-thick Lone Land Formation, which commences at the base with a very resistant, 90-foot-thick member of friable orthoquartzitic sandstone. This rock is mainly white with local pink and purple patches, medium grained and well sorted, and contains layers of granules and minor beds of quartz grit. Throughout the succeeding 300 feet, the basal sands are replaced upward by progressively increasing amounts of intercalated, partly silty and sandy, pale green, olive-green, and dark grey shale. The sands become very fine grained and thin-bedded upward. Shrinkage cracks and ripple-marks are ubiquitous. The remainder of the Lone Land is uniform in character, and is composed of 80-90 per cent brownish grey to olive-grey, very fissile, mostly silty shale, and 10-20 per cent quartzose, grey to pale greenish grey, very fine grained sandstone, in thin beds with thin shaly laminae and paper thin shale clasts. Scour-and-fill, load casts, ripple-marks and ripple drift crosslamination are prominent."

"... the writers carefully re-examined the base of the Lone Land Formation. The contact is structurally concordant and nonerosional, and the only evidence suggestive of an unconformity is the grit layers in the basal Lone Land sandstone."

GEOCHRONOLOGY

Methods

Following the separation of heavy minerals using heavy liquids, samples were passed through a Frantz LB-1™ magnetic separator to purify zircon with the least magnetic susceptibility. Crystals were then hand picked for analysis based on criteria that optimized for their clarity, lack of cloudiness, and lack of fractures, and to provide a suite of crystals representative of the population as a whole. All zircons were abraded prior to analysis to increase concordance by removing the outer portions of the grains where much of the Pb loss and alteration take place (Krogh, 1982).

Following abrasion, photography, and final mineral selection, single zircon grains were analyzed according to methods summarized in Parrish et al. (1987). Data have been reduced and errors have been propagated using software written by J.C. Roddick; error propagation was done by numerical methods (Roddick, 1987, Parrish et al., 1987). Error ellipses on concordia diagrams are shown at the 2-sigma (95% confidence) level of uncertainty. Final errors are indicated on Table 1. Linear regressions on discordant arrays of data use a modified York (1969) method that takes into account the scatter of the points about the line (*see* a discussion in Parrish et al., 1987). Fraction letters shown on concordia diagrams are keyed to the fraction letters in Table 1.

Uranium/Lead Results

Three small (<500 g) samples of poorly indurated medium- to very coarse-grained sandstone, representing map units 1, 2 and 3, were processed for detrital zircon analysis. All samples gave reasonable yields of relatively large (+105 microns, equivalent spherical diameter), clear zircons having highly abraded, irregular, polished surfaces, and minor fractures (Fig. 4). Some grains contain clear, rod-shaped inclusions and remnants of fluid inclusions pockmark the surface of many grains. These characteristics point towards prolonged abrasion of good-quality zircons and winnowing of poor-quality zircons during sedimentary transport and suggests that the grains are far-travelled or recycled.

With few exceptions, the zircons have low U and are <2% discordant (Table 1, Fig. 5). It is difficult to determine accurate provenance ages from analyses that are more discordant as they may be indicative of zircons containing inherited cores, and thereby represent a mixed age, with an undefined lower intercept representing the source age, or they may be

indicate postcrystallization Pb loss and therefore the $^{207}Pb/^{206}Pb$ age represents a minimum age of source. Further complicating matters is the low U (and hence Pb) content of most of the grains, resulting in poor analytical precision. In addition, analytical Pb blanks are typically less than 5 pg, yet measures of total common Pb range up to 20 pg (Table 1), suggesting that much of the common Pb may reside in the small fractures and clear inclusions within the crystals, or the blanks suffer from the difficulty in laboratory handling of the single grains. The net result is to increase the proportion of common Pb relative to the already small amount of radiogenic Pb in these fractions and significantly increase errors

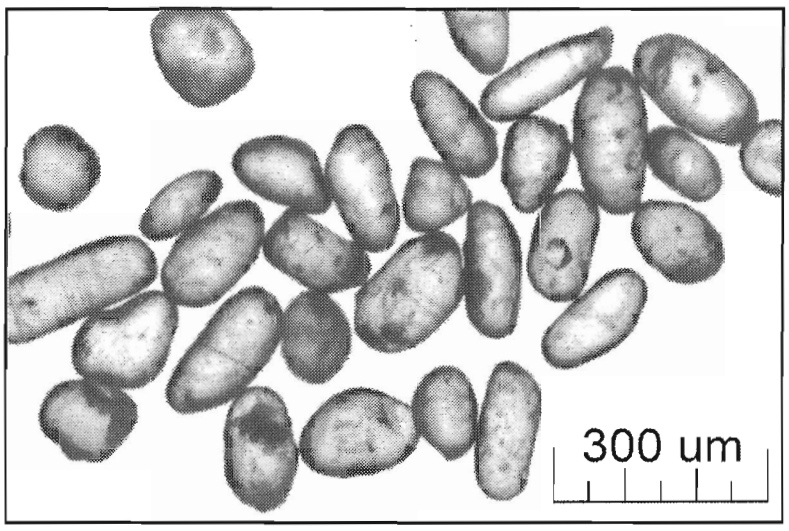

Figure 4.

Rounded and naturally abraded zircons from unit 2 sample. Zircons from units 1 and 3 show a similar morphology.

Table 1. U-Pb analytical data.

Fraction[a]	Wt.[b] µg	U ppm	Pb[c] ppm	$^{206}Pb/^{204}Pb$[d]	Pb[e] pg	$^{208}Pb/^{206}Pb$[f]	Radiogenic ratios (± 1σ, %)[f] $^{207}Pb/^{235}U$	$^{206}Pb/^{238}U$	$^{207}Pb/^{206}Pb$	$^{207}Pb/^{206}Pb$ Age (Ma)[g]	Discord.[h] %
Cap Mountain unit 1											
A1 (Z)	6	60	13	540	8	0.318	1.880 ± 0.34	0.1822 ± 0.19	0.07484 ± 0.26	1064 ± 10	-1.51
A2 (Z)	3	145	26	1529	4	0.123	1.766 ± 0.21	0.1742 ± 0.17	0.07351 ± 0.16	1028 ± 6	-0.78
A3 (Z)	2	139	24	453	8	0.068	1.842 ± 0.58	0.1785 ± 0.22	0.07485 ± 0.50	1065 ± 20	0.59
A4 (Z)	5	256	56	1720	10	0.079	2.609 ± 0.14	0.2190 ± 0.11	0.08640 ± 0.08	1347 ± 3	5.77
A6 (Z)	4	194	70	5474	3	0.343	4.081 ± 0.11	0.2913 ± 0.10	0.10162 ± 0.04	1654 ± 2	0.41
A8 (Z)	10	65	13	1089	8	0.129	2.151 ± 0.17	0.1978 ± 0.12	0.07885 ± 0.12	1168 ± 5	0.44
A9 (Z)	4	342	105	7374	3	0.098	4.358 ± 0.10	0.2978 ± 0.09	0.10613 ± 0.04	1734 ± 1	3.50
A10 (Z)	4	113	28	674	10	0.155	2.843 ± 0.22	0.2352 ± 0.13	0.08764 ± 0.16	1375 ± 6	1.03
Cap Mountain unit 2											
A1 (Z)	4	262	140	3730	7	0.156	10.612 ± 0.12	0.4700 ± 0.11	0.16375 ± 0.04	2495 ± 1	0.54
A2 (Z)	4	82	19	240	20	0.178	2.330 ± 0.58	0.2082 ± 0.27	0.08114 ± 0.47	1225 ± 18	0.48
A4 (Z)	4	75	17	185	20	0.394	1.807 ± 0.81	0.1752 ± 0.31	0.07478 ± 0.67	1063 ± 27	2.21
A5 (Z)	3	95	18	316	11	0.130	1.955 ± 0.61	0.1854 ± 0.37	0.07647 ± 0.50	1107 ± 20	1.07
A6 (Z)	2	112	27	466	7	0.110	2.827 ± 0.45	0.2354 ± 0.34	0.08712 ± 0.28	1363 ± 11	0.03
A7 (Z)	3	86	18	958	3	0.278	1.873 ± 0.36	0.1815 ± 0.30	0.07483 ± 0.23	1064 ± 9	-1.15
A8 (Z)	4	141	31	2383	3	0.081	2.584 ± 0.21	0.2224 ± 0.19	0.08427 ± 0.08	1299 ± 3	0.38
A9 (Z)	4	71	24	622	10	0.166	4.305 ± 0.36	0.3012 ± 0.32	0.10365 ± 0.16	1691 ± 6	-0.45
A10 (Z)	3	63	21	1100	4	0.237	4.051 ± 0.48	0.2927 ± 0.44	0.10037 ± 0.19	1631 ± 7	-1.68
Cap Mountain unit 3											
A1 (Z)	3	123	45	1794	5	0.123	5.782 ± 0.14	0.3437 ± 0.13	0.12199 ± 0.06	1986 ± 2	4.70
A3 (Z)	3	95	53	645	12	0.324	9.429 ± 0.28	0.4426 ± 0.25	0.15452 ± 0.11	2397 ± 4	1.71
A4 (Z)	3	81	11	388	6	0.195	1.095 ± 0.63	0.1221 ± 0.27	0.06505 ± 0.54	776 ± 22	4.55
A5 (Z)	1	106	27	298	5	0.361	2.370 ± 0.63	0.2078 ± 0.44	0.08272 ± 0.51	1263 ± 20	3.94
A6 (Z)	3	77	50	511	14	0.269	12.887 ± 0.36	0.5171 ± 0.34	0.18074 ± 0.15	2660 ± 5	-1.25
A7 (Z)	1	112	28	294	5	0.331	2.375 ± 1.53	0.2089 ± 0.65	0.08247 ± 1.30	1257 ± 50	2.95
A8 (Z)	1	170	59	414	9	0.116	5.122 ± 0.46	0.3312 ± 0.40	0.11215 ± 0.24	1835 ± 9	-0.61
A9 (Z)	1	333	75	855	5	0.159	2.347 ± 0.30	0.2108 ± 0.22	0.08074 ± 0.19	1215 ± 7	-1.62
A10 (Z)	2	110	25	840	2	0.153	2.370 ± 0.40	0.2110 ± 0.32	0.08148 ± 0.23	1233 ± 9	-0.11

[a]All zircon fractions are abraded; (Z)=Zircon, [b]Error on weight = ± 0.001 mg, [c]Radiogenic Pb, [d]Measured ratio corrected for spike and Pb fractionation of 0.09±0.03%/AMU, [e]Total common Pb on analysis corrected for fractionation and spike, of blank model Pb composition, [f]Corrected for blank and spike Pb and U and common Pb (Stacey-Kramers model Pb equal to the $^{207}Pb/^{206}Pb$ age), [g]Age error is ±2SE in Ma, [h]Discordance along a discordia to origin.

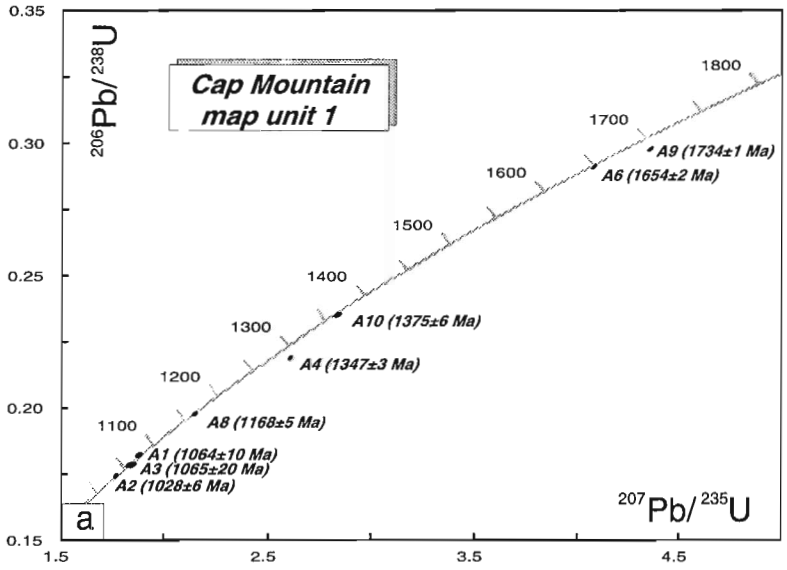

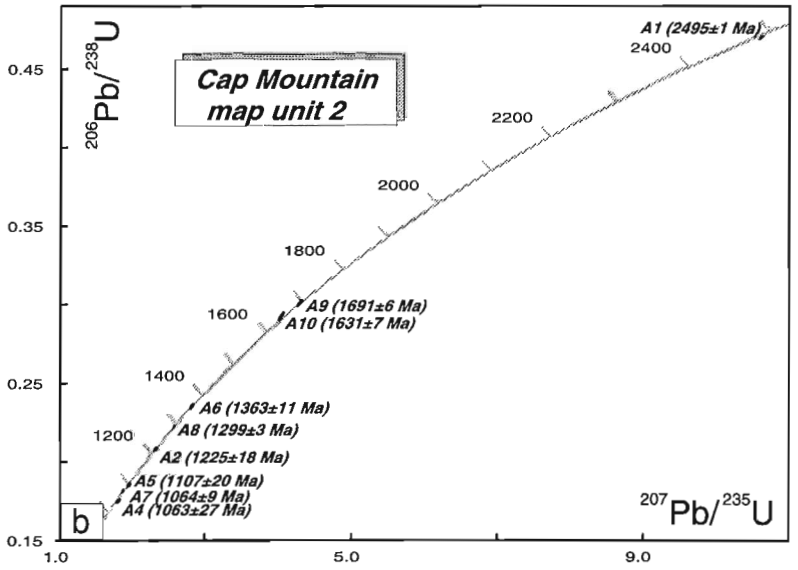

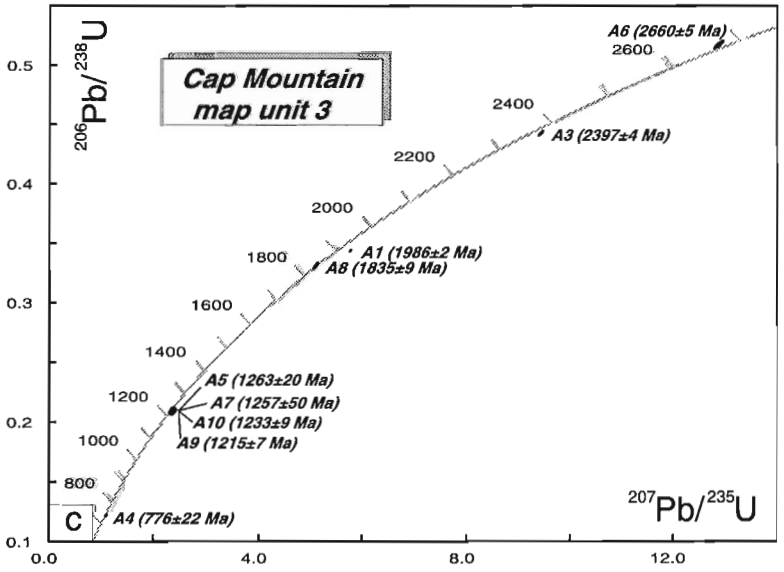

Figure 5.

***a**) Concordia diagram for unit 1. **b**) Concordia diagram for unit 2. **c**) Concordia diagram for unit 3. All errors are 2σ.*

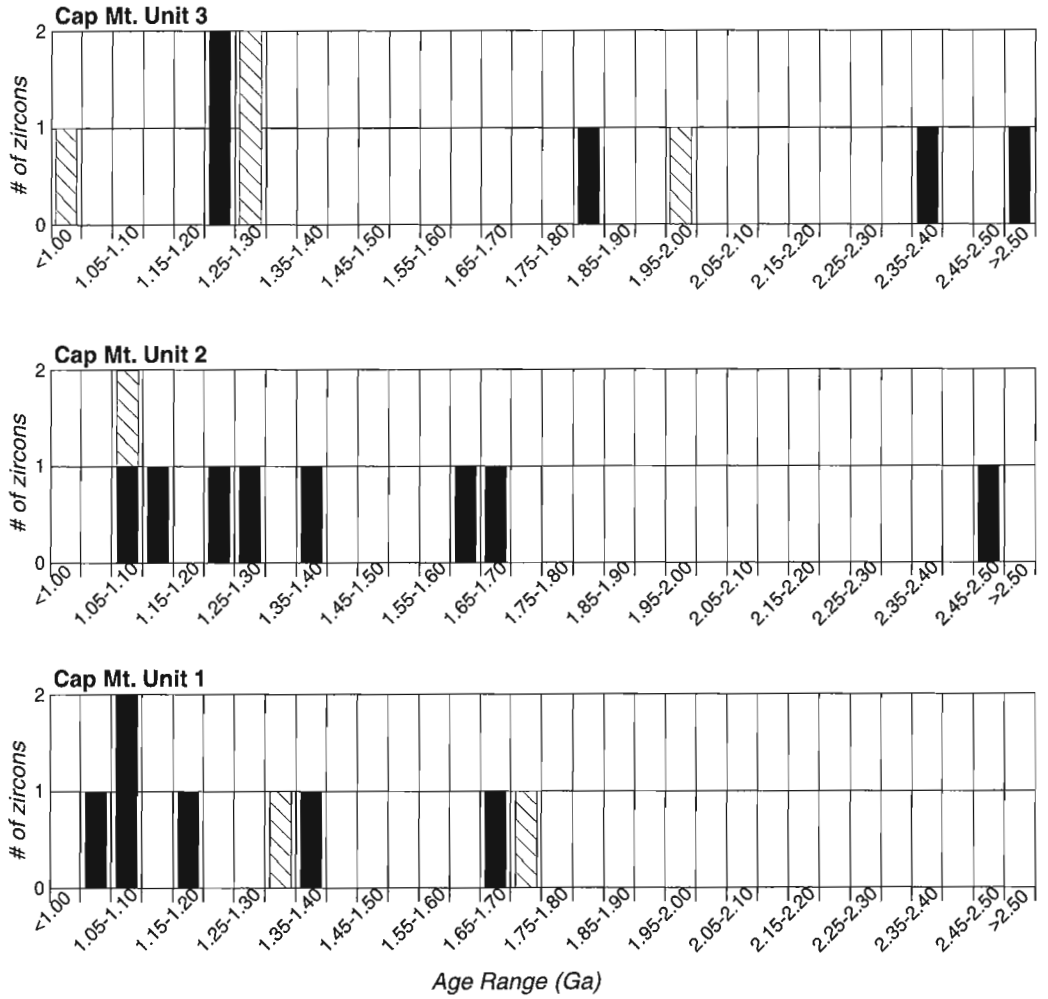

Figure 6. *Histogram (50 Ma bins) of all detrital ages. Analyses, less than 2% discordant or with $^{207}Pb/^{206}Pb$ age errors less than 20 Ma, are shown by solid bars, poor quality analyses by striped bars.*

associated with these analyses to the ± 20 Ma range. In spite of such complications, analyses that are less than 2% discordant or have larger than anticipated errors, should still be able to give reasonable approximations of the provenance age.

PROVENANCE

Disregarding analyses greater than 2% discordant or with $^{207}Pb/^{206}Pb$ analytical errors greater than 20 Ma, Figure 6 shows that the combined data for all units fall into three main groupings: 1) 1.4 Ga to 1.0 Ga, 2) 1.9 Ga to 1.6 Ga, and 3) 2.7 Ga to 2.4 Ga (Table 1), with the bulk of the analyses falling in group 1. With fewer than 10 analyses per unit, a confident (let alone statistical) measure of the diversity in zircon provenance ages cannot be provided. In a broad sense, there appears to be a shift from young ages (1.4 Ga to 1.0 Ga) in unit 1 to a more evenly mixed age spectrum in units 2 and 3. The older ages suggest a source from within Paleoproterozoic collisional belts. These include the 1.89–1.84 Ga Wopmay Orogen (Hoffman and Bowring, 1984), the 2.10–1.92 Ga Taltson Arc (Bostock and van Breemen, 1994), the 1.98–1.90 Ga Ksituan Arc, 2.0–2.4 Ga Buffalo Head Terrane (Villeneuve et al., 1993), or the 1.85 Ga Fort Simpson Arc (Villeneuve et al., 1991), all located in the northwestern Canadian Shield (Ross et al., 1991). Provenance ages of the Archean (group 3) zircons are consistent with derivation from the Archean Slave Province (Villeneuve et al., 1997).

The source of the 1.4 Ga to 1.0 Ga zircons is more enigmatic. Studies by Rainbird et al. (1992, 1996b, 1997) proposed that 'Grenville-age' detrital zircons in Neoproterozoic sequence B quartz-arenites were delivered to the northwest margin of the craton by a braided river system that drained the rising Grenville Orogen of eastern north America. The ages overlap with dated orogenic and anorogenic plutonic suites of the Grenville Province of Ontario and Quebec. Furthermore, the presence of such material appears to be a characteristic of sequence B strata, as shown by detrital zircon chronology carried out on samples from hydrocarbon exploration well H-55 (Rainbird et al., 1996b; Fig. 1), the Shaler Supergroup, and Mackenzie Mountains Supergroup (Rainbird et al., 1997, 1992).

An alternative possibility is presented by the presence of ca. 1.1 Ga to 1.6 Ga zircons in a granite clast from the diatreme at Coates Lake in the southern Mackenzie Mountains (Jefferson and Parrish, 1989). As such, there is a possibility that 'Grenville-age' basement may be present beneath at least part of the Mackenzie Mountains, although a proximal source would be at odds with the maturity of the detrital zircons, and a western source would not account for the early Proterozoic and Archean zircons. Intra-Cordilleran 'Grenville-age', xenocrystic zircons also occur in diatremes at Columbia Icefields and the Elk River field at Fernie in southern British Columbia (Parrish and Reichenbach, 1991). It should be noted that, unlike the case with the granite xenolith in Coates Lake diatreme, the xenocrystic zircons within the British Columbia diatremes could potentially come from entrained (sequence B?) sedimentary material.

One of the most intriguing avenues for follow-up study is presented by a relatively low-quality zircon analysis with a $^{207}Pb/^{206}Pb$ age of 776 ± 22 Ma (Cap Mountain unit 3, fraction A4, Table 1). Although it is 4.5% discordant and has a large error, this age agrees with estimates for the time of onset of Neoproterozoic sequence C (Windermere Supergroup) sedimentation (Ross and Villeneuve, 1997), displayed by an age of 777.7 +2.5/-1.8 Ma on a quartz diorite plug that intrudes into, and is truncated within, the Little Dal Group of the uppermost Mackenzie Mountains Supergroup (Jefferson and Parrish, 1989). A poorly defined detrital zircon age of 755 ± 18 Ma in the Sayunei Formation of the lowermost Windermere Supergroup provides a maximum age for the onset of sedimentation within sequence C (Ross and Villeneuve, 1997). Although the age of fraction A4 in unit 3 age is poorly defined, unit 3 at Cap Mountain may provide the best chance for placing tighter constraints on the age of onset of sequence C sedimentation. Furthermore, the presence of such zircons in the strata would suggest that at least some detrital material in Cap Mountain sedimentary rocks is more locally derived, given that the only known source for ca. 0.78 Ga zircons is intra-Cordilleran.

CORRELATION IMPLICATIONS

The recognition that the Cap Mountain section belongs in sequence B and is broadly correlative with Mackenzie Mountains and Shaler supergroups constitutes a major advance in our understanding of the correlation of these strata. However, within sequence B specific unit-to-unit correlations are unresolved, and the section could fall at the base, in the middle, or high in sequence B depending on which arguments and observations are applied. Three possibilities are outlined below.

1. The section may correlate with the Mackenzie Mountains Supergroup interval comprising Tsezotene Formation and Katherine Group. This conclusion would be based on the observation by Aitken et al. (1973a) that unit 1 is lithologically similar to the Tsezotene Formation, even though this correlation was rejected by Aitken et al. because they saw no lithological correspondence at the level of the overlying Katherine Group. This possibility is nonetheless viable if there exists a facies transition between the Mackenzie Mountains and Cap Mountain at the level of the Katherine Group.
2. Despite the similarities between unit 1 and Tsezotene Formation, Aitken et al. (1973a.) concluded that no Mackenzie Mountains Supergroup formation was represented in the Cap Mountain section. In such a case, the entire section may be older than all Proterozoic units that outcrop in the Mackenzie Mountains (older than unit H1 mapped by Aitken et al. (1982)). This possibility is viable because Mackenzie Mountains Supergroup strata older than H1 have been identified on seismic data by Cook and MacLean (1996) underlying the Imperial Anticline west of Norman Wells. The Escape Rapids Formation at the base of the Shaler Supergroup, about 1 km thick on Coppermine Homocline, is also considered older than H1 (Rainbird et al., 1996a).
3. The discovery of *Trachyhystrichosphaera* in the G-52 well raises the possibility that the section occurs high in sequence B. Although *Trachyhystrichosphaera* is long-ranging worldwide, in northern Canada it has only been previously identified in the Wynniatt Formation in the upper part of the Shaler Supergroup on Victoria Island and the possibility of G-52 correlating with Wynniatt must be entertained. This, combined with correlation of G-52 with unit 1 on Cap Mountain (Aitken and Pugh, 1984) raises the interesting possibility that the entire Cap Mountain section occurs very high in the Mackenzie Mountains Supergroup sequence. Counterparts in the Mackenzie Mountains Supergroup would include thick Little Dal Group carbonates, and once more a major facies change would be implied.

Interestingly, each of the above correlation rationales requires a major facies transition between Cap Mountain and potential correlatives. This is permissive considering that Cap Mountain is located cratonward, in a paleogeographic sense, from the other localities (cf. Rainbird et al., 1996a). The specific correlation within sequence B remains unresolved.

The Grenvillian zircons reported here provide further support for a pan-continental river system draining the foreland of Grenville Orogen (Rainbird et al., 1992, 1997). It is noteworthy that map unit 3 has no 1.2–1.0 Ga zircons, even though it must fall in sequence B because it overlies units 1 and 2 and underlies the Lone Land Formation. A similar situation is found in the Pinguicula Group (unit D), Wernecke Mountains, whereby 10 separate, single-grain analyses did not yield in any zircons in the age range 1.25–1.0 Ga (Rainbird et al., 1997). As such, the absence of Grenvillian zircons does not negate a sequence B age. It should be pointed out that the data from Cap Mountain does not prohibit correlation with sequence C stratigraphy. However, a number of factors argue against such an interpretation. The structure and composition of the Cap Mountain strata indicate deposition in a shallow-water, stable craton platform environment which is a uncharacteristic of sequence C. Additionally, detrital studies of sequence C stratigraphy uniformly indicate derivation from basement terranes of the northwest Canadian Shield (Ross, 1998). Finally, *Trachyhystrichosphaera* appears to be characteristic of sequence B stratigraphy and its equivalents elsewhere.

CONCLUSIONS

The presence of concordant 'Grenville-age' detrital zircons (1.6–1.0 Ga) from the lower two units of the Cap Mountain Proterozoic section establishes that the entire section is younger than 1.03 Ga and must be reassigned from sequence A to sequence B. As well, it reinforces the model of Rainbird et al. (1992, 1997) that eroded detritus from the Grenville Province was shed over a wide area of northwestern Canada. This constitutes a significant advance in our understanding of the age of these strata and establishes that the section relates in some fashion to the Neoproterozoic Mackenzie Mountains Supergroup of the Cordillera and the Shaler Supergroup of Amudsen Basin (sequence B of Young et al., 1997). This greatly constrains correlations and expands the area of known and interpreted occurrence of sequence B strata (MacLean and Cook, 1997). Unit-to-unit correlations within sequence B, however, remain equivocal.

ACKNOWLEDGMENTS

The authors would like to thank the laboratory staff of the Geochronology Laboratory at the GSC, Diane Bellerive, Jack MacRae, and Klaus Santowski for their always able assistance in analyzing the zircons. Vicki McNicoll and Reg Thériault are thanked for a thoughtful review.

REFERENCES

Aitken, J.D. and Pugh, D.C.
1984: The Fort Norman and Leith Ridge structures: major, buried, pre-Cambrian features underlying Franklin Mountains and Great Bear and Mackenzie plains; Bulletin of Canadian Petroleum Geology, v. 32, p. 139-146.

Aitken J.D., Cook, D.G., and Yorath, C.J.
1982: Upper Ramparts River (106 G) and Sans Sault Rapids (106 H) map areas, District of Mackenzie; Geological Survey of Canada, Memoir 388, 48 p.

Aitken J.D., Macqueen, R.W., and Foscolos, A.E.
1973a: A Proterozoic sedimentary succession with traces of copper mineralization, Cap Mountain, southern Franklin Mountains, District of Mackenzie (95 O); *in* Current Research, Part A, Geological Survey of Canada, Paper 73-A, p. 243-246.

Aitken J.D., Macqueen, R.W., and Usher, J.L.
1973b: Reconnaissance studies of Proterozoic and Cambrian stratigraphy, lower Mackenzie River area (Operation Norman), District of Mackenzie; Geological Survey of Canada, Paper 73-9, 178p.

Bostock, H.H. and van Breemen, O.
1994: Ages of detrital and metamorphic zircons and monazites from pre-Taltson magmatic zone basin at the western margin of the Rae Province; Canadian Journal of Earth Sciences, v. 31, p.1353-1364.

Butterfield, N. J., Knoll, A. H., and Swett, K.
1994: Paleobiology of the Neoproterozoic Svanbergfjellet Formation, Spitsbergen; Fossils & Strata 34, 84 p.

Cook, D.G. and MacLean, B.C.
1996: Imperial Anticline, a fault-bend fold with fault surfaces bedding-parallel in both ramp and flat; *in* (comp.) F. Cook and P. Erdmer; 1996 Slave–Northern Cordillera Lithospheric Evolution (SNORCLE) Transect and Cordilleran Tectonics Workshop Meeting (March 1-3), University of Calgary; Lithoprobe Report No. 50, p. 184-186

Douglas, R.J.W. and Norris, D.K.
1963: Dahadinni and Wrigley map-areas, District of Mackenzie, Northwest Territories 95 N, O; Geological Survey of Canada, Paper 62-33.

Douglas, R.J.W. And Norris, D.K. (cont.)
1974: Geology, Wrigley (NTS 95 O), District of Mackenzie; Geological Survey of Canada Map 1373A, scale 1:250 000.

Hoffman, P.F. and Bowring, S.A.
1984: Short-lived 1.9 Ga continental margin and its destruction, Wopmay orogen, northwest Canada; Geology, v.12, p. 68-72.

Hoffman, H.J. and Rainbird, R.H.
1995: Carbonaceous megafossils from Neoproterozoic Shaler Supergroup, Victoria Island, Arctic Canada, Paleontology, v. 37, p. 721-731.

Hume, G.S.
1924: Mackenzie River area, District of Mackenzie, Northwest Territories; Geological Survey of Canada, Summary Report, 1919, pt. C, p. 1-7.

Jefferson, C.W. and Parrish, R.R.
1989: Late Proterozoic stratigraphy, U-Pb ages and rift tectonics, Mackenzie Mountains, northwestern Canada, Canadian Journal of Earth Sciences, v. 26, p. 1784-1801.

Krogh, T.E.
1982: Improved accuracy of U-Pb zircon ages by the creation of more concordant systems using an air abrasion technique; Geochimica et Cosmochimica Acta, v. 46, p. 637-649.

LeCheminant, A. and Heaman, L.
1989: Mackenzie igneous events, Canada: Middle Proterozoic hotspot magmatism associated with ocean opening; Earth and Planetary Science Letters, v. 96, p. 637-649.

MacLean, B.C. and Cook, D.G.
1997: Subsurface and surface distribution of Proterozoic units, northwestern NWT: A Cambrian sub-crop map; Geological Survey of Canada, Open File 3502, scale.

Meijer Drees, N. C.
1975: Geology of the Lower Paleozoic formations in the subsurface of the Fort Simpson area, District of Mackenzie, N.W.T; Geological Survey of Canada, Paper 74-40.

Parrish, R.R. and Reichenbach, I.
1991: Age of xenocrystic zircons from diatremes of western Canada: Canadian Journal of Earth Sciences, v. 28, pp. 1232-1238.

Parrish, R.R., Roddick, J.C., Loveridge, W.D. and Sullivan, R.W.
1987: Uranium-lead analytical techniques at the Geochronology Laboratory, Geological Survey of Canada; *in* Radiogenic Age and Isotopic Studies: Report 1; Geological Survey of Canada, Paper 87-2, p .3-7.

Rainbird, R.H., Heaman, L.M. and Young, G.M.
1992: Sampling Laurentia: Detrital zircon geochronology offers evidence for an extensive Neoproterozoic river system originating from the Grenville orogen; Geology, v. 20, p. 351-354.

Rainbird, R.H., Jefferson, C.W., and Young, G.M.
1996a: The early Neoproterozoic sedimentary succession B of northwestern Laurentia: correlations and paleogeographic significance; Geological Society of America Bulletin, v. 108, p. 454-470.

Rainbird, R.H., McNicoll, V.J., Theriault, R.J., Heaman, L.M, Abbott, J.G., Long, D.G.F., and Thorkelson, D.J.
1997: Pan-continental river system draining Grenville Orogen recorded by U-Pb and Sm-Nd geochronology of Neoproterozoic quartzarenites and mudrocks, northwestern Canada; The Journal of Geology, v.105, p. 1-17.

Rainbird, R.H., Villeneuve, M.E., Cook, D.G., and MacLean, B.C.
1996b: Detrital zircon ages from two wells in the Northwest Territories: implications for the correlation and provenance of Proterozoic subsurface strata; *in* Current Research 1996-B; Geological Survey of Canada, p.29-38.

Roddick, J.C.
1987: Generalized numerical error analysis with application to geochronology and thermodynamics; Geochimica et Cosmochimica Acta, v. 51, p.359-362.

Ross, G.M.
1998: Detrital zircon geochronology of 'sequence C' grits, Dorsey Terrane (southern Yukon): provenance and stratigraphic correlation; *in* Radiogenic Age and Isotopic Studies: Report 11; Geological Survey of Canada Current Research 1998-F.

Ross, G.M. and Kerans, C.
1989: Geology, Hornby Bay and Dismal Lakes groups, Coppermine Homocline, District of Mackenzie, Northwest Territories; Geological Survey of Canada Map 1663A, scale 1:250 000.

Ross, G.M and Villeneuve, M.E.
1997: U-Pb Geochronology of stranger stones in Neoproterozoic diamictites, Canadian Cordillera: implications for provenance and ages of deposition; *in* Radiogenic Age and Isotopic Studies: Report 10; Geological Survey of Canada Current Research 1997-F, p. 141-155.

Ross, G. M., Parrish, R. R., Villeneuve, M. E., and Bowring, S. A.
1991: Geophysics and geochronology of the crystalline basement of the Alberta Basin, western Canada; Canadian Journal of Earth Sciences, v. 28, p. 512-522.

Villeneuve, M.E., Henderson, J.R., Hrabi, R.B., Jackson, V.A., and Relf, C.
1997: 2.70–2.58 Ga plutonism and volcanism in the Slave Province, District of Mackenzie, Northwest Territories; *in* Radiogenic Age and Isotopic Studies: Report 10; Geological Survey of Canada, Current Research 1997-F, p. 37-60.

Villeneuve, M. E., Ross, G. M., Theriault, R. J., Miles, W., Parrish, R. R., and Broome, J.
1993: Geophysical subdivision, U-Pb geochronology and Sm-Nd isotope geochemistry of the crystalline basement of the western Canada sedimentary basin, Alberta and northeastern British Columbia; Geological Survey of Canada, Bulletin 447, 86 p.

Villeneuve, M.E., Thériault, R.J., and Ross, G.M.
1991: U-Pb and Sm-Nd signature of two subsurface granites from the Fort Simpson magnetic high, Northwest Canada; Canadian Journal of Earth Sciences, v. 28, p.1003-1008.

York, D.
1969: Least squares fitting of a straight line with correlated errors; Earth and Planetary Science Letters, v. 5, p. 320-324.

Young, G.M., Jefferson, C.W., Delaney, G.D., and Yeo, G.M.
1979: Middle and Upper Proterozoic evolution of the northern Canadian Cordillera and Shield; Geology, v. 7, p.125-128.

– 14 –

New U-Pb ages from the Teslin area, southern Yukon, and their bearing on terrane evolution in the northern Cordillera

S.P. Gordey[1], V.J. McNicoll[2], and J.K. Mortensen[3]

Gordey, S.P., McNicoll, V.J., and Mortensen, J.K., 1998: New U-Pb ages from the Teslin area, southern Yukon, and their bearing on terrane evolution in the northern Cordillera; in *Radiogenic Age and Isotopic Studies: Report 11; Geological Survey of Canada, Current Research 1998-F, p. 129-148.*

Abstract: Highlights from a regional U-Pb, K-Ar, and $^{40}Ar/^{39}Ar$ dating program in southern Yukon include ages from metaplutonic rocks of Yukon–Tanana terrane (350–340 Ma), from peridotite of the Cache Creek terrane (ca. 245 Ma), from conglomerate clasts of the Laberge Group of Stikine terrane (229–204 Ma), and from detrital zircons (1.76–3.29 Ga) from Cassiar terrane. These, as well as ages from crosscutting plutonic suites of Early Jurassic (195–184 Ma), mid-Jurassic (ca. 176 Ma), Early Cretaceous (ca. 123 Ma), mid-Cretaceous (ca. 109 Ma) and Late Cretaceous (ca. 74 Ma) age place limits on the identification, timing of internal deformation, and age of assembly of various terranes in the northern Cordillera.

Résumé : Un programme de datation U-Pb, K-Ar et $^{40}Ar/^{39}Ar$ d'échelle régionale dans le sud du Yukon donne des âges de 350–340 Ma pour des roches plutoniques métamorphisées du terrane de Yukon-Tanana, d'environ 245 Ma pour de la péridotite du terrane de Cache Creek, de 229–204 Ma pour des clastes provenant d'un conglomérat du Groupe de Laberge du terrane de Stikine, et de 3,29–1,76 Ga pour des zircons détritiques du terrane de Cassiar. Ces âges ainsi que ceux des suites plutoniques intrusives du Jurassique précoce (195–184 Ma), du Jurassique moyen (environ 176 Ma), du Crétacé précoce (environ 123 Ma), du Crétacé moyen (environ 109 Ma) et du Crétacé tardif (environ 74 Ma) fixent des limites quant à l'identification, la chronologie de la déformation interne et l'âge du regroupement des divers terranes de la Cordillère septentrionale.

[1] Geological Survey of Canada, 101-605 Robson Street, Vancouver, British Columbia V6B 5J3
[2] Geological Survey of Canada, 601 Booth Street, Ottawa, Ontario K1A 0E8
[3] Department of Earth and Ocean Sciences, University of British Columbia, Vancouver, British Columbia V6T 1Z4

INTRODUCTION

The Intermontane and Omineca belts of the northern Cordillera are underlain by numerous terranes that record distinctive depositional, deformation, and accretion histories (Wheeler et al., 1991). The Teslin area of southern Yukon encompasses many of these terranes as well as several suites of post-tectonic plutons (Fig. 1, 2). The composition, metamorphism, and structural styles of these terranes and plutons have been recently documented through a regional geological mapping program that utilized excellent conodont and radiolarian fossil control (Gordey, 1991, 1992; Gordey and Stevens, 1994a, b; Cordey et al., 1991) as well as local detailed mapping and structural analysis (Stevens, 1991, 1992, 1993; Stevens and Erdmer, 1993; Stevens et al., 1993).

This report presents 15 new U-Pb ages and one new $^{40}Ar/^{39}Ar$ age from a regional dating program in the Teslin area and discusses the constraints these data place on terrane identification, ages of deformation, and timing of assembly. In addition, previously obtained K-Ar and $^{40}Ar/^{39}Ar$ ages from the Teslin area are summarized.

REGIONAL GEOLOGY

Terranes

Six different terranes are represented in the Teslin area, including Cassiar, Slide Mountain, Yukon–Tanana (Kootenay), Cache Creek, Quesnel, and Stikine terranes (Fig. 1, 2). Descriptions have been presented in greater detail in Gordey and Stevens (1994a, b).

Cassiar terrane

The northeast part of the area (CA, Fig. 2) is underlain by shallow-dipping quartz arenite and quartz-feldspar grit, phyllite, chert, chert-pebble conglomerate, andesite, quartzite, and carbonate. These strata are disrupted by weak to locally intense bedding-parallel mylonitization and steep normal faults. Although the nature of contacts is obscured by deformation, primary sedimentary features are preserved in many places and metamorphism is greenschist or sub-greenshist grade. The only fossiliferous unit is a regional limestone/quartz arenite marker containing corals of probable

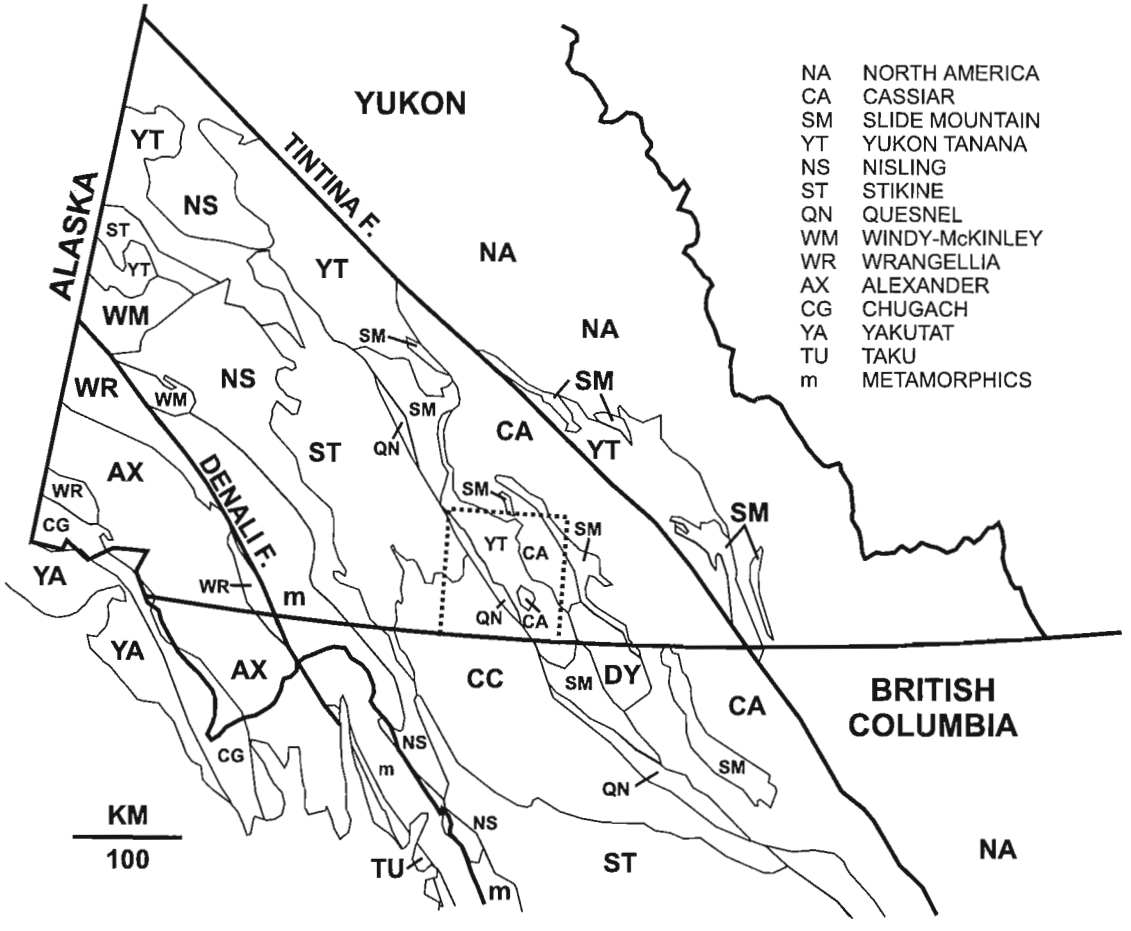

Figure 1. *Terranes in southern Yukon and regional setting of the Teslin map area (outlined by dotted line).*

Carboniferous age (Gordey and Stevens, 1994b, unit Ml). West and northwest of Thirtymile Lake, this unit changes facies to discontinuous limestone lenses within a matrix of calcareous graphitic phyllite, graphitic quartzite, and siliceous muscovite phyllite. Thick (200+(?) m), extensive exposures of aphyric massive andesite/basalt flows(?) and tuffaceous volcaniclastic rocks occur in the Englishmans Range south and northwest of Mount McCleery, and at the same latitude on the west side of the Wolf River. Similar volcanic rocks form the structural window of Cassiar terrane strata north of Nisutlin Bay.

All the above-mentioned strata were assigned to the Dorsey and Slide Mountain terranes by Wheeler et al. (1991) (described in Monger et al., 1991). However, components of the stratigraphic succession have lithological counterparts in the Proterozoic Ingenika, Early Paleozoic Road River(?), and Devono-Mississippian Earn Groups that typify North American margin strata (i.e. Cassiar terrane, Fig. 1; Fig. 3 of Gordey, 1992). The regional carbonate unit locally contains as much as 200 m of fine- to medium-grained quartz arenite, indicating a continental source. However, the provisional interpretation of all of these strata as Cassiar terrane is not without contention, particularly for the volcanic-dominated units. Harms and Stevens (1996) have suggested there are lithological and faunal similarities to the Harper Ranch and Okanagan subterranes that form the basement of Quesnellia in southern British Columbia.

Slide Mountain terrane

Rocks of the late Paleozoic Slide Mountain terrane include isolated exposures of variably serpentinized peridotite thrust above Cassiar terrane in the northeast corner of the Teslin area (SM, Fig. 2). Regionally, the terrane also includes mafic volcanic rocks, ribbon chert, and carbonate.

Yukon–Tanana (Kootenay) terrane

The Yukon–Tanana terrane (Mortensen, 1992; Kootenay terrane of Wheeler and McFeely, 1991; Teslin suture zone of Hansen et al., 1989 and Stevens et al., 1993; Teslin tectonic zone of Stevens and Erdmer, 1996) trends northwest across the central part of the map area (YT, Fig. 2). Northwest of Canol Road it consists of metamorphosed and ductile-deformed S, L-S, and L tectonites derived from sedimentary, volcanic, and plutonic rocks that form three lithotectonic assemblages (Stevens, 1993). The oldest consists of Early Mississippian or older metasedimentary rocks including quartz-muscovite±chlorite schist, muscovite-chlorite quartzite, muscovite-graphite phyllite, calcareous schist, and minor marble. Intruding these strata are foliated hornblende-bearing metagranitoids of Early Mississippian age. The last assemblage consists of mafic schist, greenstone, amphibolite, and metagabbro of probable late Paleozoic age. Inclusion of this last assemblage within the Slide Mountain terrane is also possible. Contacts between rock units are dominantly structural with rare preservation of primary depositional and intrusive relationships. Metamorphic grade is greenschist to amphibolite facies (Stevens, 1991, 1992, 1993; Stevens and Erdmer, 1993).

Between Canol Road and Nisutlin River the terrane comprises biotite quartzite to semi-schist, hornblende gneiss, biotite±hornblende metaplutonic rocks, and mylonite of greenschist to lower amphibolite facies (Gareau, 1992). Immediately east of Nisutlin Bay variably sheared originally hornblende(?)-bearing metaplutonic rocks with minor amounts of amphibole-rich schist (metavolcanic?) are dominant.

Cache Creek terrane

The Cache Creek terrane occurs southwest of Teslin valley where four main fault-bounded assemblages are recognized. Late Paleozoic (mostly(?) Permian) massive to locally crinoid-bearing carbonate (CC1, Fig. 2) occurs near Jakes Corner. The second assemblage (CC2) comprises Late Paleozoic volcanic rocks that have been subdivided into two units (*see* Gordey, 1992) of uncertain original stratigraphic relationship. One unit comprises massive, greyish-green to dark grey, aphyric andesite/basalt in which spherulites are common and pillows are locally well developed. The second unit consists of massive, grey-green to chrome-green, highly fractured and poorly indurated rocks of probable fragmental volcanic origin. This unit is distinguished by included blocks of bedded chert and carbonate from fist size to up to 30 m across.

Complexly deformed, extensive ribbon chert and greywacke with minor shale (Gordey, 1992) form the third assemblage (CC3) in the southwest part of the map area. The greywacke is well indurated, medium grey and fine to coarse grained. Radiolaria recovered from ribbon chert and argillite indicate ages as old as Middle Triassic (Ladinian) and as young as Early Jurassic (Pliensbachian or early Toarcian) (Cordey et al., 1991).

Ultramafic rocks of the Cache Creek terrane (CC4, Fig. 1) consist of massive to foliated peridotite and variably serpentinized equivalents. The foliation is defined by concentrations of large pyroxene crystals up to a few centimetres thick within a matrix of finer grained olivine and pyroxene. Irregular shaped, metre-sized masses of dunite with gradational boundaries are found locally. Ultramafic rocks in the Teslin area have the mineralogical and structural hallmarks of mantle tectonites as described for the ultramafic bodies near Atlin, British Columbia, by Ash and Arksey (1990).

Quesnel terrane

The Quesnel terrane forms a fault-bounded panel east of Teslin Lake that includes as much as 600(?) m of weakly folded clastic and minor volcanic rocks and chert (QN, Fig 2). These are intruded locally by dunite and highly altered diorite (Gordey, 1992).

The most common rock types are siliceous argillite, siltstone, and sandstone. The sandstone, in members from 1 m to at least 50 m thick, contains quartz, abundant feldspar, and as much as 10% fresh, in places euhedral, augite (±hornblende?). Many of the clastic rocks may represent primary or resedimented pyroclastic deposits. Volcanic breccia,

consisting of augite±feldspar porphyry blocks up to 20 cm across, occurs locally, as do augite porphyry dykes and sills up to 10 m thick. Thick-bedded chert that occurs low in the stratigraphic succession has yielded Upper Triassic (Norian) conodonts.

Stikine terrane

Early Jurassic clastic and minor volcanic strata of Stikine terrane (ST, Fig. 2) outcrop in the northwest part of the area. The sedimentary rocks (Laberge Group) consist predominantly of sandstone, lesser argillite, and minor conglomerate. The

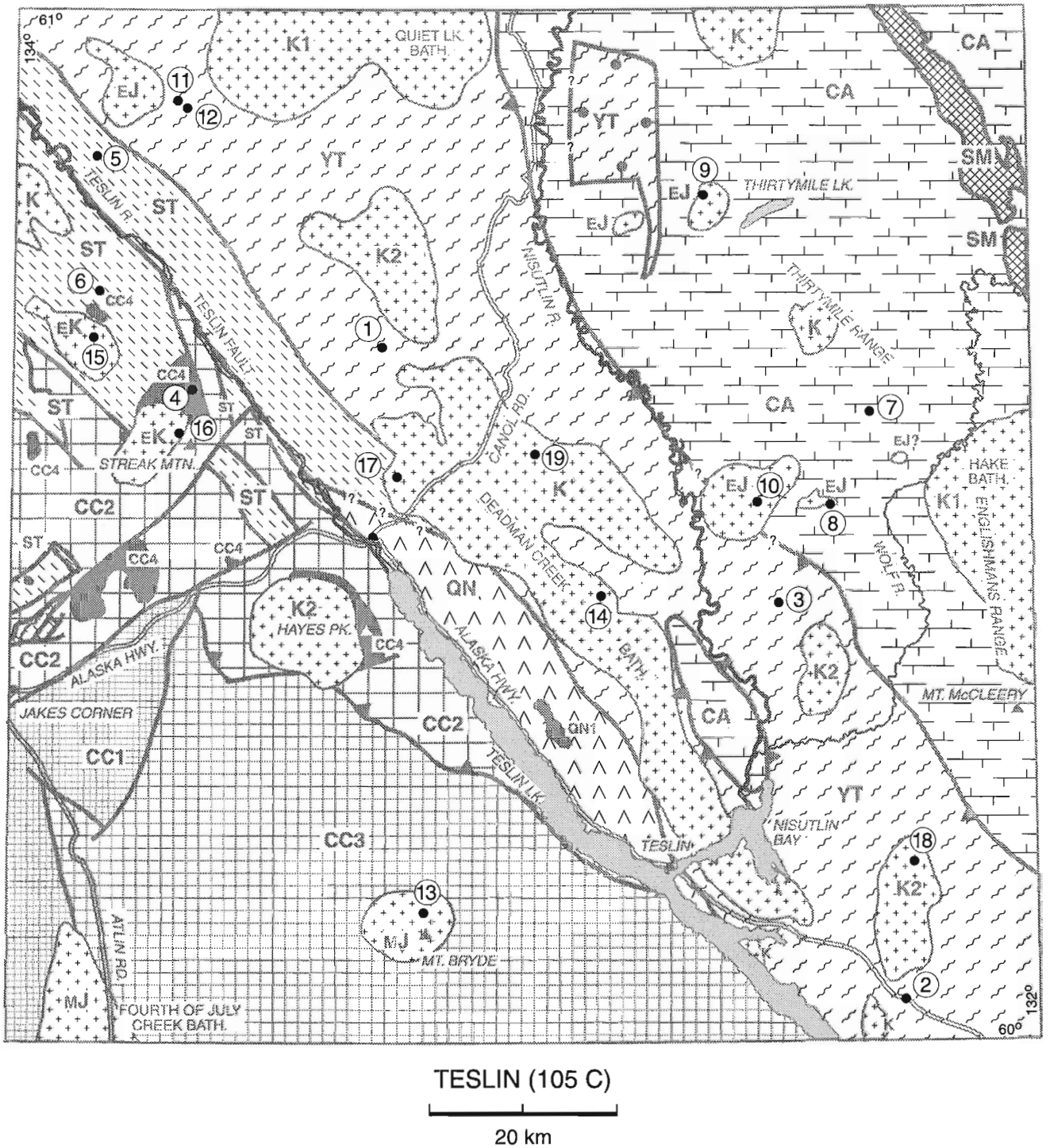

TESLIN (105 C)

20 km

Figure 2. *Terranes and post-tectonic intrusive suites in the Teslin map area. Sample sites discussed in text are indicated, and are referenced in tables 1 and 2 and Appendix 1.*

sandstone occurs as individual thin to thick beds sharply bounded by argillite, as well as in uniformly fine- to medium-grained packets from 10 m to as much as 150 m thick. The sands are composed mostly of plagioclase, lesser monocrystalline quartz and minor orthoclase, hornblende, pyroxene, and rock fragments, the last including chert(?) and aphanitic volcanic rocks. Conglomerate members from a few metres to up to 200 m thick contain pebble- to cobble-sized clasts of limestone, granitic rock, feldspar porphyry, green to grey-green volcanic(?) rock and argillite(?), chert, and dark grey argillite. Several hundred metres of massive carbonate of Late Triassic (Norian) age (Lewes River Group) occur within fault bounded panels 8.9 km and 14.7 km north-northeast of Jakes Corner (unit uTrl of Gordey and Stevens, 1994b).

Dips of bedding of the clastic rocks range from shallow to up to 70°, and reversals of dip directions indicate northwest-trending upright folds with wavelengths of a kilometre or more.

Post-tectonic plutonic suites

A tentative subdivision of plutonic rocks into three main suites comprising five main types (Fig. 2) is based on mineralogy and age (*see* discussion for comments on age).

Early Jurassic plutons (EJ) intrude the Yukon–Tanana and Cassiar terranes and consist of unfoliated, medium-grained monzodiorite and quartz monzodiorite, and minor hornblendite. Hornblende (up to 25%) is the dominant mafic mineral in the monzodiorites. It is rarely accompanied by up to a few percent biotite. Locally, the weak alignment of hornblende is interpreted as an igneous flow fabric or intrusion-related shear fabric.

The Middle Jurassic suite (MJ) intrudes the Cache Creek terrane and is represented by the Mt. Bryde pluton composed of unfoliated, medium- to coarse-grained monzodiorite and quartz monzodiorite, and minor hornblendite. The monzodiorite commonly contains about 20%, but locally up to 40% hornblende, and occurs at the east and west margins of the body. The quartz monzodiorite is characterized by twice the amount of hornblende as biotite with mafic minerals in total ranging up to about 15%. Inclusions, veins, and dykes in the pluton are rare. The closest exposures of country rock to the pluton, about 150 m distant, display minimal contact metamorphism.

Plutons of Cretaceous age are of three main types. The first type, Early Cretaceous in age (EK, Fig. 2), is dominated by medium-grained hornblende-biotite quartz monzonite and quartz monzodiorite. Hornblende and biotite occur in subequal proportions in amounts totalling up to 25%. The second main type (K1), of mid-Cretaceous age, contains biotite as the sole mafic mineral and is exemplified by the Hake and Quiet Lake batholiths (Fig. 2). The former, underlying the Englishmans Range, consists of homogeneous coarse-grained granite distinguished by up to 40% pink K-feldspar crystals to about 2 cm long, and by about 5% small fresh biotite flakes. The Quiet Lake batholith, the large body at the north margin of the map area, comprises homogeneous medium-grained biotite granite with up to 15% biotite, and local phenocrysts of pinkish K-feldspar constituting up to 10–15%. The third type (K2), also of mid-Cretaceous age, consists of unfoliated, medium- to coarse-grained, leucocratic, biotite granite. The

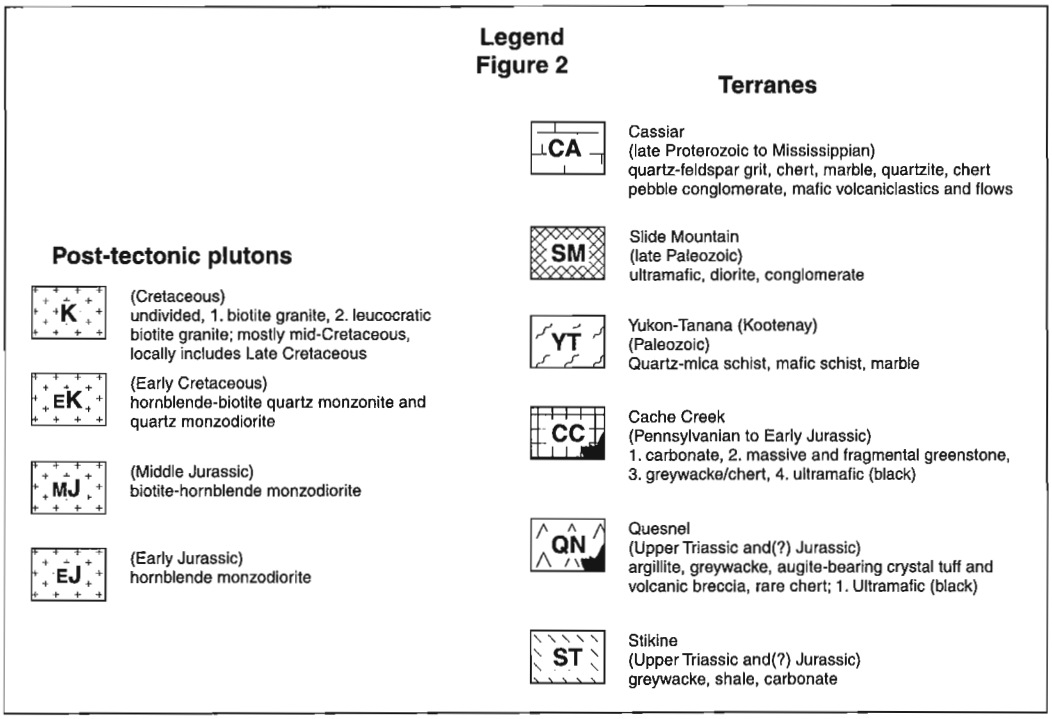

biotite occurs as small flakes, constituting up to 5% of the rock. Plutons of this suite are massive and homogeneous as typified by the bodies 25 km to the east and to the northeast of the Teslin area. Compositionally they resemble the Hake batholith, but lack the distinctive pink K-feldspar of that body. A Late Cretaceous age has been determined (*see* below) on granitic rocks otherwise resembling the mid-Cretaceous suite (K2).

ANALYTICAL METHODS

A summary of U-Pb, K-Ar, and $^{40}Ar/^{39}Ar$ age data from the Teslin area is contained in Table 1. The new data presented in this paper are highlighted; previously obtained K-Ar and $^{40}Ar/^{39}Ar$ ages are also included. Details of sample locations are provided in Appendix 1.

Table 1. Summary of U-Pb, K-Ar, and $^{40}Ar/^{39}Ar$ age data derived from samples collected during regional geological mapping in the Teslin map area.

			K/Ar and ^{40}Ar-^{39}Ar AGES		
NO.	FIELD NO.	U/Pb AGES	BIOTITE	HORNBLENDE	ROCK TYPE/SETTING
YUKON-TANANA TERRANE					
1	GGA-90-20-03B	341.6-342.5 Ma (minimum age)			blastomylonitic(?) foliated aplite
2	GGA-93-37-04B	349.5 ± 0.6 Ma			muscovite-biotite quartzofeldspathic schist; metaplutonic rock
3	GGAS-93-22-04	340.5 ± 0.7 Ma			biotite-muscovite +/- chlorite quartzofeldspathic schist; metaplutonic rock
CACHE CREEK TERRANE					
4	GGA-90-46-03C	245.4 ± 0.8 Ma			fresh pyroxenite-peridotite
STIKINE TERRANE					
5	GGA-90-25-03E	229.6 ± 1.4 Ma			quartz-feldspar porphyry; clast in Laberge Group conglomerate
6	GGA-90-03-06C	203.6 ± 0.6 Ma			coarse-grained, K-feldspar megacrystic, hornblende granite; clast in Laberge Group conglomerate
CASSIAR TERRANE					
7	GGA-90-39-05B	1.76-2.03 Ga; 2.68-2.95 Ga; 3.29 Ga			coarse grained, gritty, quartzose sandstone to quartz-feldspar pebble conglomerate; detrital zircon ages
EARLY JURASSIC PLUTONS					
8	GGA-91-38-04C			185 ± 3 (94-49)	medium-grained biotite-hornblende quartz monzodiorite
9	GGAS-93-05-02B	194.5 ± 1 Ma		193 ± 2 Ma	medium-grained hornblende quartz monzodiorite
10	GGAJ-94-19-11D	184.2 ± 0.2 Ma			coarse-grained biotite syenite to monzonite
11	GGA-90-28-04B		187.4 ± 5.2 (92-31)		near monomineralic unfoliated mosaic of large biotite flakes derived from recrystallization and/or metasomatism of aphanitic greenstone
12	GGA-90-28-01B			183.6 ± 2 (92-30)	near monomineralic unfoliated mosaic of large hornblende prisms derived from recrystallization and/or metasomatism of aphanitic greenstone
MID-JURASSIC PLUTONS					
13	GGA-91-40-11C	175.7 ± 1.4 Ma	169 ± 2 (94-51)	173 ± 3 (94-50)	medium-grained biotite-hornblende quartz monzodiorite
EARLY CRETACEOUS PLUTONS					
14	GGA-90-21-12D	123.1 ± 1.7 Ma			strongly foliated and lineated hornblende biotite granite
15	GGA-90-46-04B	123.7 +4.6/-2.8 Ma	119.8 ± 1.3 (94-48)	120.2 ± 2.2 (94-47)	medium-grained hornblende-biotite quartz monzodiorite
16	GGA-90-46-02B		118.1 ± 3.3 (94-46)		medium-grained hornblende-biotite quartz monzodiorite
MID-CRETACEOUS PLUTONS					
17	GGA-92-05-02C	109 ± 2 Ma			medium-grained biotite granite
18	GGAJ-94-20-01A	108 ± 0.3 Ma			medium- to coarse-grained biotite granite
LATE CRETACEOUS PLUTONS					
19	GGA-94-24-04C	74 +6/-1 Ma			medium-grained biotite granite

Note: Shaded boxes indicated ages presented in this paper. Non-shaded boxes indicate data have been presented elsewhere. For the latter, the number in brackets refers to the GSC publication number. For numbers 92-30,31 see Hunt and Roddick (1992). For numbers 94-46, 47, 48, 49, 50, 51, see Hunt and Roddick (1994). Analytical and detailed sample location data are presented in tables 2 and 3 and Appendix 1.

Zircon and titanite were concentrated from crushed samples using standard Wilfley™ table, heavy liquid, and magnetic separation techniques. The U-Pb analytical methods used in this study are those outlined in Parrish et al. (1987) and Parrish et al. (1992). Treatment of analytical errors follows Roddick (1987), with regression analysis modified after York (1969). All of the zircon fractions analyzed were multigrain fractions that were air abraded following the method of Krogh (1982) unless otherwise noted. U-Pb analytical results are presented in Table 2 and displayed in the concordia plots (Figs. 3–6), with errors reported at the 2 sigma level. Procedures for $^{40}Ar/^{39}Ar$ analytical techniques are described in Roddick (1990).

URANIUM-LEAD RESULTS AND DISCUSSION

Yukon–Tanana (Kootenay) terrane

Sample 1: GGA-90-20-03B

Sample 1 is a foliated aplite collected from the Yukon–Tanana terrane (Fig. 2). Zircons from this sample form stubby, subhedral to euhedral, colourless to pale brown prisms. Many of the grains are fractured and contain rare to abundant clear bubble- and rod-shaped inclusions. Four abraded fractions (A, B, C, DA) and one unabraded fraction (DB) of zircon were analyzed (Fig. 3, Table 2). Although no inherited cores were observed in any of the grains, the data array suggests that an inherited component was present in every fraction analyzed. Fraction C plots near concordia at about 345 Ma, and the other three abraded fractions give much older $^{207}Pb/^{206}Pb$ ages. Two-point discordia lines through fraction C and fractions B and A give lower intercepts of 341.6–342.5 Ma, and upper intercepts of 1.91–2.41 Ga. Assuming that the inherited zircon component is all of Early Proterozoic or older age, the range of lower intercept ages is interpreted to give a minimum age of emplacement for the aplite body. The upper intercepts give a minimum range of ages for the inherited zircon component that is present in the zircon concentrate. Fraction DB was unabraded, and gives a much younger $^{206}Pb/^{238}U$ age, reflecting significant postcrystallization Pb loss.

Sample 2: GGA-93-37-04B

This sample is from a foliated muscovite-biotite quartzofeldspathic schist collected from a sheared granitoid body from the Yukon–Tanana terrane (Fig. 2). Four zircon fractions representing the various morphologies in the sample were analyzed. Zircon fractions B and D are composed of small, stubby prisms with 2:1 length-to-width aspect ratios and contain some minor fluid inclusions. Analyses from fractions B and D overlap and intersect concordia (Fig. 3, Table 2). The age of the rock is interpreted to be 349.5 ± 0.6 Ma, which is an average of the $^{206}Pb/^{238}U$ ages and related uncertainties of fractions B and D. Fraction A, which is composed of larger prismatic crystals (+105 microns) with minor inclusions, is interpreted to contain an inherited component. Fraction C, which contains small, equant, multifaceted crystals that were only weakly abraded is interpreted to reflect postcrystallization Pb loss.

Sample 3: GGA-93-22-04

Sample 3 is from a biotite-muscovite±chlorite quartzofeldspathic schist, interpreted to be meta-plutonic in origin, collected from Yukon–Tanana terrane (Fig. 2). Three zircon fractions were analyzed from this sample. Fractions A and B are composed of small, colourless to pale yellow, stubby, prismatic grains with fluid inclusions. The age of concordant zircon fraction A is 340.5 ± 0.7 Ma and is interpreted to represent the age of the rock (Fig. 3, Table 2). The analysis for fraction B, which slightly overlaps fraction A at 2 sigma, is in agreement with the $^{206}Pb/^{238}U$ age. Fraction C, which is composed of small, colourless to pale yellow, equant, multifaceted crystals is interpreted to contain a minor inherited component.

Discussion

The U-Pb ages from samples 1 to 3 of ca. 342 Ma, 349.5 ± 0.6 Ma, and 340.5 ± 0.7 Ma (Fig. 2, Table 1) are characteristic of ages derived from metaplutonic bodies elsewhere in Yukon–Tanana terrane which are predominantly of Devono-Mississippian age (Mortensen, 1992). The ages support the continuation of the terrane, based on lithological characteristics, to the south margin of the Teslin map area. Sample 1 is from a foliated aplite that has been deformed along with its immediate host, a foliated amphibolite, both contained within a succession dominated by quartz-muscovite schist. There is no nearby exposed pluton to which the aplite may be related. Samples 2 and 3 are from biotite-muscovite±chlorite quartzofeldspathic schist which represent strongly deformed metaplutonic bodies, of uncertain extent, but each probably extends a minimum of several hundred metres across.

Cache Creek terrane

Sample 4: GGA-90-46-03C

This sample of fresh peridotite collected from the Cache Creek terrane (Fig. 2) yielded a small amount of zircon, which comprised clear, colourless, broken fragments of originally coarser grains. Three strongly abraded fractions all give concordant analyses. The weighted average of the $^{206}Pb/^{238}U$ ages is 245.4 ± 0.8 Ma (Fig. 4, Table 2), which is considered to be the crystallization age of the unit.

Discussion

The Permo-Triassic age of 245.4 ± 0.8 Ma obtained for peridotite of the Cache Creek terrane (sample 4, Fig. 2, Table 1) is the first age from alpine ultramafic rocks of this terrane in the northern Cordillera. The age reflects a temperature decline of the mantle peridotite from mantle temperatures, possibly by being brought near surface through processes of sea-floor spreading. Because uppermost mantle material would likely

be cooled within the first few millions of years after spreading (Nicolas, 1986), the age indicates that Cache Creek ocean crust was likely forming in Permo-Triassic time. This age is consistent with the Permian age of associated mafic volcanic rocks (Gordey and Stevens, 1994b). The date also provides an older limit to incorporation of the peridotite as a thrust slice within the Cache Creek terrane. Because of their spatial association in other places with Mississippian volcanic rocks, Monger (1975) had suggested a largely Mississippian age for ultramafic rocks in the northern Cache Creek terrane. These data show that the age may be much younger.

Stikine terrane

Sample 5: GGA-90-25-03E

Both zircon and titanite were recovered from sample 5, a quartz-feldspar porphyry clast from a Laberge Group conglomerate in Stikine terrane (Fig. 2). The zircon form clear, colourless to pale brown, stubby to elongate, euhedral prisms with rare to abundant, clear, bubble-shaped inclusions. Four fractions of strongly abraded zircon were analyzed. Two fractions (C and D) yield concordant analyses (Fig. 5, Table 2) with a total range of $^{206}Pb/^{238}U$ ages of 229.6 ± 1.4 Ma, which is considered to be the best estimate for the crystallization age of the sample. Fraction B gives slightly older

Table 2. U-Pb analytical data.3. $^{40}Ar/^{39}Ar$ analytical data.

Fraction[a]	Wt.[b] µg	U ppm	Pb[c] ppm	$^{206}Pb/^{204}Pb$[d]	Pb[e] pg	^{208}Pb[f] %	Radiogenic ratios (±1σ, %)[g] $^{206}Pb/^{238}U$	$^{207}Pb/^{235}U$	$^{207}Pb/^{206}Pb$	Ages (Ma, ±2σ)[h] $^{206}Pb/^{238}U$	$^{207}Pb/^{235}U$	$^{207}Pb/^{206}Pb$
1. GGA-90-20-03B[1]												
A	19	417.6	31.80	2233	16	12.38	0.07174 ± 0.09	0.8014 ± 0.13	0.08101 ± 0.08	446.6 ± 0.8	597.6 ± 1.1	1221.7 ± 3.1
B	86	427.2	28.46	6634	22	14.05	0.06260 ± 0.09	0.5452 ± 0.11	0.06316 ± 0.04	391.4 ± 0.7	441.8 ± 0.8	713.7 ± 1.7
C	383	453.1	26.58	10240	58	14.54	0.05525 ± 0.12	0.4147 ± 0.13	0.05444 ± 0.03	346.7 ± 0.8	352.3 ± 0.8	389.2 ± 1.5
DA	29	265.4	18.72	65	637	17.91	0.06331 ± 0.91	0.5467 ± 3.63	0.06262 ± 3.07	395.7 ± 7.0	442.8 ± 26	695 ± 137
DB	16	343.5	18.33	641	28	14.50	0.05028 ± 0.12	0.3785 ± 0.37	0.05460 ± 0.31	316.2 ± 0.8	325.9 ± 2.0	395.7 ± 14
2. GGA-93-37-04B[2]												
A	66	379.8	22.66	7325	12	13.57	0.05679 ± 0.09	0.4327 ± 0.10	0.05526 ± 0.04	356.1 ± 0.6	365.1 ± 0.6	422.9 ± 1.7
B	23	309.1	18.14	6992	4	13.89	0.05575 ± 0.09	0.4112 ± 0.12	0.05349 ± 0.08	349.7 ± 0.6	349.7 ± 0.7	349.8 ± 3.6
C	58	530.9	30.26	11670	9	13.69	0.05427 ± 0.09	0.3998 ± 0.10	0.05343 ± 0.04	340.7 ± 0.6	341.5 ± 0.6	346.9 ± 1.9
D	37	327.5	19.19	11230	4	13.90	0.05566 ± 0.09	0.4107 ± 0.10	0.05352 ± 0.04	349.2 ± 0.6	349.4 ± 0.6	350.9 ± 2.0
3. GGAS-93-22-04[2]												
A	26	424.8	24.21	7851	5	13.74	0.05423 ± 0.10	0.3985 ± 0.15	0.05328 ± 0.11	340.5 ± 0.7	340.5 ± 0.8	340.9 ± 4.8
B	42	497.4	28.28	8310	9	13.69	0.05412 ± 0.09	0.3987 ± 0.10	0.05342 ± 0.04	339.8 ± 0.6	340.7 ± 0.6	346.9 ± 2.0
C	24	344.0	19.71	4983	5	13.78	0.05449 ± 0.09	0.4015 ± 0.12	0.05345 ± 0.07	342.0 ± 0.6	342.8 ± 0.7	347.9 ± 3.2
4. GGA-90-46-03C[1]												
BA	207	266.4	9.79	5825	23	4.45	0.03886 ± 0.09	0.2738 ± 0.11	0.05110 ± 0.05	245.7 ± 0.4	245.7 ± 0.5	245.4 ± 2.1
BB	284	149.3	5.40	5657	18	3.24	0.03875 ± 0.09	0.2733 ± 0.11	0.05115 ± 0.05	245.1 ± 0.4	245.3 ± 0.5	247.6 ± 2.4
C	245	360.2	13.29	12660	17	4.98	0.03879 ± 0.09	0.2736 ± 0.11	0.05116 ± 0.04	245.3 ± 0.5	245.6 ± 0.5	248.2 ± 1.8
5. GGA-90-25-03E[1]												
A	28	162.3	5.54	832	12	6.93	0.03514 ± 0.10	0.2464 ± 0.30	0.05085 ± 0.25	222.6 ± 0.4	223.6 ± 1.2	234.2 ± 12
B	9	155.1	5.59	265	13	8.13	0.03666 ± 0.21	0.2588 ± 0.92	0.05121 ± 0.81	232.1 ± 1.0	233.7 ± 3.8	250.3 ± 37
C	15	130.4	4.55	355	13	6.29	0.03622 ± 0.17	0.2533 ± 1.07	0.05071 ± 0.96	229.4 ± 0.7	229.2 ± 4.4	227.8 ± 45
D	26	147.6	5.16	428	21	6.60	0.03616 ± 0.13	0.2529 ± 0.63	0.05072 ± 0.56	229.0 ± 0.6	228.9 ± 2.6	228.2 ± 26
T1	127	52.95	2.51	106	154	38.40	0.03223 ± 0.51	0.2215 ± 1.83	0.04985 ± 1.52	204.5 ± 2.1	203.2 ± 6.7	187.8 ± 72
T2	146	48.22	2.40	112	150	41.38	0.03220 ± 0.48	0.2208 ± 1.75	0.04974 ± 1.47	204.3 ± 1.9	202.6 ± 6.4	182.9 ± 70
6. GGA-90-03-06C[1]												
A	11	287.9	10.24	384	19	9.34	0.03558 ± 0.18	0.2619 ± 0.74	0.05339 ± 0.65	225.4 ± 0.8	236.2 ± 3.1	345.6 ± 30
B	9	275.1	8.76	406	13	8.98	0.03208 ± 0.14	0.2222 ± 0.68	0.05023 ± 0.60	203.6 ± 0.6	203.7 ± 2.5	205.8 ± 28
C	8	308.2	10.01	457	11	9.22	0.03260 ± 0.24	0.2295 ± 0.69	0.05106 ± 0.60	206.8 ± 1.0	209.8 ± 2.6	243.7 ± 28
T1	263	90.60	3.93	152	356	32.73	0.03224 ± 0.38	0.2234 ± 1.25	0.05025 ± 1.03	204.6 ± 1.5	204.7 ± 4.7	206.7 ± 48
7. GGA-90-39-5B[1]												
AB	9	82.92	39.75	1603	11	25.22	0.3697 ± 0.12	6.3817 ± 0.14	0.12518 ± 0.06	2028 ± 4	2030 ± 2	2031 ± 2
BA	7	82.78	30.95	816	16	11.06	0.3457 ± 0.21	5.6232 ± 0.24	0.11798 ± 0.15	1914 ± 7	1920 ± 4	1926 ± 5
BB	10	41.43	26.65	1115	13	10.76	0.5544 ± 0.16	15.5171 ± 0.16	0.20302 ± 0.06	2843 ± 7	2848 ± 3	2851 ± 2
CA	12	78.08	46.23	3007	10	12.39	0.5096 ± 0.10	12.8325 ± 0.11	0.18264 ± 0.04	2655 ± 4	2667 ± 2	2677 ± 1
CB	7	75.08	61.61	1117	20	12.20	0.6601 ± 0.17	24.3922 ± 0.18	0.26801 ± 0.04	3268 ± 9	3284 ± 3	3294 ± 1
DA	18	168.5	59.85	2266	26	16.52	0.3109 ± 0.09	4.6222 ± 0.11	0.10782 ± 0.06	1745 ± 3	1753 ± 2	1763 ± 2
DB	7	183.5	117.10	2760	17	6.08	0.5735 ± 0.11	17.0208 ± 0.12	0.21526 ± 0.04	2922 ± 5	2936 ± 2	2945 ± 1

[a] All zircon fractions are very strongly abraded; T = titanite
[b] Error on weight = ±1 µg
[c] Radiogenic Pb
[d] Measured ratio corrected for spike and Pb fractionation of 0.09 ± 0.03%/AMU
[e] Total common Pb on analysis corrected for fractionation and spike
[f] Radiogenic Pb
[g] Corrected for blank Pb and U and common Pb (Stacey-Kramers model Pb composition equivalent to the $^{207}Pb/^{206}Pb$ age)
[h] Corrected for blank and common Pb
All analyses completed at the GSC geochronology laboratory by [1] J. Mortensen and [2] V. McNicoll

$^{206}Pb/^{238}U$ and $^{207}Pb/^{206}Pb$ ages, although it still overlaps concordia, indicating the presence of a minor inherited zircon component. Fraction A gives a younger $^{206}Pb/^{238}U$ age, reflecting significant postcrystallization Pb loss. Two unabraded fractions of clear, pale brown, euhedral titanite (T1, T2) give overlapping concordant analyses with $^{206}Pb/^{238}U$ ages of 204.5 ± 2.1 Ma. These data are interpreted to result from relatively slow cooling of the sample through the closure temperature of the U-Pb system in titanite prior to incorporation into the conglomerate.

Sample 6: GGA-90-03-06C

Sample 6 is a coarse-grained, K-feldspar-megacrystic, hornblende granite clast from a Laberge Group conglomerate in Stikine terrane (Fig. 2). Zircons recovered from this sample form clear, pale brown, euhedral, stubby to elongate prisms. One strongly abraded fraction (B) yields a concordant analysis with a $^{206}Pb/^{238}U$ age of 203.6 ± 0.6 Ma, which is considered to be the best estimate for the crystallization age of this clast (Fig. 5, Table 2). The three zircon fractions (A, B, C) define a short linear array with calculated upper intercept age of 1.10 Ga, which gives an average age for a cryptic inherited zircon component that is present in fractions A and C. A single unabraded fraction of clear, pale brown, euhedral titanite

Table 2 (cont.)

Fraction[a]	Wt.[b] µg	U ppm	Pb[c] ppm	$^{206}Pb/^{204}Pb$[d]	Pb[e] pg	^{208}Pb[f] %	Radiogenic ratios (±1σ, %)[g] $^{206}Pb/^{238}U$	$^{207}Pb/^{235}U$	$^{207}Pb/^{206}Pb$	Ages (Ma, ±2σ)[h] $^{206}Pb/^{238}U$	$^{207}Pb/^{235}U$	$^{207}Pb/^{206}Pb$
9. GGAS-93-05-02B[2]												
A	102	91.99	2.99	553	34	12.54	0.03136 ± 0.13	0.2310 ± 0.34	0.05341 ± 0.28	199.1 ± 0.5	211.0 ± 1.3	346.2 ± 13
B	176	275.3	8.71	6098	15	12.40	0.03068 ± 0.09	0.2122 ± 0.11	0.05017 ± 0.04	194.8 ± 0.3	195.4 ± 0.4	202.7 ± 1.9
C	59	343.6	10.95	3849	10	13.08	0.03066 ± 0.10	0.2121 ± 0.12	0.05017 ± 0.06	194.7 ± 0.4	195.3 ± 0.4	203.1 ± 3.0
D	56	215.2	6.86	5333	4	12.42	0.03091 ± 0.10	0.2142 ± 0.12	0.05026 ± 0.06	196.2 ± 0.4	197.1 ± 0.4	206.8 ± 2.6
T1	91	124.2	6.83	167	145	49.52	0.03062 ± 0.29	0.2111 ± 1.65	0.04999 ± 1.48	194.4 ± 1.1	194.5 ± 5.8	194.6 ± 70
T2	161	119.0	6.39	214	186	48.30	0.03063 ± 0.23	0.2107 ± 1.32	0.04988 ± 1.18	194.5 ± 0.9	194.1 ± 4.7	189.2 ± 56
10. GGAJ-94-19-11D[2]												
A	99	302.5	9.03	9257	6	12.24	0.02900 ± 0.09	0.1991 ± 0.10	0.04981 ± 0.04	184.3 ± 0.3	184.4 ± 0.3	186.0 ± 1.7
B	213	855.3	25.42	27360	12	11.95	0.02898 ± 0.09	0.1991 ± 0.11	0.04985 ± 0.03	184.1 ± 0.3	184.4 ± 0.4	187.8 ± 1.4
C	176	547.1	12.14	8725	20	12.14	0.02901 ± 0.09	0.1993 ± 0.10	0.04982 ± 0.03	184.3 ± 0.3	184.5 ± 0.3	186.7 ± 1.6
D	106	551.0	16.26	13980	7	11.43	0.02895 ± 0.09	0.1988 ± 0.10	0.04980 ± 0.03	184.0 ± 0.3	184.1 ± 0.3	185.6 ± 1.5
E	320	673.0	20.18	42290	9	12.66	0.02900 ± 0.10	0.1991 ± 0.11	0.04981 ± 0.03	184.3 ± 0.4	184.4 ± 0.4	186.0 ± 1.3
F	213	467.3	13.91	5949	30	12.09	0.02896 ± 0.09	0.1991 ± 0.11	0.04986 ± 0.04	184.0 ± 0.3	184.4 ± 0.4	188.2 ± 1.8
13. GGA-91-40-11C[1]												
A	233	240.1	6.63	5803	16	11.42	0.02709 ± 0.10	0.1852 ± 0.11	0.04959 ± 0.05	172.3 ± 0.3	172.5 ± 0.4	175.6 ± 2.3
B	151	267.1	7.36	3873	18	11.37	0.02707 ± 0.08	0.1850 ± 0.11	0.04958 ± 0.06	172.2 ± 0.3	172.4 ± 0.4	175.2 ± 2.7
C	183	243.1	6.74	5460	14	11.78	0.02708 ± 0.09	0.1852 ± 0.11	0.04960 ± 0.05	172.3 ± 0.3	172.5 ± 0.4	176.2 ± 2.6
14. GGA-90-21-12D[1]												
A	180	631.7	12.25	1314	99	15.24	0.01822 ± 0.10	0.1219 ± 0.17	0.04853 ± 0.12	116.4 ± 0.2	116.8 ± 0.4	125.2 ± 5.5
B	198	752.6	15.04	2606	65	17.20	0.01833 ± 0.12	0.1226 ± 0.14	0.04851 ± 0.06	117.1 ± 0.3	117.4 ± 0.3	124.1 ± 3.1
C	108	979.6	20.32	2869	42	19.90	0.01841 ± 0.10	0.1231 ± 0.13	0.04848 ± 0.07	117.6 ± 0.2	117.8 ± 0.3	122.8 ± 3.2
D	189	710.6	14.58	2433	63	19.23	0.01836 ± 0.11	0.1227 ± 0.14	0.04846 ± 0.07	117.3 ± 0.2	117.5 ± 0.3	121.6 ± 3.2
T1	316	401.2	8.60	112	1510	24.27	0.01796 ± 0.47	0.1224 ± 1.68	0.04942 ± 1.40	114.8 ± 1.1	117.2 ± 3.7	167.6 ± 67
T2	332	405.9	8.55	91	2120	22.32	0.01810 ± 0.63	0.1247 ± 2.18	0.04996 ± 01.81	115.6 ± 1.4	119.3 ± 4.9	193.0 ± 86
15. GGA-90-46-04B[1]												
A	87	421.2	8.74	2140	20	17.66	0.01893 ± 0.10	0.1266 ± 0.14	0.04850 ± 0.10	120.9 ± 0.2	121.0 ± 0.3	123.7 ± 4.7
B	63	458.9	9.65	1818	19	18.59	0.01896 ± 0.09	0.1269 ± 0.14	0.04854 ± 0.09	121.1 ± 0.2	121.3 ± 0.3	125.4 ± 4.4
C	378	495.0	10.29	1325	169	17.43	0.01901 ± 0.77	0.1278 ± 1.01	0.04875 ± 0.84	121.4 ± 1.8	122.1 ± 2.3	135.6 ± 40
17. GGA-92-05-02C[2]												
A	72	1552.1	27.46	1041	113	14.95	0.01668 ± 0.14	0.1112 ± 0.42	0.04837 ± 0.38	106.6 ± 0.3	107.1 ± 0.9	117.2 ± 18
B	110	1083.8	19.94	9992	13	13.93	0.01755 ± 0.11	0.1173 ± 0.12	0.04845 ± 0.04	112.2 ± 0.2	112.6 ± 0.2	121.2 ± 2.0
C	136	825.9	14.88	9014	13	13.14	0.01735 ± 0.09	0.1157 ± 0.11	0.04837 ± 0.04	110.9 ± 0.2	111.2 ± 0.2	117.4 ± 2.0
D	34	1770.7	31.80	7335	9	13.40	0.01724 ± 0.09	0.1148 ± 0.11	0.04829 ± 0.04	110.2 ± 0.2	110.3 ± 0.2	113.3 ± 2.1
E	37	1152.3	21.10	3106	15	14.07	0.01744 ± 0.10	0.1169 ± 0.14	0.04860 ± 0.09	111.5 ± 0.2	112.2 ± 0.3	128.7 ± 4.3
18. GGAJ-94-20-01A[2]												
A1	23	833.1	13.98	1530	14	9.21	0.01690 ± 0.10	0.1125 ± 0.15	0.04827 ± 0.10	108.0 ± 0.2	108.2 ± 0.3	112.8 ± 4.8
A2	35	741.3	12.35	991	29	8.48	0.01691 ± 0.10	0.1126 ± 0.21	0.04830 ± 0.16	108.1 ± 0.2	108.3 ± 0.4	113.7 ± 7.3
B1	48	863.0	14.36	12950	3	8.94	0.01681 ± 0.09	0.1119 ± 0.10	0.04829 ± 0.04	107.4 ± 0.2	107.7 ± 0.2	113.6 ± 1.7
B2	44	336.9	5.56	2971	5	9.37	0.01657 ± 0.09	0.1144 ± 0.14	0.05011 ± 0.10	105.9 ± 0.2	110.0 ± 0.3	199.9 ± 4.6
19. GGA-94-24-04C[2]												
A1	20	905.8	9.23	1025	12	4.62	0.01078 ± 0.11	0.07194 ± 0.21	0.04840 ± 0.17	69.1 ± 0.2	70.5 ± 0.3	119.1 ± 7.8
A2	20	924.6	10.26	911	15	6.81	0.01147 ± 0.11	0.07542 ± 0.22	0.04767 ± 0.17	73.5 ± 0.2	73.8 ± 0.3	83.0 ± 7.9
B	71	493.2	5.38	4652	5	7.65	0.01119 ± 0.10	0.07380 ± 0.12	0.04783 ± 0.06	71.7 ± 0.1	72.3 ± 0.2	90.7 ± 3.0
C1	25	939.5	11.77	3276	6	7.65	0.01282 ± 0.10	0.08733 ± 0.13	0.04941 ± 0.08	82.1 ± 0.2	85.0 ± 0.2	167.1 ± 3.7
C2	42	721.2	8.65	642	37	7.78	0.01227 ± 0.12	0.08132 ± 0.31	0.04806 ± 0.25	78.6 ± 0.2	79.4 ± 0.5	102.1 ± 12
D	45	1143.6	13.62	4837	8	6.04	0.01241 ± 0.09	0.08315 ± 0.11	0.04860 ± 0.05	79.5 ± 0.1	81.1 ± 0.2	128.5 ± 2.3

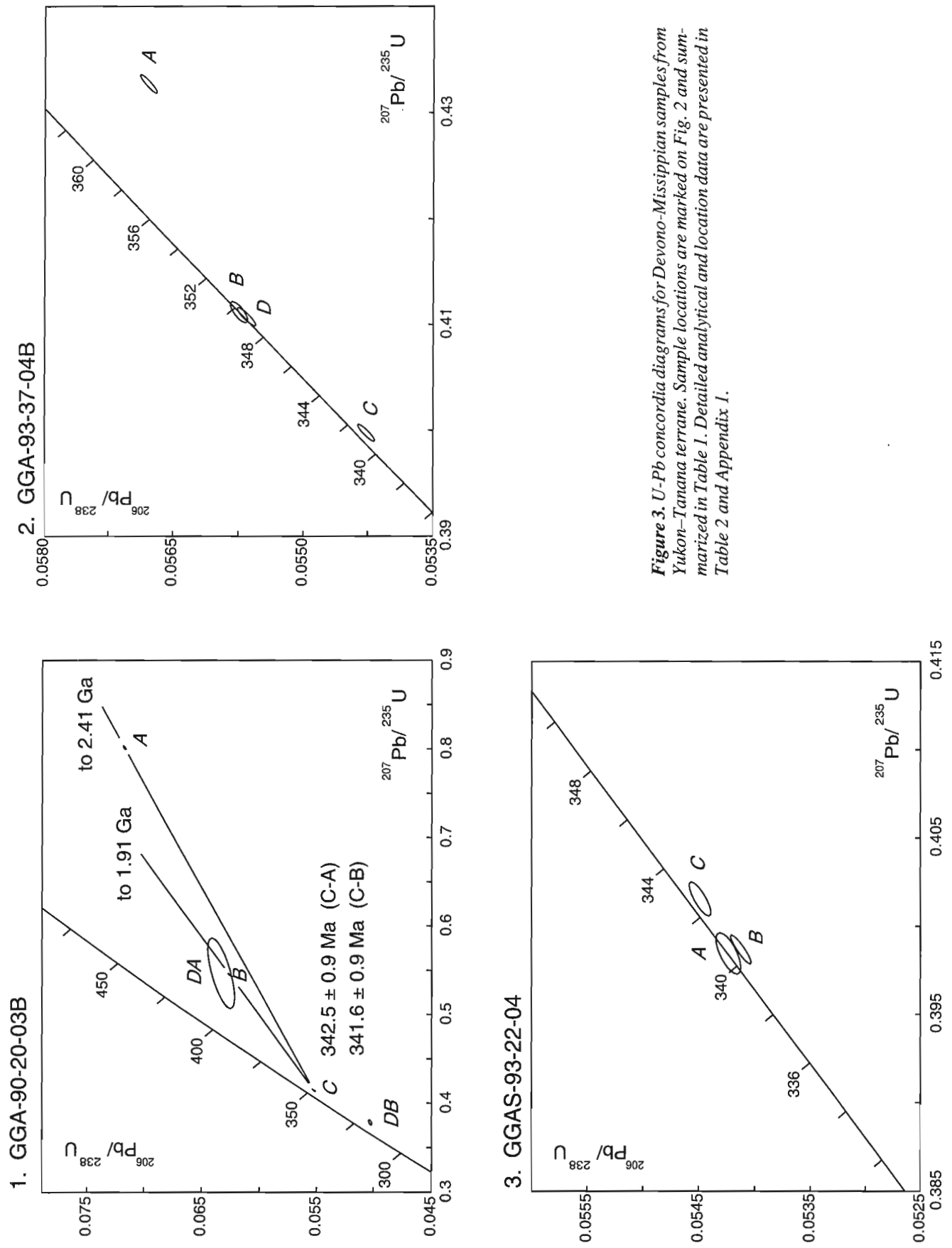

Figure 3. *U-Pb concordia diagrams for Devono-Missippian samples from Yukon–Tanana terrane. Sample locations are marked on Fig. 2 and summarized in Table 1. Detailed analytical and location data are presented in Table 2 and Appendix 1.*

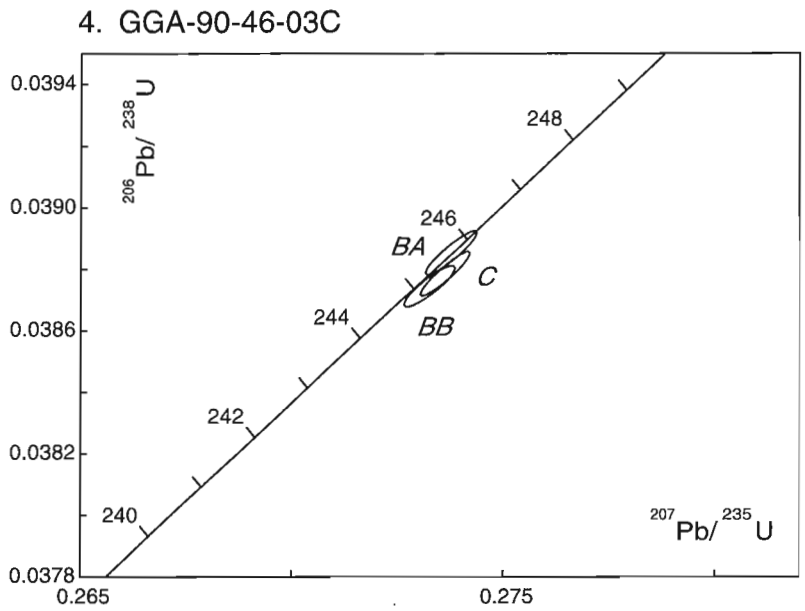

Figure 4.

U-Pb concordia diagram for a Permo-Triassic sample from Cache Creek terrane. The sample location is marked on Fig. 2 and summarized in Table 1. Detailed analytical and location data are presented in Table 2 and Appendix 1.

(T1) gives a concordant, but relatively imprecise analysis with a $^{206}Pb/^{238}U$ age of 204.6 ± 1.5 Ma, which is in good agreement with the age determined from the concordant zircon analysis.

Discussion

Late Triassic to Early Jurassic ages (229.6 ± 1.4 Ma and 203.6 ± 0.6 Ma) for samples 5 and 6 respectively (Fig. 2, Table 1) are from clasts of quartz-feldspar porphyry and hornblende granite from within the Laberge Group of the Stikine terrane. The younger clast ages provide an older limit to the age of the host strata (i.e. Early Jurassic) and confirms assignment of the containing beds to the Laberge Group. Reliable ages from Laberge group clasts elsewhere are rare. Most previously published K-Ar ages are too young for their host strata, or corrections for radiogenic Ar are uncertain (summarized in Hart et al., 1995). Hart et al. (1995) obtained U-Pb zircon ages of 215 to 208 Ma on proximal granitoid clasts from the western margin of the Laberge Group basin (i.e. Whitehorse trough) for which a probable local plutonic source in Stikinia was identified. Johannson et al. (1997) and Johannson and McNicoll (1997) reported an age of 186.6 +0.5/-1 Ma (U-Pb zircon) for a hornblende monzogranite clast in the Inklin Formation of the Laberge Group, a clast also attributed to a Stikinian source. The clasts dated herein are from the eastern limit of outcrop of the Laberge Group. The ages are not readily correlated with known plutons nor can the clasts be sedimentologically tied to a source area (i.e. Stikinia or Quesnelia).

Cassiar terrane

Sample 7: GGA-90-39-5B

Detrital zircons were analyzed from a sample of coarse-grained, gritty, quartzose sandstone to quartz-feldspar pebble conglomerate collected from Cassiar terrane (Fig. 2). Zircons recovered from this sample are clear, pale pink to medium pinkish-brown, and range from euhedral, sharp-faceted, equant to stubby prismatic grains to smoothly rounded grains. Seven strongly abraded single zircon grains were analyzed (Fig. 6, Table 2). The analyses range from 0.2–1.1% discordant, and yield a wide range of $^{207}Pb/^{206}Pb$ ages. Although the data are limited, three age populations are indicated: one population gives Early Proterozoic ages (1763–2032 Ma); a second population gives Late Archean ages (2677–2946 Ma), and a single grain gives a considerably older age of ca. 3294 Ma (Fig. 6, Table 2).

Discussion

A sample for detrital zircon analysis was collected from immature unfossiliferous quartzofeldspathic grits in northeast Teslin map area to test for provenance and maximum age, and to determine terrane affinity. Although the number of analyses is small, the detrital zircon data demonstrate derivation from a source region that included a wide range of Precambrian crystalline rocks. The lack of a Paleozoic age component is permissive to correlation of the strata to the lithologically similar upper Proterozoic Ingenika Group of Cassiar terrane (Gordey, 1992; 1995). Other samples collected from the same unit by T. Harms were analyzed by Ross (Ross and Harms, 1998). His conclusion, based on a range of single-grain crystallization ages from 1777 Ma to 1600 Ma, is that the source of the grits was likely crystalline basement of western Canada, confirming a North American affinity for these rocks and their correlation with Cassiar terrane.

Post-tectonic plutonic suites

Early Jurassic plutons

Sample 9: GGAS-93-05-02B

This sample is from a massive, post-tectonic, medium-grained, hornblende quartz monzodiorite pluton intruding Cassiar terrane (Fig. 2). Zircons in this rock are stubby, well

faceted, prismatic crystals with minor inclusions. Four zircon fractions were analyzed from this sample. Zircon fractions A and D are interpreted to contain an inherited component. Fractions B and C overlap and plot just below concordia; a weighted average of their $^{206}Pb/^{238}U$ ages is 194.8 ± 0.2 Ma (Fig. 7, Table 2). The sample also contained abundant titanite. Titanite fractions T1 and T2 are composed of subhedral, light yellow crystals and dark orange to brown subhedral grains, respectively. The two titanite analyses overlap each other and intersect concordia with a weighted average $^{206}Pb/^{238}U$ age of 194.5 ± 0.7 Ma. The zircon and titanite ages are in agreement and an age of 194.5 ± 1 Ma is taken to be the best estimate for the crystallization age of the rock. $^{40}Ar/^{39}Ar$ step-heating analyses were completed on hornblende from this sample (Table 3, Fig. 7). The standard utilized for these analyses was FCT-3, biotite, the age of which is 27.89 Ma (M. Kunk, pers. comm.). The analyses are composed of three heating steps. The first step liberated most of the atmospheric argon. The next two heating steps resulted in age measurements which are in agreement and which, when combined, result in an interpreted age of 193 ± 2 Ma. This hornblende age is in agreement with the interpreted U-Pb crystallization age of the rock (Table 1).

Sample 10: GGAJ-94-19-11D

Sample 10 is a coarse-grained biotite syenite to monzonite from the Nisutlin River pluton that possibly intrudes both Cassiar and Yukon–Tanana terranes (Fig. 2). The rock contains

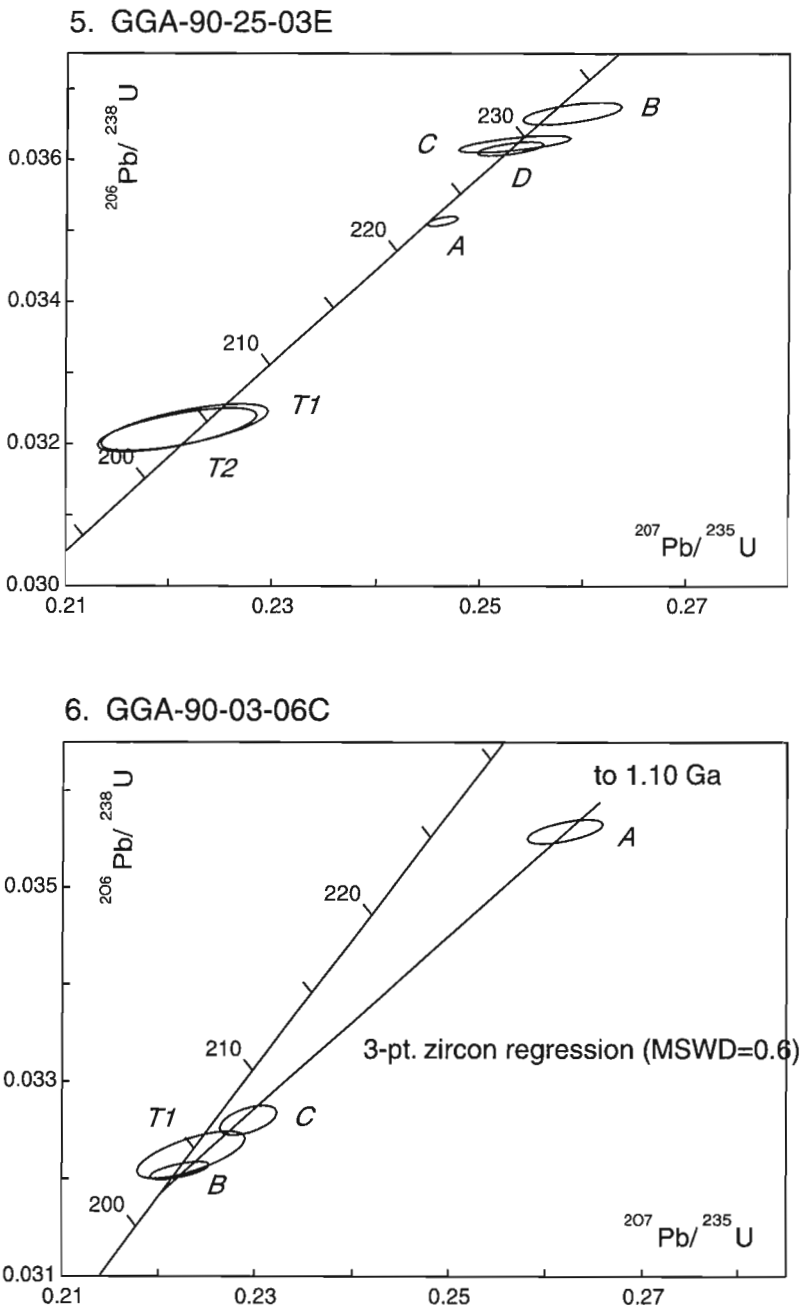

Figure 5.

U-Pb concordia diagrams for Late Triassic to Early Jurassic samples from Stikine terrane. Sample locations are marked on Fig. 2 and summarized in Table 1. Detailed analytical and location data are presented in Table 2 and Appendix 1.

abundant clear, good-quality, prismatic to more elongate zircon crystals. Six zircon fractions were analyzed from this sample; all of the analyses overlap each other and intersect concordia. A weighted average of all of the $^{206}Pb/^{238}U$ ages and associated errors is 184.2 ± 0.2 Ma, which is interpreted to be the age of the rock (Fig. 7, Table 2).

Mid-Jurassic plutons

Sample 13: GGA-91-40-11C

Sample 13 is medium-grained biotite-hornblende quartz monzodiorite from the Mount Byrd pluton that intrudes Cache Creek terrane (Fig. 2). Zircon fractions A and B are composed of very clear, pale yellow to colourless, multifaceted, equant prisms. Fraction C contains very clear, pale yellow to colourless, elongate prisms. Inclusions are rare in these zircons; zoning and cores are not apparent. All three fractions give overlapping, slightly discordant analyses (Fig. 7, Table 2). It is suggested that the discordance is due to postcrystallization Pb loss, and the best estimate for the crystallization age of the unit is therefore given by the weighted average of the $^{207}Pb/^{206}Pb$ ages of the three fractions, at 175.7 ± 1.4 Ma. A minimum age of ca. 172.0 Ma is given by the minimum $^{206}Pb/^{238}U$ age of the three fractions.

Early Cretaceous plutons

Sample 14: GGA-90-21-12D

Sample 14 is strongly foliated and lineated hornblende biotite granite from the Deadman Creek batholith (Fig. 2). Zircons in this sample display a range of morphologies, including thin tabular grains, thick tabular grains, and stubby and elongate

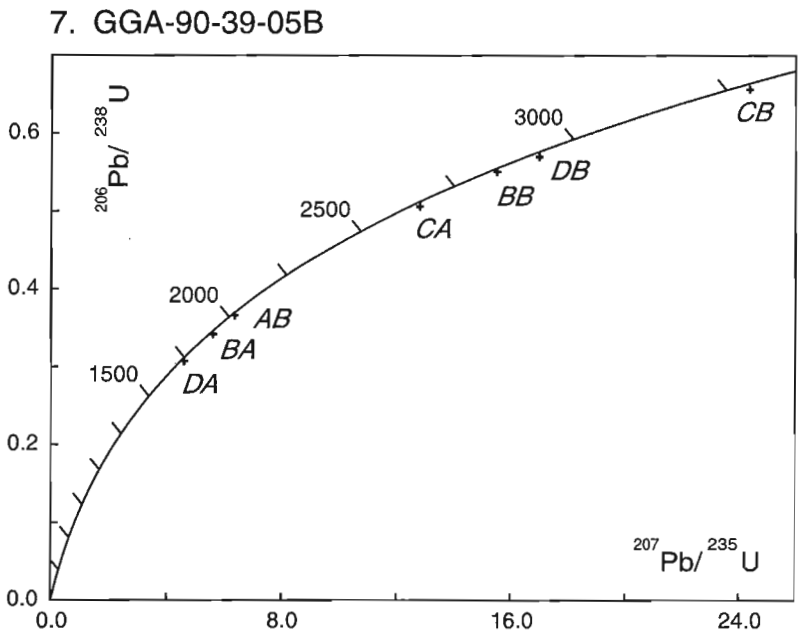

Figure 6.

U-Pb concordia diagram for a detrital zircon sample from Cassiar terrane. The sample location is marked on Fig. 2 and summarized in Table 1. Detailed analytical and location data are presented in Table 2 and Appendix 1.

Table 3. $^{40}Ar/^{39}Ar$ analytical data.

TEMP	$^{36}Ar_{tr}$	$^{37}Ar_{Ca}$	$^{38}Ar_{Cl}$	$^{39}Ar_{K}$	^{40}Ar	% Atmos. ^{40}Ar	Apparent Age	^{39}Ar
(°C)	($x10^{-9}$ cm^3 STP)[a]						Ma +/- 2σ[b]	(%)
GGAS-93-05-02B; Hornblende; J = .016086 ± 0.50 % (1 sigma)								
700	0.018	0.573	0.039	0.167	6.28	85.7	150.2 ± 34.9	0.6
1080	0.055	37.087	3.112	7.586	69.51	23.5	192.7 ± 0.5	27.6
1500	0.018	98.512	10.783	19.770	144.29	3.7	193.3 ± 0.4	71.8
Total[c]	**0.09**	**136.17**	**13.93**	**27.52**	**220.1**	**12.3**	**192.9 ± 1.9**	**100.0**
Conc.(/g)	**3.39**	**5045**	**516.3**	**1020**	**8154**			

[a]Gas quantities corected for decay, isotopes derived from interfering neutron reactions; tr denotes trapped Ar and Ca, Cl and K denote Ar derived from these elements. ^{40}Ar denotes trapped plus radiogenic Ar. Atmos. ^{40}Ar assumes a trapped Ar component of atmospheric composition.
[b]Errors are analytical only and do not reflect error in irradiation parameter J
[c]Integrated age uncertainty includes error in J (0.5% at 1 sigma).

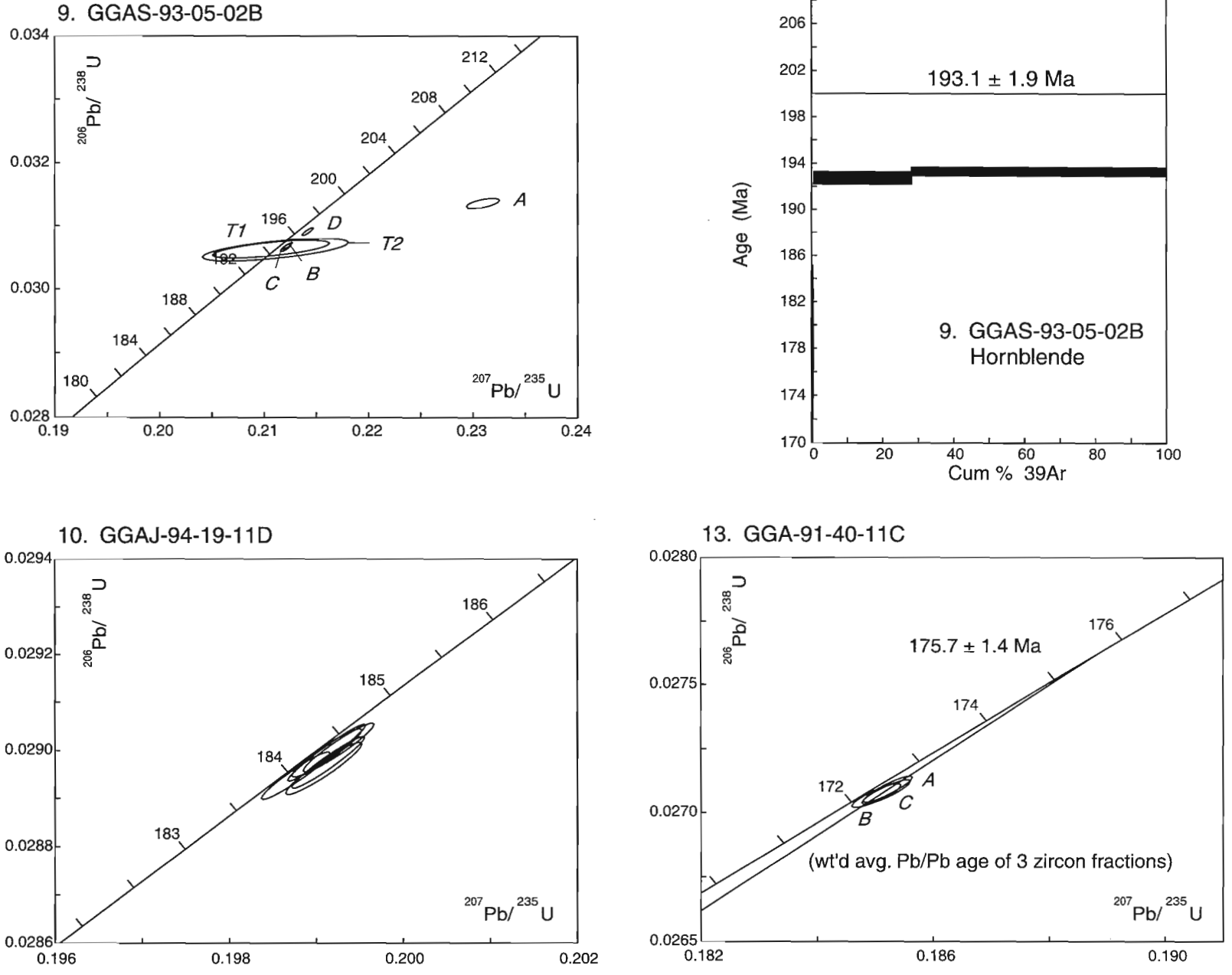

Figure 7. *U-Pb concordia diagrams and $^{40}Ar/^{39}Ar$ step-heating diagram for Early Jurassic and mid-Jurassic plutons. Sample locations are marked on Fig. 2 and summarized in Table 1. Detailed analytical and location data are presented in Table 2, Table 3 and Appendix 1.*

prismatic grains. The grains are colourless to pale yellow, and commonly contain bubble-, tube-, and rod-shaped clear inclusions. No zoning or cores were visible in any of the grains analyzed. One sample of each grain morphology was analyzed; the four analyses (A, B, C, D) are slightly discordant with identical $^{207}Pb/^{206}Pb$ ages (Fig. 8, Table 2). The data array is thought to result from minor postcrystallization Pb loss from zircons of a single age population. The best estimate for the crystallization age of the sample is therefore given by the weighted $^{207}Pb/^{206}Pb$ age for the four fractions, at 123.1 ± 1.7 Ma. Two fractions of clear, pale yellow-brown, euhedral titanite (T1, T2) were also analyzed. The analyses are relatively imprecise (Table 2), with $^{206}Pb/^{238}U$ ages ranging from 114.8–115.6 Ma. These ages are interpreted to reflect either relatively slow cooling through the closure temperature of the U-Pb system in titanite following emplacement of the pluton, or cooling following an immediate postemplacement deformation event that produced the foliation in this rock unit.

Sample 15: GGA-90-46-04B

Sample 15 is a medium-grained biotite-hornblende monzodiorite that intrudes Stikine terrane (Fig. 2). This sample contains colourless to pale yellow, stubby, multifaceted prismatic zircons. The zircons contain abundant bubble-, tube-, and rod-shaped clear inclusions and rare opaque ones. Many of the grains show evidence of magmatic resorption on the surfaces. Three fractions of zircon were analyzed from this sample. Fraction A is concordant and the best estimate for the crystallization age of the rock is given by the $^{207}Pb/^{206}Pb$ and $^{206}Pb/^{238}U$ ages of this fraction at 123.7 +4.6/-2.8 Ma (Fig. 8, Table 2). Fraction C is also concordant, but is of much lower precision. Fraction B has a slightly older $^{207}Pb/^{206}Pb$ age, indicating the presence of a minor component of older inherited zircon. This age is in agreement with previously determined K-Ar ages on biotite and hornblende of 119.8 ± 1.3 Ma and 120.2 ± 2.2 Ma, respectively, from this sample (Table 1).

Mid-Cretaceous plutons

Sample 17: GGA-92-05-02C

Sample 17 is an unfoliated, medium-grained biotite-granite from the Deadman Creek Batholith (Fig. 2). The rock contained abundant small, sharply faceted, elongate zircons with fluidal inclusions. Zircon fraction A is interpreted to have undergone postcrystallization Pb loss; this analysis also has a low $^{206}Pb/^{204}Pb$ ratio. The other zircon fractions are all interpreted to contain an inherited component. A linear regression through all of the remaining analyses (fractions B, C, D, E) has a lower intercept of 109 +1/-60 Ma (MSWD=9.91). A linear regression, including fractions B, C, and D, has a lower intercept of 109 +1/-2 Ma (MSWD=1.02). The $^{206}Pb/^{238}U$ age of fraction D, the most concordant analysis, is 110.2 ± 0.2 Ma (Fig. 8, Table 2). The best interpretation for the age of the rock is taken to be 109 ± 2 Ma, which takes into account the lower intercept of the linear regressions and the age of fraction D.

Sample 18: GGAJ-94-20-01A

This sample is from a medium- to coarse-grained biotite granite pluton that intrudes Yukon–Tanana terrane (Fig. 2) and contains abundant good quality zircons. Fractions A1 and A2 are composed of small, stubby, sharply faceted, prismatic crystals with some fluidal inclusions. These two analyses overlap each other and intersect concordia (Fig. 8, Table 2). Fractions B1 and B2 are composed of very elongate, well faceted crystals with fluidal and some opaque inclusions. Fraction B1 is interpreted to have undergone some Pb loss. The zircons in fraction B2 contain more inclusions than those in fraction B1 and are interpreted to contain an inherited component. The best estimate for the age of the rock is taken to be 108.0 ± 0.3 Ma which is an average of the $^{206}Pb/^{238}U$ ages of fractions A1 and A2 and takes into account their associated errors.

Late Cretaceous plutons

Sample 19: GGA-94-24-04C

Sample 19 is a medium-grained biotite granite from the Deadman Creek batholith (Fig. 2) which contains abundant zircon. Six zircon fractions representing the various zircon morphologies were analyzed from this rock. Zircon fractions A1 and A2 are stubby prismatic crystals with minor fluidal inclusions. Fraction A2, which intersects concordia, was abraded significantly longer than fraction A1; the $^{206}Pb/^{238}U$ age of fraction A2 is 73.5 ± 0.2 Ma (Fig. 9, Table 2). Fraction B is composed of equant, multifaceted crystal with fluidal inclusions. Fractions A1 and B are interpreted to have undergone significant postcrystallization Pb loss. A linear regression through fractions A1, A2 and B has an upper intercept of 74 +6/-1 Ma (MSWD=4.53). Fractions C1 and C2 are composed of very elongate to needle-like crystals containing minor inclusions; fraction D is composed of flat, prismatic grains with abundant inclusions. All three of these analyses contain an inherited component. A linear regression through analyses C1, C2, and D has a lower intercept of 76.5 ± 1 Ma (MSWD=4.58). The best estimate for the age of the rock is interpreted to be 74 +6/-1 Ma which takes into account the age of the most concordant analysis fraction A2, and the results of the two linear regressions.

Discussion

Early Jurassic ages were obtained from three different plutons in northeast Teslin area that intrude strata assigned to Cassiar terrane. One of the ages, 185 ± 3 (sample 8, Table 1), was obtained by the $^{40}Ar/39Ar$ method on hornblende and is interpreted to represent a cooling age. Sample 9 has a U-Pb crystallization age of 194.5 ± 1 Ma which is in agreement with an $^{40}Ar/^{39}Ar$ age on hornblende of 193 ± 2 Ma (Table 1). The third sample (sample 10, Table 1) has an age of 184.2 ± 0.2 Ma obtained by the U-Pb method (zircon) and is interpreted to be a crystallization age. Stevens et al. (1993) obtained a concordant U-Pb titanite age of 193 ± 4.2 Ma for a pluton of this suite in northwesternmost Teslin map area (EJ, Fig. 2) that intrudes Yukon–Tanana terrane, as well as

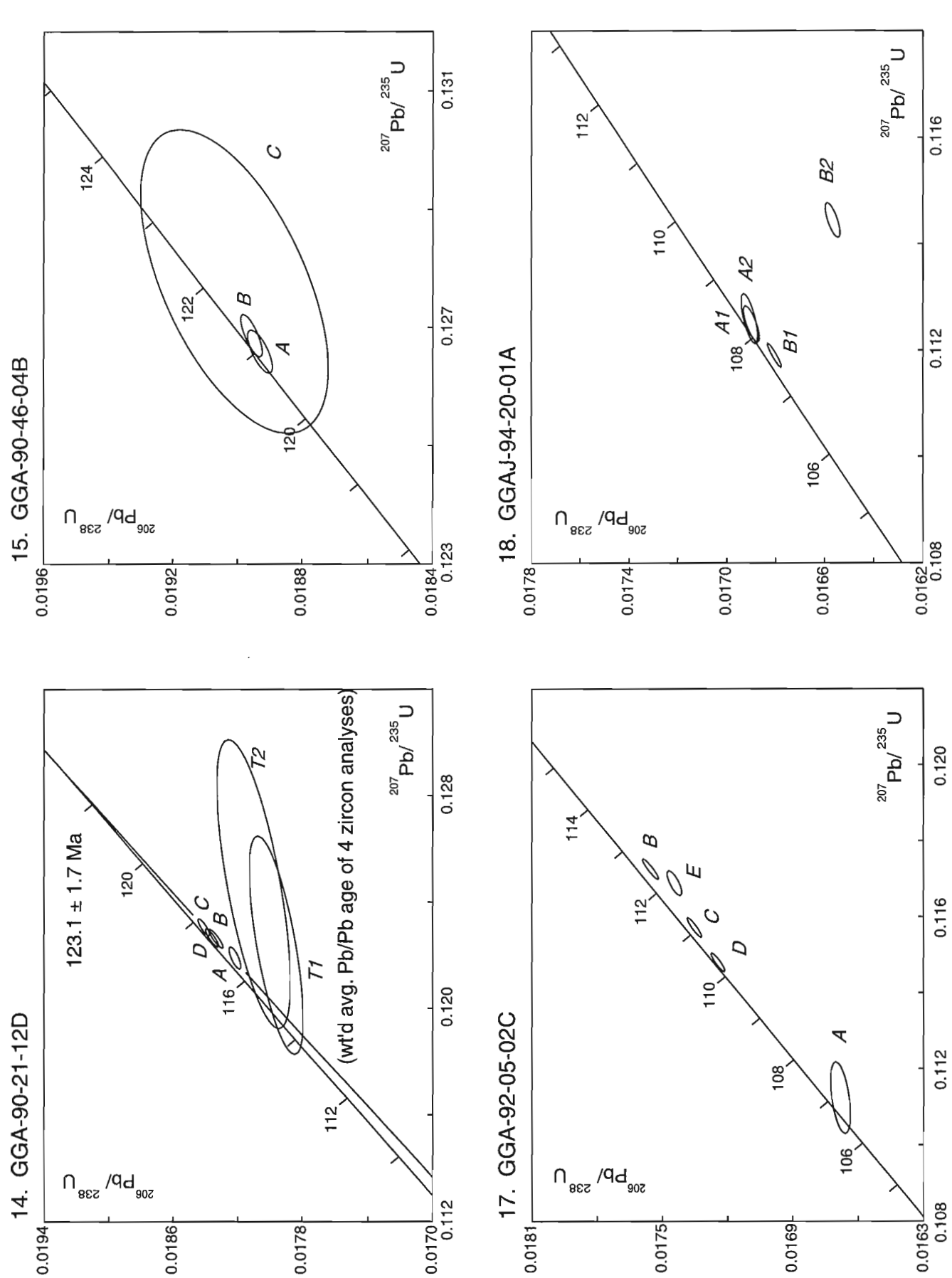

Figure 8. *U-Pb concordia diagrams for Early Cretaceous and mid-Cretaceous plutons. Sample locations are marked on Fig. 2 and summarized in Table 1. Detailed analytical and location data are presented in Table 2 and Appendix 1.*

$^{40}Ar/^{39}Ar$ ages on hornblende and biotite of 182 ± 2 and 179 ± 0.2 Ma respectively. They interpreted the difference in ages to represent moderate cooling from about 600°C (closure temperature of titanite in U-Pb system) to 500°C (closure temperature of hornblende in $^{40}Ar/^{39}Ar$ system) and then rapid cooling through 300°C (closure temperature of biotite). In this same general area, Early Jurassic $^{40}Ar/^{39}Ar$ cooling ages of 187.4 ± 5.2 Ma on unfoliated metamorphic/metasomatic biotite and 183.6 ± 2 Ma on hornblende of similar origin were obtained from a greenstone body in the Yukon–Tanana terrane (samples 11, 12; Table 1). Metamorphic cooling ages reported from nearby areas of Yukon–Tanana terrane range from 195–184 Ma (Hansen et al., 1991; summarized in Stevens et al., 1993). Although cooling histories of individual plutons and areas may vary in detail, the above data collectively reflect postkinematic intrusion of a suite of hornblende-dominant plutons from about 193–182 Ma and cooling through argon closure temperatures for hornblende and biotite of both host schist (in Yukon–Tanana terrane) and plutons within the same time frame. The pluton ages provide an Early Jurassic minimum age for mylonitic schistose fabrics in Yukon–Tanana terrane (Stevens et al., 1993) and for the weaker shear fabrics developed at lower metamorphic grade in Cassiar terrane. The Jurassic plutons form a 'stitching' plutonic suite implying proximity of Yukon–Tanana and Cassiar terranes by about 184 Ma. Whether the fault between these terranes is truncated by an Early Jurassic pluton or whether there has been post-Jurassic displacement along this boundary is uncertain; relationships portrayed for the Early Jurassic pluton near Nisutlin River (Fig. 2) are extrapolated beneath overburden. The Early Jurassic bodies in northeast Teslin area are likely part of the Black Lake Suite (Woodsworth et al., 1991), a belt of hornblende-bearing plutons found to the southeast in British Columbia. The nearest large bodies, the Simpson Peak and Nome Lake batholiths, just south of the British Columbia–Yukon border, (Gabrielse, 1969) intrude strata included within the Slide Mountain and Dorsey terranes (Wheeler and McFeely, 1991). The Teslin area plutons are also contemporaneous with the compositionally similar Klotassin Suite (Woodsworth et al., 1991), which intrudes Yukon–Tanana terrane in southwest Yukon.

Three mid-Jurassic ages were obtained from the unfoliated Mt. Bryde pluton (sample 13, Table 1). Although uncertainties of each of three ages on different minerals overlap, they essential indicate progressive cooling from a crystallization age of 175.7 ± 1.4 Ma, through the closure temperatures in the Ar system of hornblende at 173 ± 3 Ma and then biotite at 169 ± 2 Ma. The Mount Bryde pluton is unfoliated and crosscuts severely deformed ribbon chert and greywacke of the Cache Creek terrane, implying an upper limit for Cache Creek deformation of early Middle Jurassic (Aalenian) age (timescale of Harland et al., 1990). The deformation is closely bracketed as Pleinsbachian to Aalenian, considering that radiolarian ages of the beds involved are as young as Pleinsbachian or early Toarcian (Cordey et al., 1991). The ages from the Mt. Bryde pluton are similar to a U-Pb age on zircon for the Fourth of July Creek batholith near the southwest corner of the Teslin area reported by Mihalynuk et al. (1992) at 171.7 ± 3 Ma. Plutons of Middle Jurassic age are rare in northernmost British Columbia and Yukon. In the Yukon, the Teslin Crossing stock and some nearby small intrusions, predominantly hornblende monzonite (Woodsworth et al., 1991), are the only known correlatives, and intrude Mesozoic sediments of the Stikine terrane. The Three Sisters plutonic suite, which intrudes the Cache Creek and Stikine terranes in north central British Columbia, is correlative and compositionally similar to the Mt. Bryd pluton.

Samples 14, 15, and 16 (Table 1) represent a suite of Early Cretaceous hornblende-biotite bearing plutons that occurs on both sides of Teslin fault. Zircon (U-Pb), biotite and hornblende (K-Ar and $^{40}Ar/^{39}Ar$) ages overlap within uncertainties indicating fairly rapid cooling after crystallization at about 123 Ma. Southwest of Teslin fault, the ages provide an upper constraint to the age of deformation of the Lower to

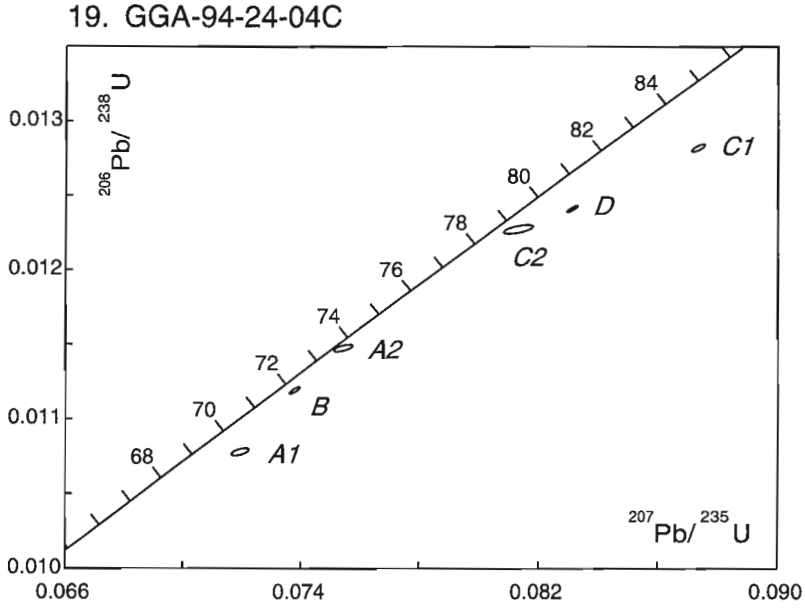

Figure 9.

U-Pb concordia diagram for a Late Cretaceous pluton. The sample location is marked on Fig. 2 and summarized in Table 1. Detailed analytical and location data are presented in Table 2 and Appendix 1.

Middle Jurassic Laberge Group greywacke (Stikine terrane). Plutons of recognized Early Cretaceous age are rare in the Cordillera. In the Teslin map area, these plutons were heretofore considered of mid-Cretaceous age (eg. Woodsworth et al., 1991).

Two samples of leucocratic biotite granite have yielded mid-Cretaceous U-Pb zircon ages of 109 ± 2 Ma and 108 ± 0.3 Ma (samples 17, 18 respectively, Table 1). The represented plutons are more felsic than the Early Cretaceous suite and also lack hornblende. The pluton near Hayes peak, although undated, appears to be a composite body, containing an early mafic phase resembling the Middle Jurassic suite intruded by a felsic phase resembling the mid-Cretaceous suite. Sample 17, dated at 109 ± 2 Ma, provides a minimum age on displacement of the fault bounding the southwest margin of Yukon–Tanana terrane, which is truncated by the Deadman Creek Batholith (Fig. 2). Truncation of this fault by the older Early Cretaceous phase (123.1 ± 1.7 Ma) of the batholith (*see* Fig. 2) is not demonstrated.

A Late Cretaceous age of 74 +6/-1 Ma (U-Pb zircon) was obtained from Sample 19 (Table 1), a massive, unfoliated fine- to medium-grained biotite granite that is difficult to distinguish from the mid-Cretaceous suite (K2). It represents a previously unsuspected northward extension of the Late Cretaceous Surprize Lake suite, a Late Cretaceous belt of hornblende-biotite and biotite-hornblende granite, alkali-feldspar granite, granodiorite, and hornblende quartz syenite that occurs in north-central British Columbia (Woodsworth et al., 1991). The new ages from the Deadman Creek batholith clearly show it is a composite body containing phases of Early Cretaceous, mid-Cretaceous, and Late Cretaceous age, of which the latter two are particularly difficult to distinguish in the field.

ACKNOWLEDGMENTS

Staff of the Geochronology laboratory (in particular Klaus Santowski, Jack MacRae, and Diane Bellerive) are thanked for their assistance in generating the U-Pb data. Critical reviews by Mike Villeneuve and Reg Thériault improved the paper.

REFERENCES

Ash, C.H. and Arksey, R.L.
1990: The Atlin ultramafic allochthon: ophiolitic basement within the Cache Creek terrane; tectonic and metallogenic significance (104 N/12); *in* Geological Fieldwork 1989, British Columbia Ministry of Energy, Mines and Petroleum Resources, Geological Survey Branch, Paper 1990-1, p. 365-374.

Cordey, F., Gordey, S.P., and Orchard, M.J.
1991: New biostratigraphic data for the northern Cache Creek terrane, Teslin map area, southern Yukon; *in* Current Research, Part E; Geological Survey of Canada, Paper 91-1E, p. 67-76.

Gabrielse, H.
1969: Geology of Jennings River map area, British Columbia (104-O); Geological Survey of Canada Paper 68-55, 37 p.

Gareau, S.
1992: Report on fieldwork in the southern Big Salmon metamorphic complex, Teslin map area, Yukon Territory; *in* Current Research, Part A; Geological Survey of Canada, Paper 92-1A, p. 267-277.

Gordey, S.P.
1991: Teslin map area, a new geological mapping project in southern Yukon; *in* Current Research, Part A; Geological Survey of Canada, Paper 91-1A, p. 171-178.
1992: Geological fieldwork in Teslin map area, southern Yukon Territory; *in* Current Research, Part A; Geological Survey of Canada, Paper 92-1A, p. 279-286.
1995: Structure and terrane relationships of Cassiar and Kootenay (Yukon–Tanana) terranes, Teslin map area, southern Yukon Territory; *in* Current Research 1995-A, Geological Survey of Canada, p. 135-140.

Gordey, S.P. and Stevens, R.A.
1994a: Tectonic framework of the Teslin region, southern Yukon Territory; *in* Current Research 1994-A; Geological Survey of Canada, p. 11-18.
1994b: Preliminary interpretation of the bedrock geology of the Teslin area (105 C), southern Yukon; Geological Survey of Canada, Open File 2886 (map, scale 1:250 000).

Hansen, V.L., Heizler, M.T., and Harrison, T.M.
1991: Mesozoic thermal evolution of Yukon–Tanana composite terrane: new evidence from $^{40}Ar/^{39}Ar$ data; Tectonics, v. 10, no. 1, p. 51-76.

Hansen, V.L., Mortensen, J.K., and Armstrong, R.L.
1989: U-Pb, Rb-Sr, and K-Ar isotopic constraints for ductile deformation and related metamorphism in the Teslin suture zone, Yukon–Tanana terrane, south-central Yukon; Canadian Journal of Earth Sciences, v. 26, p. 2224-2235.

Harland, W.B., Armstrong, R.L., Cox, A.V., Craig, L.E., and Smith, A.G.
1990: A geologic timescale 1989. Cambridge University Press, New York

Harms, T.A. and Stevens, R.A.
1996: A working hypothesis for the tectonostratigraphic affinity of the Stikine ranges and a portion of the Dorsey terrane (abstract); *in* Lithoprobe, Slave–Northern Cordillera Lithospheric Evolution (SNORCLE) and Cordilleran Tectonics Workshop, Report of the Combined Meeting, March 1–2, 1996, University of Calgary, Lithoprobe Report No. 50, p. 93-95.

Hart, C.J.R., Dickie, J.R., Ghosh, D.K., and Armstong, R.L.
1995: Provenance constraints for Whitehorse Trough conglomerate; U-Pb zircon dates and initial Sr ratios of granitic clasts in Jurassic Laberge Group, Yukon Territory; *in* (ed.) D.M. Miller. and C. Busby, Jurassic Magmatism and Tectonics of the North American Cordillera, Boulder, Colorado, Geological Society of America, Special Paper 299, p. 47-63.

Hunt, P.A. and Roddick, J.C.
1992: A compilation of ^{40}Ar-^{39}Ar ages: Report 22; *in* Radiogenic age and isotopic studies, Report 6; Geological Survey of Canada Paper 92-2, p. 179-226.
1994: A compilation of ^{40}Ar-^{39}Ar ages: Report 24; *in* Radiogenic age and isotopic studies, Report 8; Geological Survey of Canada Paper 1994-F, p. 125-155.

Johannson, G.G. and McNicoll, V.J.
1997: New U-Pb data from the Laberge Group, northwest British Columbia: implications for Stikinian arc evolution and Lower Jurassic time scale calibrations; *in* Radiogenic age and isotopic studies, Report 10; Geological Survey of Canada Paper 1997-F, p. 121-129.

Johannson, G.G., Smith, P.L., and Gordey, S.P.
1997: Early Jurassic evolution of the northern Stikinian arc: evidence from the Laberge Group, northwestern British Columbia; Canadian Journal of Earth Sciences, v. 34, p. 1030-1057.

Krogh, T.E.
1982: Improved accuracy of U-Pb ages by the creation of more concordant systems using an air abrasion technique; Geochimica et Cosmchimica Acta, v. 46, p. 637-649.

Mihalynuk, M.G., Smith, M.T., Gabites, J.E., Runkle, D., and LeFebure, D.
1992: Age of emplacement and basement character of the Cache Creek terrane as constrained by new isotopic and geochemical data; Canadian Journal of Earth Sciences, v. 29, no. 11, p. 2463-2477.

Monger, J.W.H.
1975: Upper Paleozoic rocks of the Atlin terrane, northwestern British Columbia and south-central Yukon; Geological Survey of Canada Paper 74-47, 63 p.

Monger, J.W.H., Wheeler, J.O., Tipper, H.W., Gabrielse, H., Harms, T., Struik, L.C., Campbell, R.B., Dodds, C.J., Gehrels, G.E., and O'Brien, J.
1991: Part B. Cordilleran terranes; *in* Upper Devonian to Middle Jurassic assemblages, Chapter 8 of Geology of the Cordilleran Orogen in Canada, (ed.) H. Gabrielse and C.J. Yorath ; Geological Survey of Canada, Geology of Canada, no. 4, p. 281-327 (*also* Geological Society of America, The Geology of North America, v. G-2).

Mortensen, J.K.
1992: Pre-mid-Mesozoic tectonic evolution of the Yukon–Tanana terrane, Yukon and Alaska; Tectonics, v. 11, no. 4, p. 836-853.

Nicolas, A.
1986: Structure and petrology of peridotites: clues to their geodynamic environment; Reviews of Geophysics, v. 24, no. 4, p. 875-895.

Parrish, R.R., Bellerive, D., and Sullivan, R.W.
1992: U-Pb chemical procedures for titanite and allanite in the Geochronology Laboratory, Geological Survey of Canada; *in* Radiogenic age and isotopic studies: Report 5, Geological Survey of Canada, Paper 91-2, p. 187-190.

Parrish, R.R., Roddick, J.C., Loveridge, W.D., and Sullivan, R.W.
1987: Uranium-lead analytical techniques at the geochronology laboratory, Geological Survey of Canada; *in* Radiogenic age and isotopic studies: Report 1, Geological Survey of Canada, Paper 87-2, p. 3-7.

Roddick, J.C.
1987: Generalized numerical error analysis with applications to geochronology and thermodynamics; Geochimica et Cosmchimica Acta, v. 51, p. 2129-2135.
1990: ^{40}Ar-^{39}Ar evidence for the age of the New Quebec Crater, northern Quebec; *in* Radiogenic age and isotopic studies: Report 3, Geological Survey of Canada, Paper 89-2, p. 7-16.

Ross, G.M. and Harms, T.A.
1998: Detrital zircon geochronology of 'Sequence C' grits, Dorsey Terrane (Thirtymile Range, southern Yukon): provenance and stratigraphic correlation; *in* Radiogenic age and isotopic studies: Report 11, Geological Survey of Canada Current Research 1998-F.

Stevens, R.A.
1991: The Teslin suture zone in northwest Teslin map area, Yukon; *in* Current Research, Part A; Geological Survey of Canada, Paper 91-1A, p. 271-277.
1992: Regional geology, fabric and structure of the Teslin suture zone in northwest Teslin map area, Yukon Territory; *in* Current Research, Part A; Geological Survey of Canada, Paper 92-1A, p. 287-295.
1993: Teslin suture zone; *in* Field Guide to Accompany the 1993 Nuna Conference on The Northern Intermontane Superterrane, Johnson et al. (ed.); p. 44-45.

Stevens, R.A. and Erdmer, P.
1993: Geology and structure of the Teslin suture zone and related rocks in parts of Laberge, Quiet Lake, and Teslin map area, Yukon Territory; *in* Current Research, Part A; Geological Survey of Canada, Paper 93-1A, p. 11-20.
1996: Structural divergence and transpression in the Teslin tectonic zone, southern Yukon Territory; Tectonics, v. 15, no. 6, p. 1342-1363.

Stevens, R.A., Mortensen, J.K., and Hunt, P.A.
1993: U-Pb and ^{40}Ar-^{39}Ar geochronology of plutonic rocks from the Teslin suture zone, Yukon Territory; *in* Radiogenic Age and Isotopic Studies; Report 7, Paper 93-2, p. 83-90.

Wheeler, J.O. and McFeely, P.
1991: Tectonic assemblage map of the Canadian Cordillera and adjacent parts of the United States of America; Geological Survey of Canada, Map 1712A, scale 1:2 000 000.

Wheeler, J.O., Brookfield, A.J., Gabrielse, H., Monger, J.W.H., Tipper, H.W., and Woodsworth, G.J.
1991: Terrane map of the Canadian Cordillera, Geological Survey of Canada, Map 1713A, scale 1:2 000 000.

Woodsworth, G.J., Anderson, R.G., and Armstrong, R.L.
1991: Plutonic regimes, Chapter 15 *in* Geology of the Cordilleran Orogen in Canada, (ed.) H. Gabrielse and C.J. Yorath; Geological Survey of Canada, Geology of Canada, no. 4, p. 491-531 (*also* Geological Society of America, The Geology of North America, v. G.-2).

York, D.
1969: Least squares fitting of a straight line with correlated errors; Earth and Planetary Science Letters, v. 5, p. 320-324.

APPENDIX 1

Detailed sample location data.
Sample numbers are referenced in Fig. 2 and tables 1 and 2.

SAMPLE		UTM COORDINATES			GEOGRAPHIC LOCATION			
NO.	FIELD NO.	ZONE	EAST	NORTH	NTS	LAT	LONG	DESCRIPTION
1	GGA-90-20-03B	8	594169	6727443	105C/11	60°40.40'N	133°16.59'W	6.4 km bearing 95° from Cone Mountain
2	GGA-93-37-04B	8	652429	6658807	105C/01	60°02.40'N	132°15.81'W	6.5 km bearing 210° from Mount Morley; roadcut on Alaska Highway
3	GGAS-93-22-04	8	637549	6701152	105C/07	60°25.50'N	132°30.09'W	16.8 km bearing 8° degrees from the confluence of the Wolf and Nisutlin rivers
4	GGA-90-46-03C	8	573785	6722275	105C/12	60°37.88'N	133°39.08'W	6.0 km bearing 0° from Streak Mountain
5	GGA-90-25-03E	8	562755	6747258	105C/13	60°51.45'N	133°50.69'W	5.3 km bearing 5° from the confluence of Swift and Teslin rivers
6	GGA-90-03-06C	8	563521	6732722	105C/12	60°43.61'N	133°50.13'W	20.4 km bearing 328° from Streak Mountain
7	GGA-90-39-05B	8	646894	6721963	105C/09	60°36.50'N	132°19.00'W	14.3 km bearing 270° from the south tip of Fish Lake
8	GGA-91-38-04C	8	642752	6711873	105C/09	60°31.16'N	132°23.97'W	20.9 km bearing 245° from the south tip of Fish Lake
9	GGAS-93-05-02B	8	628194	6744742	105C/15	60°49.15'N	132°38.58'W	5.5 km bearing 310° degrees from the southwest end of Thirtymile Lake
10	GGAJ-94-19-11D	8	634920	6711851	105C/10	60°31.31'N	132°32.52'W	7.1 km bearing 107° from confluence of Thirtymile Creek (south branch) and Nisutlin River
11	GGA-90-28-04B	8	571356	6753477	105C/13	60°54.71'N	133°41.06'W	14.6 km bearing 38° from the confluence of Swift River and Teslin River
12	GGA-90-28-01B	8	572293	6752661	105C/13	60°54.26'N	133°40.04'W	14.6 km bearing 43° from the confluence of Swift River and Teslin River
13	GGA-91-40-11C	8	600309	6666641	105C/03	60°07.58'N	133°11.68'W	2.3 km bearing 337° from Mt. Bryde
14	GGA-90-21-12D	8	618452	6701263	105C/07	60°25.92'N	132°50.88'W	23.9 km bearing 315° from the confluence of Nisutlin and Wolf rivers
15	GGA-90-46-04B	8	563032	6727701	105C/12	60°40.91'N	133°50.77'W	15.8 km bearing 315° from Streak Mountain
16	GGA-90-46-02B	8	572584	6717625	105C/12	60°35.39'N	133°40.50'W	2.0 km bearing 315° from Streak Mountain
17	GGA-92-05-02C	8	596150	6713520	105C/11	60°32.88'N	133°14.82'W	4.0 km bearing 315° from Haircut Lake
18	GGAJ-94-20-01A	8	653013	6673776	105C/01	60°10.44'N	132°14.51'W	13.0 km bearing 43° from confluence of Hays Creek and Morley River
19	GGA-94-24-04C	8	610938	6716379	105C/10	60°34.19'N	132°58.56'W	17.3 km bearing 284° from confluence of Thirtymile Creek (south branch) and Nisutlin River

Other publications containing geochronological data generated by the Geochronology Subdivision

Ansdell, K.M. and Stern, R.A.
1997: SHRIMP detrital geochronology in the Trans-Hudson Orogen: detrital zircons in turbiditic and fluvial sedimentary rocks; Lithoprobe Trans-Hudson Orogen Transect, Report No. 62, p. 119-129.

Bingen, B. and van Breemen, O.
1996: U-Pb titanite geochronology in Rogaland–Vest Agder (SW Norway): regional temperature at the time of intrusion of the Rogaland anorthosites; *in* Petrology and Geochemistry of Magmatic Suites of Rocks in the Continental and Oceanic Crusts, a Volume Dedicated to Professor Jean Michot, (ed.) D. Demaiffe; Université Libre de Bruxelles, Royal Museum for Central Africa (Tervuren), p. 145-160.
1998: Tectonic regimes and terrane boundaries in the high-grade Sveconorwegian belt of SW Norway, inferred from U-Pb zircon geochronology and geochemical signature of augen gneiss suites; Geological Society of London, Journal, v. 155, p. 143-154.

Bingen, B., Demaiffe, D., and van Breemen, O.
1996: Rb-Sr isotopic signature of augen gneiss suites in the Sveconorwegian Province of SW Norway; *in* Petrology and Geochemistry of Magmatic Suites of Rocks in the Continental and Oceanic Crusts, a Volume Dedicated to Professor Jean Michot, (ed.) D. Demaiffe; Université Libre de Bruxelles, Royal Museum for Central Africa (Tervuren), p. 161-174.

Cadman, A.C., Tarney, J., and Hamilton, M.A.
1997: Petrogenetic relationship between Paleoproterozoic tholeiitic dykes and associated high-Mg noritic dykes, Labrador, Canada; Precambrian Research, v. 82, p. 63-84.

Corrigan, D. and van Breemen, O.
1997: U-Pb age constraints for the lithotectonic evolution of the Grenville Province along the Mauricie transect, Quebec; Canadian Journal of Earth Sciences, v. 34, p. 299-316.

Davis, W.J.
1997: U-Pb zircon and rutile ages from granulite xenoliths in the Slave Province: evidence for mafic magmatism in the lower crust coincident with Proterozoic dike swarms; Geology, v. 25, p. 343-346.

Davis, W.J. and Kjarsgaard, B. A.
1997: A Rb-Sr isochron age for a kimberlite from recently discovered Lac de Gras field, Slave Province, Northwest Canada; Journal of Geology, v. 105, p. 503-509.

Emslie, R.F., Hamilton, M.A., and Gower, C.F.
1997: The Michael Gabbro and other Mesoproterozoic lithospheric probes in southern and central Labrador; Canadian Journal of Earth Sciences, v. 34, p.1566-1580.

Evenchick, C.A., Alldrick, D.J., Currie, L.D., Haggart, J.W., McCuaig, S., McNicoll, V.J., and Woodsworth, G.J.
1997: Status of research in the Nass River multidisciplinary geoscience project, British Columbia; *in* Current Research 1997-A; Geological Survey of Canada, p. 21-30.

Lin, S., Percival, J.A., and Skulski, T.
1996: Structural constraints on the tectonic evolution of a late Archean greenstone belt in the northeastern Superior Province, northern Quebec (Canada); Tectonophysics, v. 265, p. 151-167.

Percival, J.A., Skulski, T., and Nadeau, L.
1997: Granite-greenstone terranes of the northern Minto block, northeastern Quebec: Pelican–Nantais, Faribault–Leridon, and Duquet belts. *in* Current Research 1997-C; Geological Survey of Canada, p. 211-221.

Sandeman, H.A., Clark, A.H., Styles, M.T., Scott, D.J., Malpas, J.G., and Farrar, E.
1997: Geochemistry and U-Pb and ^{40}Ar-^{39}Ar geochronology of the Man of War Gneiss, Lizard Complex, SW England: pre-Hercynian arc-type crust with a Sudeten–Iberian connection; Geological Society of London, Journal, v. 145, p. 403-417.

Scott, D.J.
In press: U-Pb geochronology of the eastern Hall Peninsula, southern Baffin Island, Canada: a northern link to the Archean of West Greenland and the Paleoproterozoic Torngat Orogen of northern Labrador; Precambrian Research.

Stern, R.A.
1996: A SHRIMP II ion microprobe at the Geological Survey of Canada; Geoscience Canada, v. 23, p. 73-76.

Wodicka, N. and Scott, D.J.
1997: A preliminary report on the U-Pb geochronology of the Meta Incognita Peninsula, southern Baffin Island, Northwest Territories; *in* Current Research 1997-C, Geological Survey of Canada, p. 167-178.

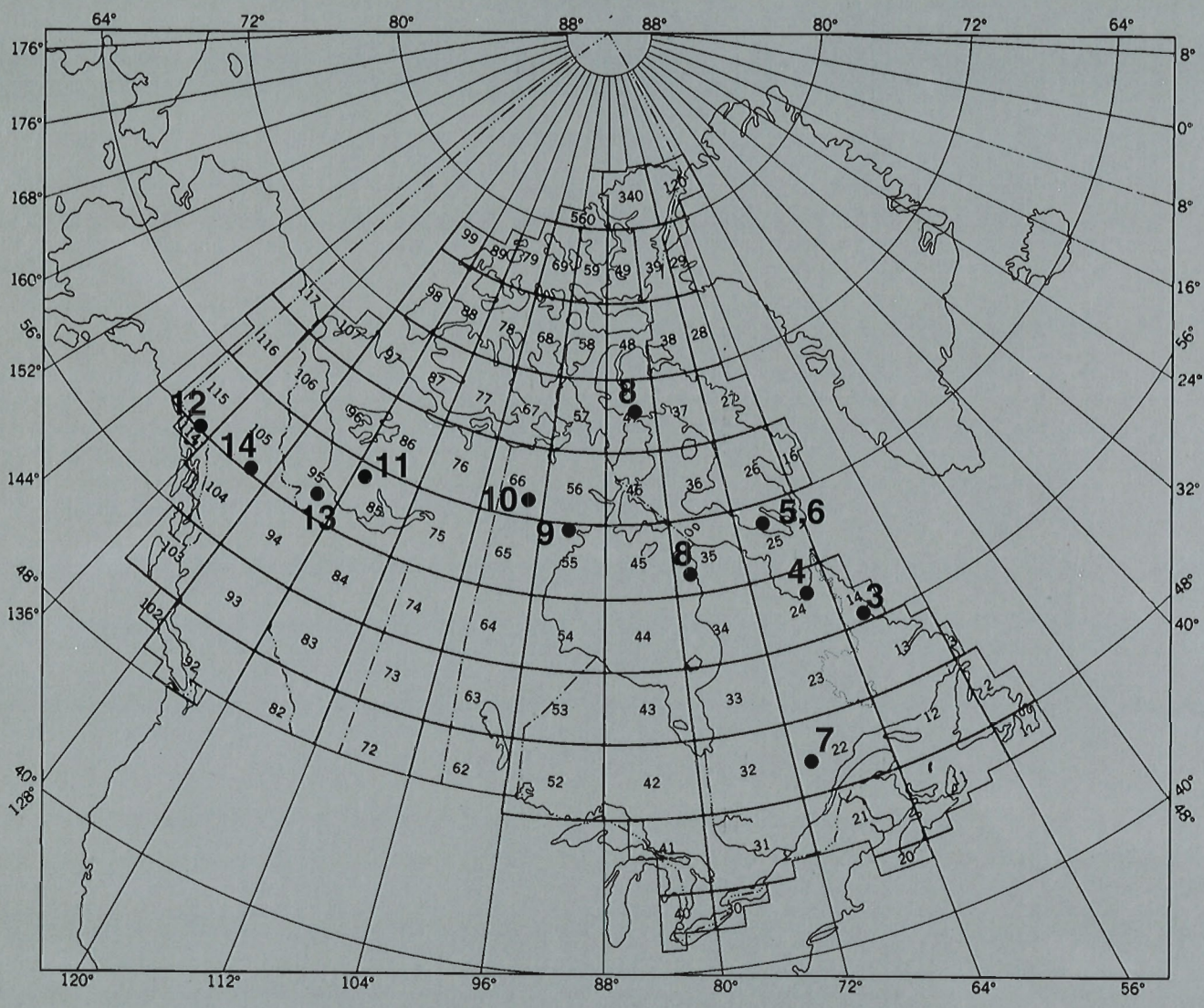

Locations on the map refer to reports in this volume
Les localités indiquées sur la carte correspondent aux rapports contenus dans le présent volume